# HIGH REYNOLDS NUMBER INCOMPRESSIBLE FLOW SIMULATION

# ABOUT PARACHUTE CANOPIES AND SIMILAR BLUFF BODIES

By

Yaacov I. Frucht

The thesis submitted to the University of Leicester for the degree of Doctor of Philosophy.

December 1987

TO MY PARENTS AND MY WIFE.

## ABSTRACT

A model for the flow around bluff bodies has been developed. It is applied to an investigation of parachute canopy aerodynamic characteristics. Since the model assumes an axisymmetric incompressible high Reynolds number flow, it is only applicable to the calculation of aerodynamic characteristics at zero angle of attack.

The flow is assumed to separate from the canopy at its surface discontinuity, i.e. the canopy hemline. The vorticity created in the boundary layer over the canopy upper surface is carried downstream, forming a free shear layer.

In the flow field vorticity is confined to the this shear layer, outside it the flow is irrotational. Consequently, in this part of the fluid field a velocity potential can be defined.

The wake flow created by bluff canopies is found to consist of a cluster of vortex rings which are shed periodically to the wake. Consequently, the axial aerodynamic force developed on the canopy will exhibit periodic behaviour. The resulting Strouhal number, has been determined to be about 0.13, based on the canopy projected area diameter.

For all axisymmetric bluff canopies considered the calculated mean axial force coefficient,based on the canopy projected diameter, was found to be between 1.20 and 1.45. These values, together with the calculated pressure distribution and the wake flow periodicity, are in good agreement with known experiments. For parachute canopies performing an oscillatory axial motion the calculated results compare well with experimental data. However, it is shown that Morison's formula for this axial force is, generally, inadequate.

Limited calculations of axial forces developed on the inflating parachute canopies agree with the sparse experimental data available.

In the model the real flow field is simulated, basically, by a potential model.

The canopy surface is replaced by a vortex ring panel lattice. Each panel contains a circular bound vortex ring which is located at one quarter panel length. For each panel the flow boundary conditions on the canopy surface are fulfilled along a control circle at three quarters of the panel length.

A standing eddy which is generated by the high back-flow developed near the canopy hemline, on the canopy under surface is simulated by a standing vortex ring.

The simulation of a two-dimensional discrete vortex separated wake is extended to the axisymmetric case by representing the separated wake with axisymmetric discrete vortex rings. The free shear layer emanating from the canopy hemline is represented by discrete free vortex rings which leave the canopy surface tangentially. At each time step in the calculation process a newly-created vortex ring is shed to the wake.

In the vortex modelling of the separated wake a number of new elements have been introduced:

-improvement of the near wake simulation by accounting for the standing eddy on the canopy under surface;
-a simple method of calculating the newly created vortex ring strength & location;
-reduction of the free parameters from two, the time step and the number of panels representing the canopy surface to one,i.e. the number of panels.

Further model validation & implementation have been suggested. Methods of model development for asymmetric canopy representation have been discussed.

## AKNOWLEDGEMENTS

The author wishes to express his profound gratitude to Dr. David J. Cockrell for his supervision and valuable criticism. Without his continuous support and encouragement the completion of this work would not have been possible.

The writer has received an important assistance in computing aspects of the research from Dr. Dimitrios Papadakos.

The author wishes to express his appreciation to Mrs. Judith Levy, his sister, for the preparation of the drawings.

Finally, the author is grateful to Professor G.D.S. MacLellan the Head of the Engineering Department for allowing facilities in the department for the present research to be used.

# LIST OF CONTENTS


| | PAGE |
|---|---|
| 1. INTRODUCTION | 1 |
| 2. WAKE FLOW - PHYSICAL BACKGROUND | 4 |
| 3. THE FLOW AROUND BLUFF BODIES - LITERATURE REVIEW | 8 |
| 3.1 EXPERIMENTAL INVESTIGATION OF THE AERODYNAMICS OF THREE-DIMENSIONAL BLUFF BODY | 11 |
| 3.2 BLUFF BODY WAKE FLOW SIMULATION | 19 |
| 3.3 THEORETICAL APPROACHES TO AERODYNAMIC LOAD CALCULATION ON PARACHUTE CANOPIES | 26 |
| 4. THE PROPOSED MODEL | 30 |
| 4.1 THE VELOCITY INDUCED BY A VORTEX RING IN AXISYMMETRIC FLOW | 37 |
| 4.2 THE VORTEX RING SELF INDUCED VELOCITY | 42 |
| 4.3 VISCOUS CORE RADIUS EVALUATION | 45 |
| 4.4 CANOPY SURFACE SIMULATION | 48 |
| 4.5 POROSITY INFLUENCE | 51 |
| 4.6 THE SHEDDING STRENGTH | 53 |
| 4.7 THE SEPARATED WAKE SIMULATION AND THE REQUIRED TIME STEP EVALUATION | 57 |
| 4.8 STANDING VORTEX RING STRENGTH & LOCATION EVALUATION | 59 |
| 4.9 DIFFERENTIAL PRESSURE CALCULATION | 63 |
| 4.10 THE MODEL LIMITATIONS | 66 |
| 5. THE CALCULATION METHOD & COMPUTER PROGRAMME DESCRIPTION | 70 |
| 6. NUMERICAL INVESTIGATION RESULTS | 76 |
| 6.1 THE AERODYNAMIC PROPERTIES DEVELOPED ON A | |

RIGID CANOPY IN ASYMPTOTICALLY STEADY MOTION 77

6.1.1 THE INFLUENCE OF THE CANOPY SHAPE ON THE TIME-DEPENDENT AXIAL FORCE 87

6.1.2 MEAN AERODYNAMIC PROPERTIES OF THE NEAR WAKE 96

6.1.3 POROSITY EFFECTS ON THE AXIAL AERODYNAMIC FORCE 100

6.1.4 THE MEAN PRESSURE DISTRIBUTION 108

6.1.5 THE FREE-STREAM REYNOLDS NUMBER EFFECT 112

6.2 THE AERODYNAMIC PROPERTIES OF A RIGID CANOPY IN AN UNSTEADY STREAM 115

6.2.1 ACCELERATED FLOW 119

6.2.2 DECELERATED FLOW 124

6.2.3 FREE DECELERATION 131

6.2.4 OSCILLATORY MOTION 137

6.3 THE PARACHUTE CANOPY INFLATION PROCESS 142

7. THE MODEL SENSITIVITY 145

8. RECOMMENDATIONS FOR FURTHER WORK 150

8.1 RECOMMENDATIONS FOR FUTURE EXPERIMENTAL STUDIES 151

8.2 RECOMMENDATIONS FOR FUTURE THEORETICAL STUDIES 152

9. SUMMARY AND CONCLUSIONS 154

REFERENCES 157

APPENDIX: COMPUTER PROGRAMME "PARACHUTE" LISTING A-1

## LIST OF SYMBOLS

A - axial force

C - dimensionless aerodynamic coefficient, e.g.:

$A=0.5\rho V_\infty^2 S_{ref} C_A$ ; $P=0.5\rho V_\infty^2 C_p$

$\bar{C}$ - mean, dimensionless coefficient (defined in section 6.1.1)

D - drag or diameter

E - the first kind elliptic integral

K - the second kind elliptic integral

I - impulse or moment of inertia

P - pressure

R - projected area radius

$\vec{R}$ - the radius vector from the canopy apex to a point on its surface

Re - Reynolds number $Re=V_\infty * l_{ref}/\nu$

S - surface

St - Strouhal number $St=f * l_{ref}/V_\infty$

$V,\vec{V}$ - velocity

Vol - reference volume for $k_{11}$

X, Y, Z - coordinate system defined in figure 5.3

X1, X2, Y1 - canopy shape parameters defined in figure 5.1

a - vortex ring radius

f - frequency [Hertz]

$k_{11}$ - added mass coefficient based on "Vol"

m - mass

$\hat{n}$ - unit vector normal to body surface

t - time

$\bar{t}$ - dimensionless time :

$$\bar{t}=t*V_\infty/(2R)$$

r - radius vector to a field point

u - linear velocity along x axis

v - linear velocity along y axis

w - linear velocity along z axis

$\Gamma$ - circulation

$\Delta$ - difference, e.g. $\Delta C_p=C_{p_1}-C_{p_2}$

$\Phi$ - velocity potential

$\alpha$ - small arc defined in figure 4.3

$\beta$ - circulation reduction factor

$\lambda$ - geometric porosity (the ratio of open area to total surface area)

$\nu$ - kinematic viscosity [length$^2$/time]

$\varepsilon$ - small length or vortex core radius

$\bar{\varepsilon}$ - dimensionless vortex core radius :

$$\bar{\varepsilon}=\varepsilon/a$$

$\delta$ - acceleration modulus:

$$\delta=2R*\dot{V}_\infty/V_\infty^2$$

$\rho$ - fluid density

$\vec{\omega}$ - vorticity

## MAIN INDICES

$_{A}$ - axial

$_{D}$ - drag

$_{can}$ - canopy

$_{f}$ - fluid, inflation time

$_{ind}$ - induced

$_{n}$ - normal

$_{p}$ - pressure

$_{por}$ - porosity

$_{ref}$ - reference

$_{si}$ - self-induced

$_{svr}$ - standing vortex ring

$_{tot}$ - total

$_{x}$, $_{y}$, $_{z}$ - associated with axes X,Y,Z respectively

$_{\infty}$ - infinite, undisturbed fluid field conditions

## OPERATORS

$$\nabla \equiv \partial/\partial x \cdot \hat{x} + \partial/\partial y \cdot \hat{y} + \partial/\partial z \cdot \hat{z}$$

$$\nabla^2 \equiv \partial^2/\partial x^2 + \partial^2/\partial y^2 + \partial^2/\partial z^2$$

$$D/Dt \equiv \partial/\partial t + \vec{V} \cdot \nabla$$

# LIST OF FIGURES

PAGE

FIGURE 2.1 : A SKETCH OF THE FLUID FIELD IN THE NEAR WAKE 7

FIGURE 3.1 : SCHEMATIC REPRESENTATION OF THE WAKE BEHIND A SQUARE PLATE (based on EDEN- 1911) 16

FIGURE 3.2 : THE EVOLUTION OF A VORTEX RING OF AN INITIALLY, HIGHLY NON-UNIFORMLY DISTRIBUTED SELF-INDUCED VELOCITY 17

FIGURE 3.3 : THE ASSUMED WAKE PATTERN BEHIND A BLUFF BODY IN AXISYMMETRIC FLOW 18

FIGURE 3.4 : KIRCHHOFF'S FREE-STREAM LINE THEORY 19

FIGURE 3.5 : THE STABLE ARRANGEMENT OF VORTICES IN A VORTEX STREET 22

FIGURE 3.6 : DIFFERENTIAL PRESSURE DISTRIBUTION ABOUT AN HEMISPHERICAL CUP, IN ATTACHED FLOW (based on Ibrahim,1965, calculations) 29

FIGURE 4.1 : THE REAL FLOW AND THE MODEL 35

FIGURE 4.2 : THE CIRCUIT FOR PROVING CONSERVATION OF CIRCULATION 36

FIGURE 4.3 : THE VORTEX RING INDUCED VELOCITY 37

FIGURE 4.4 : THE TANGENTIAL VELOCITY, $U_\theta$, DEVELOPED ABOUT A TWO-DIMENSIONAL VISCOUS VORTEX 47

FIGURE 4.5 : CANOPY SURFACE MODELLING 50

FIGURE 4.6 : THE FLOW THROUGH A POROUS SCREEN 51

FIGURE 4.7 : THE VORTEX SHEDDING FROM A SALIENT, TWO-DIMENSIONAL EDGE 54

FIGURE 4.8 : STANDING VORTEX RING LOCATION 62

FIGURE 4.9 : DIFFERENTIAL PRESSURE DISTRIBUTION CALCULATION 65

FIGURE 4.10: THE DETERMINATION OF SHED VORTEX RINGS CANCELLATION DISTANCE 69

FIGURE 5.1 : THE COORDINATE SYSTEM FOR FLOW SIMULATION 70

FIGURE 5.2 : THE LOW-LEVEL FLOW CHART FOR THE CALCULATION PROCEDURE 74

FIGURE 5.3 : A HIERARCHICAL SCHEME OF THE MAIN COMPUTER PROGRAMME PROCEDURES 75

FIGURE 6.1 : THE VORTEX SHEDDING MECHANISM AT SUCCESSIVE TIME INTERVALS 78

FIGURE 6.2 : THE WAKE FLOW PATTERN DEVELOPED AT SUCCESIVE TIME INTERVALS BY THE CANOPY X1/Y1=0.7 , X2/Y1=0.6 82

FIGURE 6.3 : THE WAKE FLOW PATTERN DEVELOPED AT SUCCESIVE TIME INTERVALS BY THE CANOPY X1/Y1=0.7 , X2/Y1=0.7 83

FIGURE 6.4 : THE WAKE FLOW PATTERN DEVELOPED AT SUCCESIVE TIME INTERVALS BY THE CANOPY X1/Y1=1 , X2/Y1=1.2 84

FIGURE 6.5 : THE WAKE FLOW PATTERN DEVELOPED AT SUCCESIVE TIME INTERVALS BY THE CANOPY X1/Y1=0.7 , X2/Y1=0.8 85

FIGURE 6.6 : THE WAKE FLOW AND THE AXIAL FORCE COEFFICIENT, $C_A$,DEVELOPED ON A HEMISPHERE 86

FIGURE 6.7 : TYPICAL AXIAL FORCE COEFFICIENT, $C_A$, DEVELOPMENT 88

FIGURE 6.8 : THE MEAN AXIAL FORCE COEFFICIENT, $\overline{C}_A$, AND THE STROUHAL NUMBER , St, FOR VARIOUS CANOPIES 90

FIGURE 6.9 : THE FLOW REATTACHMENT TREND FOR HIGHLY BLUFF CANOPIES 92

FIGURE 6.10: THE BASE PRESSURE COEFFICIENT, $C_p$ BASE OF CONES (based on Calvert's experiments, 1967 b) 95

FIGURE 6.11: THE NEAR WAKE STRUCTURE FOR CANOPIES OF DIFFERENT BLUFFNESS 98

FIGURE 6.12: THE MEAN RESULTANT VELOCITY DISTRIBUTION IN THE WAKE DEVELOPED BEHIND A FLAT CANOPY 99

FIGURE 6.13: THE POROSITY, $\lambda$, INFLUENCE ON THE MEAN, AXIAL FORCE COEFFICIENT, $\overline{C}_A$. 104

FIGURE 6.14: THE POROSITY,$\lambda$ ,ON THE STROUHAL NUMBER, St. 105

FIGURE 6.15: WAKE FLOW PERIODICITY SUPPRESSION BY THE POROSITY 106

FIGURE 6.16: A DISTRIBUTED GEOMETRIC POROSITY RESULTING IN AN ALMOST UNIFORM PRESSURE DISTRIBUTION (X1/Y1=0.7 , X2/Y1=0.7) 107

FIGURE 6.17: THE DIFFERENTIAL PRESSURE COEFFICIENT, $\Delta C_p$, ACROSS THE CANOPY CALCULATED BY DIFFERENT APPROACHES (a qualitative description) 110

FIGURE 6.18: THE DIFFERENTIAL PRESSURE COEFFICIENT, $\Delta C_p$, DEVELOPED ON VARIOUS CANOPIES (calculated and experimental results) 111

FIGURE 6.19: FREE STREAM REYNOLDS NUMBER, Re, EFFECT ON THE MEAN AXIAL FORCE COEFFICIENT, $\overline{C}_A$,

AND ON THE STROUHAL NUMBER, St. 114

FIGURE 6.20: THE AXIAL FORCE COEFFICIENT , $\overline{C}_A$, AND ITS ADDED MASS COMPONENT, $k_{11}$. (based on IVERSEN & BALENT,1951) 118

FIGURE 6.21: THE CALCULATED AXIAL FORCE COEFFICIENT, $C_A$, DEVELOPED ON A HEMISPHERE MOVED AT A CONSTANT ACCELERATION MODULUS, δ. 121

FIGURE 6.22: THE WAKE FLOW PATTERN GENERATED BY A HEMISPHERE MOVING AT A CONSTANT ACCELERATION MODULI, δ 122

FIGURE 6.23: THE WAKE FLOW PATTERN DEVELOPED BEHIND A DECELERATING HEMISPHERE 126

FIGURE 6.24: THE AXIAL FORCE COEFFICIENT, $C_A$, AND THE WAKE FLOW PATTERN DEVELOPED AT SIMILAR ACCELERATION MODULI IN A DECELERATING MOTION WHICH RESULT FROM DIFFERENT FLOW HISTORIES 127

FIGURE 6.25: THE AXIAL FORCE COEFFICIENT, $C_A$, DEVELOPED ON A FREELY-DECELERATING PARACHUTE/PAYLOAD SYSTEM (X1=X2=1.4m, Y1=2m) 133

FIGURE 6.26: THE AXIAL FORCE COEFFICIENT, $C_A$, DEVELOPED ON A FREELY-DECELERATING PARACHUTE/PAYLOAD SYSTEM (based on experimental results presented in "PERFORMANCE OF AND DESIGN CRITERIA FOR DEPLOYABLE AERODYBAMIC DECELERATOR", 1963 and by Ewing, 1972) 136

FIGURE 6.27 : THE AXIAL FORCE COEFFICIENT, $C_A$, DEVELOPED ON A HEMISPHERICAL CANOPY IN AXIAL OSCILLATORY MOTION (calculations and Harwood R., 1986

& 1987 experiments) 139

FIGURE 6.28: THE CALCULATED ADDED MASS COEFFICIENT, $k_{11}$, VARIATION DURING THE AXIAL OSCILLATORY MOTION OF A HEMISPHERE 141

FIGURE 6.29: THE CALCULATED AXIAL FORCE DEVELOPED ON AN INFLATING CANOPY 144

FIGURE 7.1 : THE DIFFERENTIAL PRESSURE COEFFICIENT, $\Delta C_p$, DISTRIBUTION ON SPHERICAL CANOPIES IN ATTACHED FLOW (comparison with analytical calculations by Ibrahim, 1965) 148

FIGURE 7.2 : THE INFLUENCE OF THE NUMBER OF PANELS, NP, ON AXIAL FORCE 149

# 1. INTRODUCTION

Parachutes are the most common form of aerodynamic decelerators, but although they are widely used the techniques available for their aerodynamic design are very limited and are mainly experimentally based.

The pressure distribution developed on the parachute canopy is affected by several factors, the most important among them being:

-the unsteady wake flow behind the canopy;

-the canopy basic shape, e.g. square, round, cross etc;

-the canopy shape changes which result from the fluctuations in pressure distribution;

-canopy porosity.

Due to the complexity of the flow around bluff canopies, analytic determination of the aerodynamic loads presents a serious challenge to the designer and only in the last 1-2 years have encouraging results, based on relatively recent techniques, been reported.

The purpose of this research is to develop a method for simulating the flow around an axisymmetric bluff body. The method is applied to investigate the flow field and calculate the aerodynamic loads on bluff parachute canopies in both steady and unsteady flight.

The basic assumptions are:

-the canopy is axisymmetrical;

-its angle of attack is zero;

-the flow is incompressible and its Reynolds number is high.

The approach adopted is to simulate the unsteady, separated flow by using a potential flow model.

In this model the canopy surface is replaced by a bound vortex sheet and the shear layer carrying fluid of high vorticity from the under, unwetted, surface part of the canopy leaves the canopy surface tangentially at the hemline. The free part of this shear layer, which envelops the wake is simulated by a free discrete vortex sheet. The standing eddy developed by the high back-flow in the vicinity of the separation line on the canopy under surface is modelled by a standing vortex ring.

The fluid flow viscous effects are considered by letting the flow separate along the canopy hemline and by assuming small regions of concentrated vorticity in the cores of the ring vortices forming the free vortex sheet. Outside these small regions of concentrated vorticity the flow field is irrotational.

The flow about two-dimensional bluff bodies has been throughly investigated, both theoretically and experimentally. Its simulation is based on Kirchhoff's free stream-line theory and on Prandtl's boundary layer concept. Von Karman's vortex street revealed the wake flow periodicity. The numerical investigation of the separated two-dimensional wake has been facilitated by Rosenhead's pioneering work. Among other contributions, these fundamental works will be reviewed later. However, unlike

two-dimensional bluff body flow, few investigations have been made into flow around bluff three-dimensional bodies.

The three-dimensional flow complexity will here be considered in its simplest form i.e., axisymmetric flow. Thus, this research is considered to be a necessary first step in understanding flow phenomena which occur around three-dimensional bluff bodies, particularly when flow separation from those bodies is determined by salient edges. It provides a significant improvement of the existing aerodynamic design techniques for parachute canopies.

The thesis consists of five parts:

In part -I-, chapters 1-2, are presented some of the basic phenomena which occur in separated flow.

In part -II-, chapter 3, experiments on separated flow about three-dimensional bodies and methods for simulating the flow around such bodies are reviewed.

In part -III-, chapters 4 and 5, the nature of the proposed model and the calculation method are outlined.

In part -IV-, chapter 6, the results obtained from the numerical investigation and the model sensitivity are considered.

In part -V-, chapters 7-9, the research is summarised and possible directions for the present model validation & development are suggested.

## 2. WAKE FLOW - PHYSICAL BACKGROUND

To emphasise the main characteristics of the flow about a bluff obstacle, a disk moving through an unbounded fluid at a constant velocity with its surface normal to the velocity will be considered.

At very low Reynolds numbers (Re<<1) the flow is attached to the disk.

At higher Reynolds numbers the fluid carrying vorticity from the upper surface side of the disk to the under surface gives rise to a vortex ring in an identical manner to the development of a vortex in two-dimensional flow described by Prandtl & Tietjens (1954 article 93). This vortex ring is continuously supplied with vorticity carried from the under surface part of the disk and it diffuses vorticity at the rear.

A further increase in the Reynolds number causes variations in both the vortex ring's length and its thickness.

Above a certain Reynolds number the equilibrium between the vorticity which is supplied to the vortex ring and that diffused from it can no longer be maintained and the result is, as Rosenhead (1931, a) noticed, "a sheath of vorticity which is unstable and breaks up. The way in which this sheath breaks up is arrived at by regarding the surface of discontinuity as a series of vortex rings packed closely together".

The present research is concerned with flow at these high Reynolds numbers when the flow is characterized by an unstable free shear layer spreading from the salient edges of the bluff body. At high Reynolds number flow this shear layer is thin and the viscous decay in it can be neglected.

The free shear layer, which separates from the disk at its edge and which thereby creates a surface discontinuity, encloses a volume of fluid which moves at a much lower velocity than that of the free stream. It tends to close and reattach. During this process the layer becomes unstable and rolls up to form "packages of vortex rings" [Rosenhead 1931 a].

These vortex ring packages are shed at more or less regular intervals downstream into the wake. The part of the wake which is bound by the unwetted body surface and by the region where the shear layer tends to close and where the "vortex rings packages" are shed is henceforth defined as the near wake. Figure 2.1 shows schematically the near wake flow field structure.

Due to the strong movements of the fluid immediately downstream of the the near wake the flow there becomes turbulent. However, due to viscous dissipation, this flow may relaminarise [Batchelor 1967, 5.13] further downstream.

Since the near wake makes the main contribution to the pressure distribution the fundamental purpose of this research is to simulate the near wake fluid flow.

As pointed out by Batchelor [1967, 5.10], the free shear layer emanating from the separation line leaves the body

surface tangentially. The vorticity, shed from the boundary layer on the under surface of the disk, is convected by this shear layer at an average velocity of about one half of that at the outer part of the shear layer (figure 2.1). According to Kirchhoff's free streamline theory, reviewed in section 3.2 and Fage & Johansen's 1927 experiments, reviewed in section 5.6, the ratio between the velocity at the outer part of the free shear layer and that of the free stream will be in the range of 1.0-1.4. Therefore, the average convective velocity is anticipated to be about 0.6 of the free-stream velocity. Because of the velocity which is induced by the moving shed vortices the fluid velocity at any given point is time-dependent. Therefore, a separated flow is always unsteady, regardless of any variation in the free-stream velocity or in the body shape.

Due to its very small radius of curvature, at the salient edge the velocity is much larger than the free-stream velocity. Immediately downstream a strong back-flow occurs and this results in a "standing eddy" [Batchelor, 1967, 5.10] formed behind this edge. Physically, this eddy is "standing" only when its average centre velocity is compared with the free stream velocity. As will be shown in chapter 4 and in section 6.1.4, this standing eddy, which apparently has been neglected in the known flow simulation methods, makes a significant contribution to the aerodynamic load determination.

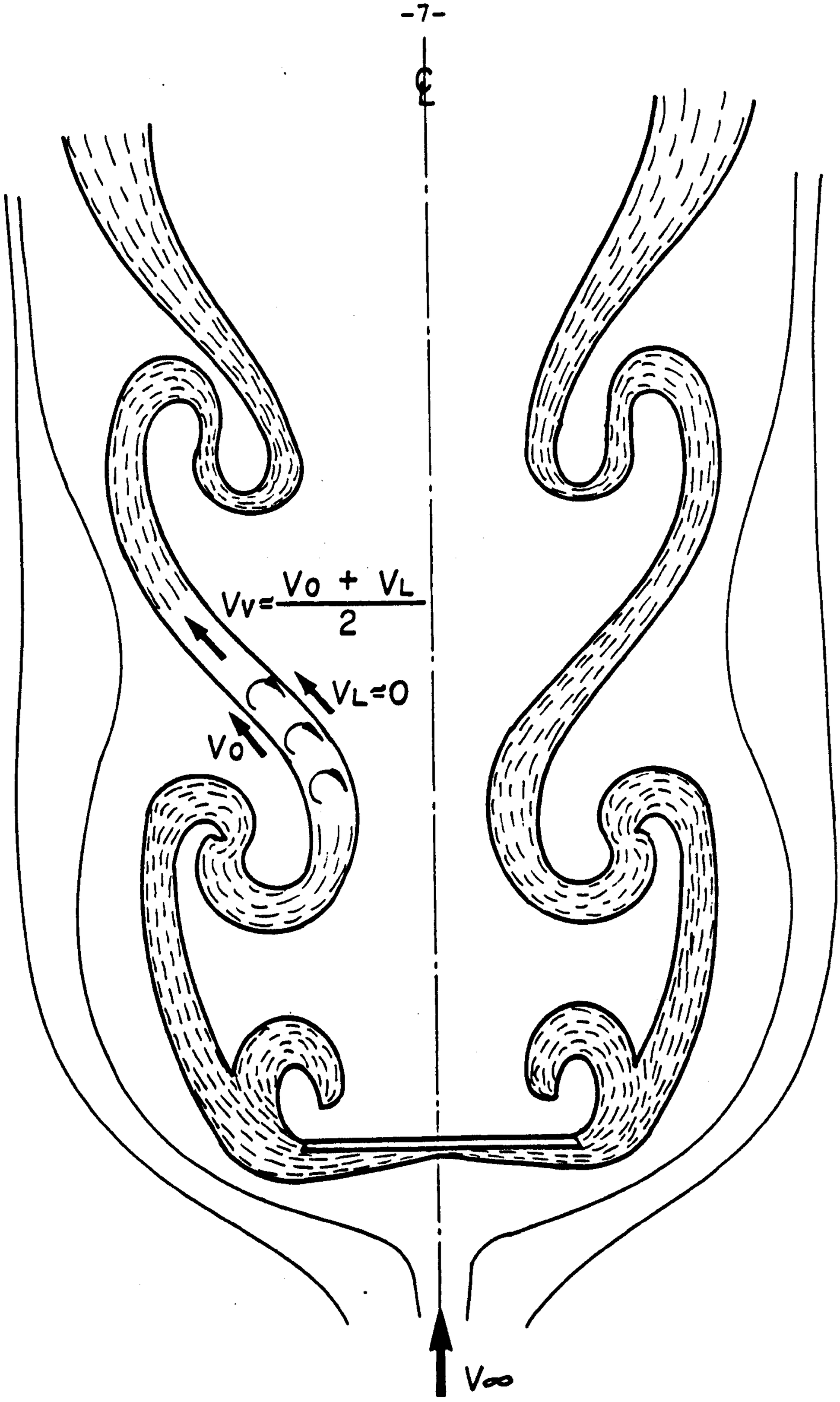


FIGURE 2.1: A SKETCH OF THE FLUID FIELD IN THE NEAR WAKE

## 3. THE FLOW AROUND BLUFF BODIES - LITERATURE REVIEW

The inability of potential flow to predict the drag occurring in steady flow (D'Alembert's paradox) has challenged the fluid dynamicists since the middle of the previous century.

Most of the research effort has been dedicated to two-dimensional flow and relatively few results, either experimental or theoretical, are applicable to three-dimensional flow.

On this ground a legitimate question is why not apply research results for the flow about two-dimensional bluff bodies to three-dimensional flow or, at least, for axisymmetric flow ?

The answer to this question lies in the significant differences in the behaviour of the fluid elements and consequently the vortex tubes in two main cases. For example, stretching of fluid elements can not occur in a two-dimensional flow.

This can be understood from the vorticity transport equation for a constant viscosity fluid [Chia Shun Yih 1969, 2.4]:

$$\frac{D\vec{\omega}}{Dt} = \vec{\omega}\nabla\vec{V} + \nu\nabla^2\vec{\omega} \qquad 3.1$$

In two-dimensional flow the first term on the right side of equation 3.1, which represents the fluid element deformation, is identically zero and therefore, at high

Reynolds numbers when the fluid viscosity can be neglected (this is mathematically exact when the Reynolds number equals infinity) equation 3.1 reduces to:

$$\frac{D\vec{\omega}}{Dt} = 0 \qquad 3.2$$

Since, in inviscid, two-dimensional flow the vorticity of a fluid element remains constant and no stretching of vortex elements can occur.

An additional significant characteristic of three-dimensional vortex filaments/tubes (Batchelor 1967, 7.1 and section 4.2 of this work) is the self-induced velocity. It was found that for a circular vortex ring the self-induced velocity direction is parallel and opposite to the free-stream velocity and its average magnitude is about $0.25V_{\infty}$ [Batchelor 1967, 7.2]. As a consequence of these two variations in fluid particle behaviour there are significant differences between two-dimensional and three-dimensional wake flows.

At Reynolds numbers which are characteristic of engineering situations the wake flow pattern of a two-dimensional bluff body is dominated by the well known vortex street, while the flow pattern in three-dimensional flow at the same Reynolds number is rather different (figure 3.1). It is therefore clear that great care must be exercised before results obtained in a two-dimensional flow are applied to the axisymmetric case.

An important feature of separated flow caused by a surface discontinuity, such as the canopy hemline, is the weak

dependence of the wake flow on Reynolds number.

The boundary layer separation region from a smooth wall is determined by interaction between the outer, potential flow and the viscous flow on the surface region. It is in this process that the flow Reynolds number makes an impact on the wake flow [Chang K., 1970, 1.2.2].

When separation is forced by a salient edge such as the canopy hemline the high velocity gradient at this edge "would separate any boundary layer" [Lighthill M. in chapter 2 of "Laminar Boundary Layers" edited by Rosenhead L. in 1963]. Thus for a disk the drag coefficient is independent of Reynolds number when the latter based on the disk diameter, is higher than about 100. By contrast the drag coefficient for a sphere manifests a strong dependence on Reynolds number [Streeter V.L., 1966]. A similar statement on the flow about bluff bodies was postulated by Ericsson G. (1980) when he reviewed experimental investigations of two-dimensional flows around bluff bodies.

Thus, in conclusion, when separation is caused by a salient edge experimental data can be applied over a wide range of Reynolds numbers, i.e. Reynolds numbers between the order of one hundred and infinity.

## 3.1 EXPERIMENTAL INVESTIGATION OF THE AERODYNAMICS OF THREE-DIMENSIONAL BLUFF BODIES

Eden (1911) presented the earliest flow visualization about three-dimensional obstacles.

By using the very basic equipment available at his time he found that the wake flow behind a square plate immersed in both water and air was periodic. The vortex wake configuration which he obtained is sketched in figure 3.1. The Reynolds number based on the square side, was about 100.

When flow visualization pictures are analysed, since it is very difficult to achieve a truly axisymmetric flow in experiments, it is therefore reasonable to assume that the flow is, to some extent, asymmetric. In such a flow, the fluid particles reach the separation line after following unequal paths which commenced at the stagnation point. It is therefore conceivable that the shed vortex rings do not possess a uniformly-distributed circumferential vorticity.

Moreover, when the vortex ring is shed from an non-axisymmetrical shape, such as Eden's square plate, the lack of symmetry manifests itself in curvature of the vortex ring as well. It will be explained in section 4.2, that a vortex tube develops a self-induced velocity which is aligned with the local curved vortex tube binormal. Its magnitude is a function of the local vortex ring vorticity, curvature and viscous core dimension. For the extreme case of a vortex filament, i.e. a vortex tube of an infinitesimally small cross section, this self induced velocity tends to infinity

as the local radius tends to zero. On this ground, it is likely that in asymmetric flow the vortex ring exhibits a nonuniformly-distributed self-induced velocity and this will result in vortex ring deformation. For example, a small angle of attack of Eden's square plate would cause a difference between the vorticity developed along the part of the vortex ring shed from the upper square side and that part shed from the lower side. This would deform the vortex ring, making it develop a tail-like shaped part along its circumference. When the variations in self-induced velocity along the vortex ring circumference are large, such as near the corners of the intially square-shaped vortex ring in Eden's experiments, it might well be torn up into four separate vortex tubes. Due to collisions & viscous interaction [experimental works: Oshima Y. & Asaka S. 1977 and Fohl T. & Turner S. 1975; simulation: Leonard A. 1975] as figure 3.2 describes qualitatively, these tubes may later form a vortex ring with a circumferentially-distributed self-induced velocity which is more uniform.

Since these differences in the self-induced velocity which is developed along the vortex ring are very large this process is very fast. It is likely to occur within a short distance downstream of the obstacle (e.g. wake part "A" in figure 3.1).

Figure 3.3 shows the assumed wake flow pattern of Eden's experiments if the flow were axisymmetric.

In 1931, Stanton.T.E. & Marshall.D found experimentally that the wake behind a disk immersed in water is characterized by periodic vortex shedding. The Reynolds

number was about 200 and the Strouhal number, based on disk diameter was about 0.12. The flow pattern which they reported was similar to that shown in figure 3.1.

In 1967 Calvert J.R., measured the velocity spectra in the wakes formed behind disks immersed in air at various angles of attack. He found that the Strouhal number in the wake was about 0.14, based on the width perpendicular to the flow. The Reynolds number was about 40,000.

As can be noticed, the large variation in the Reynolds number between the three cases quoted above does not affect the wake flow characteristics. This is in line with the conclusion stated at the end of the previous section.

Achenbach E.(1972) and Taneda S.(1978) have presented data on the flow about a sphere. They also found periodical vortex shedding. Their experiments were performed at Reynolds numbers of between 400 and 1,000,000, based on sphere diameter. At the lower Reynolds numbers the flow pattern was similar to figure 3.1. As they did not observe flow separation occurring along a well-defined line, in their work the position of the separation line may have oscillated. For this reason their experiments do not appear to be directly applicable to the present investigation.

A number of important experimental investigations have been made of the flow around parachute canopies.

Both Pepper B. & Reed J. 1976 and Heinrich G. & Uotila J. 1977, measured the pressure distribution about fabric canopies of different shapes, having various porosities. Nothing is mentioned about the periodicity of these pressure

or drag measurements. Their experiments were performed at Reynolds numbers of about 100,000 based on canopy projected diameter. The differential pressure coefficient, at a point on the canopy between the lower & upper surfaces was, on average, 1.4 decreasing to zero along the canopy hemline.

In 1977, Lingard J.S. investigated the aerodynamics of the canopy inflation process. He presented data concerning the velocity distribution about canopies and the forces acting on them at different stages of the inflation process.

In 1981, Doherr K.F. performed wind tunnel and water channel tests on hemispherical canopies. Although the flow visualization resulting from his water channel tests, for which the Reynolds number based on diameter was $2*10^3$, clearly shows periodic vortex shedding of axisymmetric vortex rings, in his wind tunnel experiments which were conducted at Reynolds numbers of $10^5$-$10^6$, the force fluctuations were stochastic. Doherr, making an analogy to the flow around a two-dimensional cylinder, related this distinction to the difference in the Reynolds numbers for the two tests. Since in both cases flow separation was caused by the surface discontinuity at the canopy hemline, the present author (following the arguments brought up at the beginning of this chapter), assumes that the Reynolds number difference could not be the main cause of this variation in the wake flow behaviour.

The experiments performed by Cockrell D.J. et al at Leicester University in the United Kingdom were mainly orientated to the measurement of stability coefficients.

Important data concerning aerodynamic forces acting in both steady and unsteady motion have been reported in various papers such as Jorgensen D. & Cockrell D.(1981), Yavuz T. (1981), Jorgensen D. (1984) and Cockrell D. et al 1986.

In 1984, Jorgensen D., found an oscillatory drag force acting on a hemispherical fabric canopy, at a Reynolds number of $6*10^5$ based on canopy projected diameter. The corresponding Strouhal number, based on canopy projected diameter, was 0.61.

During 1986-1987 Harwood.R and Cockrell D. performed experiments with different parachute models immersed under water in a ship tank. The models were moved in both constant and oscillatory motion, this allowing for both the velocity and acceleration dependent forces to be determined. These experiments will be discussed in section 6.2.4.

In 1987 Shen C. investigated experimentally the flow field around bluff parachute canopies. She found that the wake behind a rigid hemisphere manifested periodic behaviour. The wake flow periodicity was measured using a hot-wire anemometer and the Strouhal number, based on the projected diameter, was found to be about 0.16.

The conclusions arising from this review are:

1.-the flow behind a parachute canopy could well be characterized by periodic vortex shedding;

2.-only a strictly limited number of measurements of the flow about canopy-like bluff bodies have been made;

3.-only a few measurements of drag variation with a constant relative flow velocity, have been reported for bluff bodies.

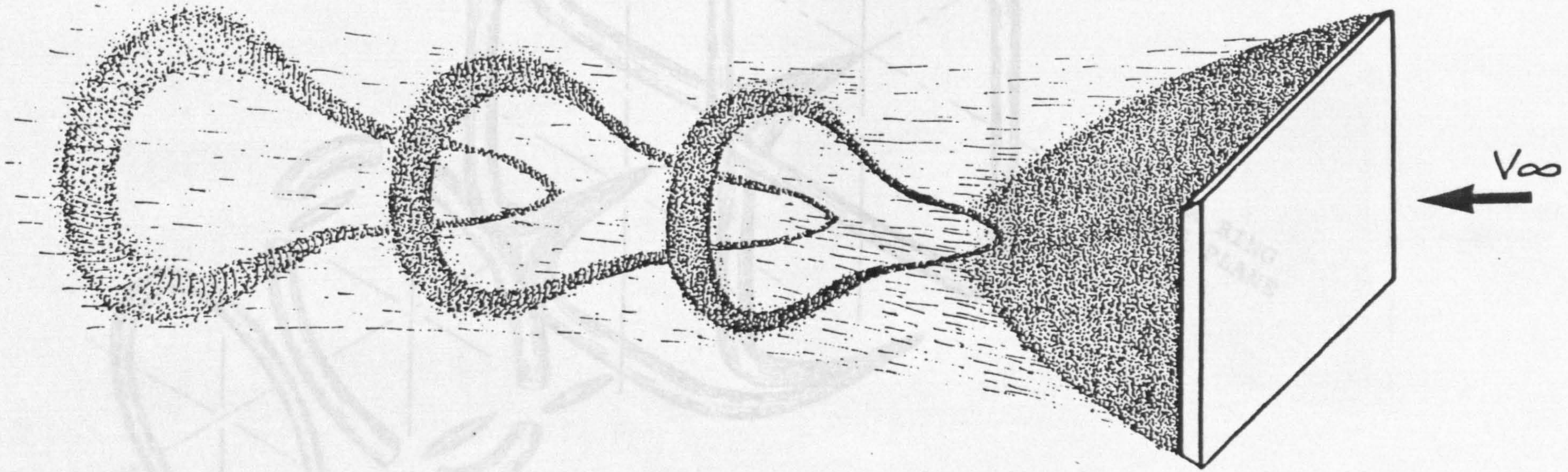


FIGURE 3.1: SCHEMATIC REPRESENTATION OF THE WAKE BEHIND A SQUARE PLATE (based on EDEN-1911)

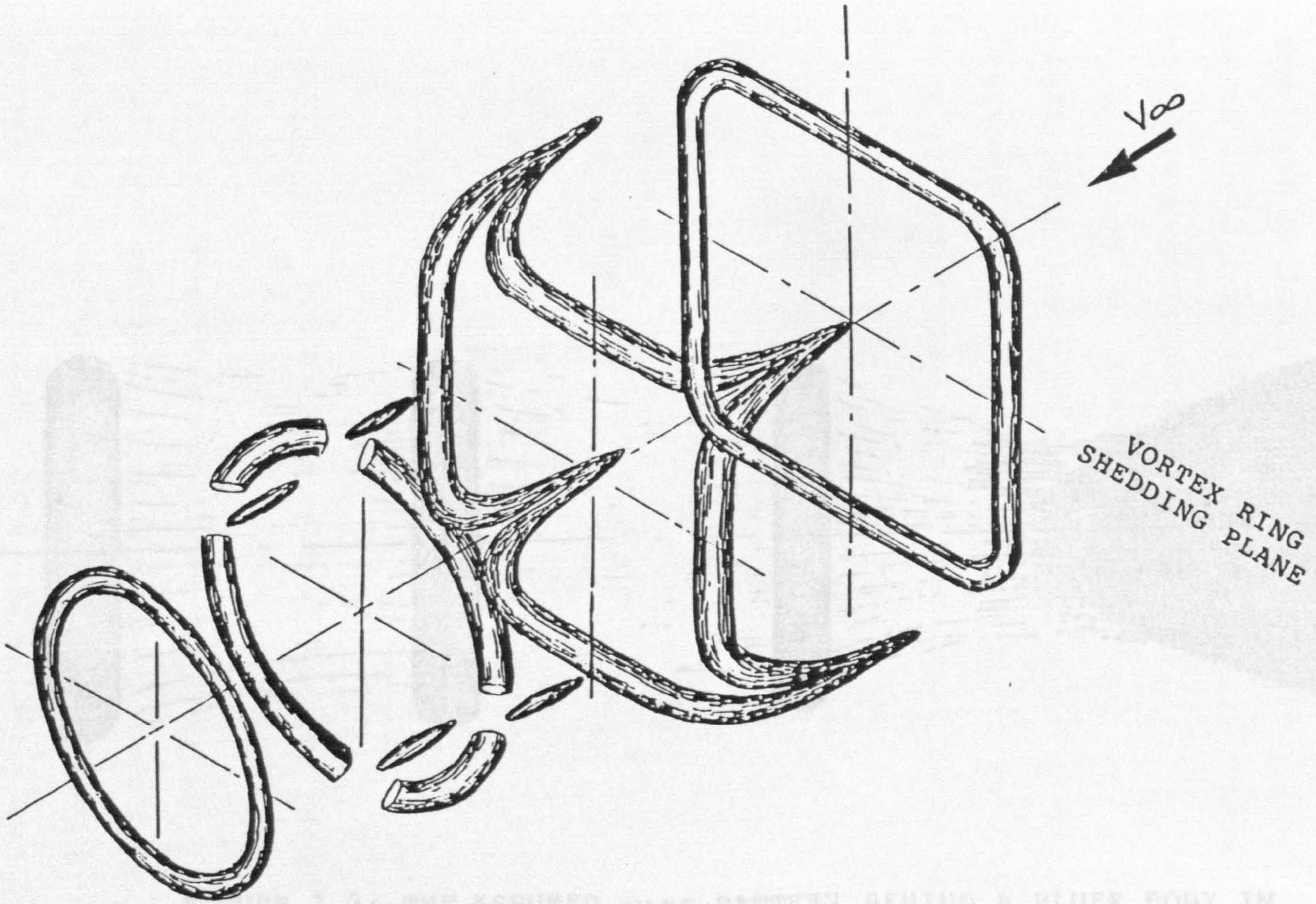


FIGURE 3.2: THE EVOLUTION OF A VORTEX RING OF AN INITIALLY HIGHLY NON-UNIFORMLY DISTRIBUTED SELF-INDUCED VELOCITY

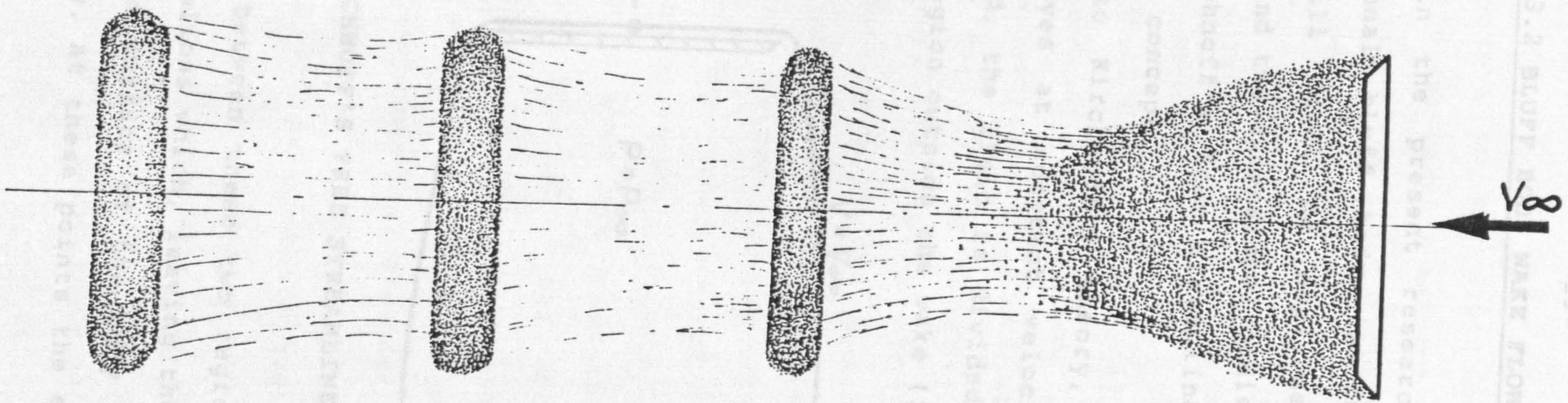


FIGURE 3.3: THE ASSUMED WAKE PATTERN BEHIND A BLUFF BODY IN AXISYMMETRIC FLOW

## 3.2 BLUFF BODY WAKE FLOW SIMULATION

Although in the present research the wake flow of a three-dimensional bluff body is investigated, the basic principles will first be explained for the wake flow developed behind two-dimensional bodies. These principles are based on Kirchhoff's free streamline theory and Prandtl's boundary layer concept.

According to Kirchhoff's theory, as a two-dimensional bluff body moves at constant velocity through an ideal, unbounded fluid, the fluid is divided into two regions: the wake and the region outside the wake (figure 3.4).

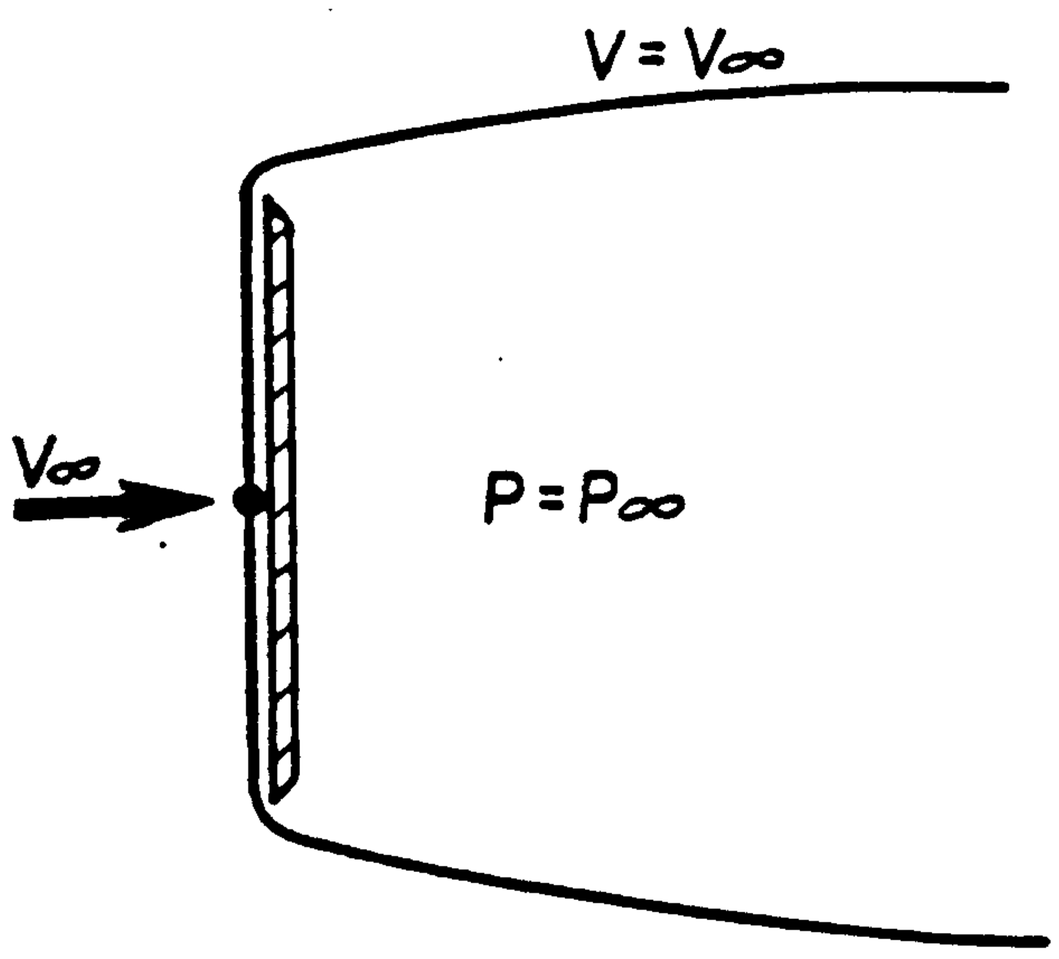


FIGURE 3.4: KIRCHHOFF'S FREE STREAMLINE THEORY

The boundary between these two regions is formed by the separating streamlines which, leaving the forward stagnation point, follow the surface of the body until they reach the separation points. At these points the streamlines leave the

body and continue to the fluid boundary downstream. The pressure inside the wake is assumed to be constant and equal to the pressure at the fluid boundary. The velocity along a streamline changes from zero at the forward stagnation point, to $V_\infty$ at the separation point. Beyond this point, the velocity and subsequently the pressure remain constant along the streamline boundary.

Using conformal mapping, Kirchhoff calculated the drag of a plate perpendicular to the stream. Since the resulting drag coefficient per unit length, based on plate width, $C_D$=0.88, was about one half of the measured drag, several authors later improved his method by introducing in the model various experimental data such as cavity length (Riabouchinsky D. 1919) and base pressure (Roshko A. 1954).

An interesting method for predicting the mean pressure distribution over the wetted part of a two-dimensional bluff body was used by Parkinson & Jandali (1970). In this method the effect of the wake was simulated by two symmetrical sources. Their position was determined by creating stagnation condition at the known separation points on the complex plane while their strength was set to satisfy an experimentally determined base pressure.

In 1975, Bearman P. & Fackrell J. extended Parkinson & Jandali's method for axisymmetric bodies by using surface distributed singularities (discrete vortices).

These methods present one extension of Kirchhoff's theory. With the aid of experimental data they predict the pressures on the wetted part of the body, the mean drag, the mean shape

of the wake and the mean velocity along the dividing streamlines.

A second extension to Kirchhoff's theory uses Prandtl's boundary layer concept. The flow field is divided into two regions, an irrotational region, where a velocity potential can be defined and a region of high vorticity. The dividing streamlines are replaced by shear layers which smooth out the discontinuity between the outer potential flow and the wake. These shear layers present a discontinuity in both the normal and the tangential velocities which develop along its opposite surfaces. At high Reynolds number the discontinuity in the normal velocity caused by the fluid viscosity and representing the vorticity diffusion vanishes. Consequently, these shear layers, carrying vorticity from the boundary layer formed on the upstream part of the body, are represented by infinitesimally thin continuous layers of vortices constituing vortex sheets. These are unstable and small disturbances result in undulations of increasing amplitude in them, creating the so called "Helmholtz instability" [Batchelor G.K., 1967, chapter 7.1].

The continuous vortex sheets can be approximated by discrete ones, facilitating the utilisation of this model in numerical simulations. The first analysis of discrete vortex sheet behaviour was presented by Rosenhead L. (1931, b). His principal conclusion was that the discrete vortex sheet is unstable to every periodic disturbance, the amplification factor being independent of disturbance frequency.

Abernathy & Kronauker (1962), studying the interaction

between two discrete vortex sheets simulating the wake formed behind a two-dimensional body, found that the vortices "arranged" themselves in "clouds" of vortices having a spacing ratio (width/length):

$$h/l=0.28*k \qquad 3.3$$

k being an integer. This result was in accordance with von Karman's vortex street model. According to von Karman's analysis [Kochin N.E.,Kibel I.A. & Roze N.V., 1964, chapter 5.18 or Goldstein S., 1938, chapter 18], a stable configuration of two parallel rows of discrete vortices is achieved when (figure 3.5):

$$h/l=0.28 \qquad 3.4$$

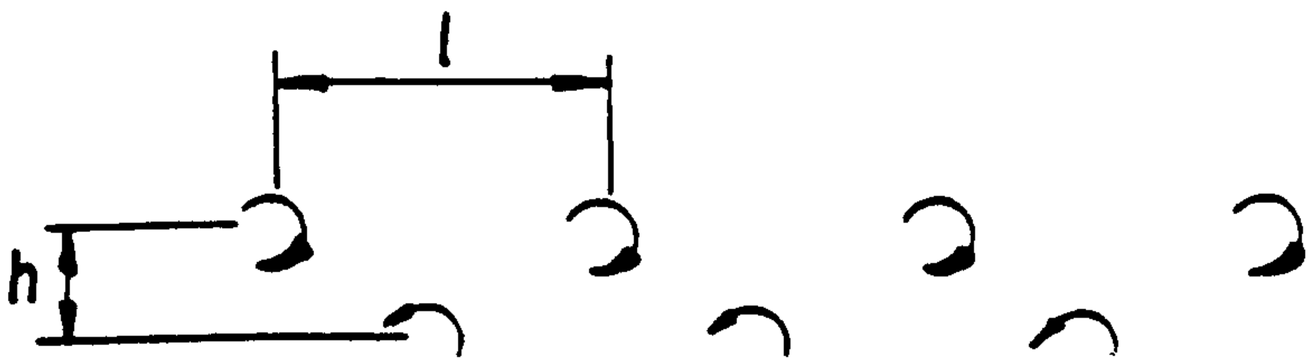


FIGURE 3.5: THE STABLE ARRANGEMENT OF VORTICES IN A VORTEX STREET

Another important result of Abernathy & Kronauker's analysis is the prediction of the trapping of vortices of one sign in "clouds" of vortices of the opposite sign. This trapping diminishes the vorticity shed from the body by approximatively 40%. Their analysis agreed with Fage &

Johansen's (1927) experiments which investigated the wake flow behind a two-dimensional plate at different angles of attack and at high Reynolds numbers.

Some of the basic theoretical work in this field was done by Gerrard J.H. (1967), Ham D.A. (1968), Clements R.(1972), Sarpkaya T.(1975) and by Kiya M. & Arie M. (1977). The discrete vortices simulating the wake were usually introduced in close vicinity to the separation points. The distance between the vortex shedding point and the separation point represents the distance required by the real flow for vortex formation. The main differences in their presentation were in the ways of calculating the strength of newly-created (nascent) vortex rings and the ways of determining the variation with time of the vortex shedding point location.

To calculate the nascent vortex ring strength and the shedding point location these methods were used:

-Prandtl's relation for the vortex shedding strength discussed in section 4.6;

-Kelvin's circulation theorem;

-Kutta's condition in various forms at the flow separation point.

These earlier methods used conformal transformation to simulate the relevant bluff body shapes. Katz J. (1981), by representation of the surface with discrete bound vortices, extended these methods to more general two-dimensional shapes.

The above mentioned methods were able to simulate unsteady flows and under these conditions they succeeded in predicting

wake flow characteristics. The forces determined by these methods where higher by approximately 25% than the appropriate experimental values. It could well be that this was because the standing eddy (chapter 2) had been neglected. It will be shown in section 6.1.4 that when the standing eddy is accounted for the aerodynamic load at the separation point is close to zero and consequently the predicted drag forces would tend to the experimental values.

Following the successful application of the discrete vortex to represent the standing eddy in two-dimensional wake simulation, this method was extended to three-dimensional wings (Atta E.H., Kandil O.A., Mook D.T. & Nayfeh 1977, Rehbach C. 1978, Katz J. 1979 etc.). In these works, the separated wake was simulated by free vortex sheets and the wing surface was replaced by a vortex lattice, using the well known method first introduced by Falkner V.M. (1943).

In 1976 Leonard A. used vortex rings to simulate the separated flow behind a sphere. These vortex rings were shed from a predetermined circle on the sphere. They were tracked downstream using a grid of 20-100 points, each one representing a segment of the vortex ring and having the vortex core size associated with it. Both the wake flow pattern and the forces which were determined exhibited a fluctuating behaviour. The mean drag force agreed with experimental values but no results for pressure distribution were presented. As mentioned by the author in a later comment [Sovran G., Morel T. & Mason W.T., 1978, page 307], the resulting Strouhal number based on sphere diameter of about

1.0 was about ten times higher than that measured in Achenbach (1972) experiments.

In 1981 Bernardinis B., Graham J.M. and Parker K.H. analysed the flow around an oscillatory disk. They used a system of bound vortices to simulate the disk surface together with a free vortex sheet which was composed of vortex rings. The predicted flow pattern was in good agreement with that determined by flow visualization but no comparison between the calculated pressure distribution over the disk and experimental measurements was made. Their approach is similar to the one adopted in the present model, the principal differences being the modelling of both the nascent vortex ring and the near wake. These points will be discussed in chapter 4.

Extensive reviews of separated flow simulation by vortex methods may be found in Clements R.R. & Maull D.J. (1975), Smith J.H.B. (1984) and in Maull D.J. (1986).

Although the trend of the three-dimensional wake simulation by discrete vortex sheets is promising, the basic theoretical analysis has only been performed for two-dimensional vortex sheets. Extension to three-dimensional wakes has so far been based on more intuitive considerations.

## 3.3 THEORETICAL APPROACHES TO AERODYNAMIC LOAD CALCULATION ON PARACHUTE CANOPIES

The state of the art in parachute aerodynamic design has recently been described by Cockrell D.J. (1987). The present section is restricted to considering theoretical methods of determining the aerodynamic loads developed on parachute canopies.

The first attempt to calculate the pressure distribution and the added masses, i.e. "the effective mass of the fluid that surrounds the body and which (in unsteady motion) must be accelerated with it" [Newman N.J., chapter 2.11, 1935], for canopy-like bodies was made by Ibrahim S. (1965). By assuming attached flow Ibrahim succeeded in developing closed expressions for the velocity potential of immersed spherical cups. Because of D'Alembert's paradox his method is not appropriate for steady drag calculation. The pressure distribution obtained is strongly affected by the high velocities occurring at the canopy hemline and by the symmetry in the location of the stagnation points about the canopy apex (figure 3.6). According to Pepper & Reed (1976) and Heinrich & Uotila (1977), this pressure distribution obtained is unrealistic.

Klimas P. (1977 and 1979) extended Ibrahim's method. Since he also assumed attached flow, his model also has limited applications. By replacing the canopy with a bound vortex sheet, Klimas calculated the flow around axisymmetric canopies of a more general shape. The strength of the bound

vortex sheet was determined by assuming that the flow velocity through the canopy was in accordance with porosity requirements. By allowing different boundary conditions on the canopy, the pressure distribution was calculated for different porosities under accelerating flow and with canopy shape changes.

In an early work, Roberts B. (1968) assumed an attached flow and used a two-dimensional, unsteady approach based on conformal mapping to calculate the aerodynamic loads on the canopy. This is the first published work in which the equations governing both the structural and aerodynamic loads on the parachute canopy were solved simultaneously.

Muramoto K.K. and Garrard W.L. (1984) used source rings to model the aerodynamic load on the canopy in order to calculate the flow field about it. Their model also assumed attached flow so it too was limited in its applicability.

Meyer J. & Purvis J.W. (1984), used a vortex lattice method for canopy modelling and the two-dimensional vorticity transport equation:

$$\frac{D\vec{\omega}}{Dt} = \nu\nabla^2\vec{\omega} \qquad 3.5$$

to simulate its wake. Because in this work two-dimensional flow was assumed, their model could well produce some unrealistic results.

According to Shirayama S.& Kuwahara K. (1986) the canopy could be represented by a vortex lattice built up by straight vortex segments which form closed vortex rings. The unsteady effects which occur in the wake were simulated by the

movement of vortex sticks, formed by shed vortex ring segments. The vorticity of each vortex stick was calculated using the vorticity transport equation and each vortex stick was tracked as it was convected by the local velocity. Based on its projected diameter, the calculated axial force coefficient for an imporous disk obtained by this method was about 0.95, i.e. approximately 25% lower than shown in the experimental data collected by Hoerner (1965). Although in steady flow the calculated axial force exhibited unsteady behaviour, no periodic variations in it were found. As reported by the authors, their method demands high computing resources.

The use of vortex methods to represent parachute canopies and an example of a typical calculation scheme has been presented by Strickland J.H. (1986).

Mc Coy H.H. & Werme T.D. (1986) developed an axisymmetric vortex lattice method which was applicable to parachute canopies. In their model the canopy was replaced by ring panels containing two counter-rotating vortex rings of equal strength. The strength of the vortices shed in the wake was a function of the variation in the strength of the bound vortices near the hemline. As was pointed out by the authors, the pressure distribution calculated by their model gave unrealistic results near the canopy hemline. No time-dependent variations in the calculated axial force developed on a steadily moving canopy were reported.

In neither of the papers by Strickland or by Mc Coy & Werme were the three-dimensional effects considered which are

discussed at the begining of this present chapter.

The main conclusion arising from the works cited above is that although by using discrete vortex representation of the wake there are good prospects of predicting the aerodynamic loads developed on parachute canopies, no current model does so satisfactorily. It is in this context that the author's model has been developed.

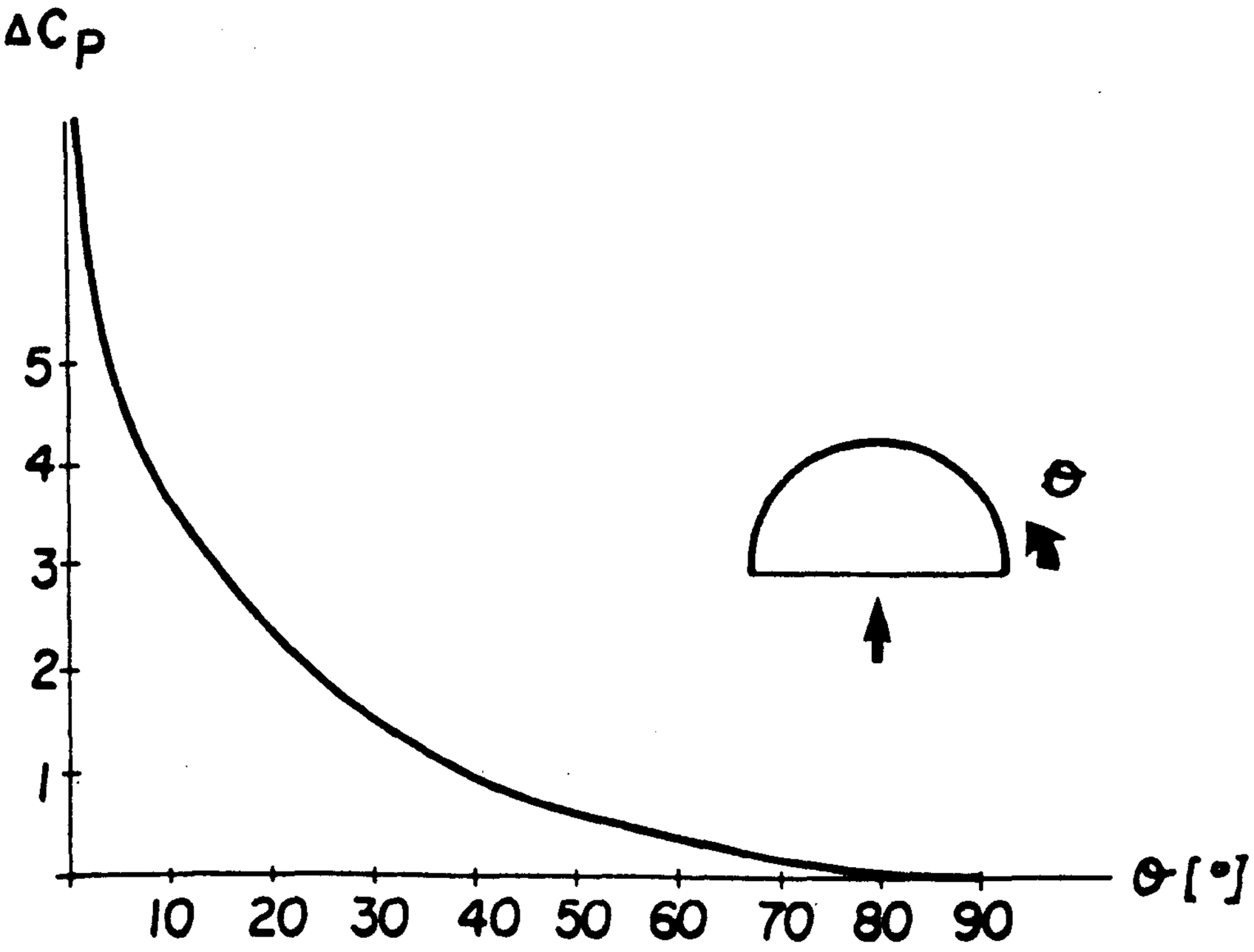


FIGURE 3.6: DIFFERENTIAL PRESSURE DISTRIBUTION ABOUT AN HEMISPHERICAL CUP, IN ATTACHED FLOW (based on Ibrahim, 1965, calculations)

# 4. THE PROPOSED MODEL

This chapter presents the model. It includes the interpretation of real flow around the canopy, the mathematical formulation of the problem and the model limitations.

The proposed model assumes high Reynolds number, incompressible axisymmetric flow around an axisymmetric canopy. The flow is divided into two parts: a viscous flow regime and the outer potential region.

Because of the assumption of high Reynolds number the shear layer resulting from the boundary layer separation from the canopy is thin [Batchelor 1967, 5.11]. Thus, the vorticity is confined to a small and well defined region of the flow field, the thin shear layer which envelops the wake developed behind the canopy [Thwaites 1960, VII.1].

The continuity equation for an incompressible fluid is:

$$\nabla \cdot \vec{V} = 0 \qquad 4.1$$

The assumption of irrotationality in the flow field outside the non-zero vorticity regions, i.e. outside the free shear layer, enables a velocity potential to be defined (e.g. Karamcheti K., 1966, 9.8):

$$\vec{V} = \nabla \Phi \qquad 4.2$$

These relationships lead to the Laplace equation:

$$\nabla^2 \Phi = 0 \qquad 4.3$$

Figure 4.1 compares the real flow about an axisymmetric canopy to the modelled flow. In this figure the canopy surface has been replaced by a system of bound vortex rings. By imposing different boundary conditions, porosity and shape changes can be introduced.

Generalising Rosenhead's (1931 b) method of two-dimensional continuous vortex sheet discretisation to the axisymmetric case, the free shear layer carrying vorticity from the boundary layer is approximated by a free layer of discrete vortex rings. This free layer, following the streamline pattern, separates from the surface and leaves it tangentially. In this proposed method when tracking the shed vortex rings, only the most energetic parts of the fluid field which make the principal contribution to the aerodynamic load generated on the canopy, are considered. Therefore, when considering the near wake only the shear layer which envelops it and the standing eddy are specifically simulated in the present model.

For any immersed body the location of the separation line can be determined by considering the interaction between the external potential flow and the boundary layer. Because this is a complex calculation, an alternative way has been developed [e.g. Gerrard 1967, Leonard 1975] in which experimental data relating the different flow parameters to the position of the separation line is used.

In the present application the flow separates from the

upper surface along a well-defined line, the canopy hemline. The model is therefore, self-contained and in order to determine the separation line there is no need to consider any kind of interaction between the viscous flow in the boundary layer generated at the body surface and the outer potential flow.

On the lower surface of the canopy and downstream of the separation line the high back-flow region creates a standing eddy near the hemline. This is simulated by a standing vortex ring.

The potential $\Phi$ consists of the canopy surface potential, the separated wake potential and the standing vortex ring potential.

The boundary conditions of the flow are:

(a)-the disturbance induced by the canopy decays far from the canopy and from the wake:

$$\lim_{r \to \infty} \nabla\Phi = 0 \qquad 4.4$$

(b)-the velocity through the canopy surface (i.e normal to it) at a general point "i" on the canopy is in accordance with the porosity requirements which will be developed in section 4.5 :

$$V_{por_i} = \vec{V}_\infty \cdot \hat{n}_i + \vec{V}_{ind_i} \cdot \hat{n}_i + \dot{\vec{R}} \cdot \hat{n}_i \qquad 4.5$$

where $V_{ind_i}$ is the velocity induced by the whole field; $\vec{R}$ is the vector from the canopy apex to the canopy point "i" and its time derivative

represents any canopy shape changes.

In order to satisfy irrotationality of the fluid field Kelvin's circulation theorem, which implies that in an inviscid fluid the circulation around any closed material curve is invariant, must be obeyed. Thus :

$$\frac{d\Gamma(t)}{dt} = 0 \qquad 4.6$$

For a three-dimensional flow the meaning of this theorem is that a vortex tube must be closed and that the circulation is zero around any closed fluid circuit which can be contracted without crossing the vortex tube [Karamcheti K. 1966, 18.5].

To satisfy spatial vorticity conservation [Karamcheti K., 1966 18.4], at any instant of time the flow of vorticity through any cross-sectional surface of a vortex tube is constant. Thus, for any circuit around a cross section of the vortex tube a constant circulation is found. It is usually defined as the vortex tube/ring strength ($\Gamma$).

Figure 4.2 shows a fluid circuit enveloping the canopy and a part of the wake. As can be noticed, this circuit can be contracted to zero without touching either the canopy or the shed vortex rings. Therefore, spatial vorticity conservation dictates that the circulation around this circuit is zero and the model obeys Kelvin's circulation theorem.

In section 4.1 the velocity induced by a vortex ring will be developed. As the velocity induced by such a ring

(equations 4.13 and 4.15) tends to zero far from it, the model fulfils the boundary condition expressed by equation 4.4.

Consequently, the main equation which is to be solved is 4.5, expressing the flow boundary conditions on the canopy surface.

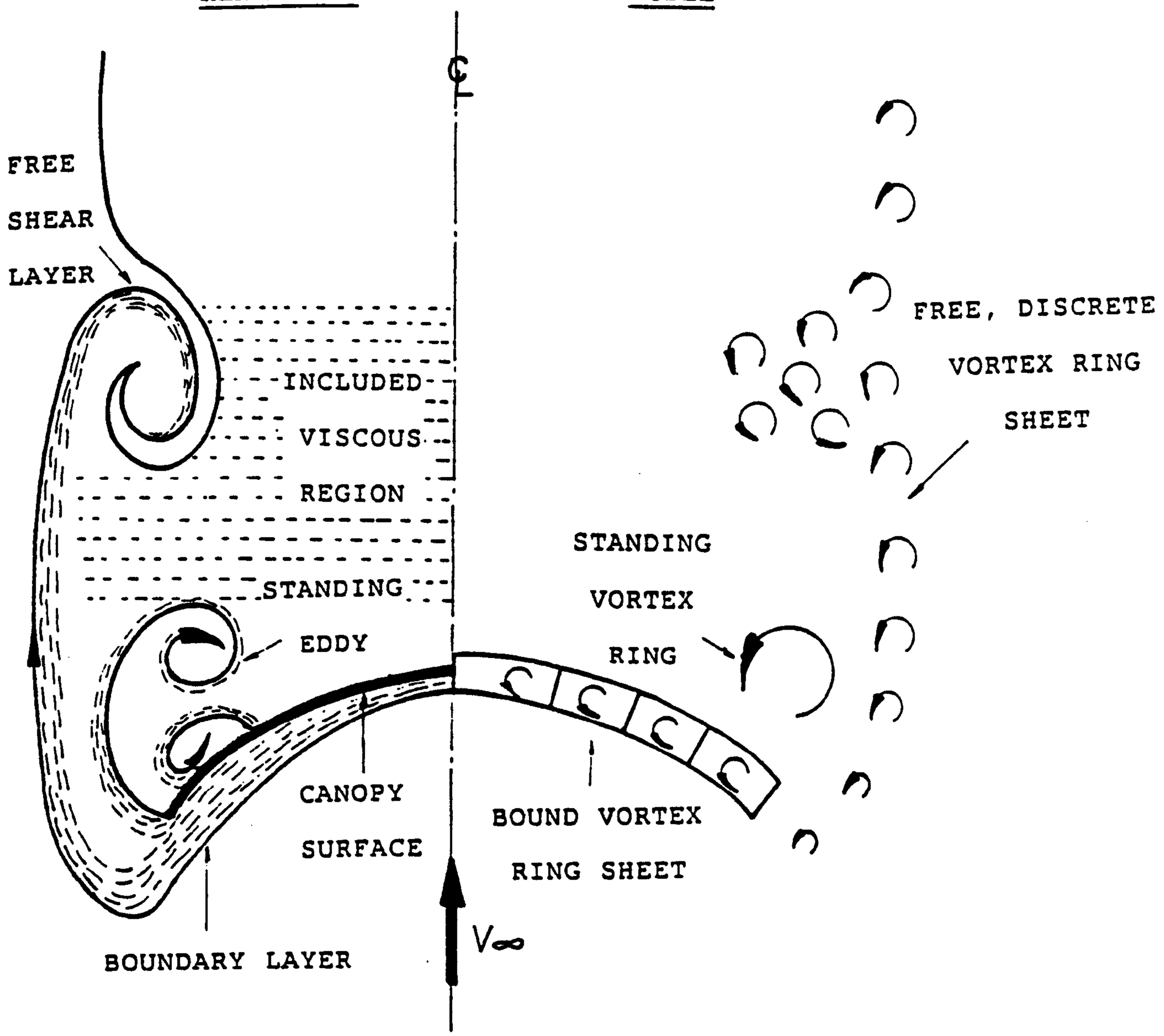


FIGURE 4.1 :THE REAL FLOW AND THE MODEL

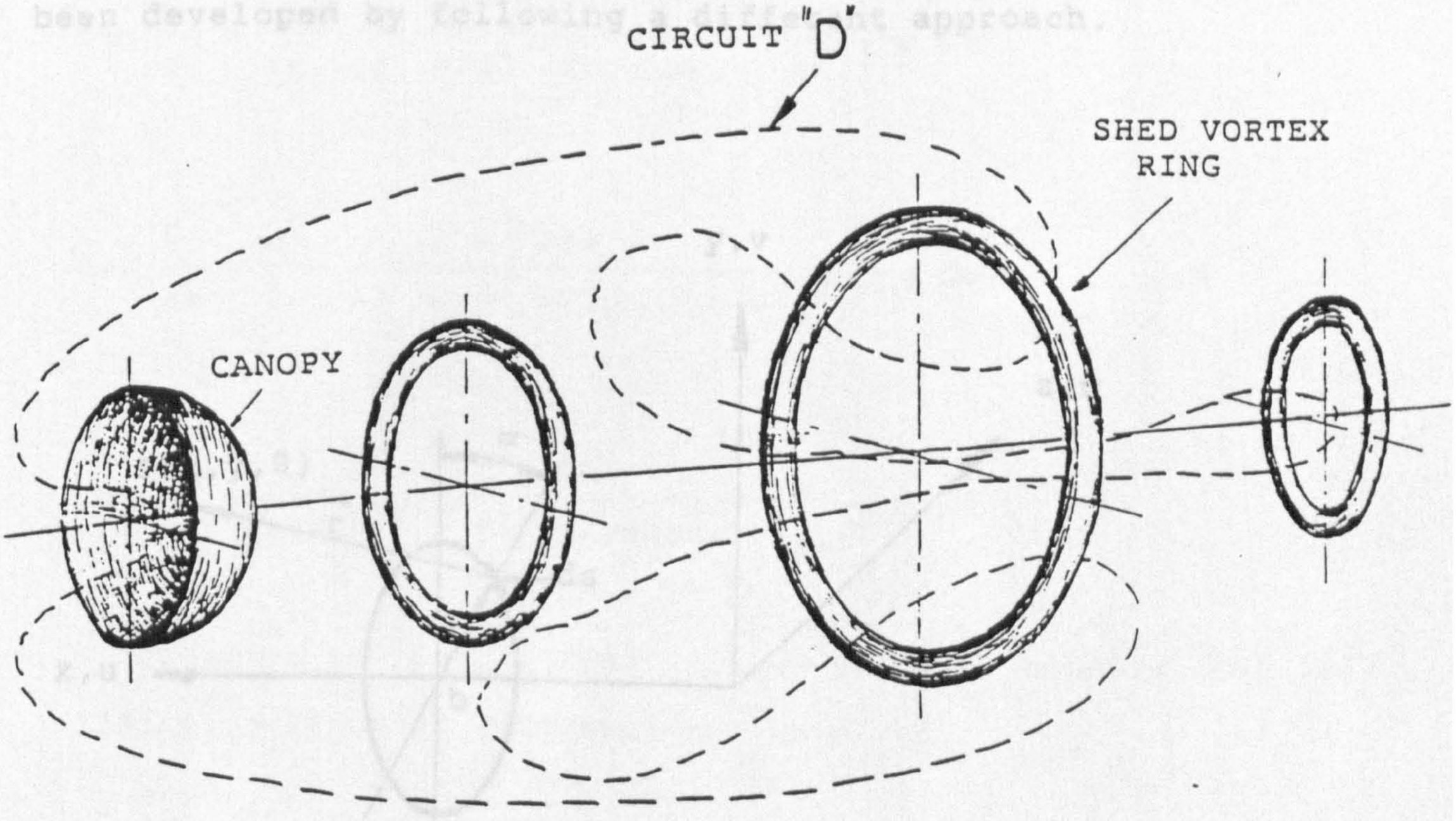


FIGURE 4.2: THE CIRCUIT FOR PROVING CONSERVATION OF CIRCULATION

## 4.1 THE VELOCITY INDUCED BY A VORTEX RING IN AXISYMMETRIC FLOW

The velocity induced by a vortex ring can be calculated from Lamb's (1932, article 161) solution for the stream function. In this section, because computational advantages can be seen the velocity field induced by a vortex ring has been developed by following a different approach.

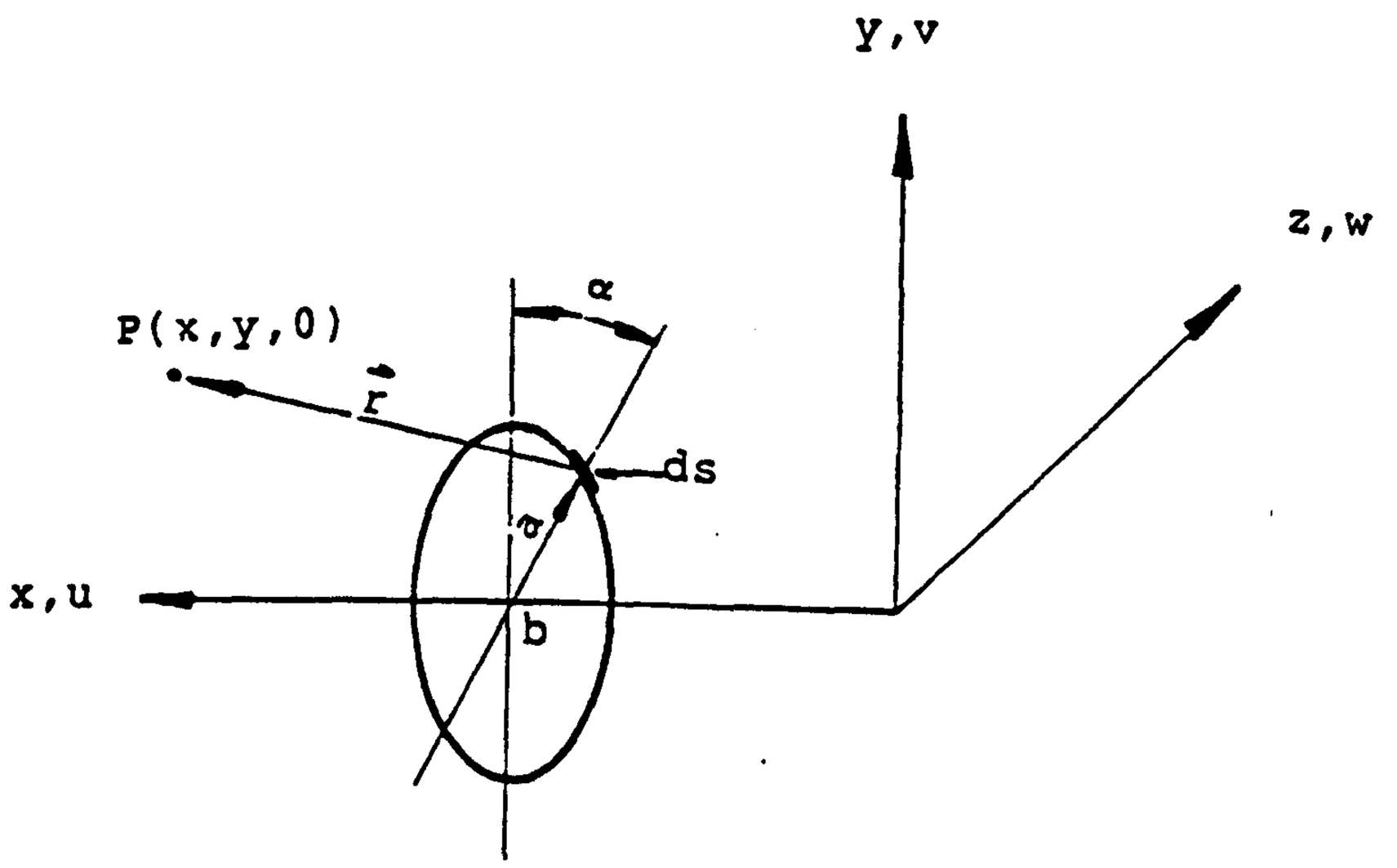


FIGURE 4.3: THE VORTEX RING INDUCED VELOCITY

From the Biot-Savart law [e.g. Karamcheti, 1966, 18.7], the velocity induced at P(x,y,0) (figure 4.3) by an infinitesimally long vortex filament is :

$$d\vec{V} = -\frac{\vec{r}}{4\pi} * \frac{\vec{r}\times d\vec{s}}{|\vec{r}|^3} \qquad 4.7$$

After the vector operations are performed the components of the incremental velocities shown in figure 4.3 become:

$$du = \frac{\Gamma}{4\pi} a \frac{(a - y\cos\alpha)}{[(x-b)^2 + y^2 - 2ya\cos\alpha + a^2]^{1.5}} d\alpha$$

$$dv = \frac{\Gamma}{4\pi} a \frac{(x-b)\cos\alpha}{[(x-b)^2 + y^2 - 2ya\cos\alpha + a^2]^{1.5}} d\alpha \qquad 4.8$$

$$dw = \frac{\Gamma}{4\pi} a \frac{(x-b)\sin\alpha}{[(x-b)^2 + y^2 - 2ya\cos\alpha + a^2]^{1.5}} d\alpha$$

Thus, in the vortex ring induced velocity calculation, the following types of integrals are involved:

$$I_1 = \int_0^{2\pi} \frac{d\alpha}{[(x-b)^2 + y^2 - 2ya\cos\alpha + a^2]^{1.5}}$$

$$I_2 = \int_0^{2\pi} \frac{\cos\alpha\, d\alpha}{[(x-b)^2 + y^2 - 2ya\cos\alpha + a^2]^{1.5}} \qquad 4.9$$

$$I_3 = \int_0^{2\pi} \frac{\sin\alpha \, d\alpha}{[(x-b)^2 + y^2 - 2ya\cos\alpha + a^2]^{1.5}}$$

To facilitate these integrations the denominators are written in a new form:

$$[(x-b)^2 + y^2 - 2ya\cos\alpha + a^2]^{1.5} =$$

$$= [(x-b)^2 + (y+a)^2]^{1.5} * [1 - \frac{4ay}{(x-b)^2+(y+a)^2} \sin^2 \frac{\pi-\alpha}{2}]^{1.5} \qquad 4.10$$

By using the following definitions:

$$A \equiv [(x-b)^2 + (y+a)^2]^{-1.5} \qquad 4.11$$

$$k^2 \equiv \frac{4ay}{(x-b)^2+(y+a)^2}$$

the integrals from 4.9 become [Gradstein I.S. & Ryshik I.M. ,1963]:

$$I_1 = \frac{4A}{1-k^2} E(k)$$

$$I_2 = \frac{4A}{k^2(1-k^2)} [(2-k^2)E(k) - 2(1-k^2)K(k)] \qquad 4.12$$

$$I_3 = 0$$

where K(k) is a complete elliptic integral of the first kind and E(k) of the second kind [Gradstein I.S. & Ryshik I.M.

,1963].

Finally, the velocities induced by the vortex ring at P(x,y,0) are:

$$u_P = \frac{\Gamma a A}{\pi k^2(1-k^2)} [(ak^2 - 2y + yk^2)E(k) + 2y(1-k^2)K(k)]$$

$$v_P = \frac{\Gamma a A(x-b)}{\pi k^2(1-k^2)} [(2-k^2)E(k) - 2(1-k^2)K(k)] \qquad 4.13$$

$$w_P = 0$$

The latter result reflecting the flow symmetry.

By using power expansion for K(k) and E(k) [Gradstein I.S. & Ryshik I.M. ,1963] they become:

$$K(k) = \frac{\pi}{2} [1+ (\frac{1}{2})^2 k^2 + (\frac{1*3}{2*4})k^4 - ....] = \frac{\pi}{2} [1 + k^2(\frac{1}{4} + S_K k^2)]$$

4.14

$$E(k) = \frac{\pi}{2} [1- (\frac{1}{2})^2 k^2 - (\frac{1*3}{2*4})\frac{1}{3}k^4 - ....] = \frac{\pi}{2} [1 - k^2(\frac{1}{4} + S_E k^2)]$$

With these, the velocities induced at P(x,y,0) can be written:

$$u_P = \frac{\Gamma a A}{\pi(1-k^2)} \{(y-a)E(k) - 2yK(k) + 2y\pi[0.5 + k^2(S_E+S_K)]\}$$

$$v_P = \frac{\Gamma a A}{\pi(1-k^2)} k^2 \left[0.75 - S_E(1-k^2) + S_K(2k^2+1)\right] \qquad 4.15$$

Equations 4.13 & 4.15 show some characteristics of the velocity field induced by a circular vortex ring :

-for $x = b$ , $v_P = 0$

-for $y = 0$ , $v_P = 0$

-for x,y tending to $\infty$ both $u_P$ and $v_P$ tend to 0.

-when $k^2$ tends to 1 both $u_P$ and $v_P$ tend to infinity. The significance of this result will be clarified in the next section.

## 4.2 THE VORTEX RING SELF-INDUCED VELOCITY

To show the cause of the self induced velocity developed by a vortex ring, a simplified analysis will be performed. It assumes an infinitesimal core (i.e. the vortex tube reduces to a vortex filament) and small arcs $\alpha$ (figure 4.3). This results in:

$$\cos\alpha \simeq 1 - \alpha^2/2 \qquad \text{and} \qquad \sin\alpha \simeq \alpha - \alpha^3/6 \ .$$

Thus, equations 4.8 become:

$$du = \frac{\Gamma a}{4\pi} \frac{1}{[(x-b)^2 + (y-a)^2 + ay\alpha^2]^{1.5}} [(a-y) + \alpha^2 y/2] \, d\alpha$$

$$dv = \frac{\Gamma}{4\pi} \frac{1}{[(x-b)^2 + (y-a)^2 + ay\alpha^2]^{1.5}} (x-b)(1-\alpha^2/2) \, d\alpha$$

4.16

To find the velocity field in the vicinity of the vortex filament, equation 4.16 will be integrated under the following conditions:

$$y-a=\varepsilon$$

and

$$x=b$$

The same result may be found by taking $x-b=\varepsilon$ and $y=a$ .

The velocity induced by the small curved vortex filament at P(b,a,0) is:

$$\vec{V}_P = u_P \hat{x} = \left( \int_{-\alpha}^{\alpha} du \right) \hat{x} = \left[ \frac{\Gamma}{4\pi a} \int_0^{\alpha} \frac{\Theta^2 - \bar{\varepsilon}^2}{(\Theta^2 + \bar{\varepsilon}^2)^{1.5}} d\Theta \right] \hat{x}$$

4.17

where $\hat{x}$ is the appropriate unit vector.

Finally ,for $\bar{\varepsilon} << 1$ :

$$u_P \simeq - \frac{\Gamma}{4\pi a} \left( \frac{1}{\bar{\varepsilon}} + \ln \frac{\alpha}{\bar{\varepsilon}} \right) = u_{P_1} + u_{P_2} \qquad 4.18$$

This latter equation shows that the induced velocity has two components:

- $u_{P_1}$ represents a line vortex velocity field tending to infinity as $1/\bar{\varepsilon}$;

- $u_{P_2}$ is the self-induced velocity, tending logarithmically to infinity as $1/\bar{\varepsilon}$ .

The self-induced velocity is proportional to the curvature (1/a). Therefore, the self-induced velocity of a straight, two-dimensional vortex filament is zero. Similar results were found by Batchelor (1967, 7.1), who followed a slightly different method.

For the general case of a vortex ring with a finite core Saffman P.G (1970) developed a general relation between the

vortex core vorticity distribution and the self-induced velocity. His result for the self-induced velocity in the limiting case of small core vortex rings with uniformly distributed vorticity :

$$V_{si} = \frac{\Gamma}{4\pi a}\left( \ln \frac{4}{\varepsilon} - \frac{1}{4} \right) \qquad 4.19$$

was identical with that obtained by Helmholtz's [Lamb H.,1932, article 163] and this relation can be compared with equation 4.18 for an arc of the vortex ring.

For the parachute model at high Reynolds number flow the shear layer is thin and consequently, the vortex cores are small. For such, a uniformly-distributed vorticity appears to be an appropriate assumption, thus, in the present model the self-induced velocity is calculated by equation 4.19.

## 4.3 VISCOUS CORE RADIUS EVALUATION

The viscous core radius is evaluated by assuming two-dimensional flow. In view of the characteristic length, i.e. the ratio between the vortex core diameter and the vortex ring diameter, involved in this specific calculation this assumption is justified.

For a real vortex in two-dimensional flow, Lamb (1932, article 334 a) found that :

$$U_\theta = \frac{\Gamma_o}{2\pi r} \{ 1 - \exp[-r^2/(4\nu t)] \} \qquad 4.20$$

where $U_\theta$ is the tangential velocity around a two-dimensional vortex, $\Gamma_o$ -the circulation around it at its creation, r -the distance from the separation line which in the present circumstances, is the canopy hemline and t -the time counted from the moment when the flow leaves the hemline.

Figure 4.4 shows schematically the variation of $U_\theta$. Its maximum value is developed at a distance $\varepsilon$ from the vortex center.

Since at $r>\varepsilon$ the potential model is appropriate, the distance from the core center to the place where $dU_\theta/dr=0$, is considered the viscous core radius (Schaefer J. & Eskenazi S. ,1959).

Then:

$$\varepsilon^2 \simeq 5\nu t \qquad 4.21$$

The circulation $\Gamma^*$ inside the viscous core at t=0 is:

$$\Gamma^* = \int_0^{2\pi} U_\theta r d\theta \simeq 0.72\Gamma_o \qquad 4.22$$

this showing that only about 70% of the shed vorticity is recirculated in the vortex ring core.

Defining $Re_D$ as the Reynolds number based on canopy projected area then:

$$\varepsilon \simeq \left( \frac{5\bar{t}D}{Re_D} \right)^{0.5} \qquad 4.23$$

where $\bar{t}$ stands for the dimensionless time step at the shedding of the newly-created vortex ring and D for the projected area diameter.

Thus :

$$\varepsilon/D = 0 \left( Re_D \right)^{-0.5} \qquad 4.24$$

This result justifies the small cores assumption made in the previous section.

From Kelvin's circulation theorem not only does the circulation around the vortex ring remain constant as the latter moves downstream but a further consequence [Karmancheti K. 1966, 18.5] is that the fluid particles which form the vortex tube at a given instant remain part of it for all time. Therefore, the vortex ring volume is preserved and:

$$( \varepsilon^2 a )_{t=t_o} = ( \varepsilon^2 a )_{t=t_n} \qquad 4.25$$

This relationship for the free vortex ring deformation is applied in the numerical model.

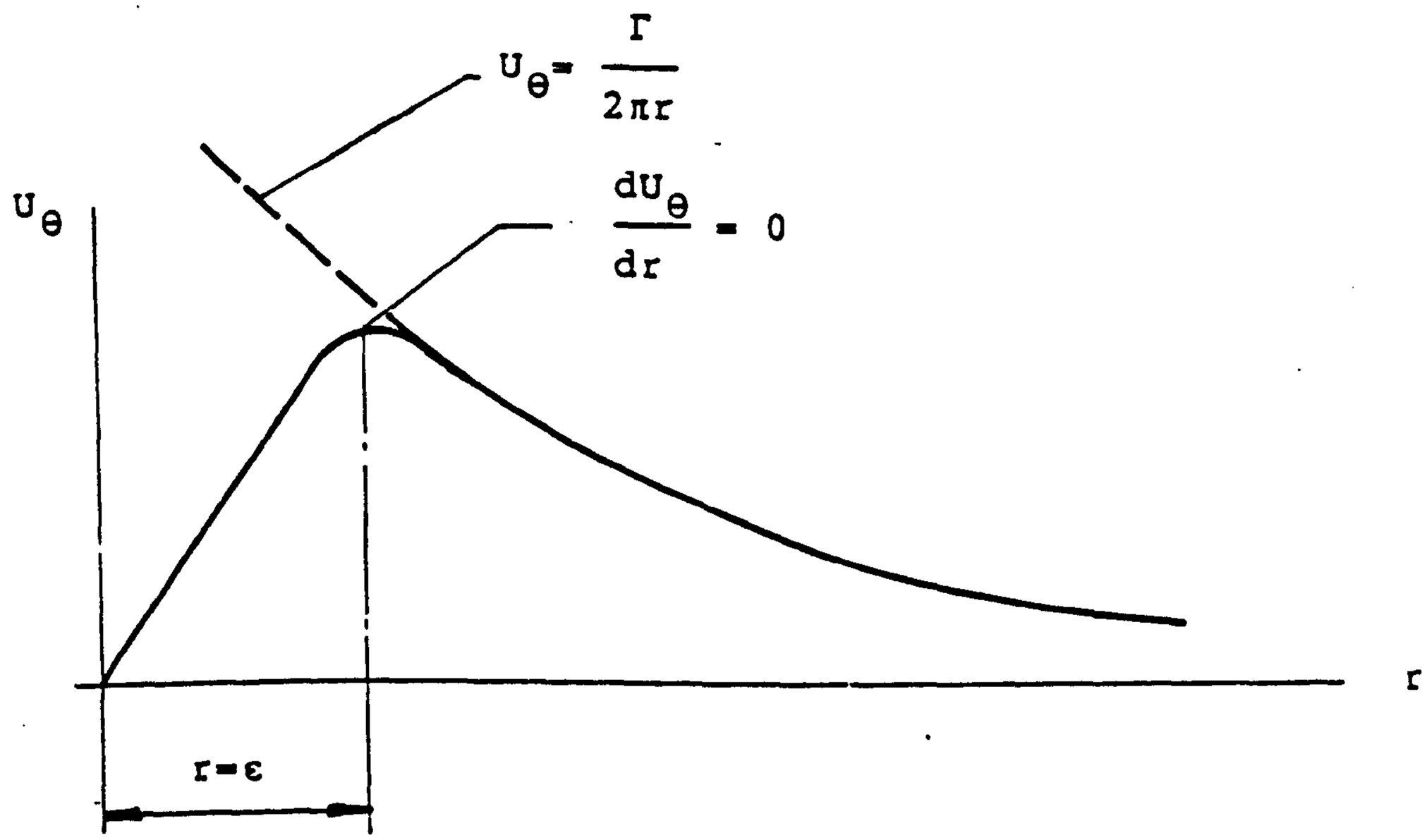


FIGURE 4.4: THE TANGENTIAL VELOCITY, $U_\theta$, DEVELOPED ABOUT A TWO-DIMENSIONAL VISCOUS VORTEX

## 4.4 CANOPY SURFACE SIMULATION

To model the canopy surface it is first replaced by panels of equal chord lengths (figure 4.5). This method, introduced in 1943 by Falkner, is widely used for aerodynamic load calculations. To simulate the panel's lifting characteristics a vortex ring of constant circumferential strength is arbitrarily placed at one quarter of the panel length. The boundary condition on the canopy surface, equation 4.5, is satisfied along a circle defined as the control circle and located at three quarters of the panel length.

The induced velocity at panel "i" has the following matrix form :

$$V_{ind_i} = [A_{can_i}]\{\Gamma_{can}\} + [A_{wake_i}]\{\Gamma_{wake}\} + A_{svr_i} * \Gamma_{svr} \qquad 4.26$$

where $A_{can}$ represents the canopy bound vortex system matrix influence coefficients , $A_{wake}$ represents the wake matrix influence coefficients and $A_{svr}$ the standing vortex ring influence coefficients (the "mn"-th influence coefficient is the velocity induced at panel "m" by a vortex ring of $\Gamma$ = 1 located at an identical axial position and of the same radius as the "n"-th vortex ring).

When a rigid canopy is assumed, the $A_{can}$ and $A_{svr}$ terms are calculated only once, at the simulation commencement. But if the canopy were to change its shape with time, they would

have to be calculated at each time step.

By substituing equation 4.26 into equation 4.5, for every panel, a linear system of equations is built up.

It is shown later (sections 4.7 and 4.8) that at the instant "t" the location and strength of both the shed vortex rings and the standing vortex ring are known. The one remaining unknown is the strength of the bound vortex rings. These will be determined by solving the linear system of equations which results when the boundary conditions, equation 4.5, are applied to every panel.

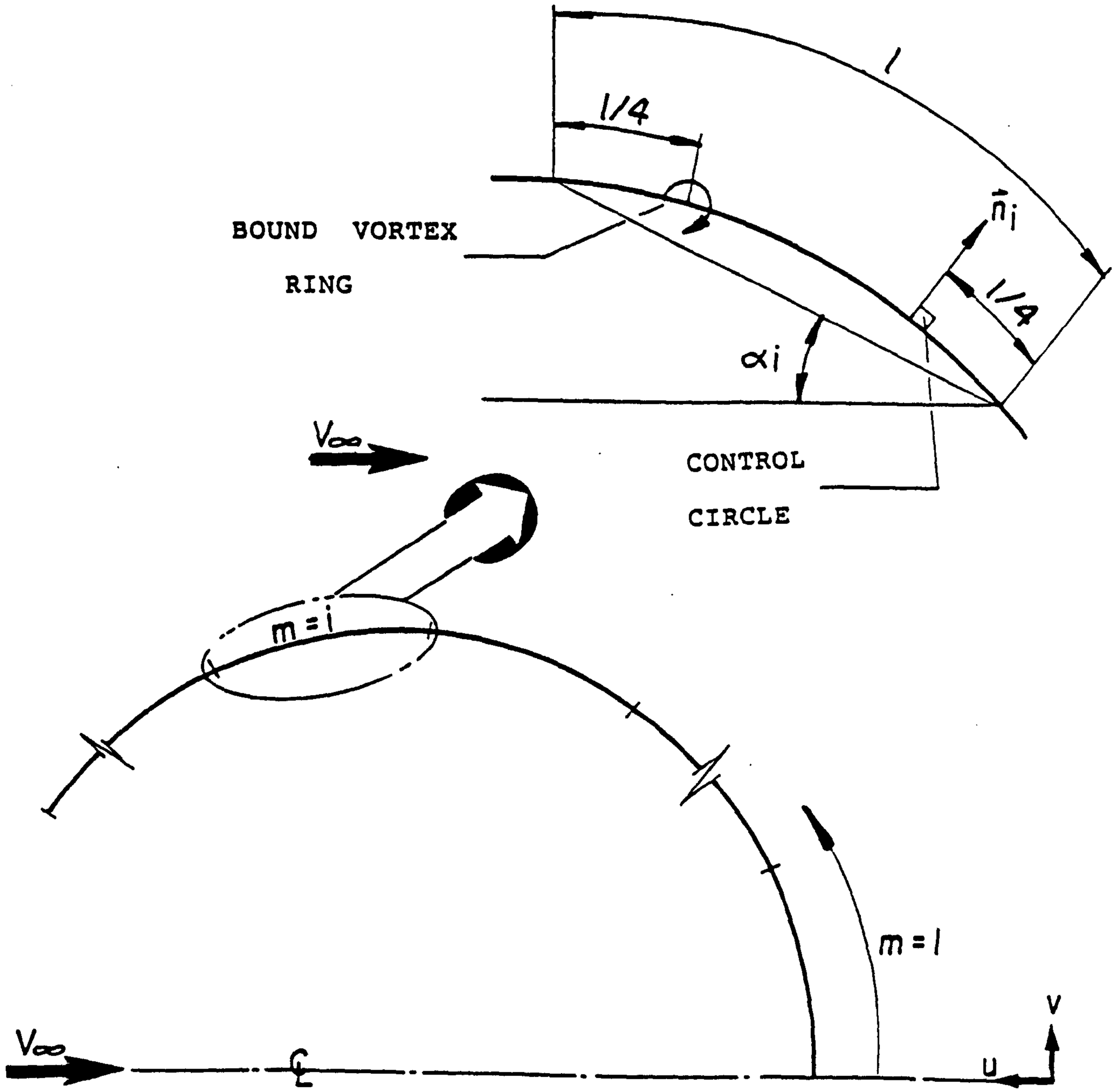


FIGURE 4.5: CANOPY SURFACE MODELLING

## 4.5 POROSITY INFLUENCE

According to Payne P.(1978) and Cockrell D.(1987) the pressure difference across a porous canopy in incompressible flow can be represented by:

$$\Delta P = P_1 - P_2 = K_1 V_{por}^2 - K_2 V_{por} \qquad 4.27$$

where $K_1$ and $K_2$ are proportional constants and $V_{por}$ is the velocity through the canopy surface.

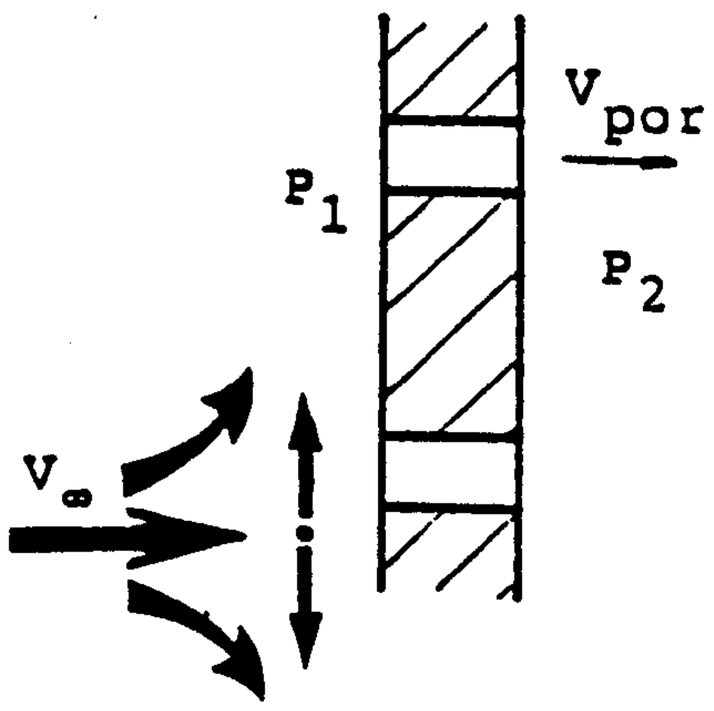


FIGURE 4.6: THE FLOW THROUGH A POROUS SCREEN

By neglecting the viscous loss term, i.e. $K_2 V_{por}$ the pressure drop across a porous screen becomes:

$$\Delta P = 0.5 K \rho V_{por}^2 \qquad 4.28$$

where K is a dimensionless, two-dimensional resistance coefficient such as that defined by Taylor G.I. and Davies R.M. ,1944.

In the empirical theory for the flow through porous

parachute canopies which Roberts B. (1979) developed, he considered the flow through a ribbon parachute to be similar to that through a screen with sharp edge elements whereas the flow through a fabric parachute is better represented by that through a porous screen made by circular elements. With such assumptions and by using the resistance coefficient concept of equation 4.28 Roberts developed two simple relationships which correlated this coefficient with the canopy's geometric porosity, $\lambda$, i.e. the ratio of open area to total surface area :

- for a ribbon canopy :

$$K \simeq (1/\lambda^2) - 1 \qquad 4.29$$

- whereas for a fabric canopy :

$$K \simeq (0.58/\lambda^2) - 1 \qquad 4.30$$

In order to preserve the validity of representing the canopy surface by a continuous vortex sheet, only porosity values which result in a normal velocities smaller than about 0.15 of the free stream velocity have been considered. Thus, equations 4.29 and 4.30 become approximately, respectively :

$$K \simeq (\lambda)^{-2}$$
$$K \simeq 0.58*(\lambda)^{-2} \qquad 4.31$$

Then by substituing equations 4.31 in equation 4.28 :

- for a ribbon canopy:

$$V_{por} \simeq (\Delta C_p)^{0.5} V_\infty \lambda \qquad 4.32$$

- for a fabric canopy:

$$V_{por} \simeq 1.3*(\Delta C_p)^{0.5} V_\infty \lambda \qquad 4.33$$

## 4.6 THE SHEDDING FREQUENCY

The shedding frequency can be calculated by using the equation ( Prandtl & Tietjens, 1957, article 93) :

$$\frac{d\Gamma}{dt} = \frac{v_u^2 - v_l^2}{2} \qquad 4.34$$

$V_u$ and $V_l$ being the velocities at the upper part and lower part of a shear layer respectively (figure 4.7). An important consequence of this equation is that the shedding frequency is not affected by the shear layer thickness.

Fage A. & Johansen F. (1927) investigated the wake flow behind a two-dimensional plate. One of their results was an experimental validation of equation 4.34. They measured the vorticity shed from the plate near the separation point and that existing in the wake at about nine plate widths downstream. It was found that only about 0.6 of the shed vorticity was recirculated. Their measurements (table VII in their previously quoted paper), show that the velocity on the lower part of the shear layer was one order of magnitude less than that on the upper side. Since near the separation point the velocity on the upper part of the shear layer was about 1.45 times the free stream velocity, the shed vorticity was, approximatelly $1.1*v^2_\infty$.

In view of Fage & Johansen's results most of the methods for separated wake simulation by discrete vortices use the following equation for shedding frequency calculation :

$$\frac{d\Gamma}{dt} = \beta \frac{v_u^2 - v_l^2}{2} \qquad 4.35$$

In this expression $\beta$ is an empirical circulation reduction factor which takes into account the difference between the vorticity shed from the body and that which is recirculated.

The value assumed for $\beta$ in some discrete vortex wake models, e.g. by Katz.J 1981, is about 0.6.

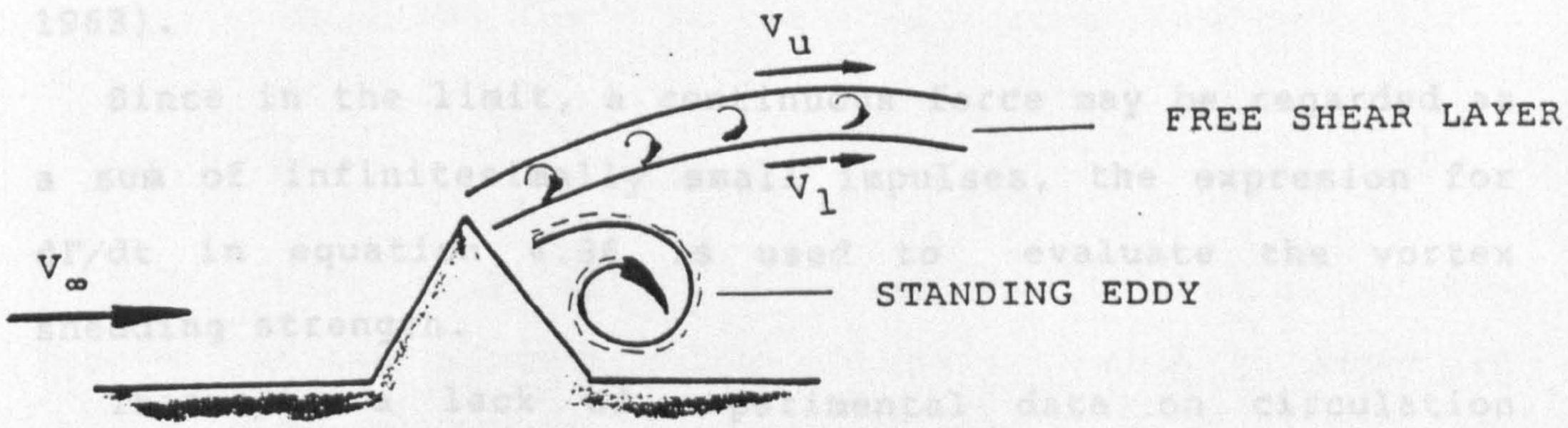


FIGURE 4.7: THE VORTEX SHEDDING FROM A SALIENT, TWO-DIMENSIONAL EDGE

A serious drawback in using this relation is that it demands velocities close to the separation point. The large changes in these induced velocities near to the shedding point can cause considerable variations in the determined forces acting on the canopy. The variations are amplified by ambiguity arising from the discrete representation of the flow field, in defining the exact point at which this velocity is to be calculated.

In order to simplify the calculation, in the present model

a different approach has been adopted.

As a differential pressure, which results in an infinitesimally-small drag force, impulsively sets in motion a disk normal to its surface, a vortex ring of strength:

$$\Delta\Gamma = \frac{1}{\rho} \Delta t \frac{\text{Drag}}{S_{disk}} = 0.5 \Delta t V_{\infty}^2 C_D \qquad 4.36$$

will be shed behind it (Durand F.W. division E chapter 3 1963).

Since in the limit, a continuous force may be regarded as a sum of infinitesimally small impulses, the expresion for $d\Gamma/dt$ in equation 4.36 is used to evaluate the vortex shedding strength.

There is a lack of experimental data on circulation reduction in axisymmetric flow so the model described in section 4.3 has been used. From equation 4.22 the circulation reduction factor is $\beta=0.72$, thus the shed vortex ring strength is smaller by about 30% than that determined by equation 4.36.

The shedding strength calculation scheme resulting from equation 4.36 implies an iterative procedure. This is because the drag force determination at instant $t=t_1$ requires the value $d\Gamma/dt$ at $t_1$. At the beginning of the model development, in the iterative calculation scheme, the calculated drag force manifested very strong variations in both its amplitude and strength. A quite similar problem was faced by Sarpkaya (1975) when he calculated the shedding strength using the instantaneus velocity near the flow separation point.

To avoid this numerical problem, in the current model an experimentally-based method has been adopted.

According to experimental data collected by Hoerner 1965, the drag coefficient ($C_D$) referred to the projected area of canopy-similar configurations, called cup-shaped bodies by Hoerner, is in the range of 1.2-1.4.

Subsequently, when an average $C_D$ is assumed, the effective shedding strength, i.e. the shedding strength of the vorticity which was found in the shed vortex ring core, is:

$$\frac{d\Gamma}{dt} \simeq 0.47\ V_\infty^2 \qquad 4.37$$

Using this relationship the sensitivity of calculated results to the assumed value of the $C_D$ value is shown in chapter 7 to be very small.

## 4.7 THE SEPARATED WAKE SIMULATION AND THE REQUIRED TIME STEP EVALUATION

Physically, the free shear layer leaves the surface tangentially. An appropriate way to model this is to assume that the canopy surface commences with an additional fictional panel. This panel lies along the tangent to the canopy, near its hemline, and its length is equal to that of the other real panels.

Therefore, the fictional panel bound vortex ring is, in fact, the newly-created vortex ring. Consequently, its strength is calculated together with the bound vortex system by solving the system of linear algebraic equations which result when equation 4.5 is expressed for each panel (section 4.1).

A method which has been widely used for the newly-created vortex strength calculation is by using equation 4.35 within a specific range of time steps whose magnitude is based on physical considerations. Hence, two free parameters have to be found empirically : the time step and the number of surface panels to be adopted (e.g. Katz.J 1981 and Levin D. & Katz J. 1980).

In the present model, once the strength of the newly-created vortex ring has been calculated the time step can be set at each instant to accord with equation 4.37. Thus, the number of free parameters is reduced to one, i.e. the number of panels representing the canopy surface. It will

be shown in chapter 7 that the sensitivity of the resulting simulation to this free parameter is found to be small.

The wake development is calculated by assuming that each free vortex ring is convected by the local velocity:

$$\begin{Bmatrix} \Delta x \\ \Delta y \end{Bmatrix}_{i_t} = \Delta t_t * \vec{V}_{t-\Delta t} \qquad 4.38$$

where $\Delta x$ and $\Delta y$ are the change in the "i-th vortex ring axial position and radius, respectively at instant "t", and $\vec{V}_{t-\Delta t}$ represents the sum of the free stream velocity, induced velocity and self-induced velocity of the "i"-th shed vortex ring, at the previous time step. This integration method results in an error whose order of magnitude is $(\Delta t)^2$ [ Henrici P., 1962].

In view of the small time step to which the present calculation method converges (chapter 5), this integration method should be satisfactory. However, the sensitivity of the solution to the integration method adopted will be discussed in chapter 7.

## 4.8 STANDING VORTEX STRENGTHS & LOCATION EVALUATION

The standing vortex ring simulates the standing eddy which develops behind salient edges, that is the canopy hemline. Owing to the dimensions involved, the separation region can be treated as locally two-dimensional, thus a Kutta-type condition requiring zero load near the hemline can be applied. This physically-based assumption is sustained by the experimental results obtained by Henrich G. & Uotilla J. (1977) and by Pepper B. & Reed J. (1976) which show that the differential pressure close to the hemline descreases to zero.

At the beginning of the model development, the standing vortex ring strength and its location were determined using an iterative procedure which ensured pressure continuity near the separation line, i.e. zero load at the hemline. Later however, the following approximate method, which results in considerable computational time saving, was used.

The fluid which is disturbed by the motion of a canopy can be divided into two main components, that included in the volume which is defined by the canopy surface and the canopy hemline plane, and that which is outside this volume. The energy of this latter fluid is approximately that of a moving disk of radius R. Thus, its added mass is [Lamb, 1932, article 120]:

$$m_f = \frac{8}{3} R^3 \rho \qquad 4.39$$

By assuming an equally-distributed impulse over the whole canopy surface :

$$I = \rho \Gamma \pi R^2 = m_f V_\infty \qquad 4.40$$

$\Gamma$ being the circulation associated with the disk movement.

Since the pressure difference across the disk decreases near its circumference this assumption is only approximate. However, due to the concavity of the canopy this pressure drop, which the disk represents, is limited to a small region (see experimental results of Pepper & Reed 1976 and Heinrich & Uotilla 1977). Therefore, for bluff canopies the approximation of an uniformly-distributed differential pressure distribution appears to be justified.

With equations 4.39 and 4.40 the strength of the vortex which accompanies the movement of a canopy is:

$$\Gamma = \frac{8R}{3\pi} V_\infty \qquad 4.41$$

Subsequently, the standing vortex ring strength is calculated by subtracting the newly-created vortex ring strength from that calculated by equation 4.41.

The location of the standing vortex ring is shown schematically in figure 4.8. The distance YVT (figure 4.8),

which ensures zero load near the canopy hemline, has been found empirically by trial and error to be about 1.15*YI. Its variation range was 1.05-1.20 for all the configurations whose aerodynamic characteristics were investigated. However, in the computer programme, the nominal YVT recommended value of 1.15*YI could be varied in order to keep the load near the hemline close to zero. The way in which this value is to be set will be described in chapter 5.

It is conceivable that this method will not give a zero load near the hemline. The maximum absolute value of the differential pressure across the nearest panel to the canopy hemline was found to be about 0.2. Since this approximate method of standing vortex ring strength & position evaluation will be shown in chapter 6 to give satisfactory results the iterative calculation procedure described earlier has been removed from the computer programme.

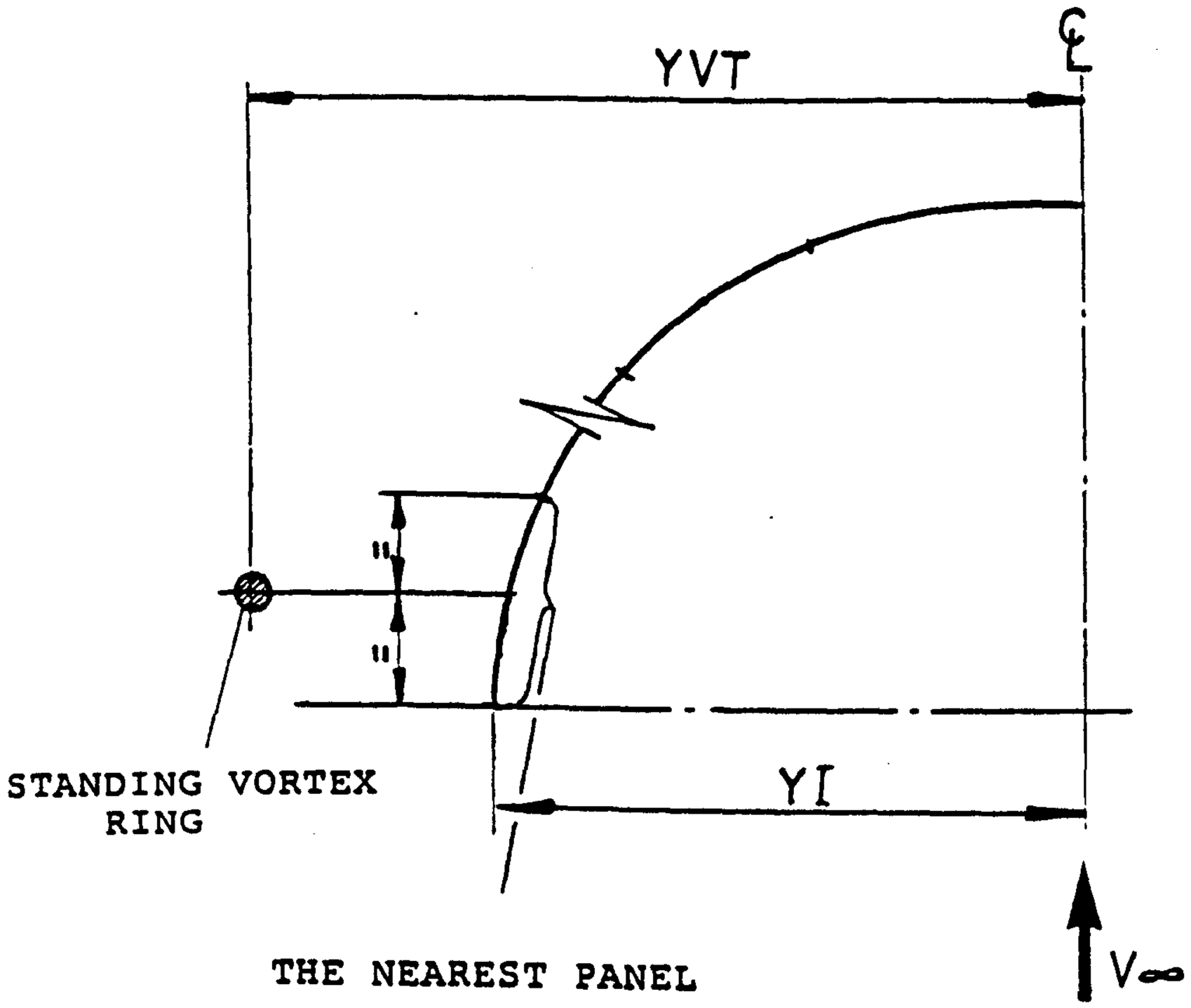


FIGURE 4.8: STANDING VORTEX RING LOCATION

## 4.9 DIFFERENTIAL PRESSURE CALCULATION

Physically, the wake developed behind the canopy is bounded by a continuous vortex sheet. Thus, the fluid field is divided into two distinct parts: the wake and the outer fluid flow. In the model the continuous vortex sheet which envelops the wake is approximated by a layer of discrete vortex rings. Following this approximation in the model the fluid field is continuous and therefore Bernoulli's theorem can be applied through the irrotational parts of the fluid field [Batchelor G.K., 1967, chapter 6.2]. Therefore, in the present model, it is assumed that the total pressure is constant across the vortex sheet whereas in the real flow the static pressure is constant. Judging by the results shown in chapter 6 and particularly in section 6.1.4, this assumption leads to good results for the differential pressure distribution and consequently for the total forces acting on a parachute canopy in both steady and unsteady motion.

From Bernoulli's theorem, the differential pressure across panel "i"-th, as shown in figure 4.9, is determined to be:

$$\Delta P = P_A - P_B = 0.5\rho(V_B^2 - V_A^2) + \rho\frac{\partial}{\partial t}(\Phi_B - \Phi_A) \qquad 4.42$$

As the canopy surface is replaced by a thin vortex sheet, the steady part in equation 4.42 gives:

$$0.5\rho(V_B^2 - V_A^2) \simeq \rho(\Gamma_{can_i}/l)V_\infty \cos^2\alpha_i \qquad 4.43$$

$\Gamma_{can_i}$ being the bound vortex ring strength of the i-th panel.

This calculation neglects both the porosity effect and any velocity which is caused by canopy shape changes or inducing pressure fluctuations which occur during the inflation process. Since these neglected velocities are shown in sections 4.6 and 6.2.3 to be small in comparison with the other terms in equation 4.43, this is a satisfactory procedure. However, these velocities were not neglected in the boundary condition given by equation 4.5.

The time-dependent part in equation 4.42 is calculated by observing the changes in the circulation around the circuit D (figure 4.9).The potential difference between points A and B (figure 4.9) is:

$$\Gamma_D = \Phi_A - \Phi_B \qquad 4.44$$

where $\Gamma_D$ is the circulation around circuit D. Its time variation is:

$$\frac{\partial}{\partial t}(\Phi_A - \Phi_B) = \frac{d}{dt}\left(\sum_1^i \Gamma_{can_k}\right) + \frac{d}{dt}\Gamma_{wake} + \frac{d}{dt}\Gamma_{svr} \qquad 4.45$$

This equation shows that the unsteady pressure distribution depends on the changes in the bound vorticity of the canopy, commencing with the hemline and proceeding up to the specific panel. It also depends on the wake circulation variation (this being the newly-created vortex ring) and on the variation in the standing vortex ring strength.

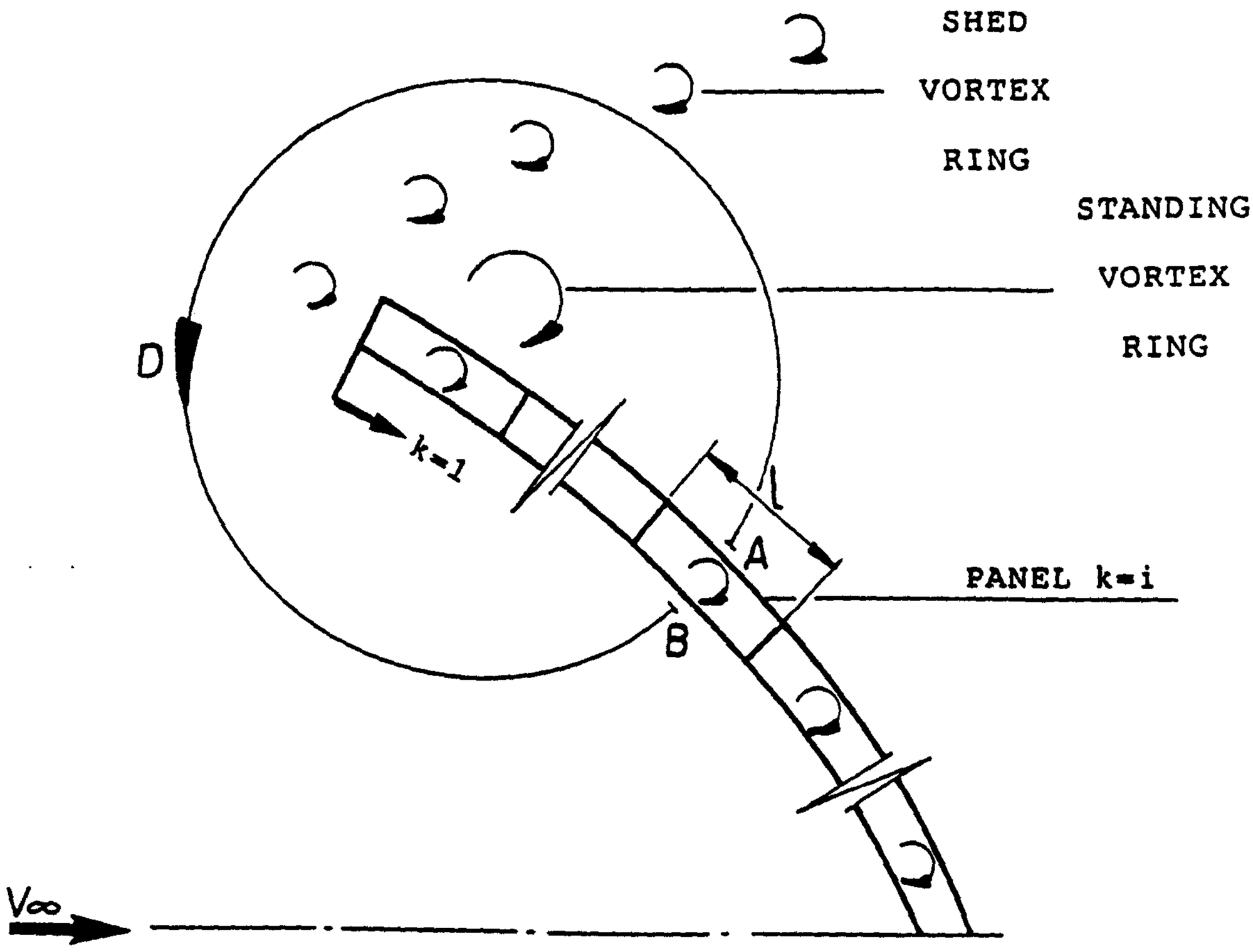


FIGURE 4.9: DIFFERENTIAL PRESSURE CALCULATION

## 4.10 THE MODEL LIMITATIONS

The principal application of the present bluff body flow model is to predict the aerodynamic characteristics developed by bluff parachute canopies.

Since a time-dependent canopy shape has been assumed, this remains to be considered. What the present model predicts is the instantaneous aerodynamic load, for a given momentary shape & velocity. In order to simulate properly complex phenomena such the inflation process and the canopy "breathing", a model which can predict the canopy shape as a function of all the applied loads is required.

Since the present model obeys Kelvin's conservation theorem, no viscous decay or viscous interaction between vortex filaments has been accounted for and neglecting these effects could lead to some unrealistic results.

Although some basic experimental data for these viscous effects are available [see Maxworthy T. 1972,1974 for the circulation decay of vortex rings and Leonard A. 1976 for modelling the viscous interaction between vortex filaments], because of the overall experimental data shortage it is premature to introduce those features into the present model. Once these data are available, the viscous effects could be modelled by schemes such as those which Sarpkaya T. & Shoaff R (1979) have adopted.

By using the present model to simulate the flow field developed about various shapes after long flight periods, it

was found that the effect of neglecting these viscous effects manifests itself when the dimensionless flight time, $tV_\infty/2R$, is higher than about 20.

In the current inviscid model, due to the rollup process vortex rings at a relatively large distance from the canopy may develop high velocities in the reverse direction to that of the free stream. These would cause them to interact with vortex rings which are situated close to the canopy surface. Both the steady axial force and the Strouhal number will be affected by this unrealistic interaction with the far wake. In order to diminish this effect, which in a real flow would be strongly damped by viscous mechanisms, the vortex rings situated at larger distances than four diameters behind the canopy were neglected. This recommended distance was chosen by examining the development in steady flow of the mean axial force coefficient (see definition in section 6.1.1). It is illustrated in figure 4.10.

Beside the near wake simulation improvement, a significant by-product of neglecting this far wake is a considerable & welcome reduction in the required computation time.

Physically, the free shear layer which envelops the wake is continuous and there is no flow through it. When the wake is approximated by discrete vortices this condition can not be fulfilled, for example, in the present model it is kept only near the shedding line. Therefore, as pointed out by Clements & Maull (1975), the fine structure of the wake is not properly simulated.

The approximation of the continuous, free vortex sheet

fails during the rollup calculation. The simulated wake flow pattern (e.g. figure 6.1 e & f) shows that during the process of vortex rings cluster creation the vortex sheet crosses through itself. This limitation of the flow simulation method based on the representation of the two-dimensional wake by discrete vortices is discussed by Clements & Maull (1975) and by Windall (1975). It could well be that the rollup of the free shear layer which occurs in the real flow involves viscous mechanisms as well and therefore it cannot be described by inviscid considerations only, as has been done in the present model. However, judging by the results presented in chapter 6 the main properties of the unsteady wake flow are well simulated and no attempt to solve this problem has been made in the present work.

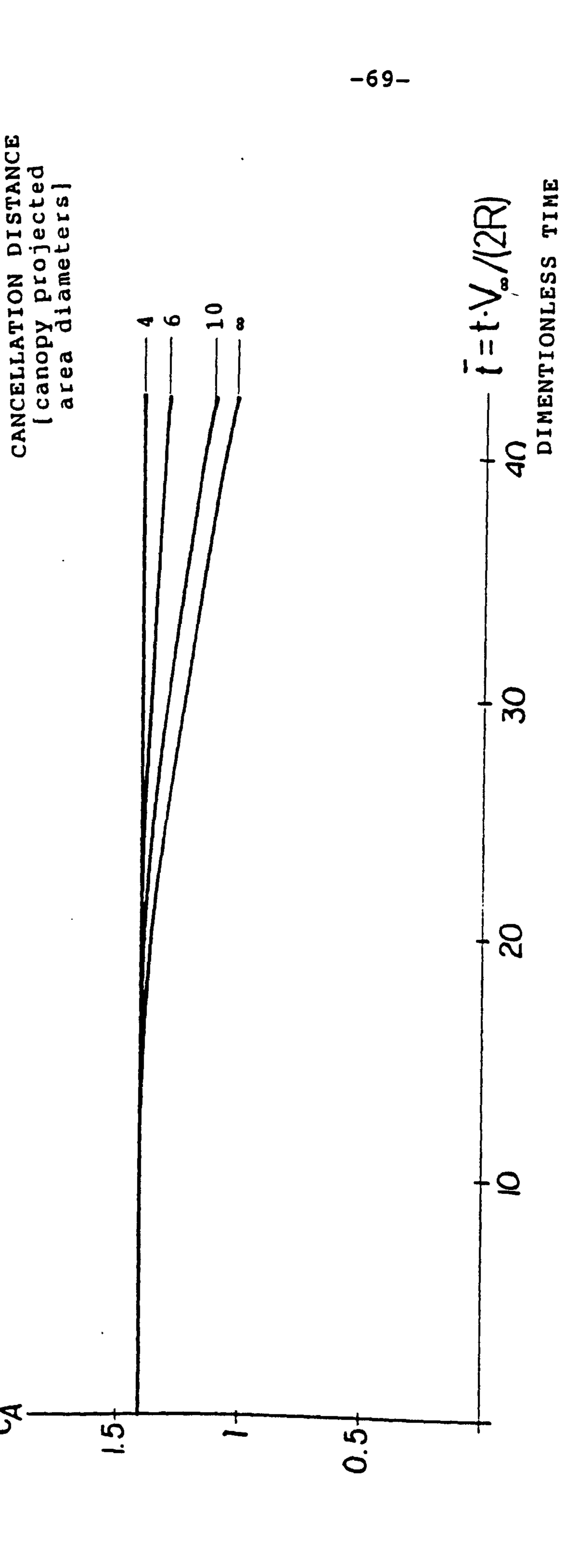


FIGURE 4.10: THE DETERMINATION OF THE CANCELLATION DISTANCE

## 5.THE CALCULATION METHOD & COMPUTER PROGRAMME DESCRIPTION

The model principles were mathematically formulated and subsequently a computer programme based on those principles was developed.

In figure 5.1 the basic flow chart for the calculation method is shown.

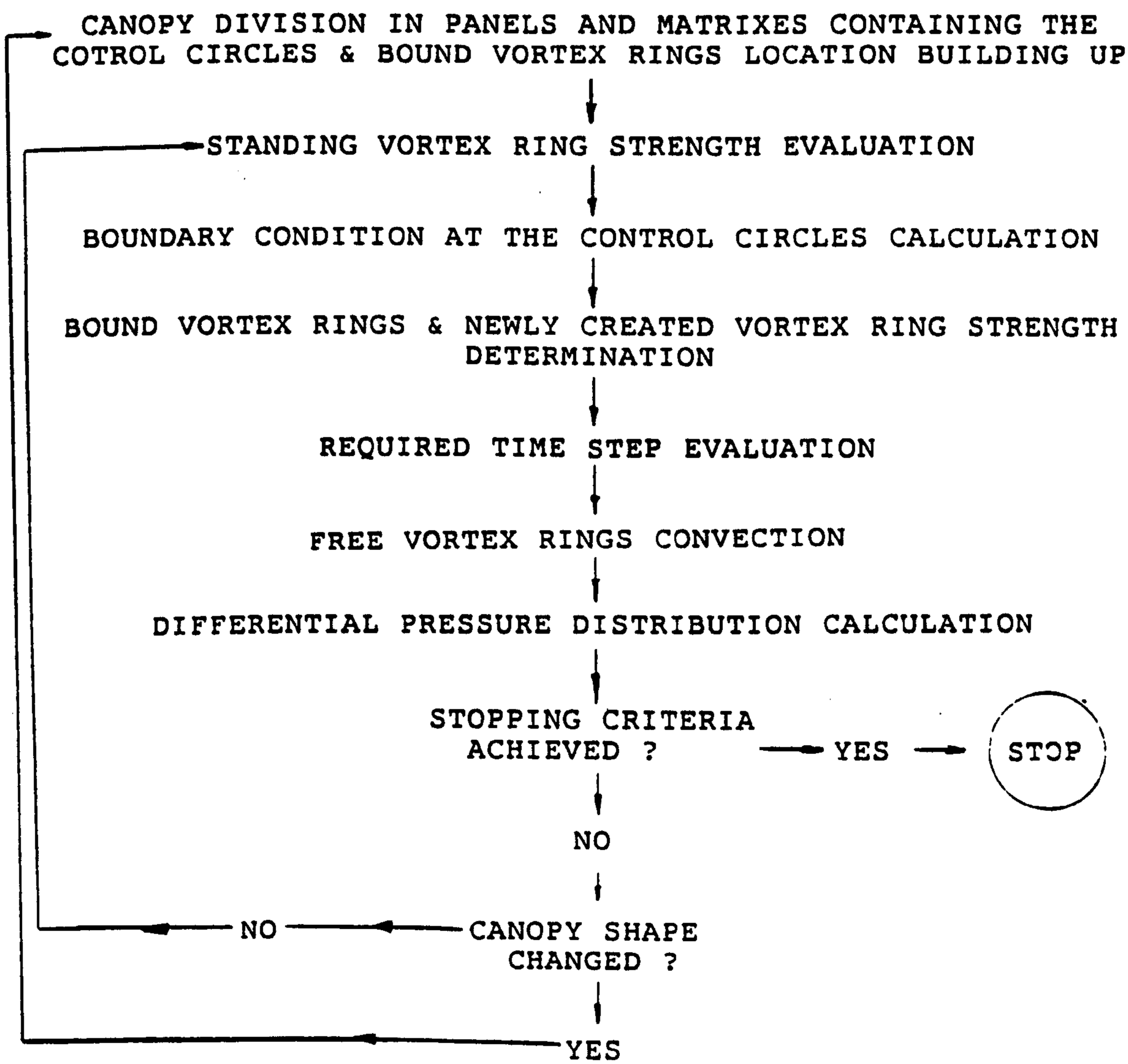


FIGURE 5.1: THE LOW-LEVEL FLOW CHART FOR THE CALCULATION PROCEDURE

Figure 5.2 shows the coordinate system used in the computer programme.

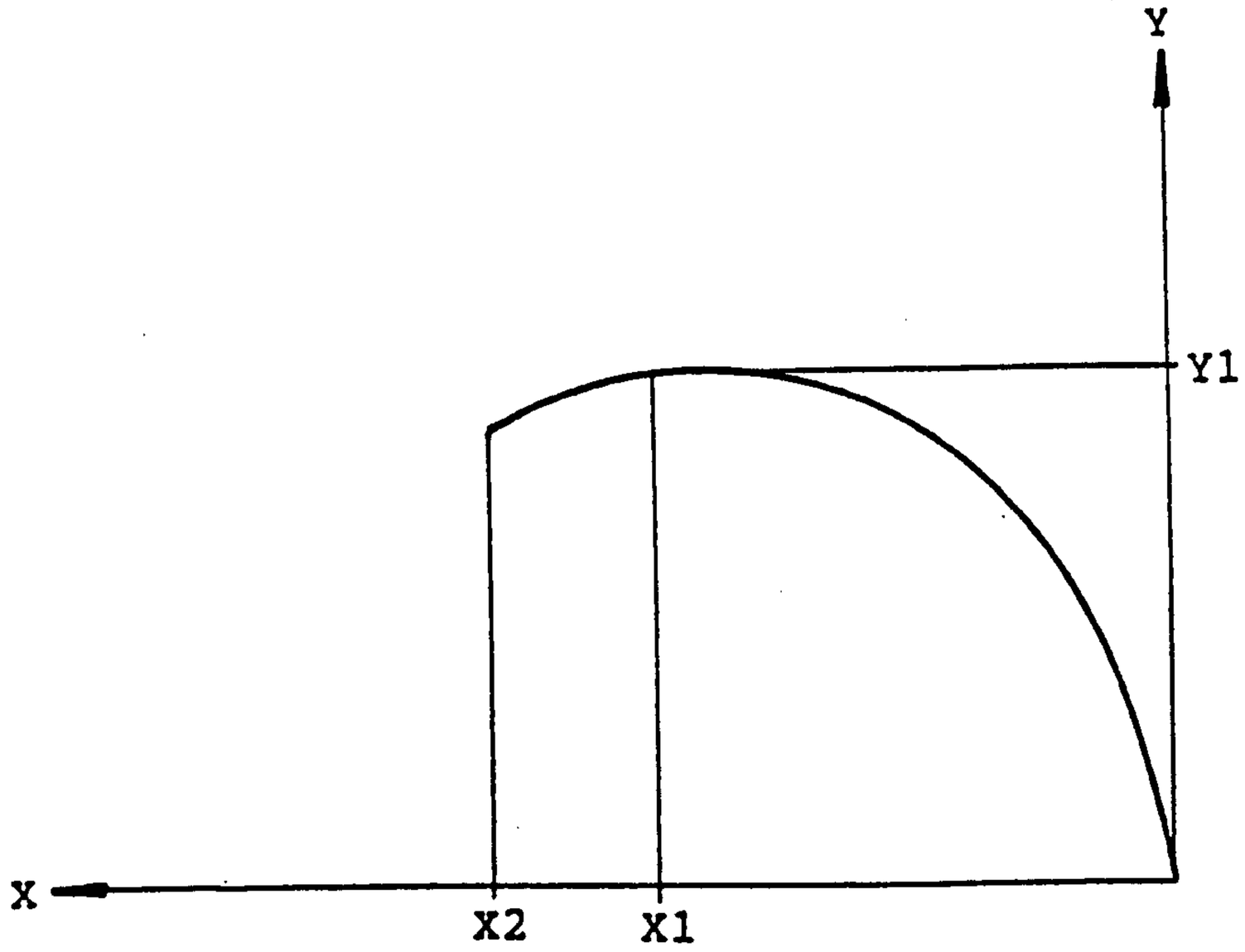


FIGURE 5.2: THE COORDINATE SYSTEM FOR FLOW SIMULATION

The canopy shape is assumed to have an elliptical cross-section and therefore three parameters, which may be a function of time, are required to define the shape: X1,X2,Y1 (see figure 5.2). Those parameters are required by the function generating the canopy shape. To allow for a discrete canopy shape or one with any other shape geometry only minor programming changes are required to the canopy shape generating function.

The velocity may be steady or it may be a tabulated function of time.

An additional way of specifying the velocity profile is through the free deceleration mode. When this option is used the mass of the parachute/payload system is also required.

The velocity is calculated by the computer program at each time step, by integrating the parachute/payload system acceleration developed by the instantaneous aerodynamic and gravitational forces.

Whichever specification method is used for the velocity profile, the boundary conditions, i.e. the normal velocity at the control circles are set to fulfil both the kinematic and the canopy porosity requirements.

The first element of the vortex system whose strength is calculated is the standing vortex ring. Following the method described in section 4.8, it is calculated by:

$$\Gamma_{SVR} = \frac{8R}{3\pi} V_\infty - \Gamma_{NC} \qquad 5.1$$

where $\Gamma_{SVR}$ and $\Gamma_{NC}$ are, respectively, the standing vortex ring and the newly-created vortex ring strength. Because at the motion commencement there is no wake, at the first time step $\Gamma_{NC}$ is zero. Its subsequent evaluation is explained in the following.

The normal velocity through the canopy surface is determined by the porosity requirements. Thus, it is calculated by the equations:

- for a ribbon canopy (equation 4.32):

$$V_{por_i} \simeq (\Delta C_p)_i^{0.5} V_\infty \lambda$$

- for a fabric canopy (equation 4.33):

$$V_{por_i} \simeq 1.3*(\Delta C_p)_i^{0.5} V_\infty \lambda$$

At the motion commencement, i.e. at the first time step it is arbitrarly set to equal zero. The induced velocity at panel

"i" has the following matrix form (equation 4.26):

$$V_{ind_i} = [A_{can_i}]\{\Gamma_{can}\} + [A_{wake_i}]\{\Gamma_{wake}\} + A_{svr_i} * \Gamma_{svr}$$

where $A_{can}$ represents the canopy bound vortex system matrix influence coefficients , $A_{wake}$ represents the wake matrix influence coefficients and $A_{svr}$ the standing vortex ring influence coefficients (the "mn"-th influence coefficient is the velocity induced at panel "m" by a vortex ring of $\Gamma$ = 1 located at an identical axial position and of the same radius as the "n"-th vortex ring).

When a rigid canopy is assumed, the $A_{can}$ and $A_{svr}$ terms are calculated only once, at the simulation commencement. But if the canopy were to change its shape with time, they would have to be calculated at each time step.

Finally, the boundary condition at the canopy surface, i.e. the velocity through the canopy surface (i.e normal to it) at a general control circle "i" is given by equation 4.5:

$$V_{por_i} = \vec{V}_\infty \cdot \hat{n}_i + \vec{V}_{ind_i} \cdot \hat{n}_i + \dot{\vec{R}} \cdot \hat{n}_i$$

where $V_{ind_i}$ is the velocity induced by the whole field;

$\vec{R}$ is the vector from the canopy apex to the canopy control circle "i" and its time derivative represents any canopy shape changes.

By substituing equation 4.26 into equation 4.5, for every panel, a linear system of equations whose only unknown is the bound vortex sheet strength, i.e. the matrix $\{\Gamma_{can}\}$, is built up. The bound vortex sheet strength is determined at each time

step. Together with this bound vortex sheet strength the strength of the newly-created vortex ring is also calculated. According with the method described in section 4.7 the newly-created vortex ring, $\Gamma_{NC}$, is considered to be the vortex ring bound to the fictional panel. In view of the relatively small dimensions (usually about 10*10) of the resulting matrix, which is related to the number of canopy panels the linear system of equations is solved by a Gaussian elimination non-iterative method.

The required time step is determined by the method described in sections 4.6 & 4.7. Thus, it is calculated by:

$$\Delta t=(0.47V_{\infty}^{2})^{-1}\Gamma_{NC} \qquad 5.2$$

At the motion commencement, when the $\Gamma_{NC}$ equals zero the non-dimensional time step is set arbitrarly to equal 0.1. For steady flows it usually converges after about five time steps to values between $\Delta\bar{t}=0.05$ and $\Delta\bar{t}=0.15$.

The wake development is calculated by convecting each of the vortex rings with the local velocity. The latter is found by summing up the contribution of the whole vortex system at the circumference of the specified vortex ring. Thus, the free vortex ring motion is calculated by equation 4.38:

$$\begin{Bmatrix}\Delta x\\ \Delta y\end{Bmatrix}_{i_t} = \Delta t_t * \vec{V}_{t-\Delta t}$$

where $\Delta x$ and $\Delta y$ are the change in the "i-th vortex ring axial position and radius, respectively at instant "t", and $\vec{V}_{t-\Delta t}$ represents the sum of the free stream velocity, induced

velocity and self-induced velocity of the "i"-th shed vortex ring, at the previous time step.

There are two mechanisms for vortex ring cancellation. In the first, the vortex rings which collide with the canopy during the roll up process are cancelled.

The second mechanism is described in section 4.6. Its purpose is to minimise any unrealistic effects which may emerge from the method of treating viscosity effects. It is recommended that vortex rings which are at a greater distance downstream of the canopy hemline than four canopy projected diameters, be cancelled.

From Bernoulli's theorem, the differential pressure across panel "i"-th, as shown in figure 4.9, is determined from equations 4.42, 4.43 and 4.45 to be:

$$\Delta P_i = \rho[(\Gamma_{can_i}/l)V_\infty \cos^2\alpha_i + \frac{d}{dt}\left(\sum_1^i \Gamma_{can_k}\right) + \Gamma_{NC}/\Delta t + \frac{d}{dt}\Gamma_{svr}] \qquad 5.3$$

Finally, the total force generated on the canopy is calculated by integrating the differential pressure over the canopy surface.

Figure 5.3 briefly describes the computer programme main procedures and their hierarchy. In the final version of the computer programme, which introduces calculation methods described in chapter 4 and whose results will be shown in the following chapter 6, there are no iterative calculations. However, if the standing vortex ring nominal location (section 4.8) does not result in a sufficiently small load near the canopy hemline, it has to be determined by trial &

error for every configuration.

As shown in figure 4.8, only the standing vortex ring coordinate in the "Y" direction (YVT) is to be determined. The recommended procedure is to chose a value of about YVT=1.15*YI and run the computer programme interactively for 10-20 time steps. If the differential pressure across the near hemline panel is not satisfactory (i.e. if it is not close enough to zero) the location of the standing vortex ring must be slightly changed (usually by up to 10%). By running the program for different configurations, it was found that 1.05*YI<YVT<1.20*YI. Within three trials it is anticipated that a sufficiently small differential pressure across the near hemline panel will be achieved.

The computation time depends mainly on the number of uncancelled free vortex rings, approximately as the square of this number.

The recommended number of panels in which to divide the canopy is between 8 and 14. When the number of panels is too small, because of the discrete representation of the canopy the resulting configuration may differ significantly from the desired one. However, dividing the canopy into too many panels unjustifiably increases the computation time. The sensitivity of solutions to this free parameter is discussed in chapter 7.

Using the recommended values, the characteristic computation time demanded by the computer programme on a VAX-8600 computer is about 450 seconds C.P.U. for about 20 units of dimensionless time, i.e. the product of time counted

from motion commencement and the average free-stream velocity, divided by the canopy projected area diameter.

The computer programme is menu driven and when run interactively, the programme prompts with questions and hints to help the inexperienced user. Its listing is given in the Appendix.

**PARACHUTE** (main)
- data input:
  - canopy geometry (it can be time-dependent)
  - free stream velocity (it can be a tabulated function of time or integrated at each time step according to the instantaneous axial force and parachute/payload system mass)
  - fluid density
  - number of panels for canopy discretisation
  - stopping criteria
- output options specifications

**CANOPY** ( the main subroutine) : integrates the axial force resulting by activating the other procedures
- **CIC** (subroutine) : calculates the canopy influence coefficients
  - **UVR, VVR** (functions) : calculate the axial and radial, respectively, velocity induced by a vortex ring of a unit strength
  - **E1, E2** (functions) :calculate the first and the second, respectively, elliptic integrals
- **SOLVE** (subroutine) : solves the linear system of equations giving the bound vortex rings & newly created strength
- **CP** (subroutine) : calculates the differential pressure distribution
- **WAKE** (subroutine) : calculates the wake development by convecting the free vortex rings
  - **UVR,VVR**
  - **E1,E2**

FIGURE 5.3: A HIERARCHICAL SCHEME OF THE MAIN COMPUTER PROGRAMME PROCEDURES.

# 6.NUMERICAL INVESTIGATION RESULTS

This chapter presents the numerical investigation results for steady and unsteady flows about both rigid canopies and those whose shape is time-dependent.

About one half of the presented results are for spherical canopies. Since they are unstable and have a relatively low drag coefficient referred to the constructed area this shape is obsolete for parachute canopies but it has some advantages for experimental purposes such as for the experimental investigation of the flow field. Results were obtained by using the computer programme "PARACHUTE" whose listing is given in the Appendix and which was briefly described in chapter 5. The canopy was divided in twelve panels and the shed vortex rings located at a distance larger than four canopy projected diameters downstream of the canopy were cancelled.

For the sake of abbreviation, the canopy configuration whose aerodynamic properties will be analyzed is defined by stating the quantities X1,X2 and Y1 shown in figure 5.1.

The axial force coefficient $C_A$ and the Strouhal number St are referred, respectively, to the canopy projected area and to the diameter of the canopy projected area.

Unless otherwise specified, the flow Reynolds number in these results is about $1.5*10^5$, based on the canopy projected diameter.

## 6.1 THE AERODYNAMIC PROPERTIES DEVELOPED BY A RIGID CANOPY IN ASYMPTOTICALLY STEADY MOTION

In chapter 2 Rosenhead's (1931 a) interpretation of Stanton T. & Marshal D.'s (1931) experiments is quoted. In this quotation the observed wake flow periodicity is explained by the unstable shear layer, "sheath of vorticity", as Rosenhead termed it, spreading from the separation line. As it breaks down it creates packages of vortex rings which are subsequently shed to the wake. Anticipating the flow simulation results, it is seen that Rosenhead's interpretation of the wake flow periodicity is remarkably accurate .

Figure 6.1 shows a sequence of the vortex shedding process occurring in the wake developed behind a hemispherical canopy. The shear layer carrying the vorticity created in the boundary layer is represented by the discrete axisymmetric layer of vortex rings which leaves the hemisphere hemline tangentially (point A in figure 6.1-a). As it does so it manifests both small scale disturbances ( point B in figure 6.1-b) and a roll-up process (point C in figure 6.1.-b). In the vicinity of the roll-up initiation region the shear layer tends to close and the concentration of the vortex rings increases (figure 6.1-c).

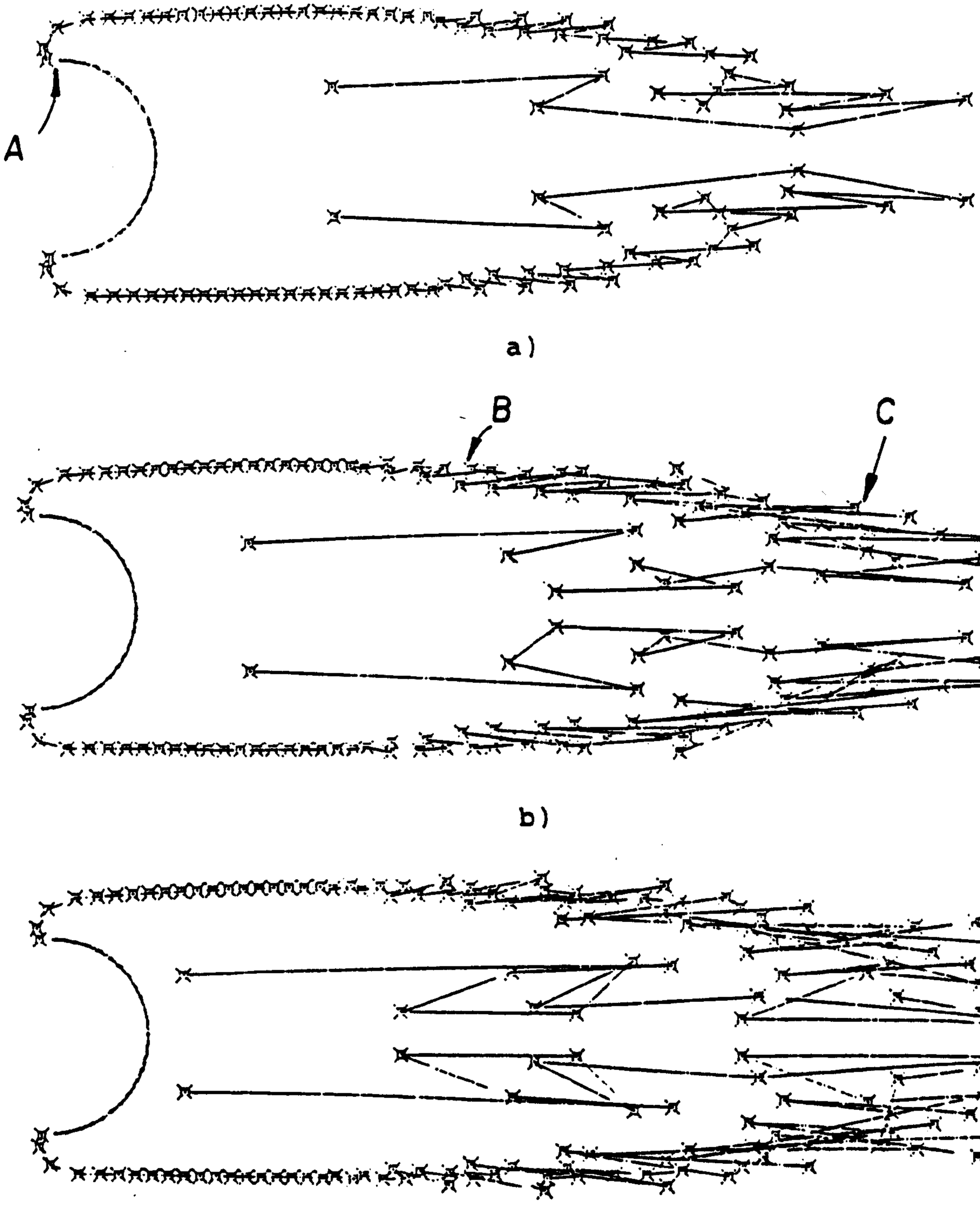


FIGURE 6.1(a-c): THE VORTEX SHEDDING MECHANISM AT SUCCESSIVE TIME ITERVALS (continued on the next page)

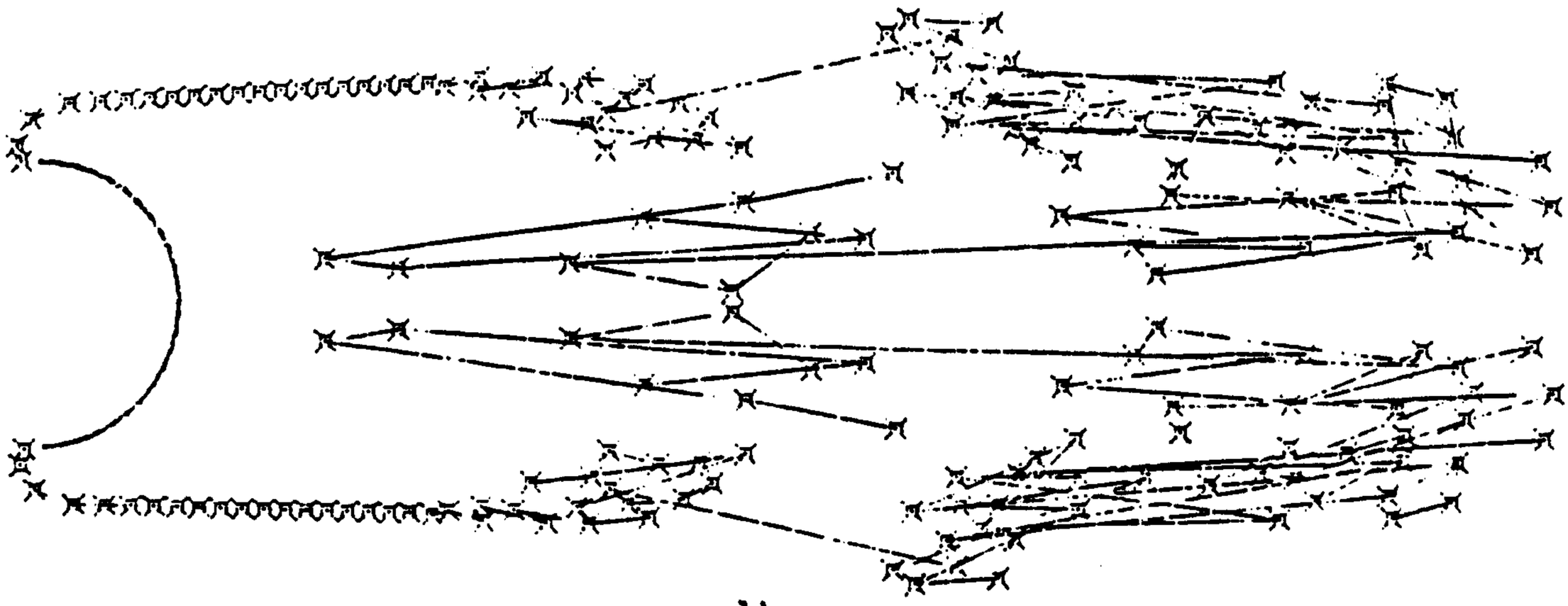

d)

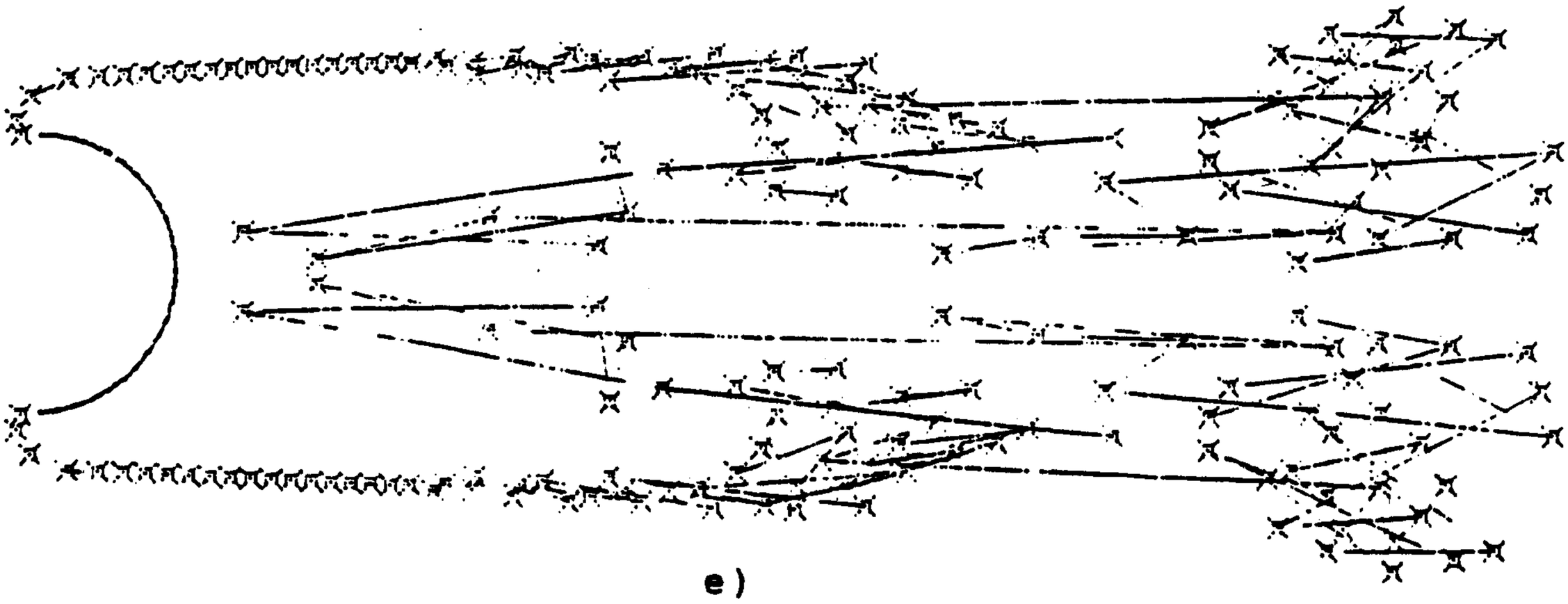

e)

FIGURE 6.1(d-e): THE VORTEX SHEDDING MECHANISM AT SUCCESSIVE TIME ITERVALS (continuation)

For a while, the cluster of vortex rings maintains its distance to the hemisphere thus, its mean, induced velocity is balanced by the free-stream velocity.

A further increase in the concentration of the vortex rings suddenly disturbs this equilibrium and a cluster of vortex rings is shed to the wake (figure 6.1-d). As this cluster moves downstream a new concentration of vortex rings is gradually created afresh(figure 6.1-e).

Figures 6.2-6.5 shows the wake flow pattern developed behind differently-shaped canopies.

This periodic behaviour exercised by the wake flow will affect the axial force developed on the canopy. Figure 6.6 shows the wake flow and the resulting time dependent axial force developed on a hemispherical canopy.

Close to the commencement of motion the flow is governed by impulsive movement of the canopy and an acceleration-dependent force develops. This kind of motion is discussed in section 6.2. In the current section the flow developed after the acceleration effect decay is

considered i.e. the dimensionless time $\bar{t}>>1$. At $\bar{t}\simeq13$ and $\bar{t}\simeq19.5$ (figure 6.6), groups of concentrated vortex rings are shed. Consequently, the axial force varies abruptly.

As shown by Sarpkaya T. (1975) the calculated axial force which is developed on a two-dimensional plate in normal flow manifests gradual periodic variations caused by the movement of the large cluster of vortices leaving the plate edges alternately and forming a vortex street.

In the axisymmetric case, due to the vortex shedding mechanism, the changes in the axial force are much more abrupt than they are in two-dimensional flow.

Since there is a clear functional dependence of this axial force fluctuation on the wake flow, the Strouhal number of the velocity variations in the wake flow can also be found by counting the fluctuations in the axial aerodynamic force. Thus, there are two ways of determining Strouhal number experimentally, one by measuring the velocity in the wake, such as with a hot-wire anemometer, and the other by considering the fluctuations in the axial aerodynamic force.

Since parachute canopies are flexible, the fluctuations developed in the aerodynamic load may affect the canopy shape. Hence, the applicability of wind tunnel results concerning the abrupt changes in the axial force which are developed on steadily-moving canopies to the design of full-scale parachute canopies depends on the availability of a model which predicts the changes in canopy shape resulting from variations in the aerodynamic load. It could well be that phenomena like canopy "breathing" (Hume R. & Stevens W., 1971) and "collapse"(Spahr R. & Wolf D., 1981) are caused by this interaction between the fluctuating aerodynamic load and the canopy structural response.

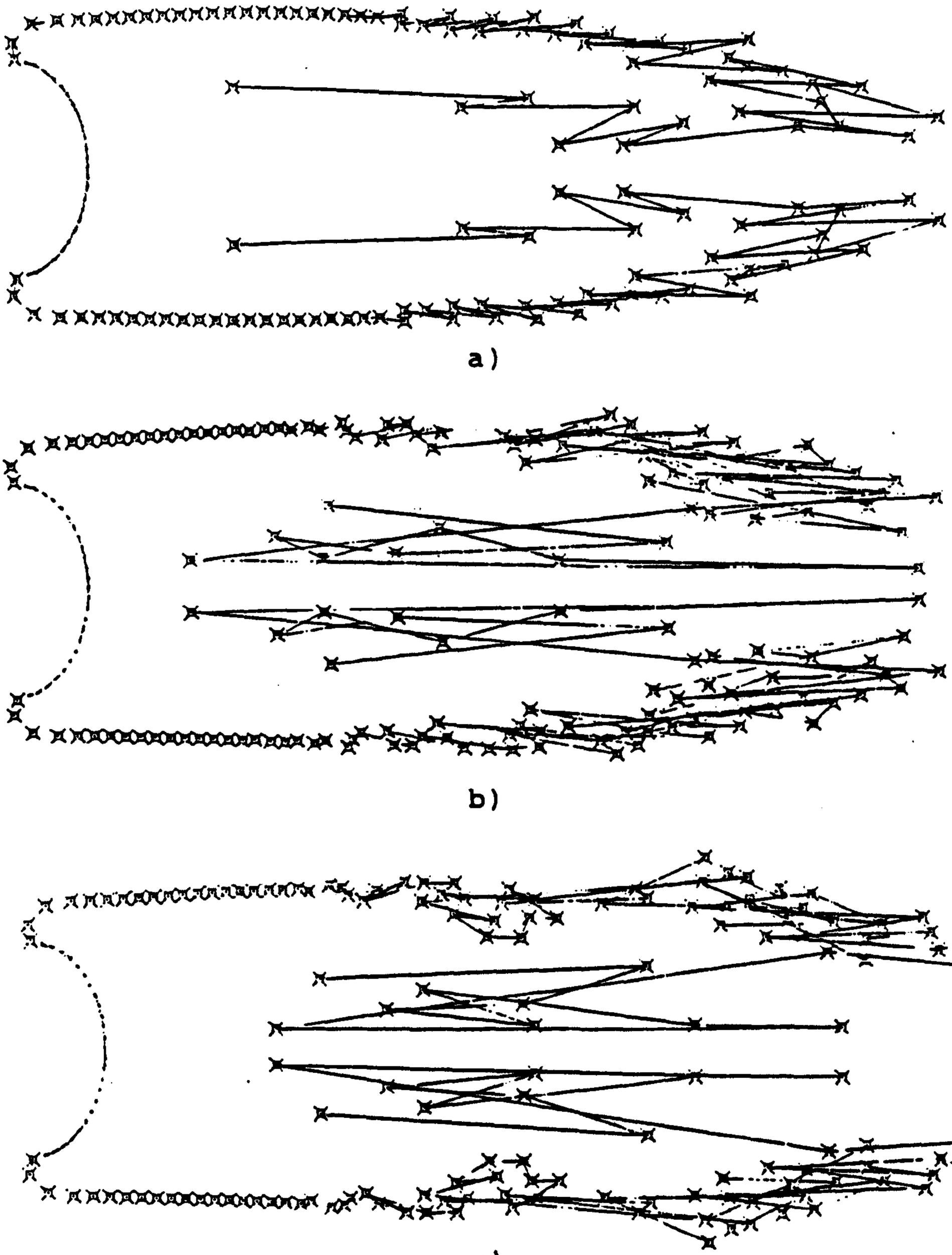

a)

b)

c)

FIGURE 6.2: THE WAKE FLOW PATTERN DEVELOPED AT SUCCESSIVE TIME INTERVALS BY THE CANOPY X1/Y1=0.7 , X2/Y1=0.6

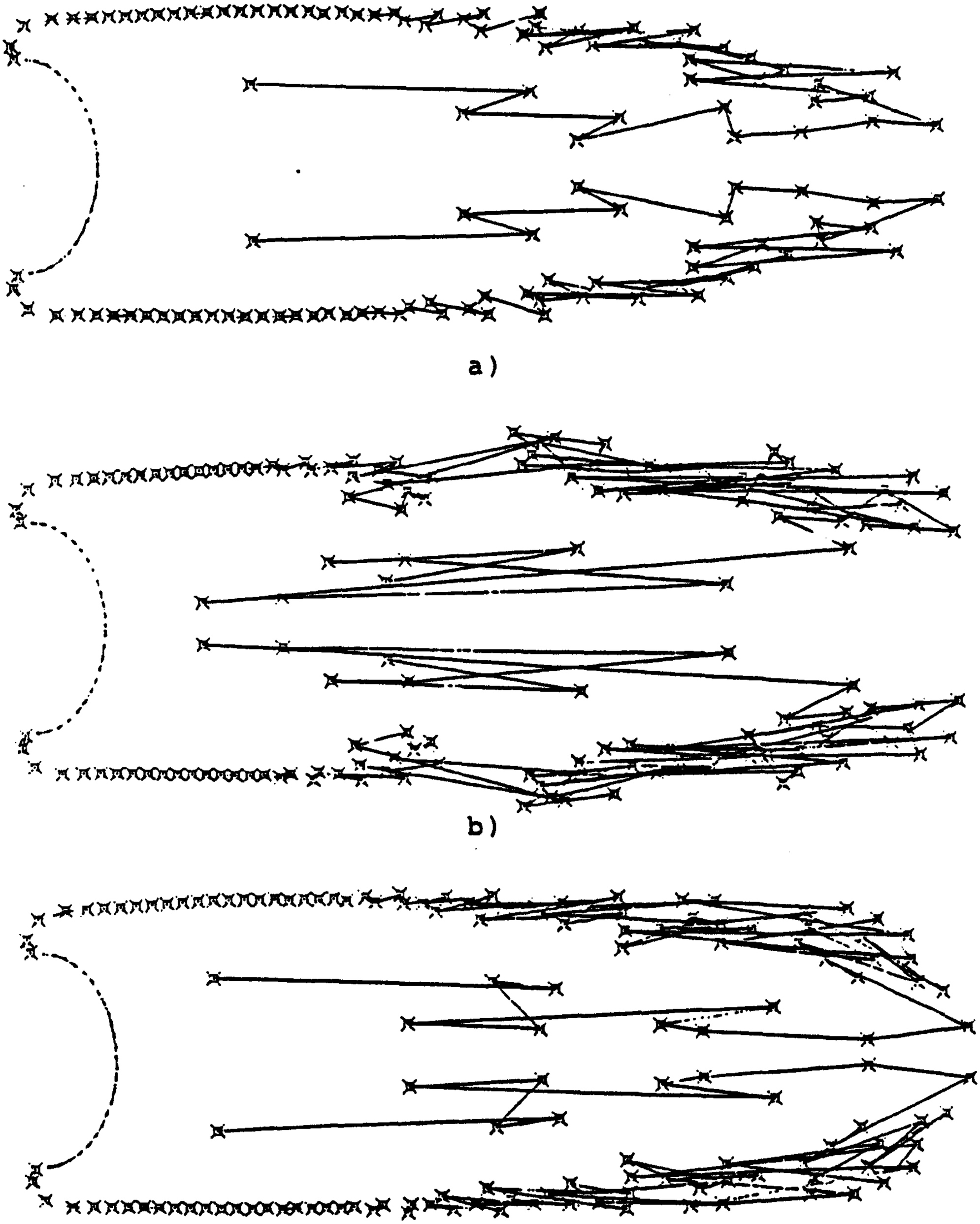

a)

b)

c)

FIGURE 6.3: THE WAKE FLOW PATTERN DEVELOPED AT SUCCESSIVE TIME INTERVALS BY THE CANOPY X1/Y1=0.7 , X2/Y1=07

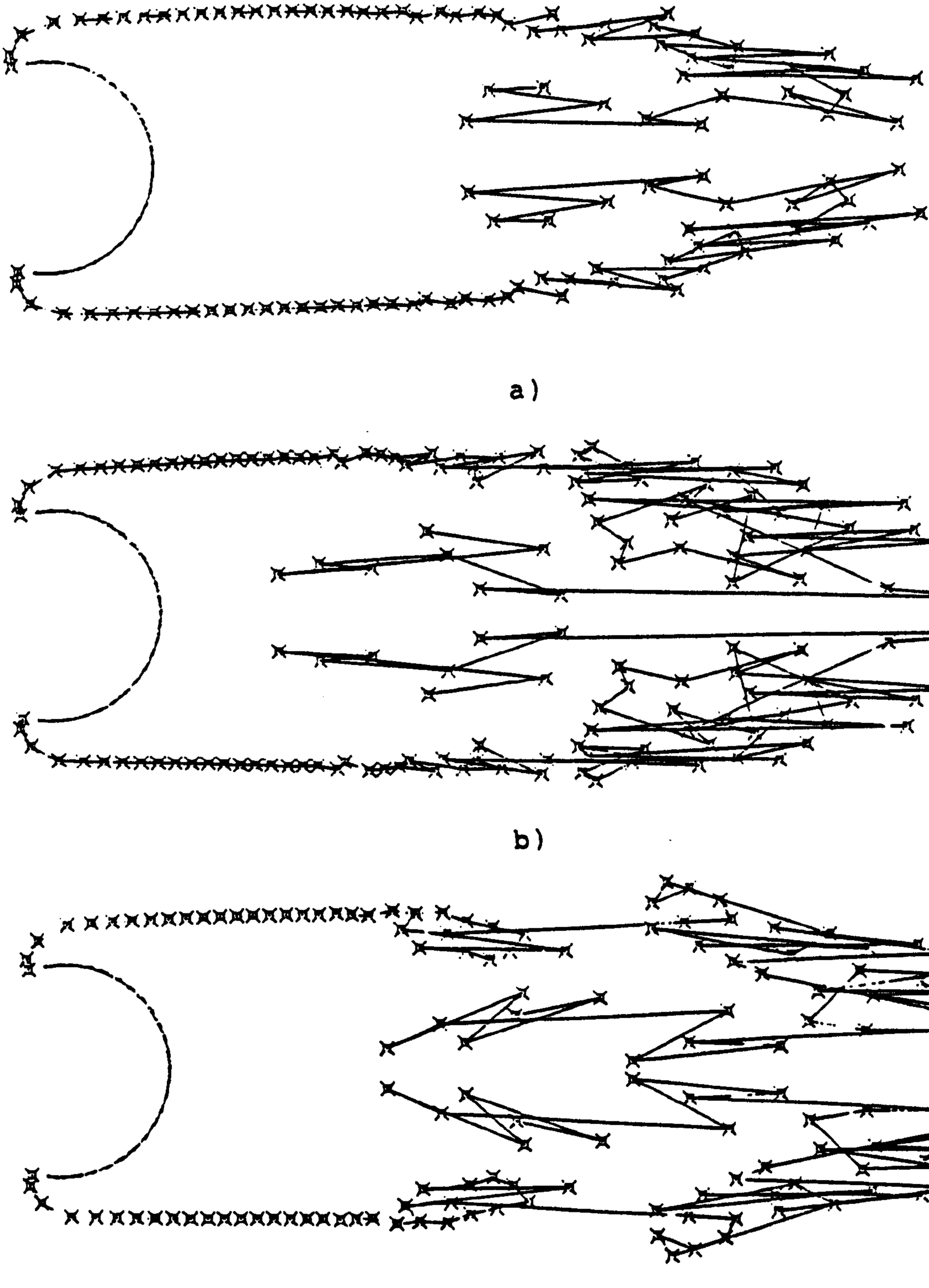

a)

b)

c)

FIGURE 6.4: THE WAKE FLOW PATTERN DEVELOPED AT SUCCESSIVE TIME INTERVALS BY THE CANOPY X1/Y1=1 , X2/Y1=1.2

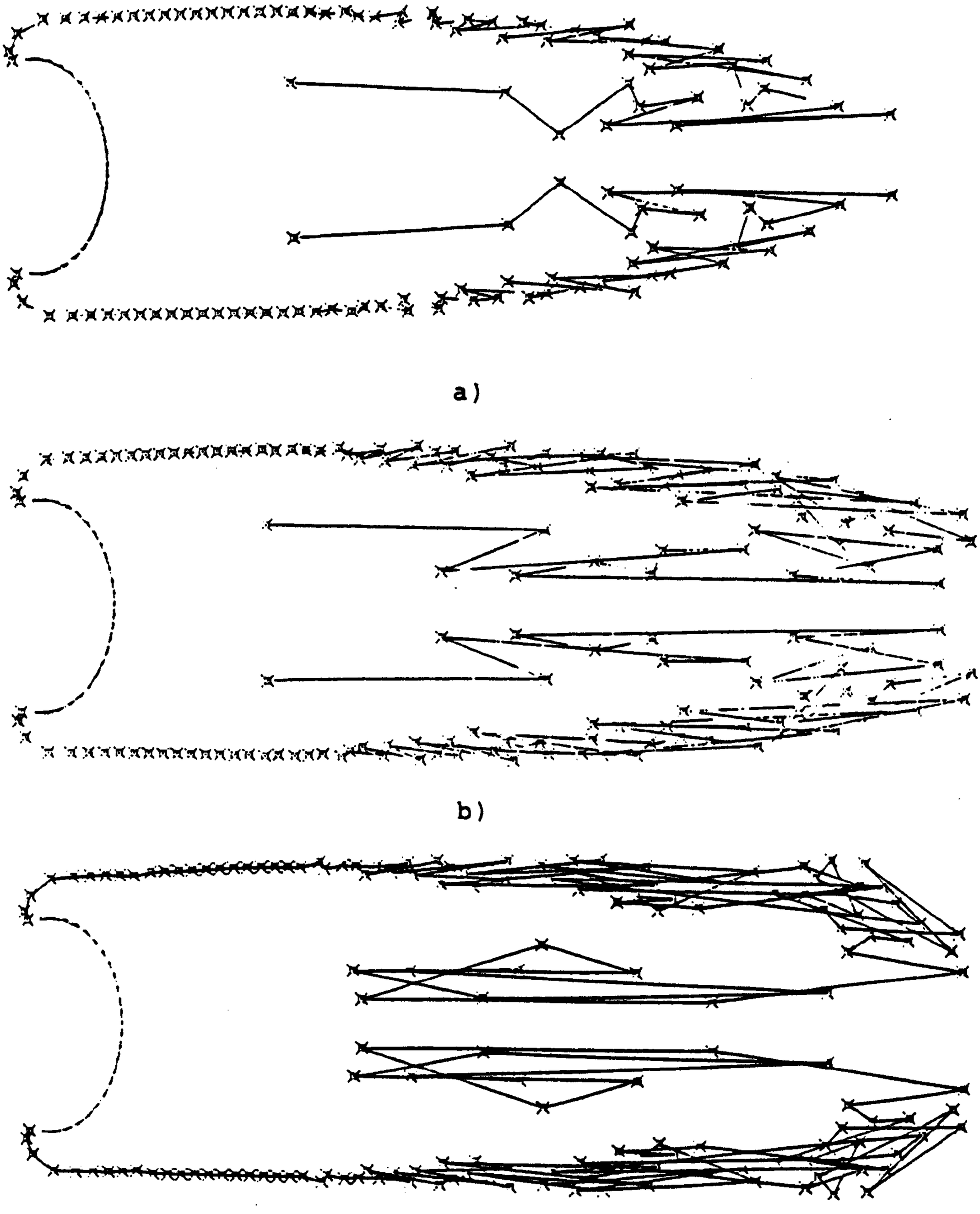

a)

b)

c)

FIGURE 6.5: THE WAKE FLOW PATTERN DEVELOPED AT SUCCESSIVE TIME INTERVALS BY THE CANOPY X1/Y1=0.7 , X2/Y1=0.8

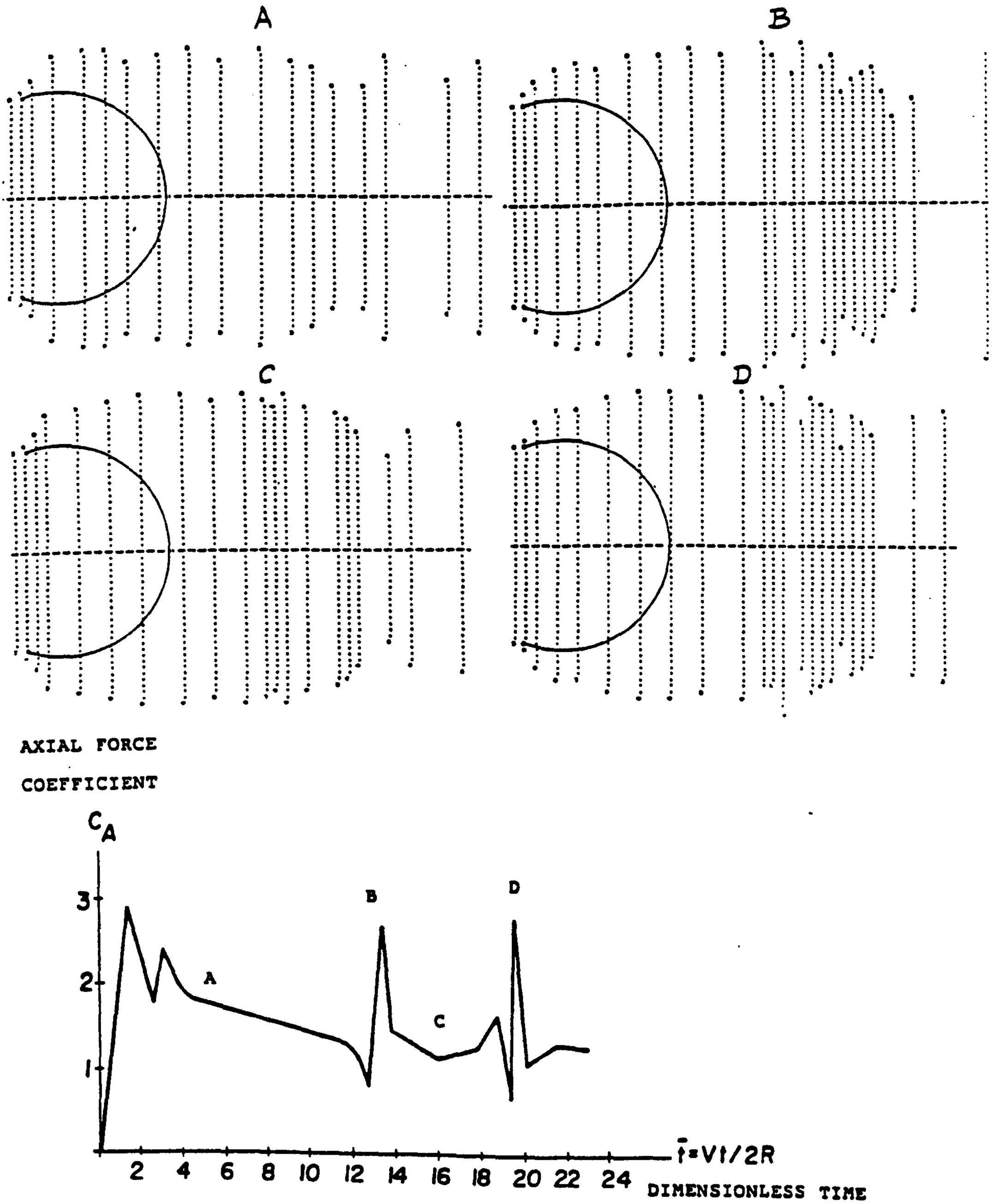


FIGURE 6.6: THE WAKE FLOW AND THE AXIAL FORCE, $C_A$, DEVELOPED ON A HEMISPHERE

## 6.1.1 THE INFLUENCE OF CANOPY SHAPE ON THE TIME-DEPENDENT AXIAL FORCE

As previously detailed, the wake periodicity determines the gross characteristic of the wake flow.

Figure 6.7 shows the time-dependent axial force developed on two different canopy shapes. The fluctuations in the axial force do not behave precisely periodically thus, for a given shape, the Strouhal number can only be defined as an average quantity.

The value of the axial force developed between two consecutive fluctuations, or spikes in figure 6.7, will be defined as the mean axial force, while the instantaneous Strouhal number will be defined as that Strouhal number which is based on the axial force fluctuation period.

Figure 6.8 show the dependence of the mean axial force coefficient ($\bar{C}_A$)and the Strouhal number developed on spherical and elliptical canopies of various bluffnesses.

Figure 6.9 shows that for highly-bluff canopies the fluid tendency is to reattach on the unwetted canopy side. When this fairing effect occurs the applicability of the present model is questionable.

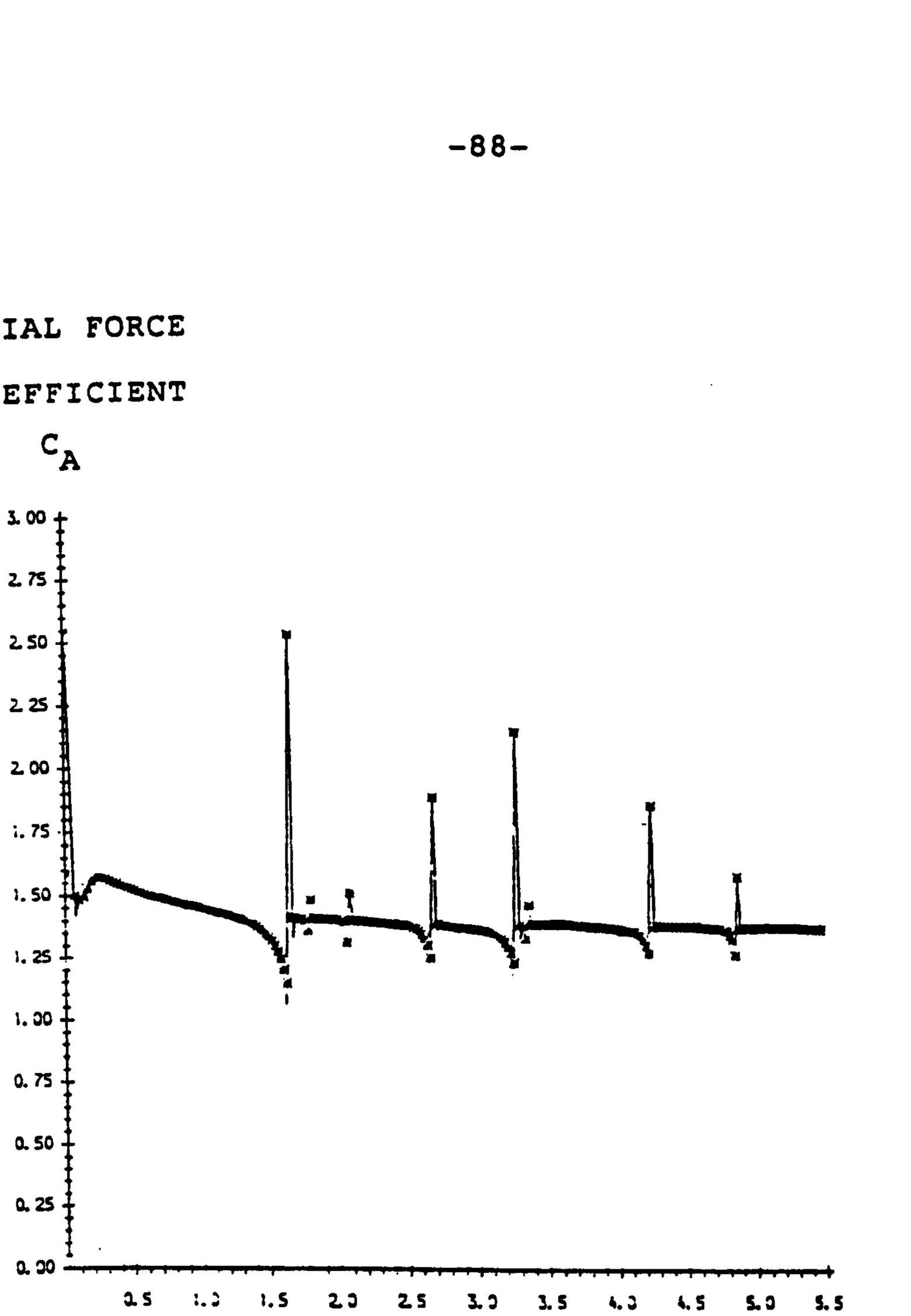


a) $X1 = 1m$ $X2 = 1m$ $Y1 = 1m$

free stream velocity = 15 m/sec

FIGURE 6.7: TYPICAL AXIAL FORCE COEFFICIENT, $C_A$, DEVELOPMENT

(continued on the next page)

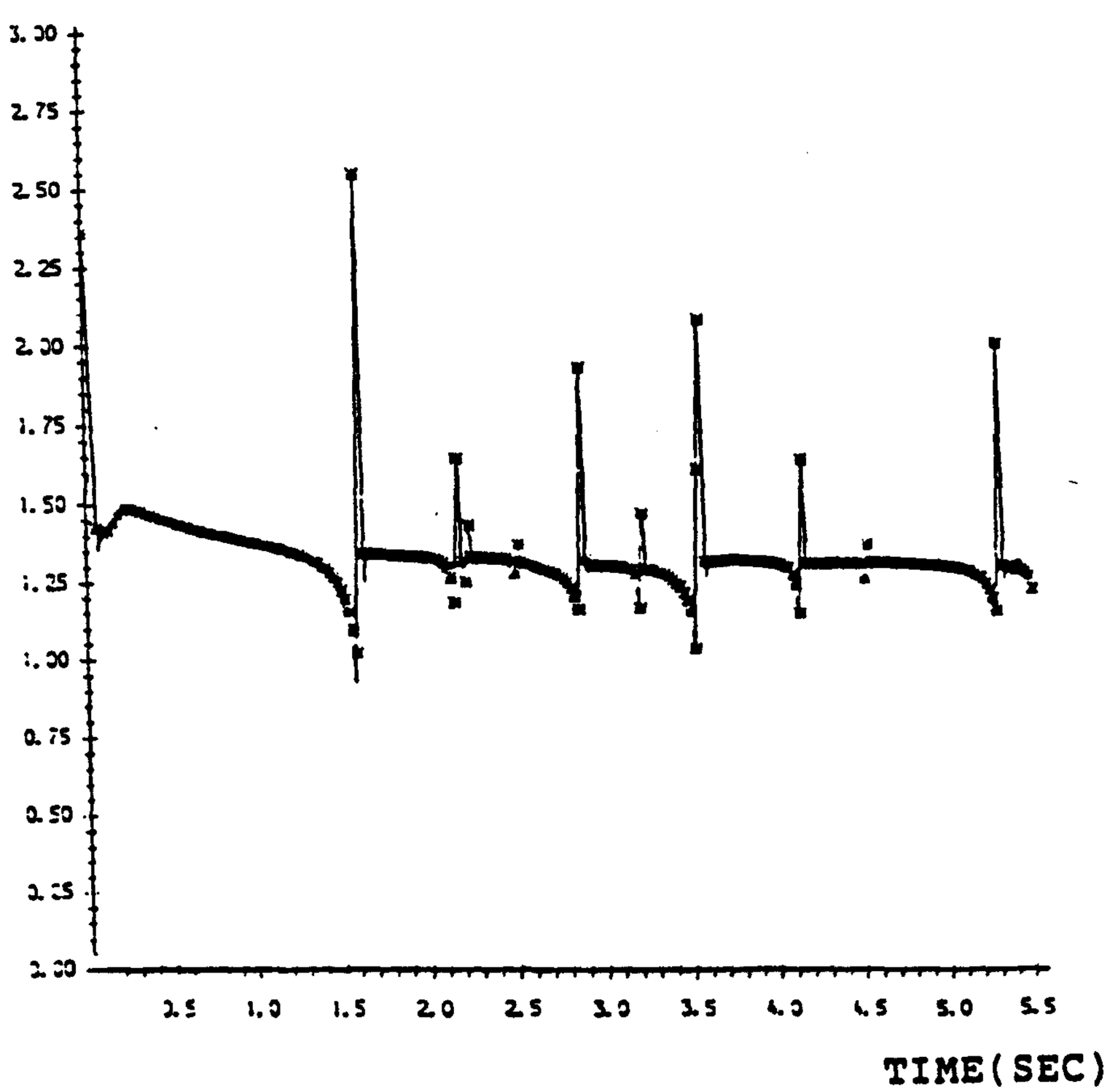


b) X1 = 1m  Y1 = 1m  X2 = 0.9 m

free stream velocity = 15 m/sec

FIGURE 6.7: TYPICAL AXIAL FORCE COEFFICIENT, $C_A$, DEVELOPMENT (continuation)

Text cut off in original

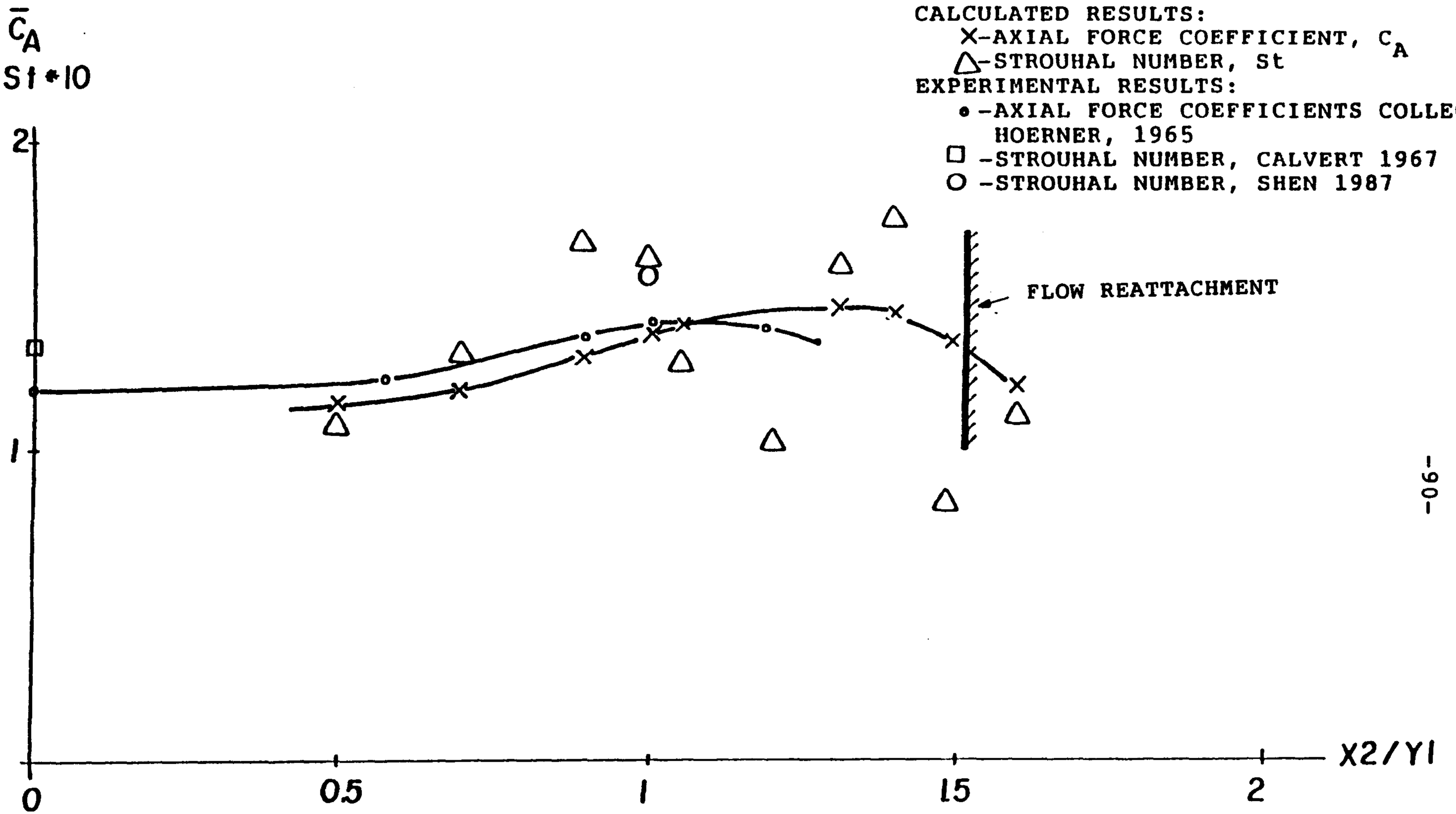


a) SPHERICAL CANOPIES

FIGURE 6.8: THE MEAN AXIAL FORCE COEFFICIENT, $\bar{C}_A$, AND THE STROUHAL NUMBER, St, FOR VARIOUS CANOPIES

(continued on the next page)

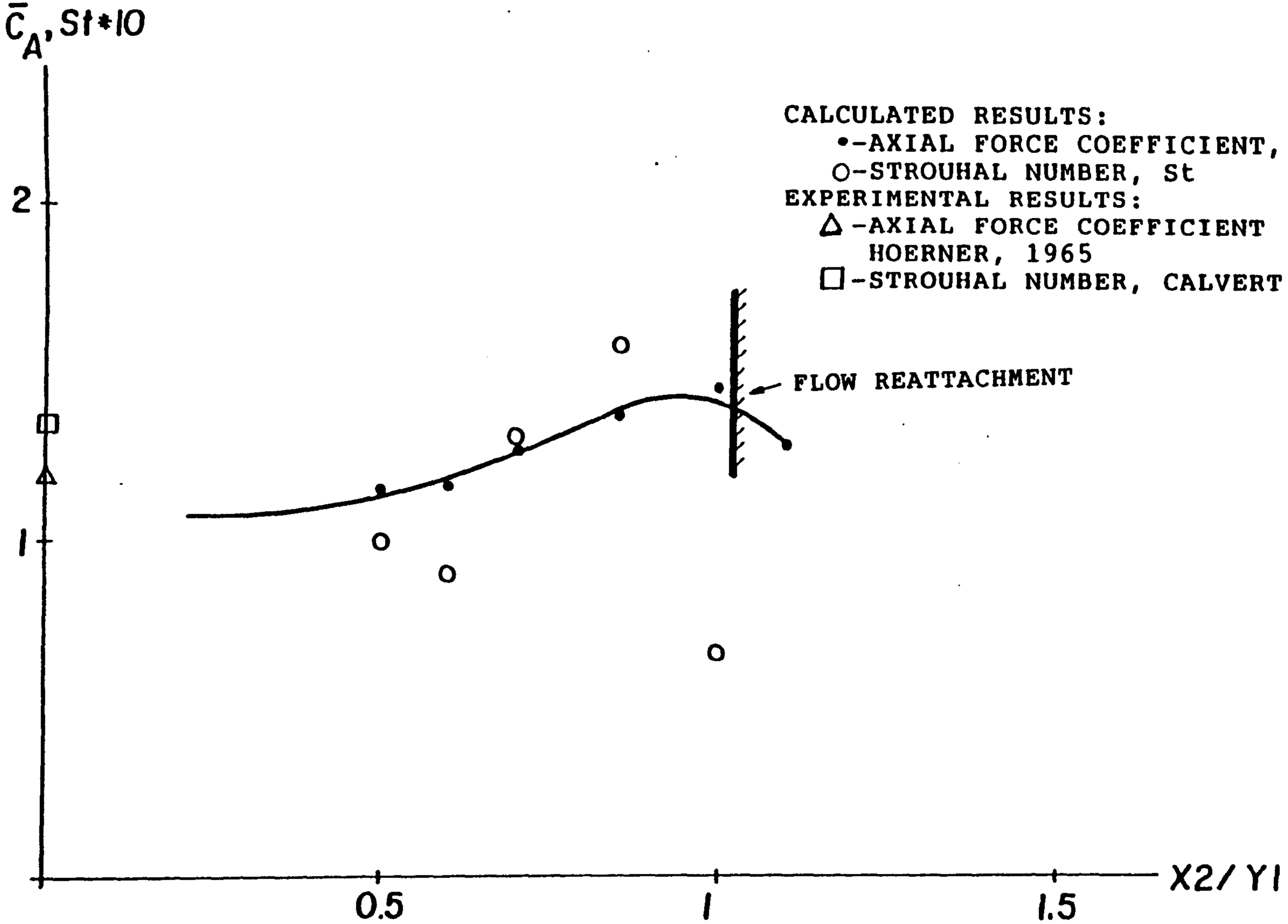


b) ELLIPTICAL CANOPIES

FIGURE 6.8: THE MEAN AXIAL FORCE COEFFICIENT , $\bar{C}_A$, AND THE STROUHAL NUMBER, St, FOR VARIOUS CANOPIES (continuation)

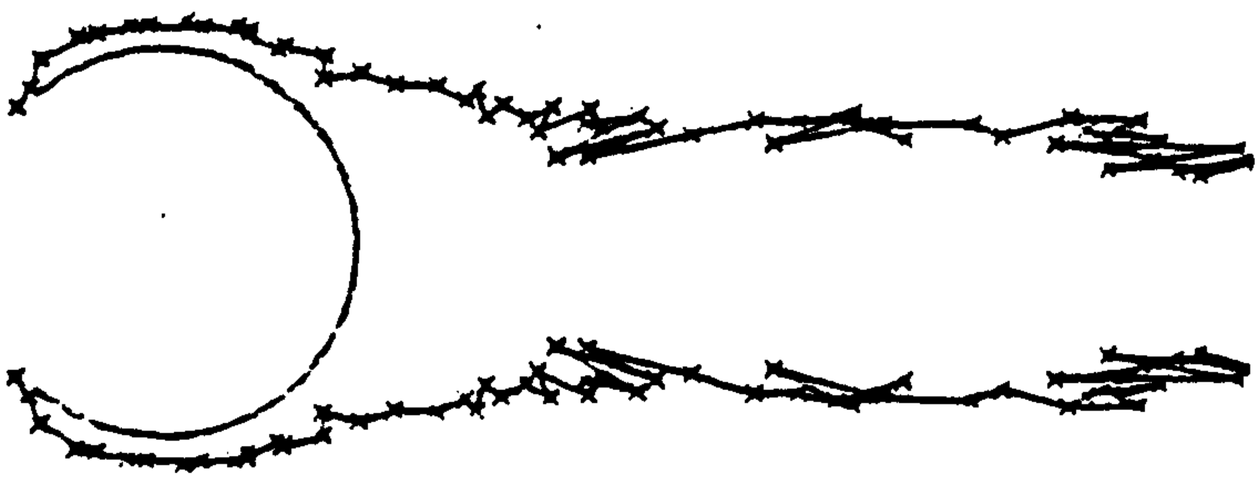

a) X2/Y1=1.65 X1/Y1=1

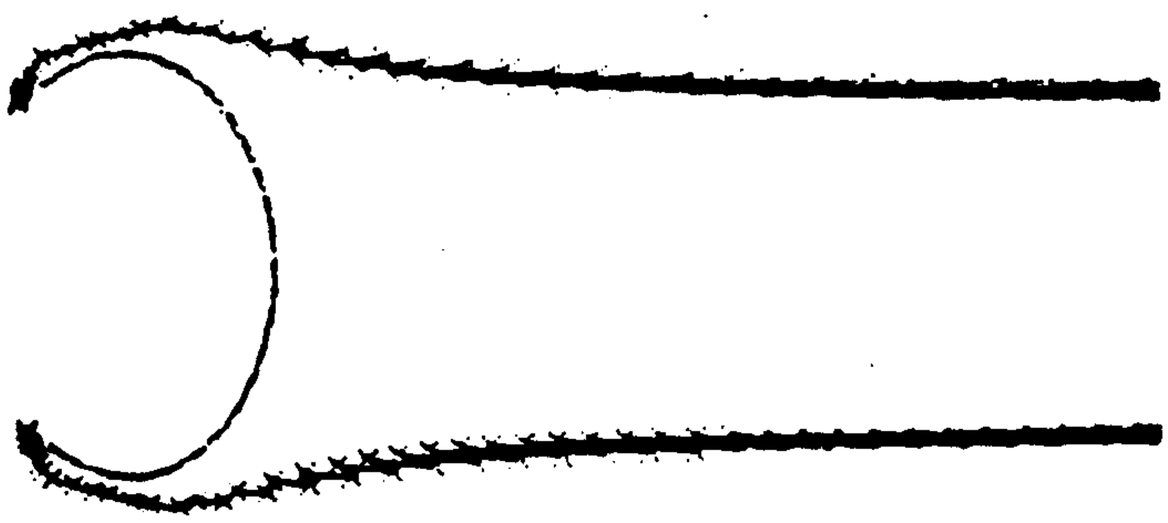

b) X2/Y1=1.1 X1/Y1=0.7

FIGURE 6.9: THE FLOW REATTACHMENT TREND FOR HIGHLY BLUFF CANOPIES

The range of variations of the instantaneous Strouhal number about the average values shown in figure 6.8 was about ±0.015 for all the configurations considered. These results are in good agreement with the known experimental data.

The mean axial force coefficient and the Strouhal number exhibit a similar dependence on the body bluffness (i.e. X1/X2).

In view of the uncertainty range in the calculated Strouhal number (±0.015), it could well be that its variation with body bluffness is smaller than that shown in figure 6.8. Thus, the Strouhal number is almost constant for all the configurations, its value being about 0.13.

Owing to the lack of experimental data concerning the three-dimensional separated flow, experimental investigations of two-dimensional separated flow are considerd in this context.

Roshko (1954 a) found experimentally that for two-dimensional bodies, the Strouhal number is a function of their bluffness. The measured Strouhal numbers, related to the projected width of the bodies, were (at a Reynolds number of about $10^4$):

| | | |
|---|---|---|
| -for a plate normal to the flow | (→ \| ) | 0.135 |
| -for a $90^o$ wedge | (→ < ) | 0.18 |
| -for a circular cylinder | (→ O ) | 0.20 |

In a subsequent experimental study, Modi V. & Slater J. (1977) found that the Strouhal number (at a Reynolds number

of $10^4$),for a $90^o$ degree structural angle section (→ > ) was 0.135.

Thus, the trend found by Roshko would appear to be valid only up to a certain bluffness magnitude; when this is exceeded the variations in the Strouhal number with the bluffness seem to have no practical significance.

A similar trend, for three-dimensional axisymmetric flow, can be found in Calvert's (1967,b) experimental data. Figure 6.10 shows the base pressure coefficient behind cones. These results also show that in axisymmetric separated flow when a certain degree of bluffness is exceeded, the base pressure and subsequently the wake flow appears to be only a weak function of the immersed body's shape.

It could thus be that the predicted tendency for both the axial force coefficient and the Strouhal number developed on bluff canopies (figure 6.8) to vary little with canopy shape is appropriate and is supported by the few experimental data available.

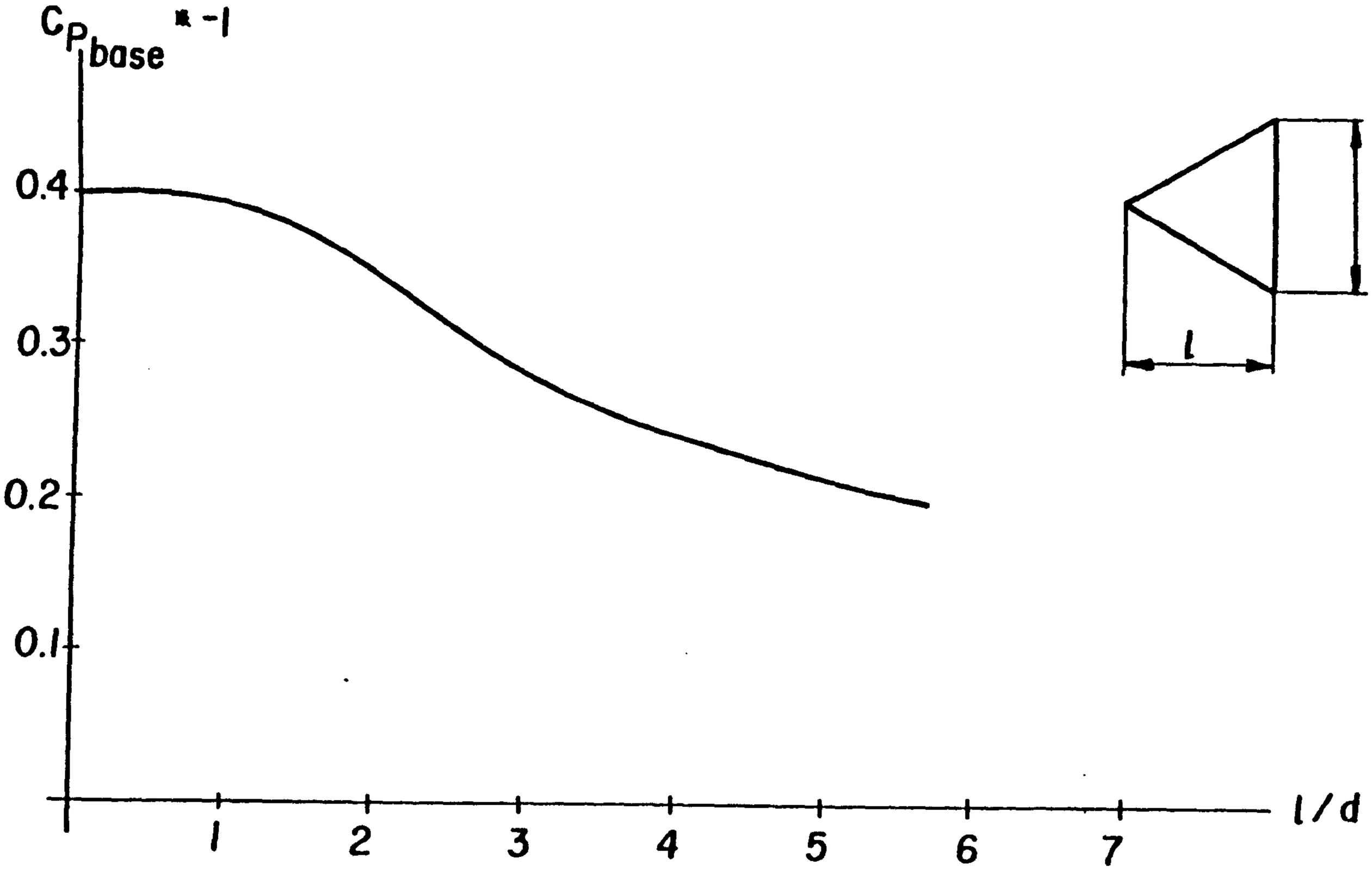





FIGURE 6.10: THE BASE PRESURE , $C_{p_{BASE}}$ OF CONES (based on Calvert's experiments,1967 b)

## 6.1.2 THE MEAN AERODYNAMIC PROPERTIES OF THE NEAR WAKE

As has been shown, axial force unsteadiness manifests itself by fluctuations occurring at almost equal intervals, the duration of such a fluctuation being much smaller than the characteristic period between two consecutive fluctuations. Therefore, during most of the flight time the canopy experiences an almost steady aerodynamic load.

On this ground, it is useful to investigate some average, aerodynamic properties such as the mean velocity distribution at different distances downstream of the canopy, together with the wake shape developed behind it.

Figure 6.11 shows the flow developed about three canopies, whose shapes are sectors of spheres after about 25 dimensionless time ($t*V_\infty/(2R)$) units, counted from the motion commencement. The near wake width has been considered to be the average vortex ring layer diameter and the near wake length as the distance between the canopy hemline and the shedding region of the vortex rings cluster. Then, by visual inspection of figure 6.11, it is seen that as the ratio X1/X2 varies between 0.5 and 1.4, this ratio X1/X2 defining canopy bluffness, both the near wake width and its length are unaffected.

Figure 6.12 shows the calculated mean resultant velocity distribution across the wake developed behind a flat canopy at several different distances downstream of the canopy hemline. The mean velocity distribution was found to be

essentially independent of the canopy shape.

The velocity profiles show the existence of a region behind the canopy behaving, on the average, as a closed bubble with a stagnation point on the wake center line at 2.1-2.5 diameters downstream of the separation line.

The lack of dependance of the mean near wake structure with the canopy shape variation helps to explain the weak variation of the mean axial force coefficient and Strouhal number with the canopy bluffness which was described in the previous section 6.1.1.

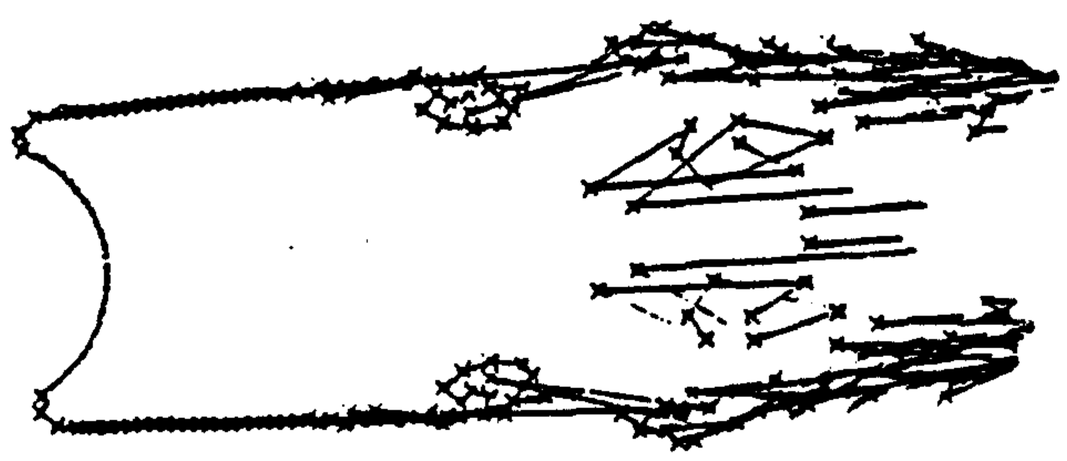

a) X1/Y1=1 X2/Y1=0.5

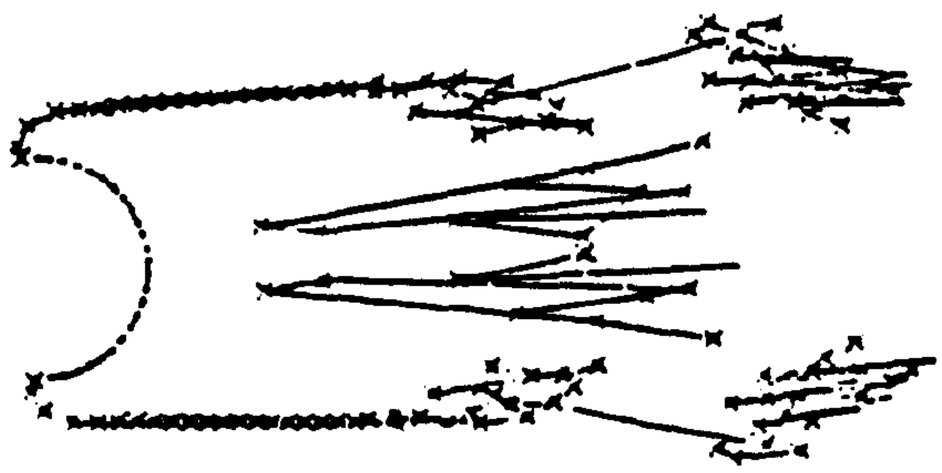

b) X1/Y1=1 X2/Y1=1

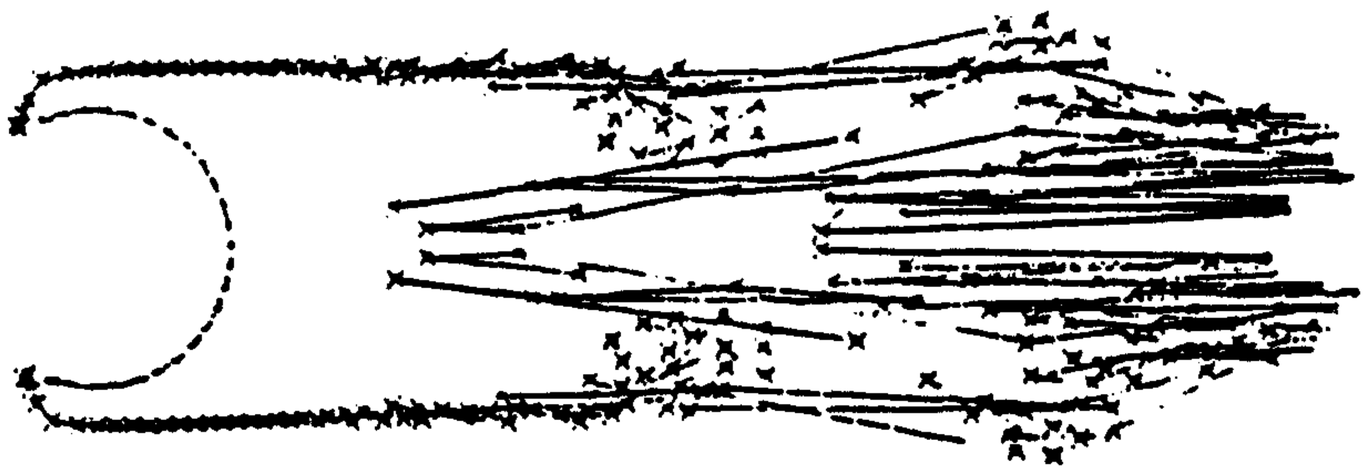

c) X1/Y1=1 X2/Y1=1.4

FIGURE 6.11: THE NEAR WAKE STRUCTURE FOR CANOPIES OF DIFFERENT BLUFFNESS

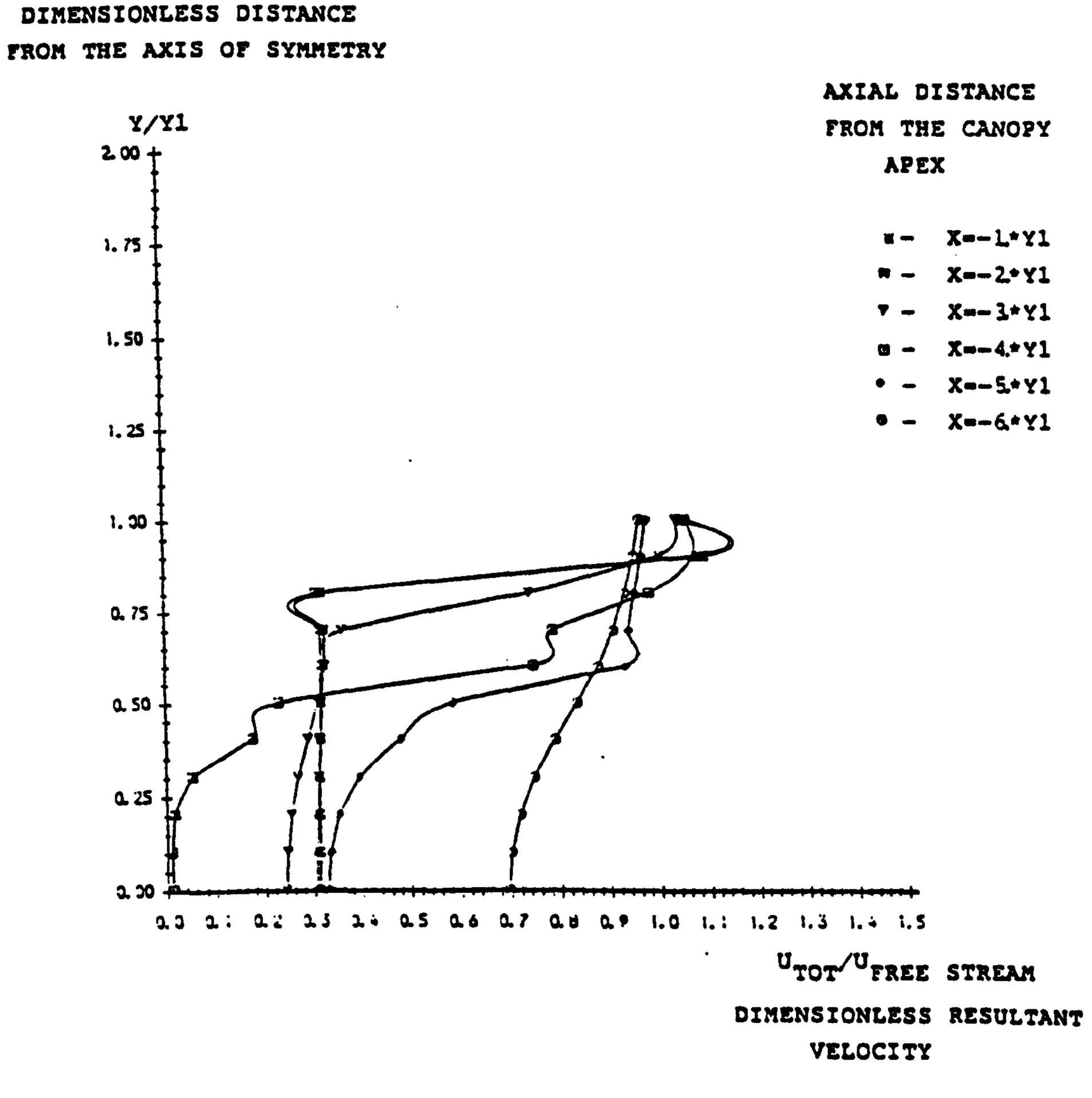


FIGURE 6.12: THE MEAN RESULTANT VELOCITY DISTRIBUTION IN THE WAKE DEVELOPED BEHIND A FLAT CANOPY; X1/Y1=1 X2/Y1=0.5

## 6.1.3 POROSITY EFFECTS ON THE AXIAL FORCE

In the present method of porosity representation the basic assumption is that porosity variation causes only second-order effects to the axial aerodynamic force.

This assumption is supported by empirical relations such as that obtained by Heinrich & Uotilla (1977). In axisymmetric, high Reynolds number, incompressibe flows they measured the differential pressure distribution on 20 degree conical ribbon parachute canopies having various geometric porosities, $\lambda$. By integrating the pressure distribution they found that:

$$C_A = 0.467 + 0.132L_C - 1.71\lambda^2 \qquad 6.1$$

where $L_C$ is the ratio between the chord length to the nominal diameter and $C_A$ is referred to the constructed area.

In the present model the porosity is represented by permitting the existence along the control circle of a velocity component normal to the canopy surface. By making such a representation the porosity can vary over the canopy.

The flow velocity through the canopy surface is calculated by using equation 4.32.

Intuitively, it appears that the canopy can only be represented by a vortex sheet if the normal velocity component caused by porosity is small. It is suggested that the maximum average normal velocity should be about 0.10-0.15 of the free stream velocity, i.e. $\lambda_{MAX} \approx 15\%$.

Figure 6.13 shows the influence of porosity on the calculated, mean axial force coefficient and on the Strouhal number developed on both a hemispherical and an elliptical canopy. Since the elliptical canopy shape is similar to those used in the Henrich & Uotilla (1977) experiments, the axial force predicted by equation 6.1 is also presented in figure 6.13.

The calculated, mean axial force diminishes as the porosity increases. This trend agrees with both the experimentally-based equation 6.1 and data presented by Cockrell D.J. (1987).

The Strouhal number varies nonlinearly with porosity. At first an increase in porosity causes a corresponding increase in Strouhal number then, following a further porosity increase the Strouhal number suddenly falls to zero, i.e. the flow ceases to be periodic (figure 6.14). Figure 6.15 shows the flow pattern when the wake flow periodicity has been suppressed by the porosity.

Because there are insufficient experiments about porosity effects on the Strouhal number in axisymmetric flows, the model predictions can only be compared with results from two-dimensional experiments. Such experiments have been performed by Bearman P. (1967). He found a functional dependence of Strouhal number on porosity which is qualitatively similar to that shown in figure 6.14.

In later experimental studies (Castro I., 1971, and Low H. & Newman B., 1986) the Strouhal number was found to increase monotonically with the porosity for $\lambda<15\%$. The flow

visualisation photographs presented by Low H. & Newman B. (1986) show a very smooth flow around porous canopies. This appears to be in contradiction to measurements which they made of the increase in the wake flow periodicity with increasing porosity.

At this stage, there is therefore no clear experimental evidence to support the calculated trend presented in figure 6.14. Moreover, it is conceivable that the real flow through porous canopies is strongly affected by both the local surface finish and the local Reynolds number. For this reason, the present porosity representation may be unsatisfactory. However, when considering the porosity influence on the axial force it may well be that the main flow field properties are well predicted by the model.

In order to find how the local porosity affects the canopy aerodynamic properties two cases were simulated. The first case was of canopies with a skirt of 20% geometric porosity and the second case was of canopies having a region of similar porosity around the apex. The canopy shape parameters used in these simulations were:

a)-an hemispherical canopy: X1/Y1=X2/Y1=1

b)-an elliptical canopy : X1/Y1=X2/Y1=0.7

The results show that by using the porous skirt the axial force development was very like that for a uniformly-distributed geometric porosity of about 2-5%. Thus, the mean axial force was slightly lowered and the wake flow periodicity suppressed. When the porous region was about the apex however, the mean drag was unaffected but the Strouhal

number was significantly increased , e.g. for the hemispherical shape, the Strouhal number was 0.2, about 25% higher than the corresponding value for an imporous canopy.

Using the present model it is possible to design a canopy possessing any desired pressure distribution. For example, figure 6.16 shows the geometric porosity distribution which results in an almost uniform pressure distribution over the entire canopy.

The basic assumption for porosity simulation in the model is that the porosity magnitude is small, so that the canopy representantion by a vortex sheet remains valid.

If an average geometric porosity significantly higher than about 15% is to be simulated a more accurate representation of canopy porosity must be adopted. In such cases it could well be that either Strickland's J. (1986) suggestion of simulating every imporous canopy segment by an independent vortex sheet or representation of the canopy surface by ring sources as suggested by Muramoto K. and Garrard W., (1984) were more suitable approaches.

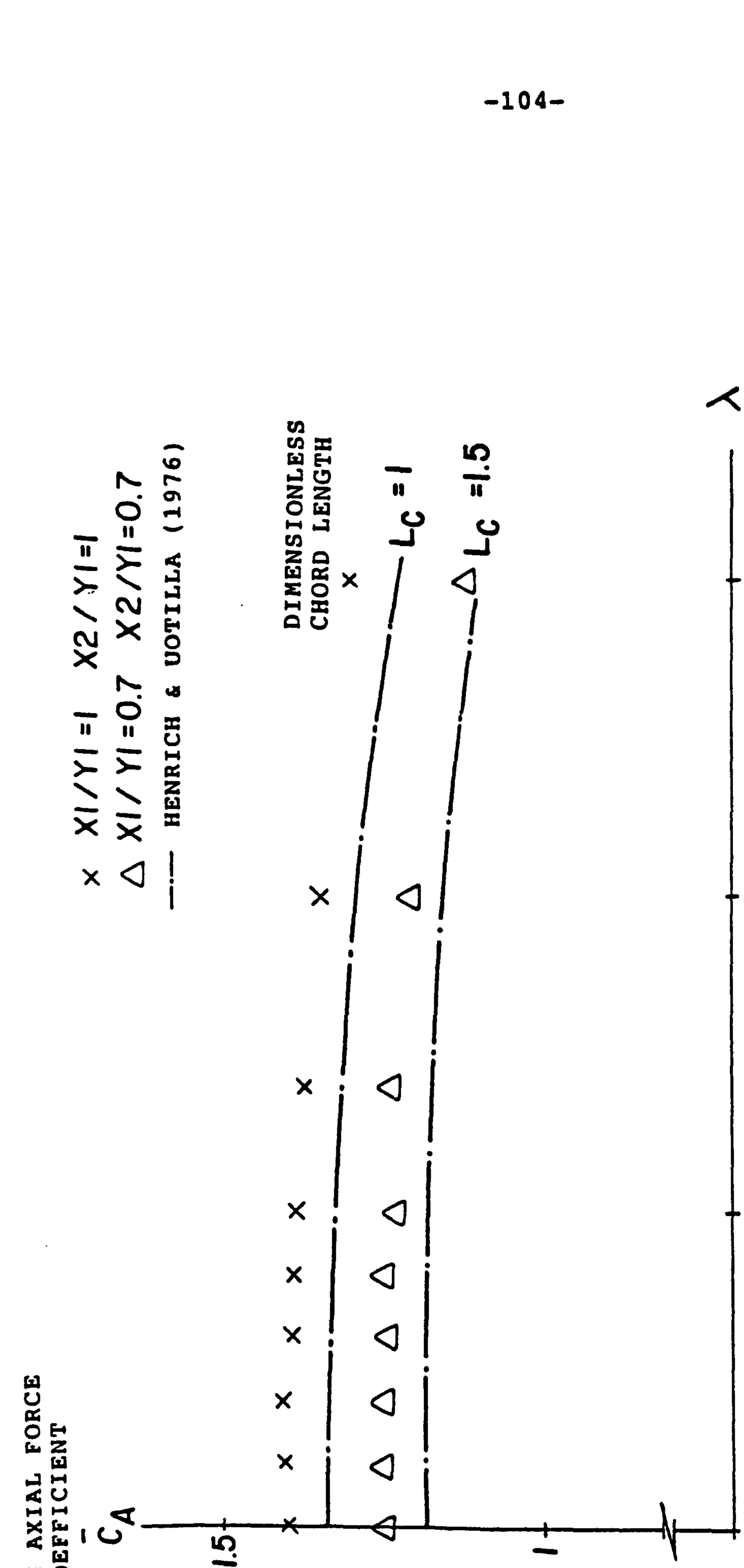


FIGURE 6.13: THE POROSITY, λ, INFLUENCE ON THE MEAN AXIAL FORCE COEFFICIENT, $\bar{C}_A$.

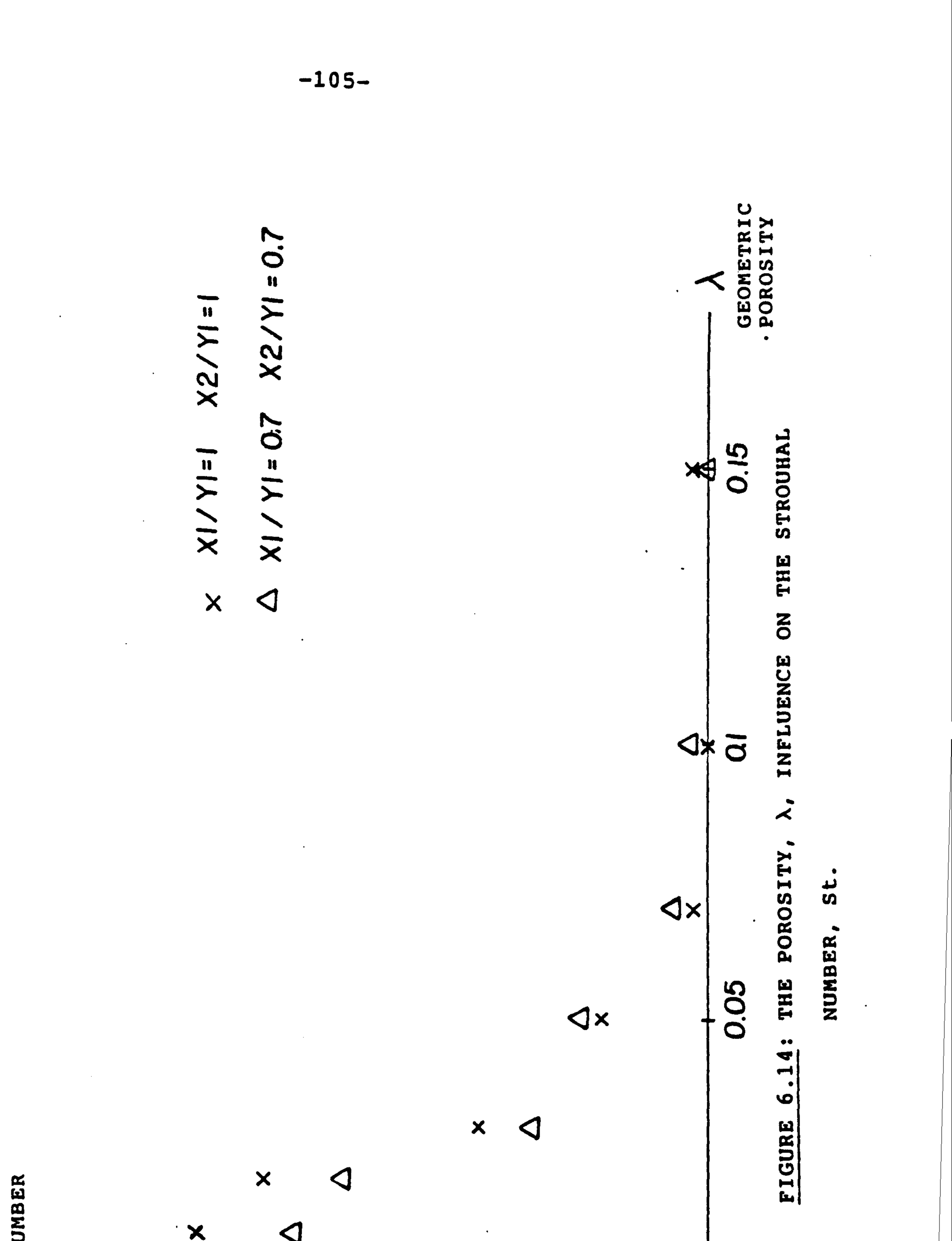


FIGURE 6.14: THE POROSITY, λ, INFLUENCE ON THE STROUHAL NUMBER, St.

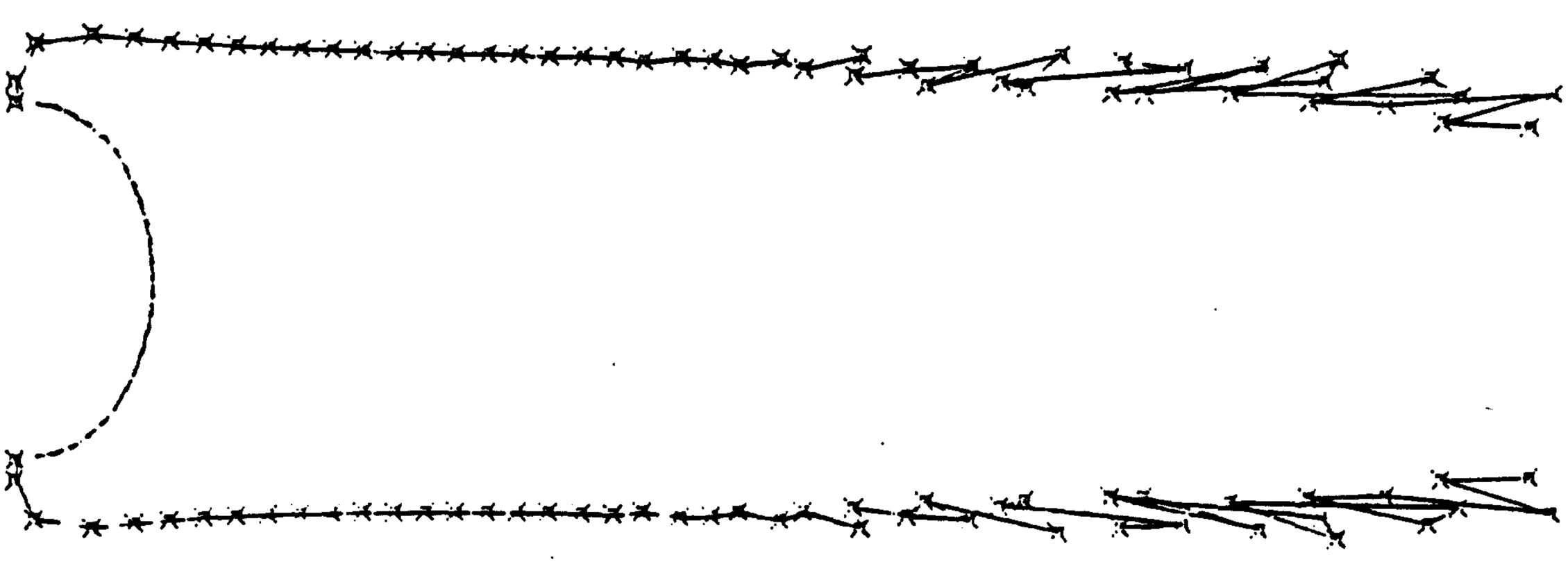

b) X1/Y1=0.7, X2/Y1=0.7

a) X1/Y1=1, X2/Y1=1

FIGURE 6.15: WAKE FLOW PERIODICITY SUPPRESSION BY THE POROSITY .

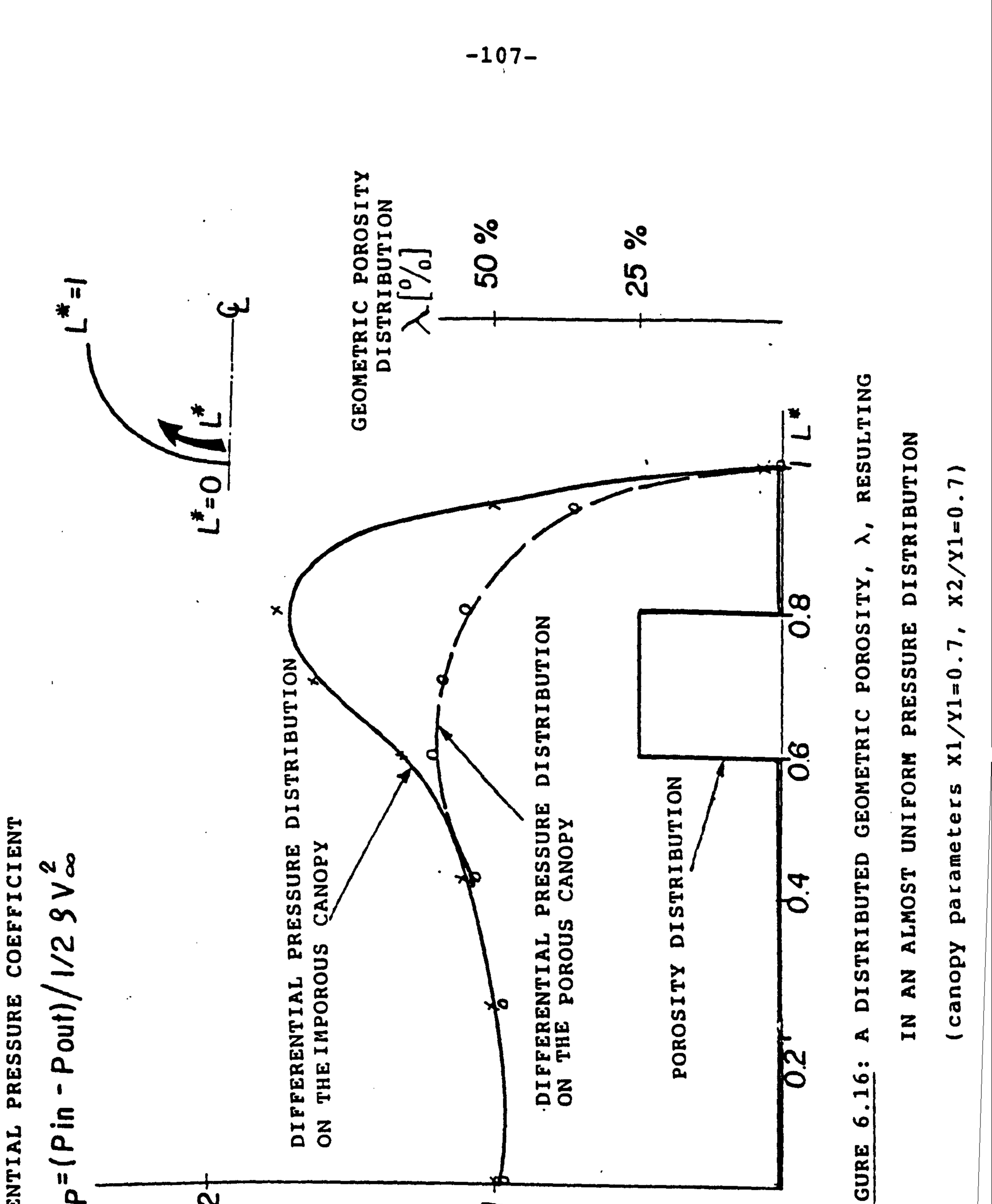


FIGURE 6.16: A DISTRIBUTED GEOMETRIC POROSITY, $\lambda$, RESULTING IN AN ALMOST UNIFORM PRESSURE DISTRIBUTION

(canopy parameters X1/Y1=0.7, X2/Y1=0.7)

## 6.1.4 THE MEAN PRESSURE DISTRIBUTION

Since pressure distribution prediction is of importance in quantifying the structural loading, special attention has been dedicated to achievement of this goal. Figure 6.17 shows qualitatively the differential pressure distribution as calculated by three different approaches.

Curve A in figure 6.17 is the pressure difference which is predicted if attached flow were assumed. Because of the symmetrical location of the stagnation points about the canopy apex the pressure difference at this point is zero and approaching the canopy skirt, near the hemline, it tends to infinity. However, since the flow which is developed around bluff parachute canopies is well separated, curve A is an unrealistic prediction.

When separated flow is assumed but the zero load condition near the separation line at the canopy hem is not accounted for, the resulting differential pressure distribution is qualitatively described by curve B in figure 6.17. Due to the velocity induced by the shed vortex rings the differential pressure near the hemline is less than that shown in curve A but the pressure difference in that region still exhibits considerably larger values than those determined experimentally. Near the canopy apex the differential pressure coefficient is about 1.0. This is because of the very low fluid velocity on the unwetted upper canopy side near its apex and the flow approaching stagnation at the apex

on its wetted lower side.

Curve C shows the pressure difference when both a separated flow is considered and the zero load condition has been imposed near the hemline. In the present model this zero load condition is achieved by simulating the standing eddy which develops downstream of the canopy hemline.

By neglecting the short periods of fluctuations figure 6.18 shows the mean pressure difference which is developed on several canopies having different shapes.

Because of the method used for the determination of the standing vortex ring location described in chapter 5 the calculated differential pressure coefficient near the hemline is not exactly equal to zero but its typical value is |0.15|.

Very good agreement is obtained with various experimental values, as shown in figure 6.18. This agreement provides significant support for the present model.

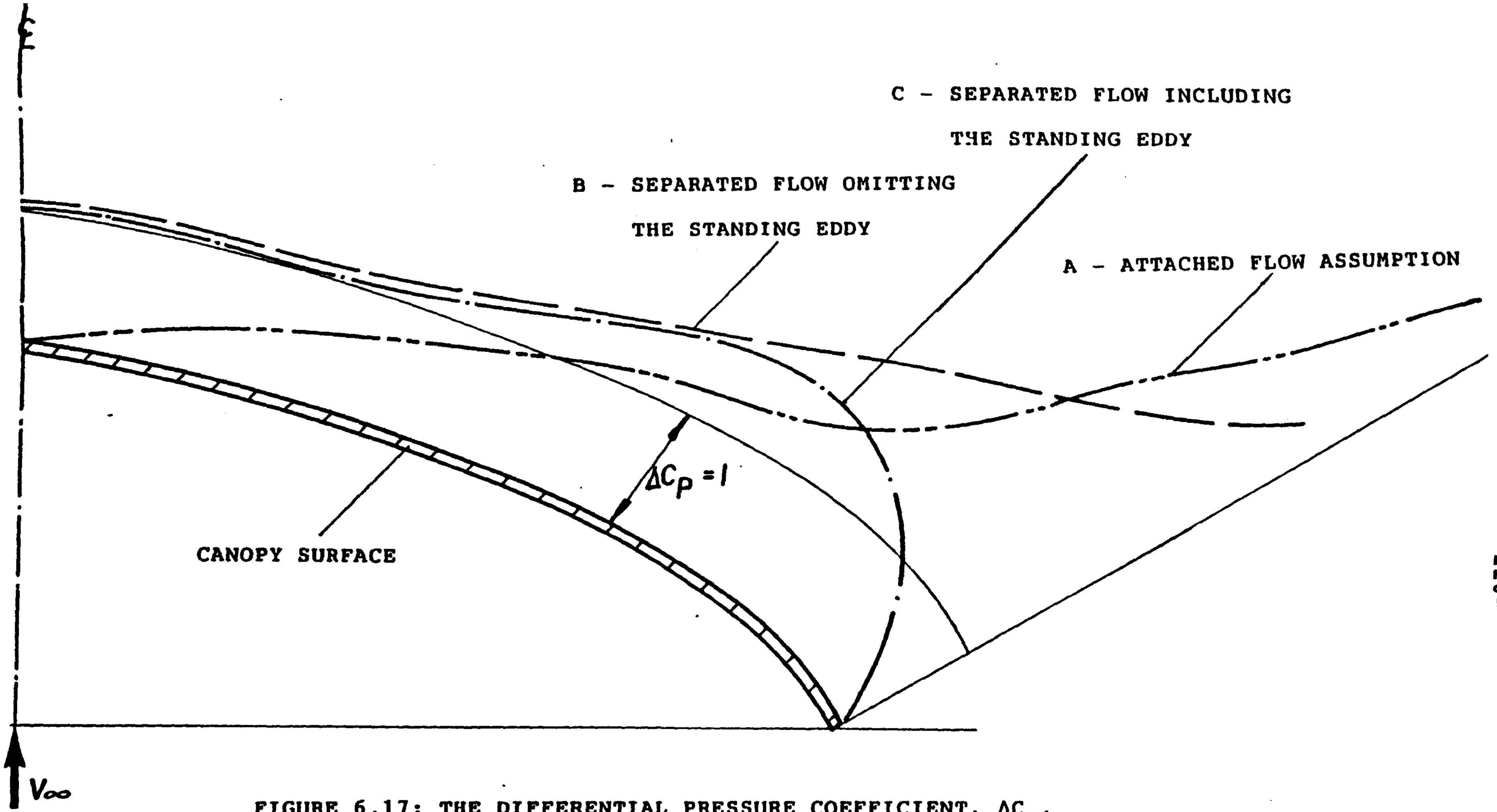


FIGURE 6.17: THE DIFFERENTIAL PRESSURE COEFFICIENT, $\Delta C_p$, ACROSS THE CANOPY CALCULATED BY VARIOUS APPROACHES (a qualitative description)

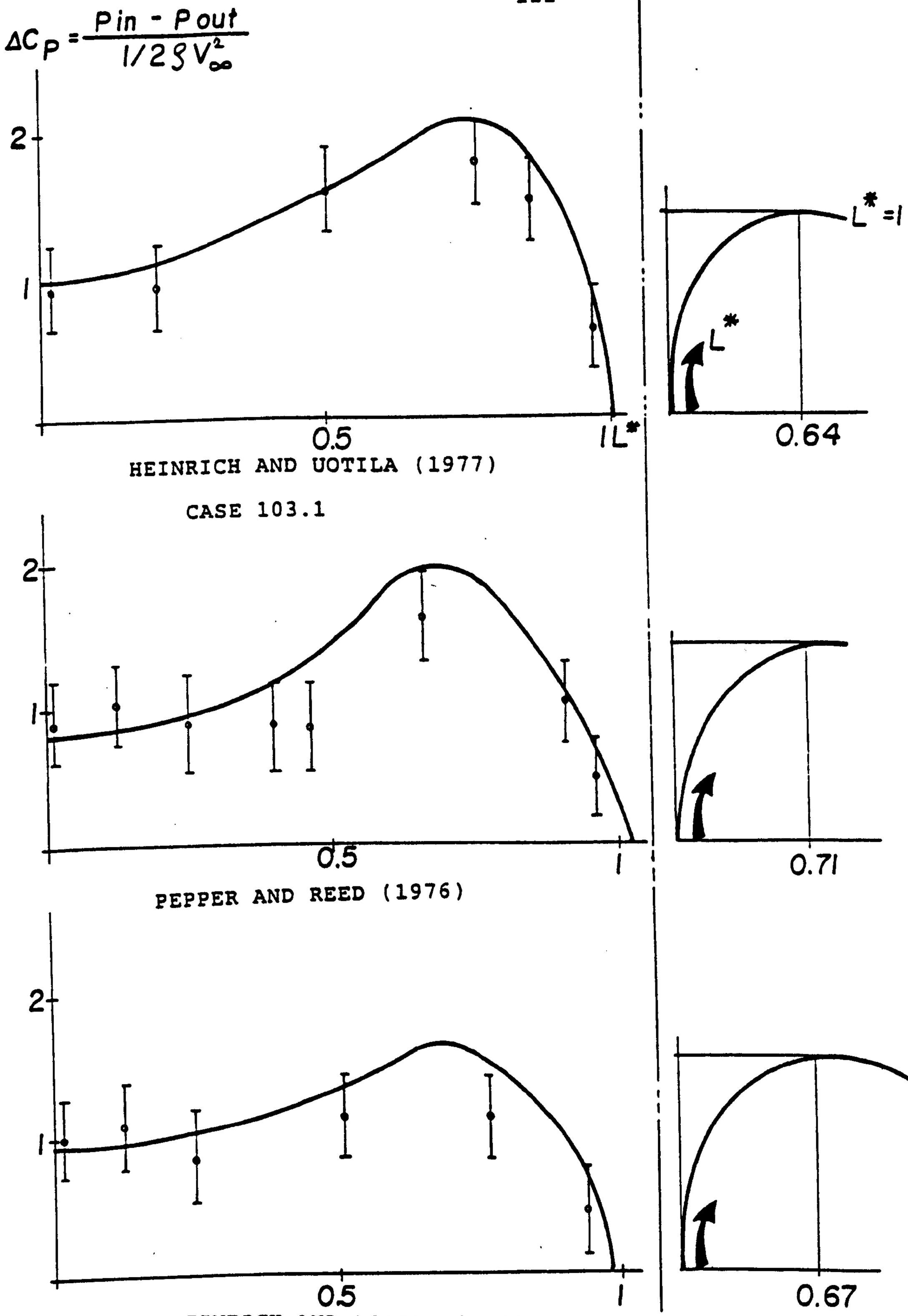


FIGURE 6.18: THE DIFFERENTIAL PRESSURE COEFFICIENT, $\Delta C_p$, DEVELOPED ON VARIOUS CANOPIES (calculation and experiments)

### 6.1.5 THE FREE STREAM REYNOLDS NUMBER EFFECT

In the present model a high free stream Reynolds number has been assumed. Under these conditions the shear layer emerging from the separation line is thin and the dissipation within it can be neglected. It can also be assumed that the vorticity is equally distributed across the vortex ring cores, thus simplifying the calculation of the self-induced velocity.

When a two-dimensional separated wake is simulated by discrete vortex methods the Reynolds number only appears explicitly in the vortex core evaluation (e.g. Sarpkaya & Shoaff, 1979). The core size is used to define a cut-off distance for the induced velocity calculation thus avoiding the infinite velocity which would otherwise occur in the model as the distance to the vortex core center tended to zero.

Since, in section 4.2 it has been shown that in three-dimensional flow the vortex core size affects the magnitude of the self-induced velocity (equation 4.19), in the present model the Reynolds number is explicitly accounted for both through the use of a cut-off distance which is set to equal the vortex core radius and through the self-induced velocity influence on the wake flow.

As Batchelor (1967, 7.2) pointed out , when the ratio between the vortex ring core radius and the vortex ring radius is greater than about 0.01 the fluid carried along by

the vortex ring extends to the axis of symmetry. Since the ratio of the vortex core radius to the vortex ring radius is of the order of magnitude of about $Re^{-0.5}$ (equation 4.24), the lowest Reynolds number which can be simulated by the present model is about $5*10^4$. This does not mean that Eden's (1911) or Stanton & Marshal's (1931) experiments at lower Reynolds number are irrelevant to this research but that for well separated flows at lower Reynolds numbers such as they considered a more exact model of vortex ring vorticity would be required. However, in view of the much higher Reynolds number characterizing the flight of full-scale parachutes, this low boundary does not seriously affect the applicability of the present model.

Figure 6.19 shows calculated results for free stream Reynolds number effects on the axial force developed by a hemispherical canopy. Increasing Reynolds number from about $10^5$ one hundred times causes an axial force coefficient reduction of less than 5% but a more substantial reduction of about 30% in the Strouhal number. Thus, within the Reynolds number range of $10^5$-$10^7$ neither the axial aerodynamic force or the wake flow are strongly dependent on the Reynolds number.

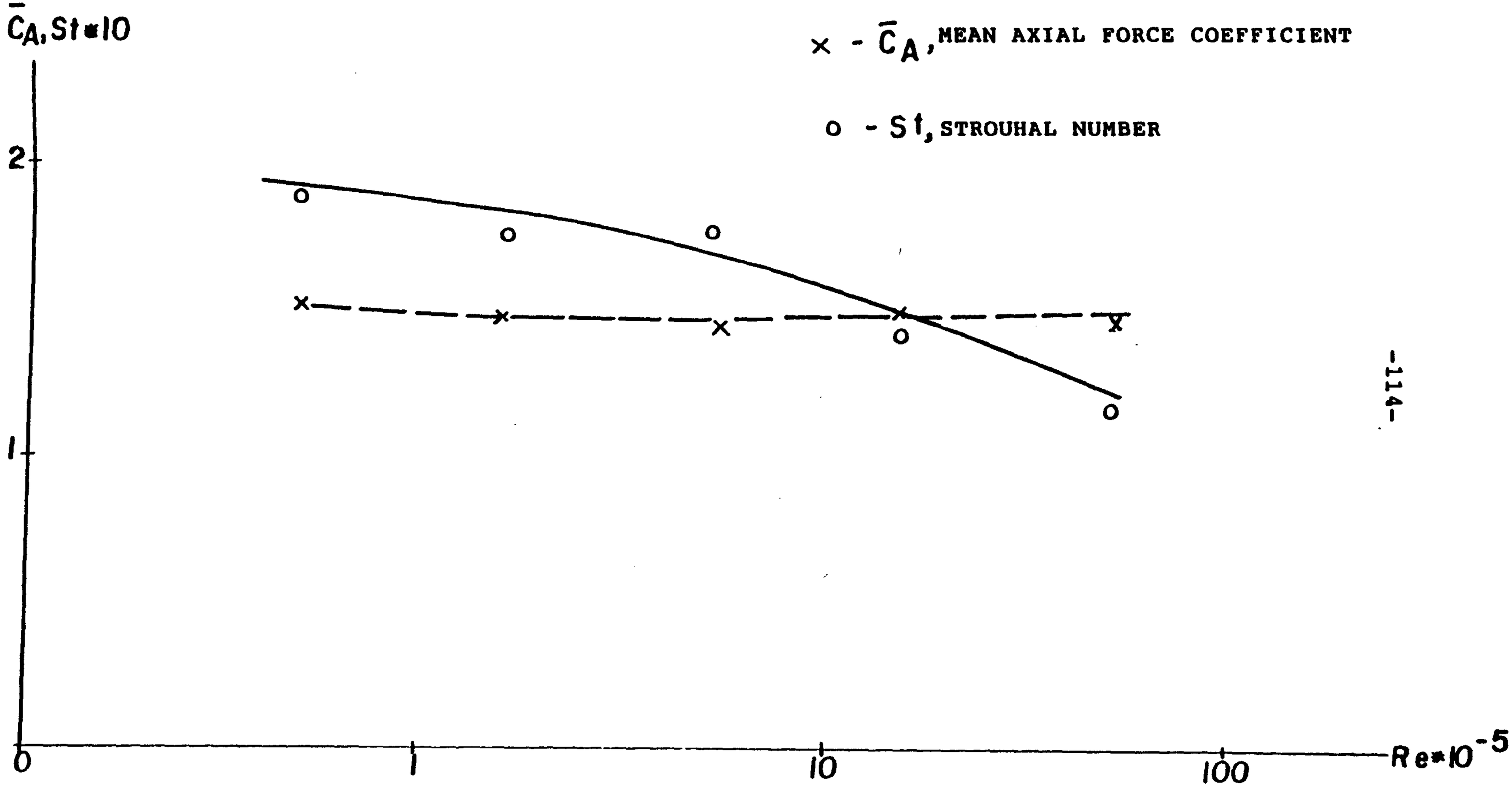


FIGURE 6.19: FREE STREAM REYNOLDS NUMBER, Re, EFFECT ON THE MEAN AXIAL FORCE, $\bar{C}_A$, AND ON THE STROUHAL NUMBER, St.

## 6.2 THE AERODYNAMIC PROPERTIES OF A RIGID CANOPY IN AN UNSTEADY STREAM

It has been explained in section 6.1, that the flow about a parachute canopy is always unsteady, regardless of the free stream conditions. However, when free stream unsteadiness is superimposed on the inherently time dependent flow developed about the canopy the resulting flow becomes very complex and simpler experimental models for force determination have been developed.

By assuming that the axial force can be represented by Morison's formula [Newman N., 1982, 2.13]:

$$A = 0.5\rho S_{ref} C_A V_\infty |V_\infty| + k_{11} \dot{V}_\infty Vol \qquad 6.2$$

and measuring the axial force developed on immersed, unsteadily moving bodies, the constants $C_A$ and $k_{11}$ can be determined. Experimental methods and the various averaging techniques involved in the calculations have been described by Yavuz T. & Cockrell D. (1981), Cockrell D. et al (1986) and Cockrell D.J. (1987).

Equation 6.2 assumes that the force developed by an accelerating body is a sum of an inertial component and a viscous component. Newman N. (1982, 2.11) shows that equation 6.2 is valid for impulsive motion, when the acceleration modulus $\delta$, defined by Iversen H. & Balent R., 1951, and by Cockrell D. , 1987, as the acceleration and projected

diameter product divided by the free-stream velocity squared, is very high.

The extension of Morison's formula towards lower acceleration moduli or high time-dependent motions such as oscillatory motion is questionable and as will be shown in the next sections will not generally lead to realistic results.

This statement is supported by some experimental data.

Iversen H. & Balent R. (1951) measured the resistance experienced by a disk driven through an undisturbed fluid by a constant force applied normal to its surface. Subsequently, by using Morison's formula, they calculated the instantaneous added mass coefficient, $k_{11}$ and found it to be a function of the acceleration modulus.

At very low acceleration moduli the spread of the measured axial force coefficient was large. This can be explained in terms of the time-dependent axial force developed in steady flow which has been previously described.

At higher acceleration moduli they showed that the envelopes of both the measured axial force coefficient and the added mass coefficient converge, the latter becoming close to the magnitude predicted by assuming ideal fluid flow (equation 4.39 developed by Lamb, 1932, article 120).

Therefore, Morison's formula, which implies constant values for both the steady axial force coefficient and the added mass coefficient, would appear to be appropriate only at high acceleration moduli.

In the following sections the model is used to analyse the

axial force development at different acceleration moduli and also in highly time-dependent states, such as oscillatory motion.

The previous history of the flow is also important and its impact on the Morison's formula model will be discussed in the following sections.

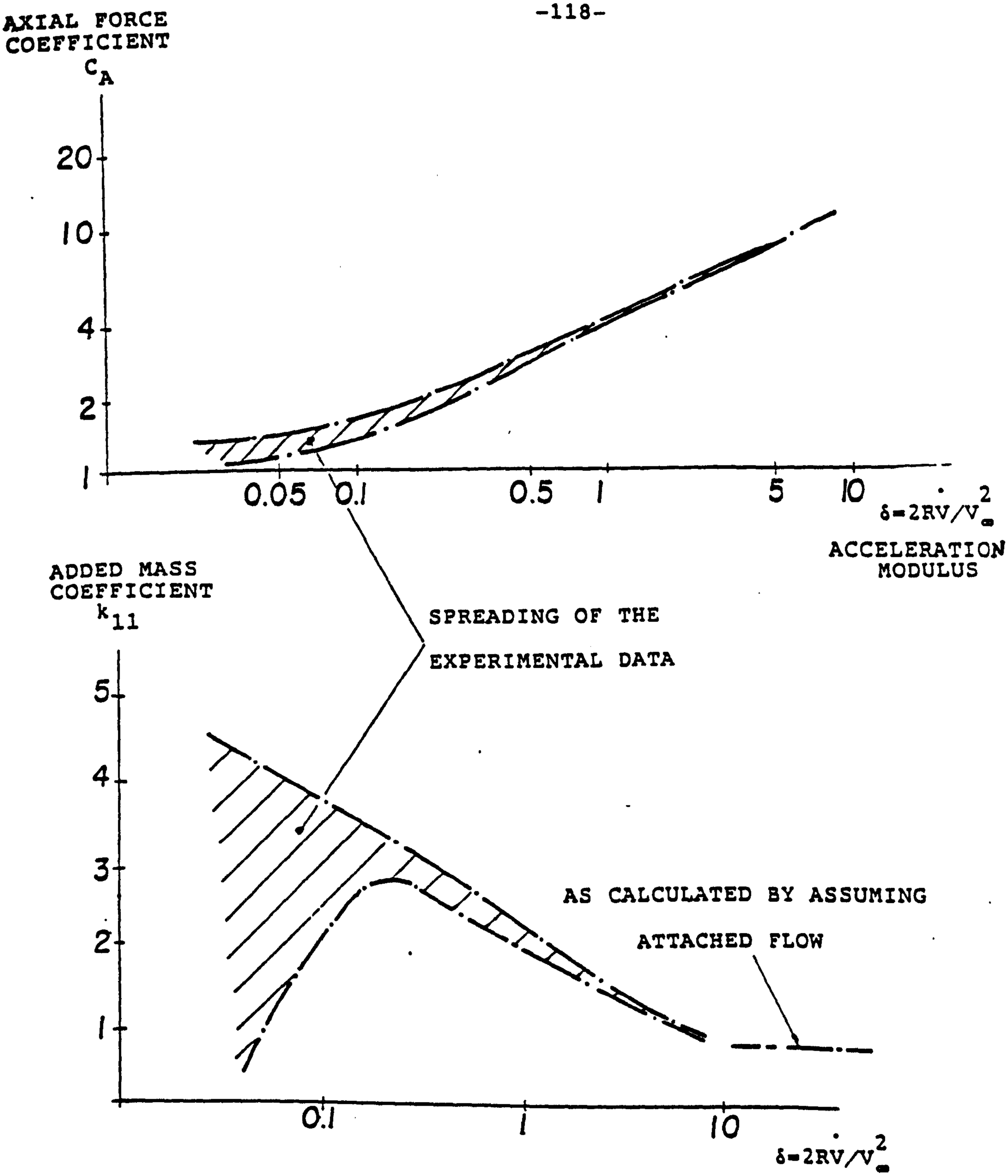


FIGURE 6.20: THE AXIAL FORCE COEFFICIENT, $C_A$, AND ITS ADDED MASS COEFFICIENT, $k_{11}$ (based on Iversen & Balent ,1951, experiments)

## 6.2.1 ACCELERATED FLOW

Figure 6.7 shows the calculated time-dependent axial force coefficient acting on a hemisphere which is subjected to a sudden axial motion.

When a body is impulsively set in motion the acceleration modulus is very high and conditions are appropriate for the application of Morison's formula. Subsequently, the added mass contribution diminishes and the axial force coefficient gradually converges towards its time-dependent behaviour in steady flow, as described in figure 6.7.

This result is qualitatively similar to Sarpkaya's experimental (1978) and calculated (1979) results for the axial force development on a circular two-dimensional cylinder which had been set in motion impulsively.

Figure 6.21 shows the calculated axial force coefficient developed on a hemisphere which is moved at a constant acceleration modulus and in figure 6.22 the consequent wake flow pattern.

At low acceleration moduli the wake pattern is essentially the same as that developed during steady flow whereas at moderate acceleration moduli the wake flow becomes less pronounced, tending to lose its periodicity.

The wake is composed of the fluid particles which carry vorticity created on the wetted part of the canopy. The changes in this shed vorticity are caused by variations in the free-stream velocity, shape changes and the fluctuations

caused by the wake flow periodicity in the velocities induced at the shedding point. Thus, the previous history of the flow manifests itself in the vorticity of the wake fluid particles and consequently in the wake's strength & structure.

The shed vorticity is convected at a velocity which is, on average, proportional to the free stream velocity (chapter 2). Therefore, the amount of vorticity which can be found within a given length downstream of the canopy becomes smaller as the acceleration modulus increases.

Thus, at high acceleration moduli the wake and consequently flow history have little effect on the aerodynamic load which is developed on the canopy.

At high acceleration moduli the added mass coefficient tends to the constant ideal flow value calculated by assuming attached flow. Under such conditions, Morison's formula is applicable .

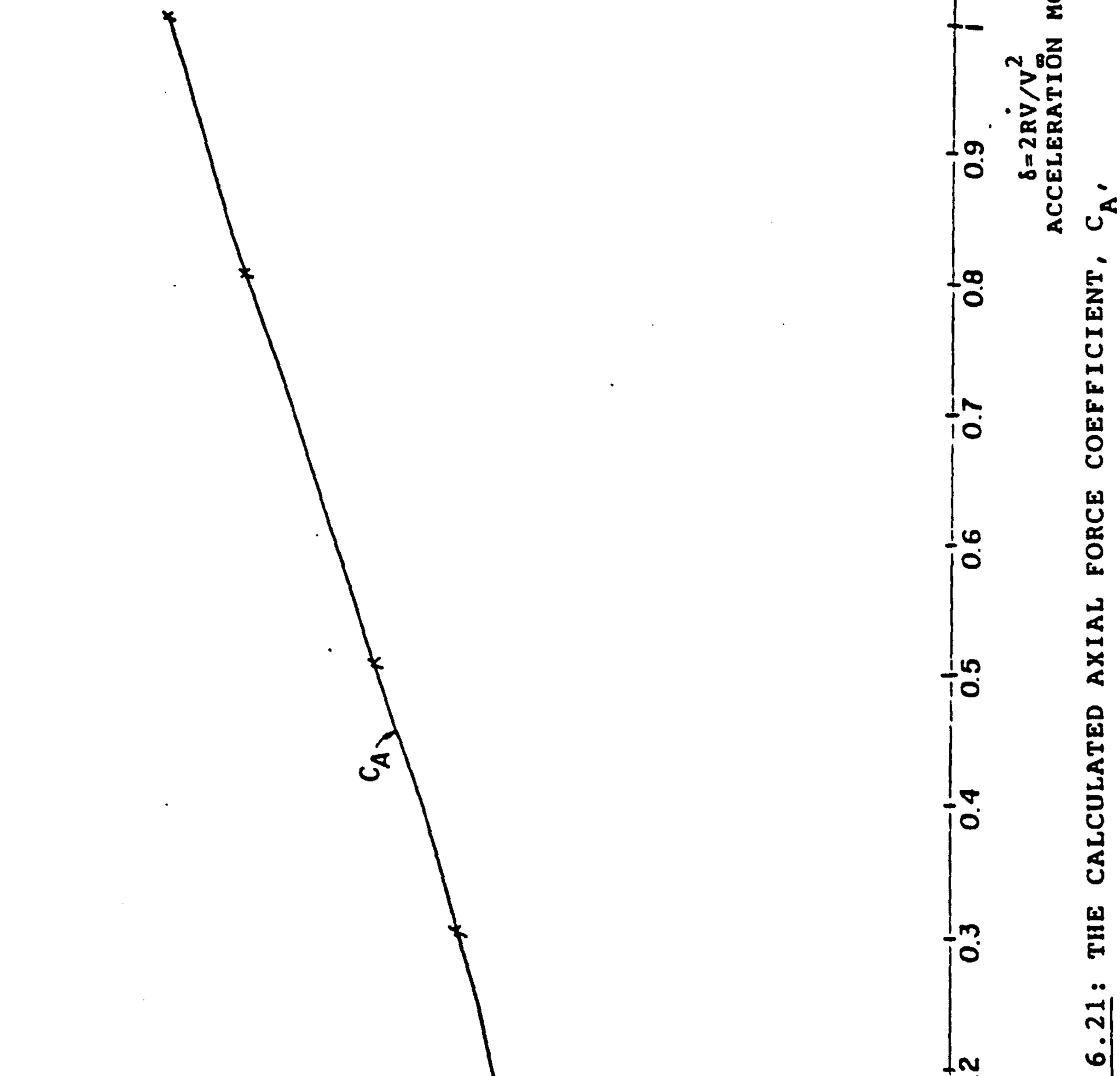


**FIGURE 6.21:** THE CALCULATED AXIAL FORCE COEFFICIENT, $C_A$, DEVELOPED ON A HEMISPHERE MOVED AT CONSTANT ACCELERATION MODULUS, $\delta$.

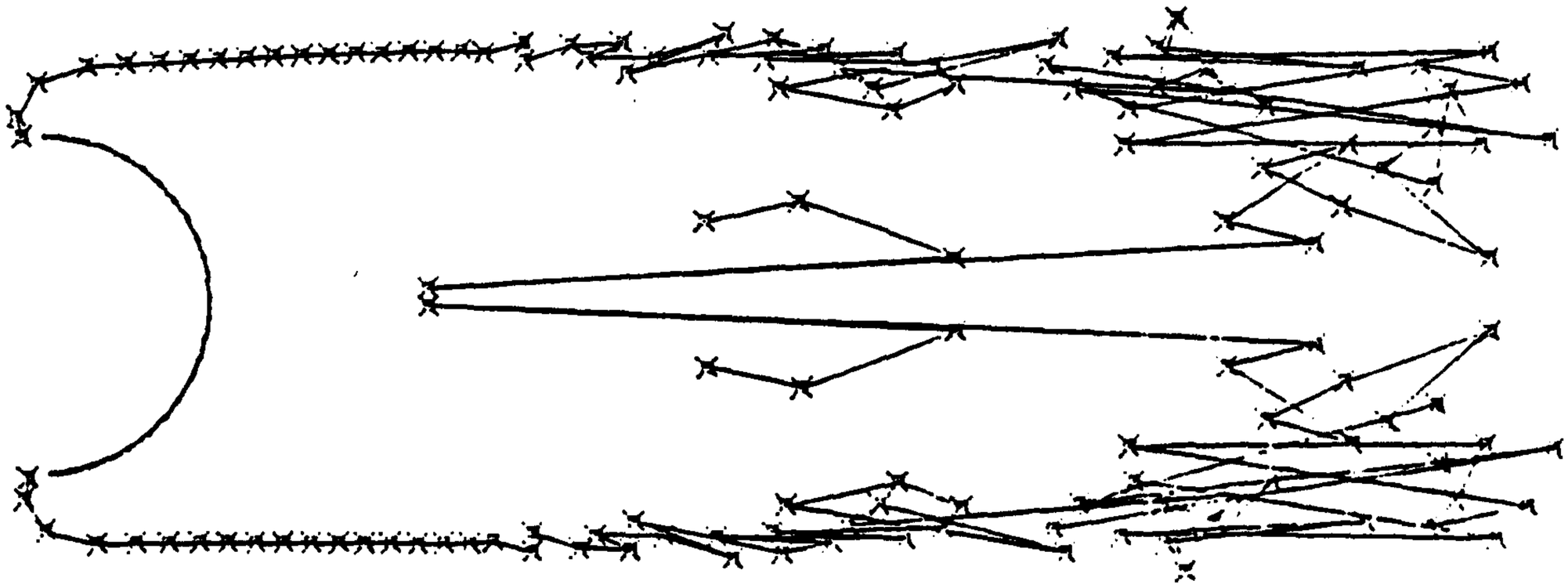

a) $\delta = 0.01$

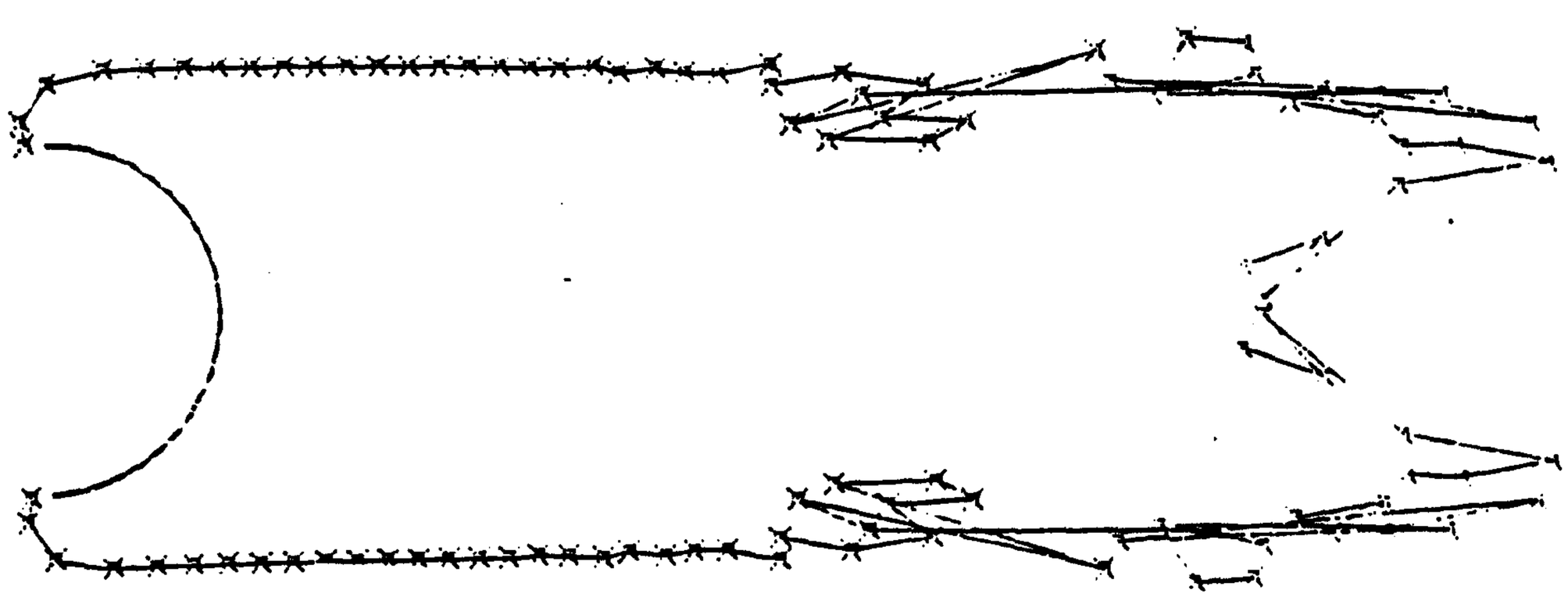

b) $\delta = 0.03$

FIGURE 6.22: THE WAKE FLOW PATTERN GENERATED BY A HEMISPHERE MOVED AT CONSTANT ACCELERATION MODULI, $\delta = 2R\dot{V}/V_\infty^2$

(continued on next page)

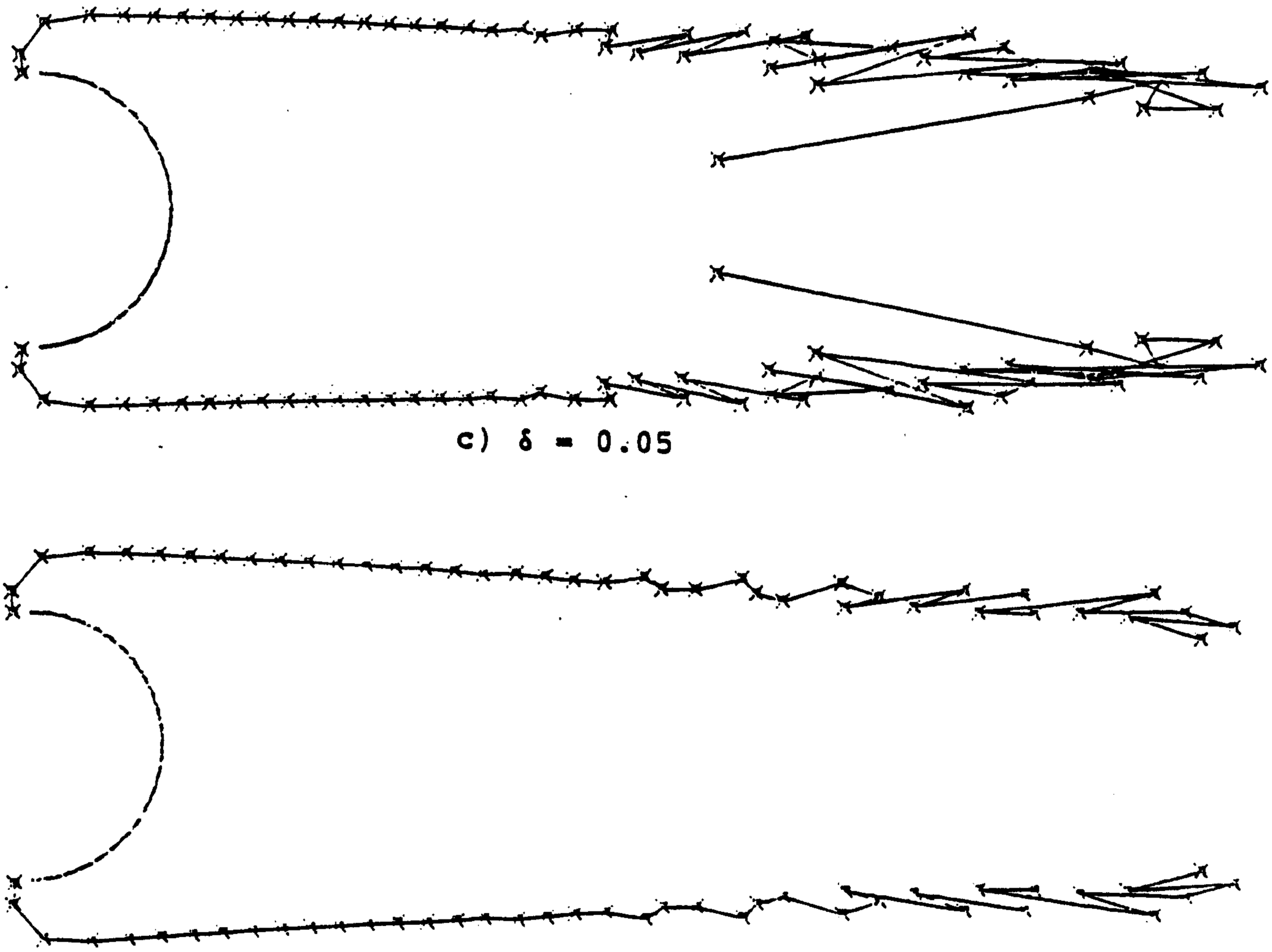

c) $\delta = 0.05$

d) $\delta = 0.1$

FIGURE 6.22: THE WAKE FLOW PATTERN GENERATED BY A HEMISPHERE MOVED AT CONSTANT ACCELERATION MODULI, $\delta=2R\dot{V}/V_\infty^2$ (continuation)

## 6.2.2 DECELERATED FLOW

From the explanation given in the previous section, the vorticity density (i.e. the amount of shed vorticity per unit length) shed into the wake behind a decelerating bluff body will be larger than the vorticity density in the wake developed behind a bluff body which moves at a constant velocity or is in accelerating motion.

Figure 6.23 shows the wake flow developed behind a bluff canopy in decelerating flow. The shed vorticity is much more dense than that shown in steady flow in figure 6.1.

The significant differences between the effect of accelerated and decelerated motion on the wake flow can be appreciated by considering the wake fluid to be composed of material particles which possess inertia. Then in decelerating motion the canopy will be exposed to a back-flow resulting from the inertia of the wake fluid particles.

Because a high-vorticity density region is developed in the near wake behind a decelerating bluff body, the flow history has a significant role in the axial force determination. Figure 6.24 shows the wake flow pattern and the consequent axial force coefficient developed on a one-meter radius hemispherical canopy in two different free-stream velocity profiles, V1 and V2 in figures 6.24 a and 6.24 b, respectively. After one second from the commencement of motion, the velocity and the deceleration in these two cases are similar, thus the acceleration moduli are

the same. However, the axial force development is dissimilar because it is a function of the flow history as well as of the instantaneous velocity and acceleration.

In a decelerating motion therefore, due to the strong dependence of the axial force on the flow history, Morison's formula does not provide a satisfactory relationship for the axial force.

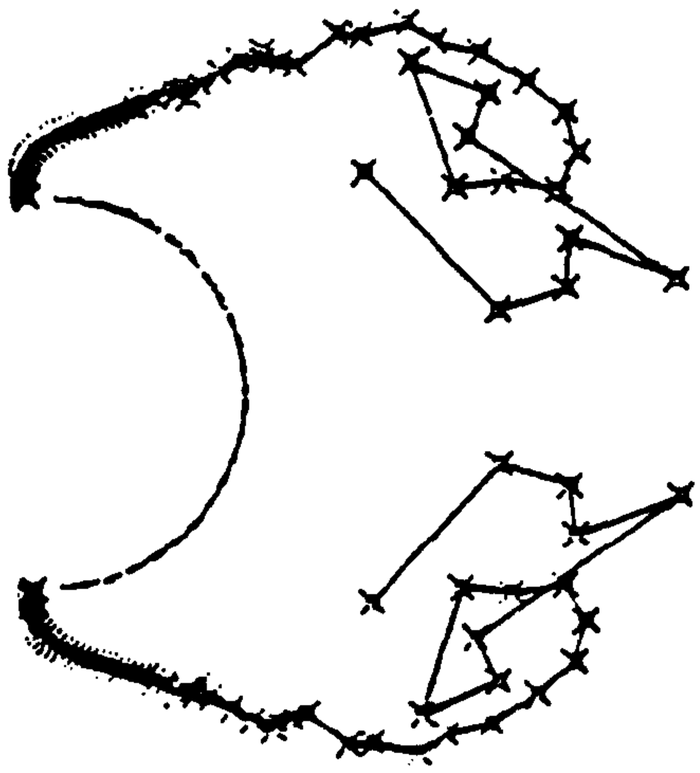

a) ACCELERATION MODULUS: $2R\dot{V}/V_\infty^2 = -0.3$

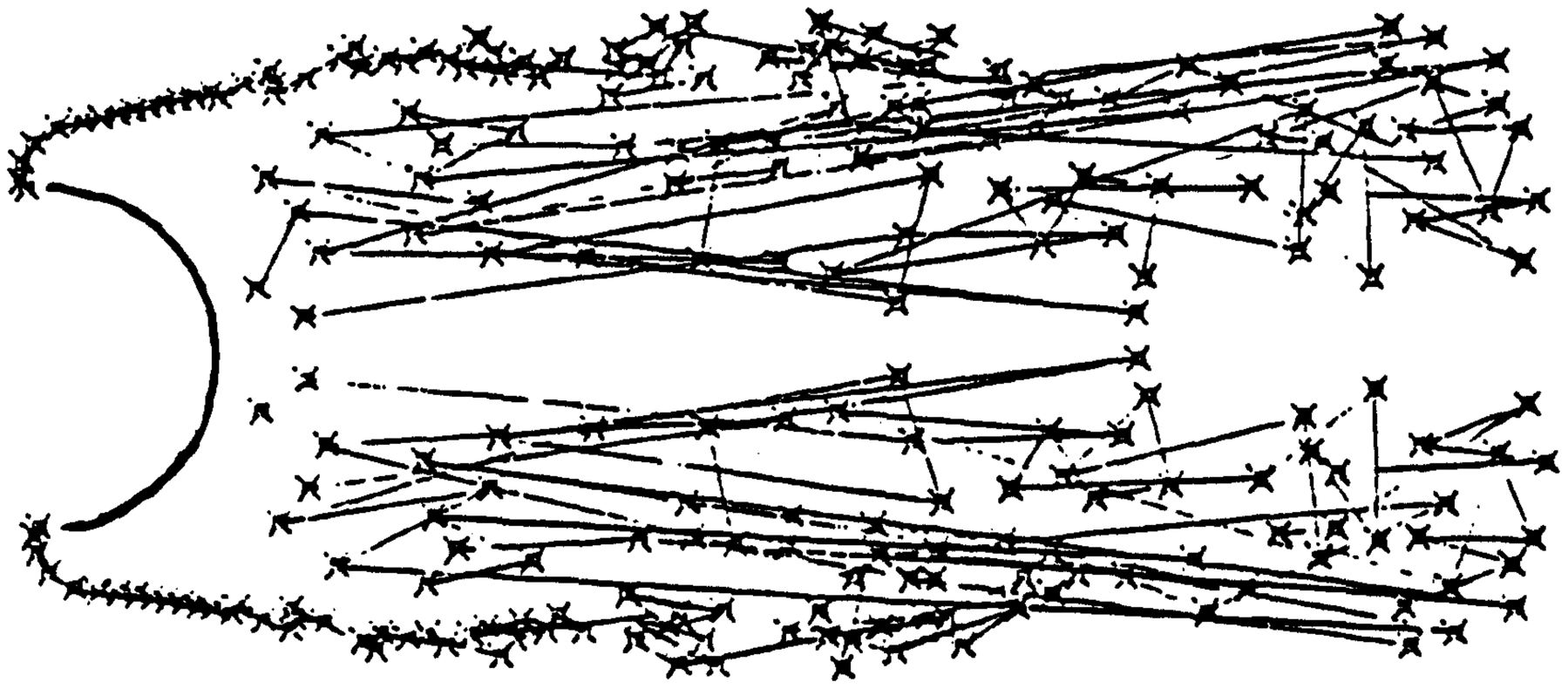

b) ACCELERATION MODULUS: $2R\dot{V}/V_\infty^2 = -0.03$

FIGURE 6.23: THE WAKE FLOW PATTERN DEVELOPED BEHIND A DECELERATING HEMISPHERE

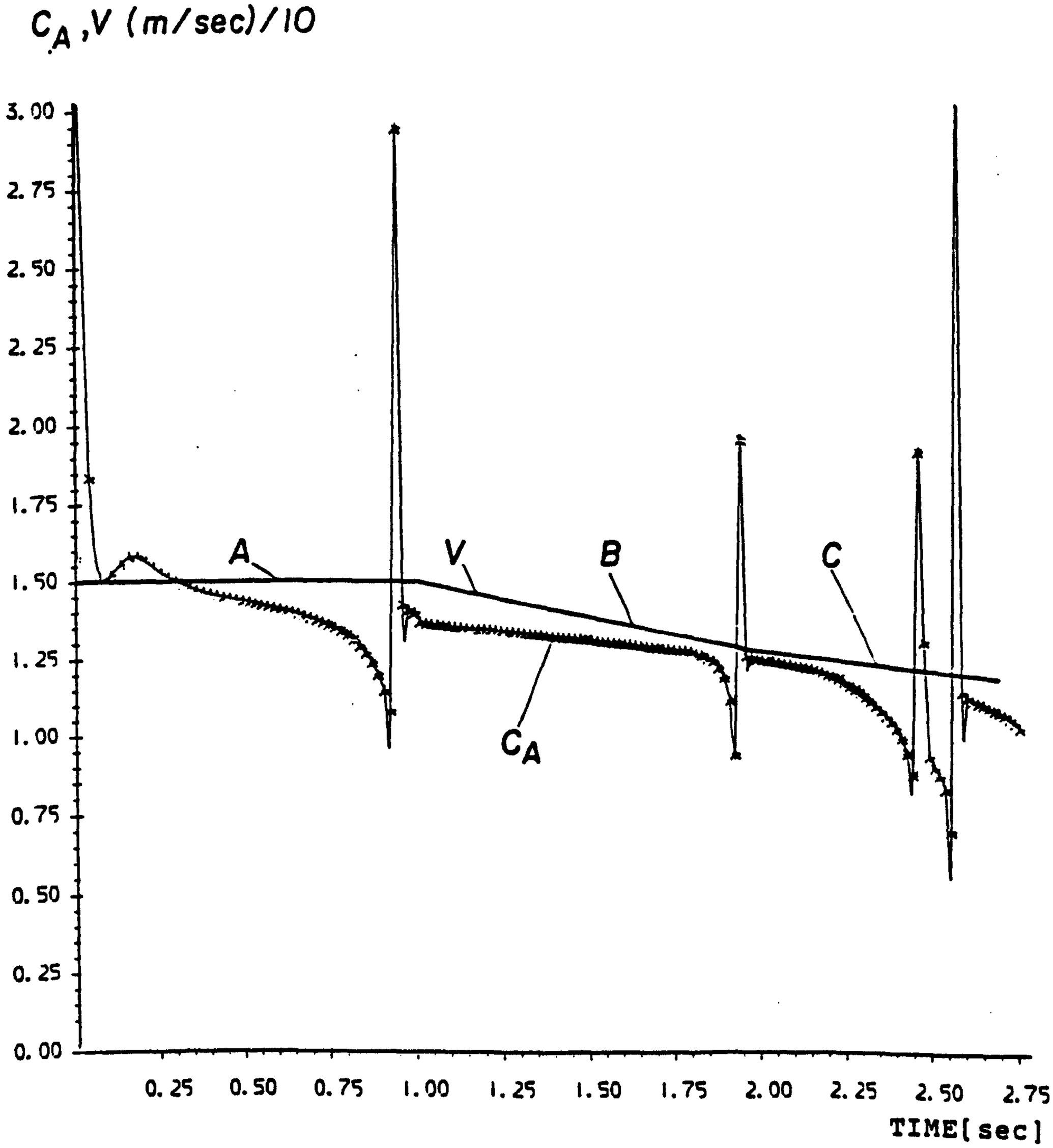


a) THE VELOCITY PROFILE V1

(i) AXIAL FORCE COEFFICIENT, $C_A$, VARIATION

FIGURE 6.24: THE AXIAL FORCE COEFFICIENT, $C_A$, AND THE WAKE FLOW PATTERN DEVELOPED RESULTING FROM DIFFERENT FLOW HISTORIES IN A DECELERATED FLOW AT SIMILAR ACCELERATION MODULUS (continued on next page)

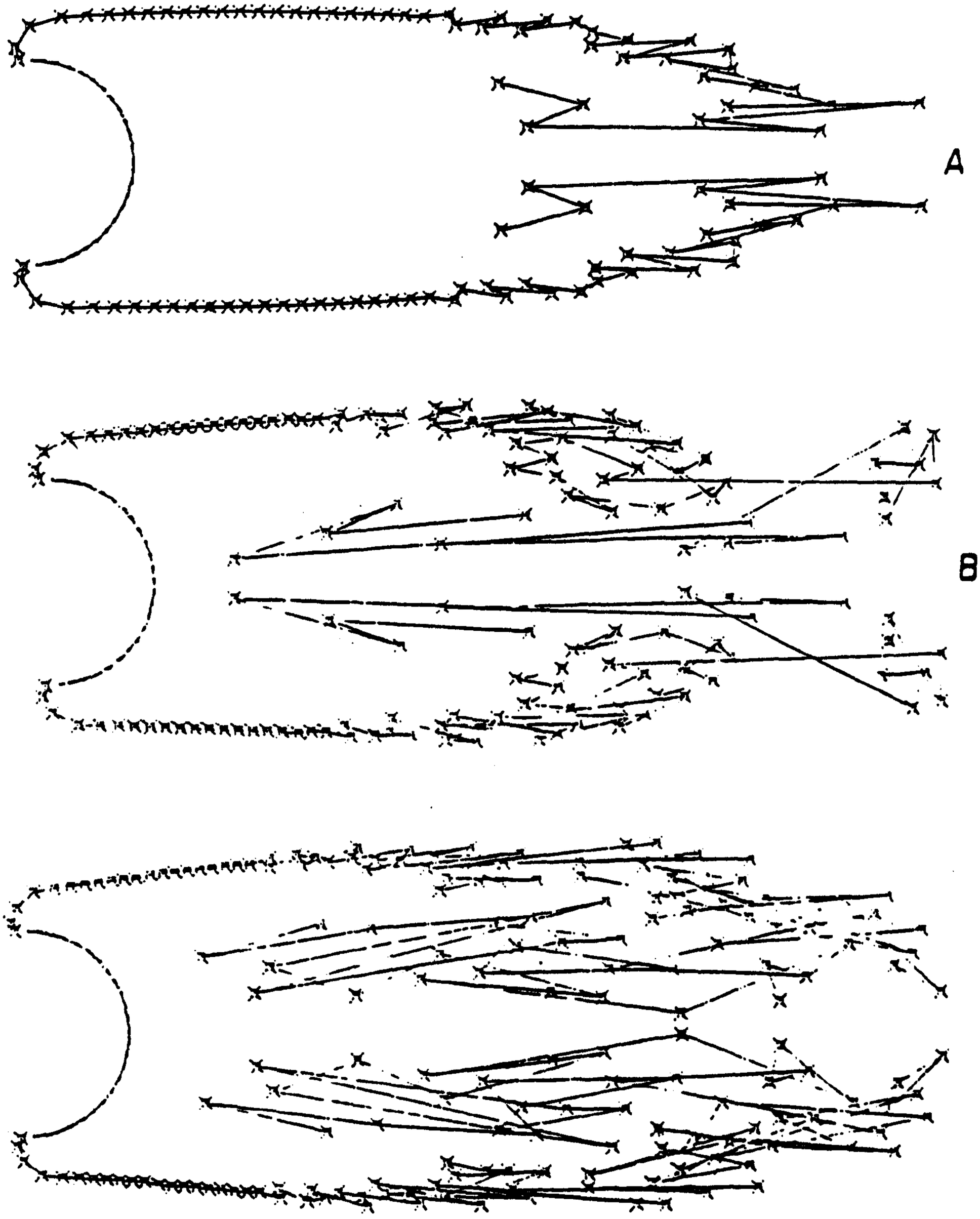


a-(ii) THE WAKE FLOW PATTERN DEVELOPED BY VELOCITY PROFILE V1 AT SUCCESSIVE TIME INTERVALS A,B,C DEFINED IN FIGURE 6.24 a(i

FIGURE 6.24: THE AXIAL FORCE COEFFICIENT, $C_A$, AND THE WAKE FLOW PATTERN DEVELOPED AT SIMILAR ACCELERATION MODULI IN A DECELERATING MOTION WHICH RESULT FROM DIFFERENT FLOW HISTORIES (continued on next page)

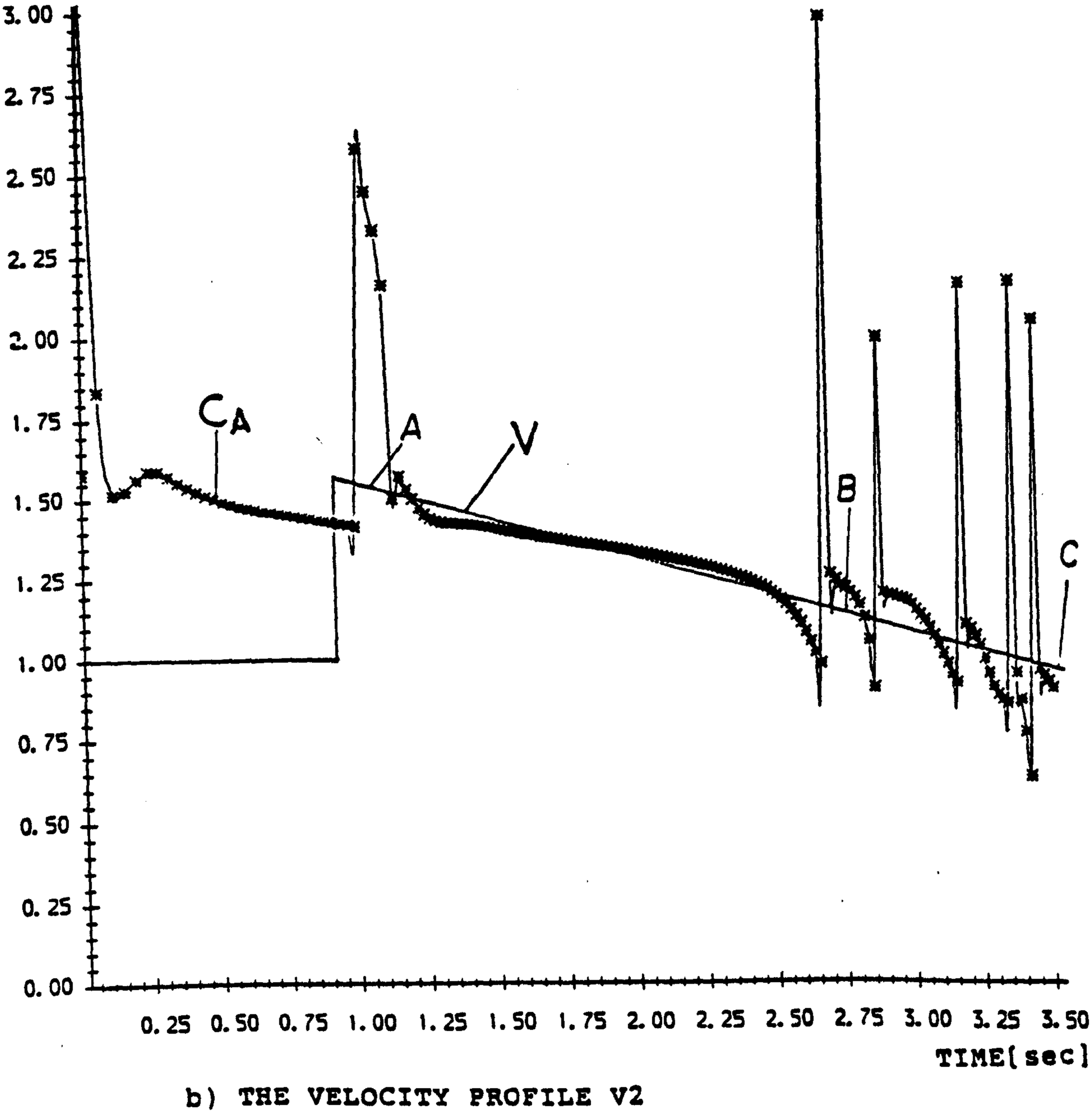


b) THE VELOCITY PROFILE V2

(i) AXIAL FORCE COEFFICIENT, $C_A$; VARIATION

FIGURE 6.24: THE AXIAL FORCE COEFFICIENT, $C_A$, AND THE WAKE FLOW PATTERN DEVELOPED AT SIMILAR ACCELERATION MODULI IN A DECELERATING MOTION WHICH RESULT FROM DIFFERENT FLOW HISTORIES (continued on next page)

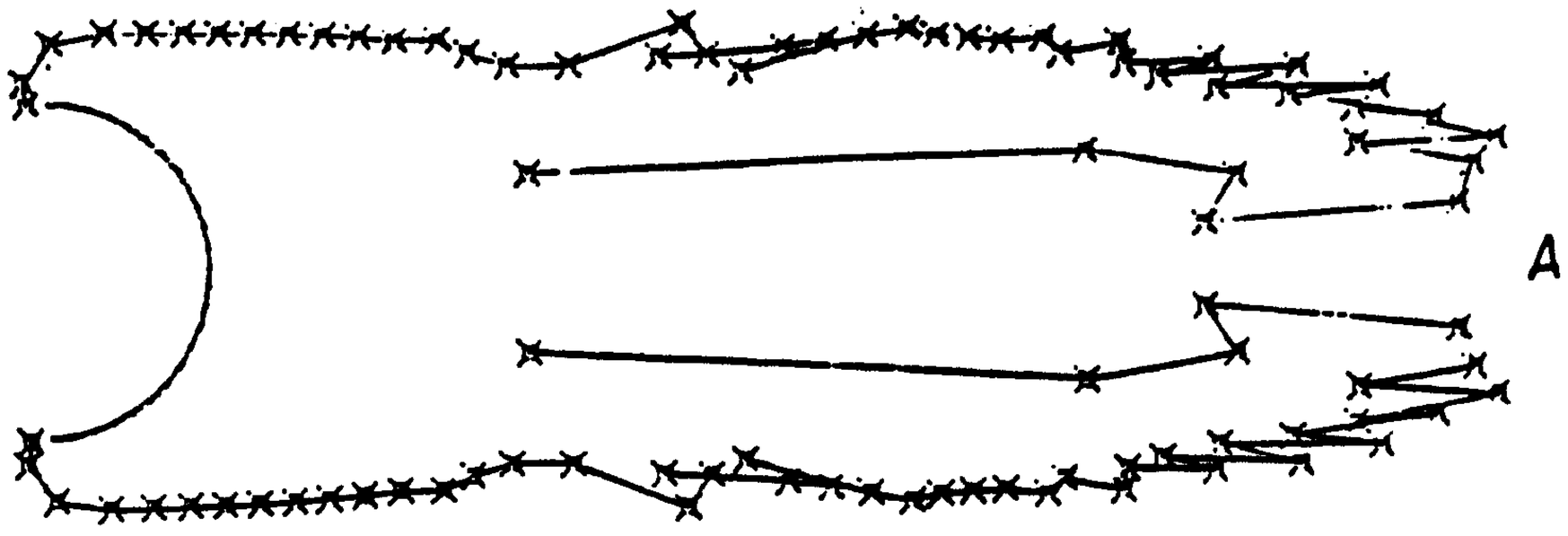


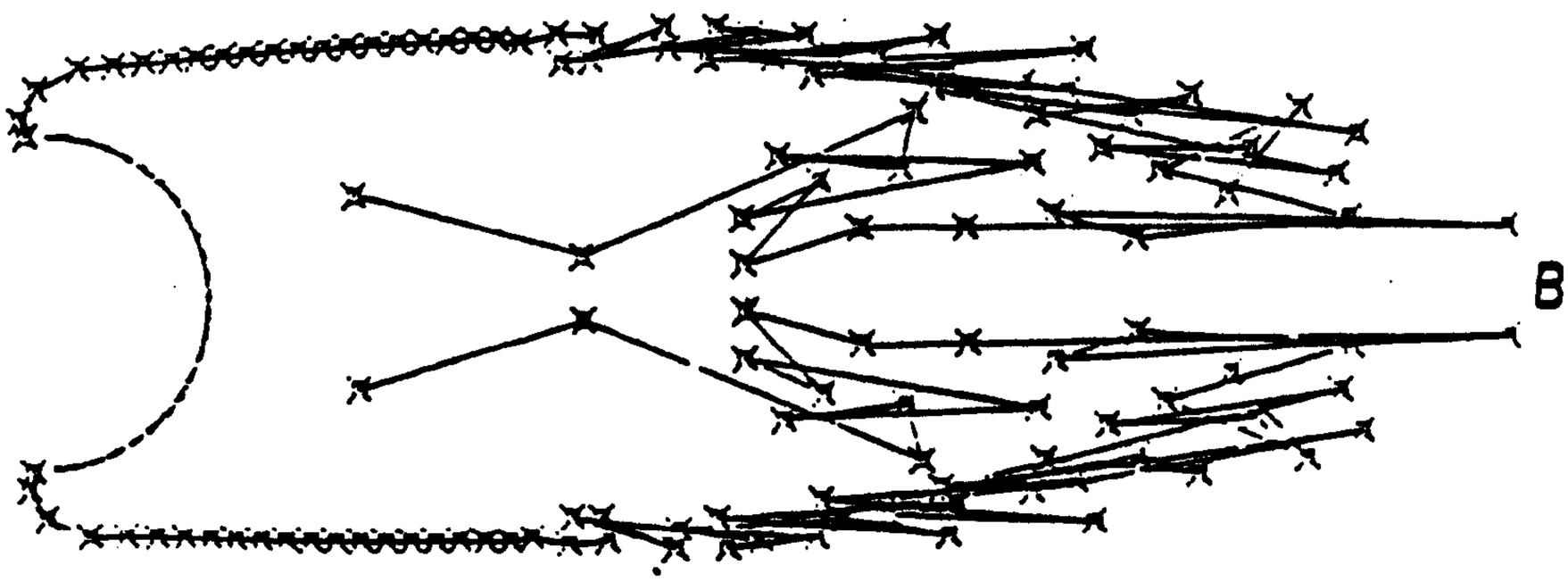


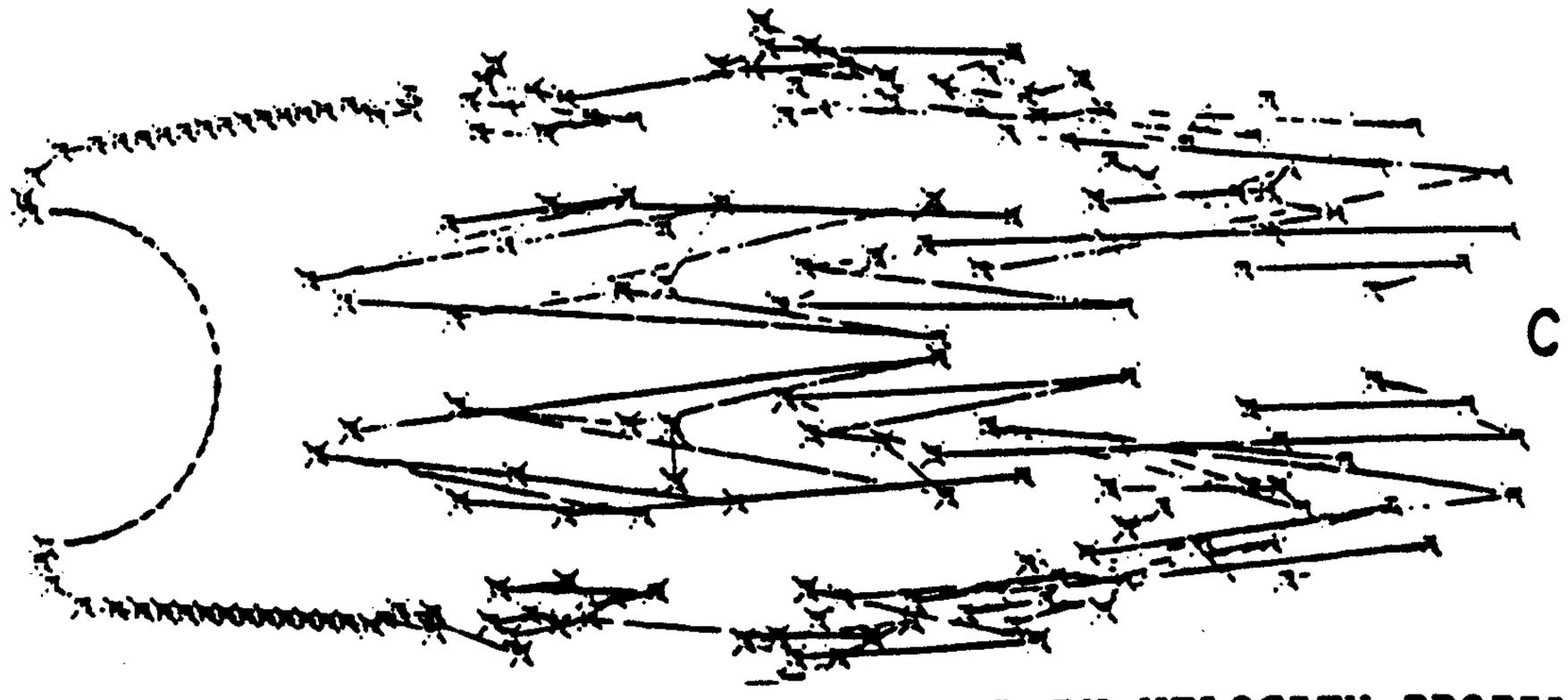


b-(ii) THE WAKE FLOW PATTERN DEVELOPED BY VELOCITY PROFILE V2 AT SUCCESSIVE TIME INTERVALS A,B,C DEFINED IN FIGURE 6.24 b(i)

FIGURE 6.24: THE AXIAL FORCE COEFFICIENT, $C_A$, AND THE WAKE FLOW PATTERN DEVELOPED AT SIMILAR ACCELERATION MODULI IN A DECELERATING MOTION WHICH RESULT FROM DIFFERENT FLOW HISTORIES (continuation)

## 6.2.3 FREE DECELERATION

Free deceleration (i.e. the movement of a decelerating system under both axial & gravitational forces) is a particular example of decelerating motion. Since this motion is basic to the application of parachutes some of its features will be analysed.

Figure 6.25.a shows the axial force coefficient development for a freely-decelerating system released at an initial descent velocity of 30 m/sec.

Close to descent commencement, the axial force coefficient fluctuations are of a higher frequency and amplitude than they are in a steady, free-stream flow, then gradually the fluctuations tend to those which are developed in steady motion.

Soon after the commencement of motion the mean axial force coefficient is about 60% of its steady value. Even after about six seconds flight at a practically constant velocity the mean axial force coefficient does not reach its steady value of 1.25 (figure 6.8 b). This is because the decelerated motion increases the vorticity density in the near wake,behind the canopy.

Figures 6.25 b & 6.25 c show the axial force coefficient developed on the same canopy, but with a different initial descent velocity and a different parachute/payload system mass.

By comparing the axial force coefficient development in figures 6.25 a, 6.25 b and 6.25 c, it can be seen that the axial force coefficient developed on a freely-decelerating parachute canopy depends on the flow history. When a rigid canopy is assumed, this flow history is a function of the systems's initial velocity and the parachute/payload system mass.

Some evidence supporting the results of this simulation is provided in "PERFORMANCE OF AND DESIGN CRITERIA FOR DEPLOYABLE AERODYNAMIC DECELERATORS" (1963) and by Ewing E.G. (1972). The experimental axial force coefficient variation trend with the descent velocity is shown in figure 6.26.

This trend can be explained partially by Reynolds number effects on the axial force developed on porous canopies (Cockrell D.J. 1987). But it could also be explained by consideration of the unsteady wake flow, as predicted by the present model.

Since a parachute canopy is not rigid, as has been assumed in the present calculations, it will change its shape during flight as it is affected by the momentary pressure distribution. Thus, a more quantitative comparison of the results from the model with experimental data, such as those which is shown in figure 6.26, would not be realistic.

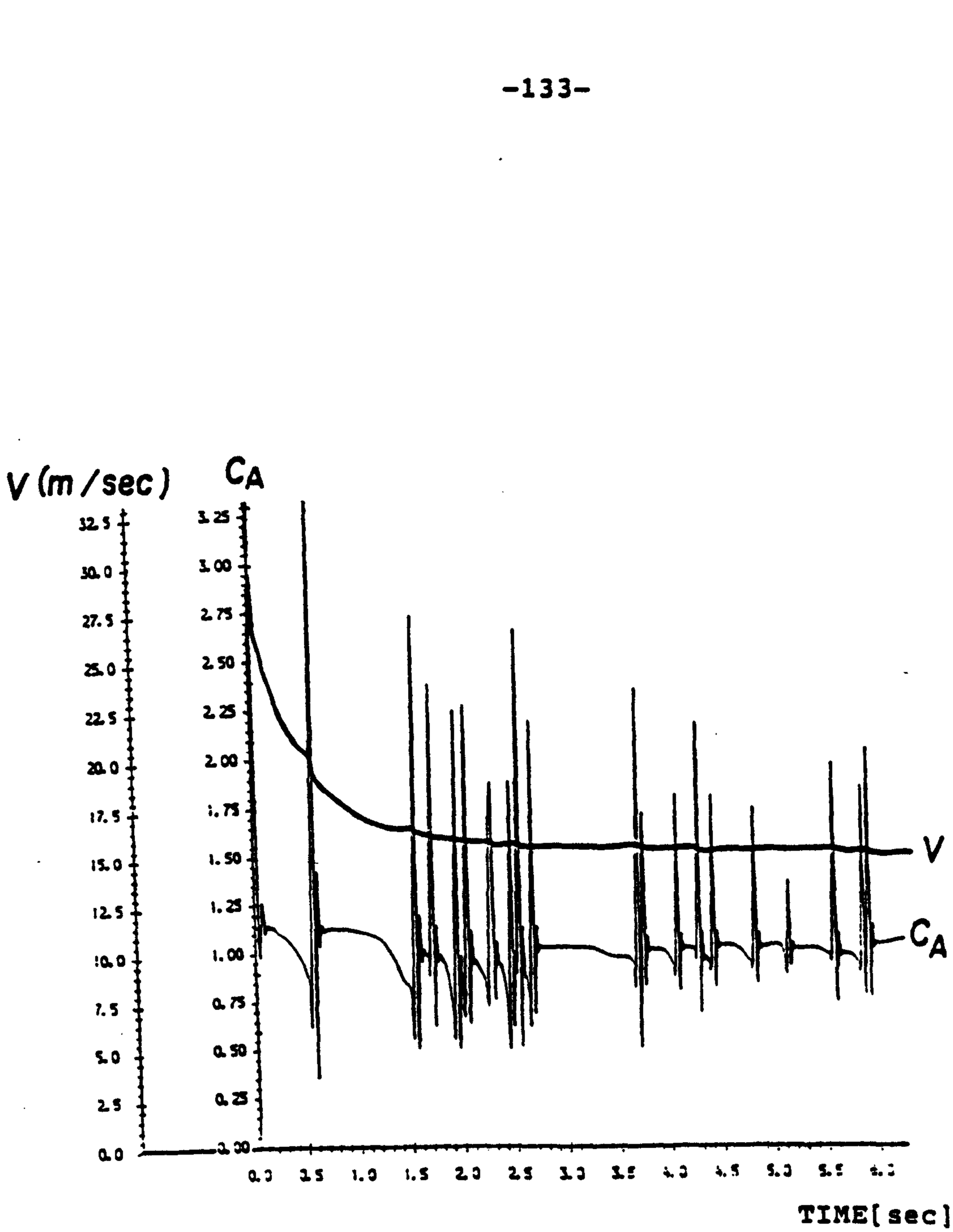


a) PARACHUTE/PAYLOAD MASS=100 Kg, INITIAL VELOCITY=30m/sec

FIGURE 6.25: THE AXIAL FORCE COEFFICIENT, $C_A$, DEVELOPED ON A FREELY-DECELERATING PARACHUTE/PAYLOAD SYSTEM ,X1=X2=1.4m Y1=2m. (continued on next page)

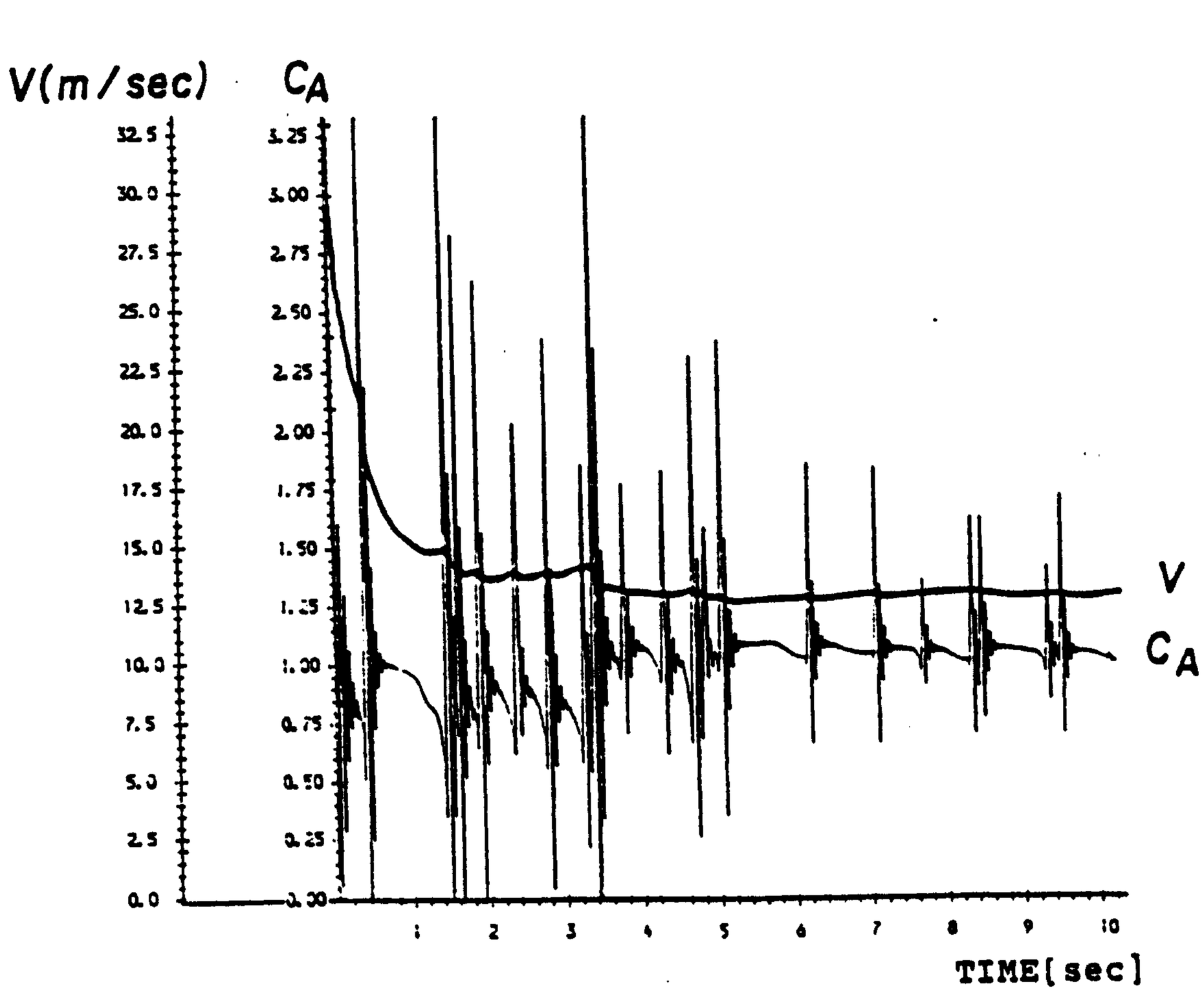


b) PARACHUTE/PAYLOAD MASS=200 Kg, INITIAL VELOCITY=30m/sec

FIGURE 6.25: THE AXIAL FORCE COEFFICIENT, $C_A$, DEVELOPED ON A FREELY-DECELERATING PARACHUTE/PAYLOAD SYSTEM ,X1=X2=1.4m Y1=2m. (continuation).

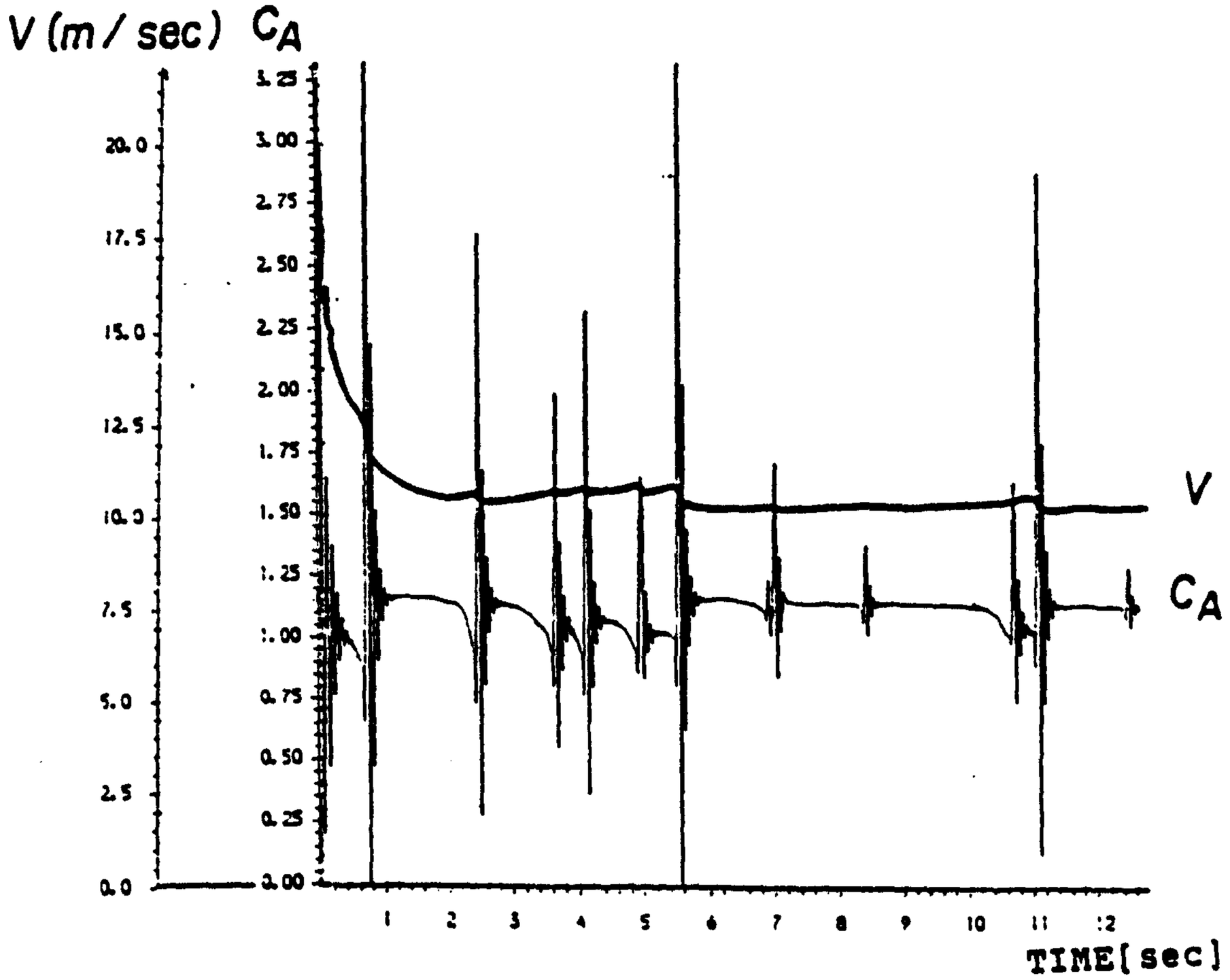


c) PARACHUTE/PAYLOAD MASS=100 Kg, INITIAL VELOCITY=20m/sec

FIGURE 6.25: THE AXIAL FORCE COEFFICIENT, $C_A$, DEVELOPED ON A FREELY-DECELERATING PARACHUTE/PAYLOAD SYSTEM ,X1=X2=1.4m Y1=2m .(continuation)

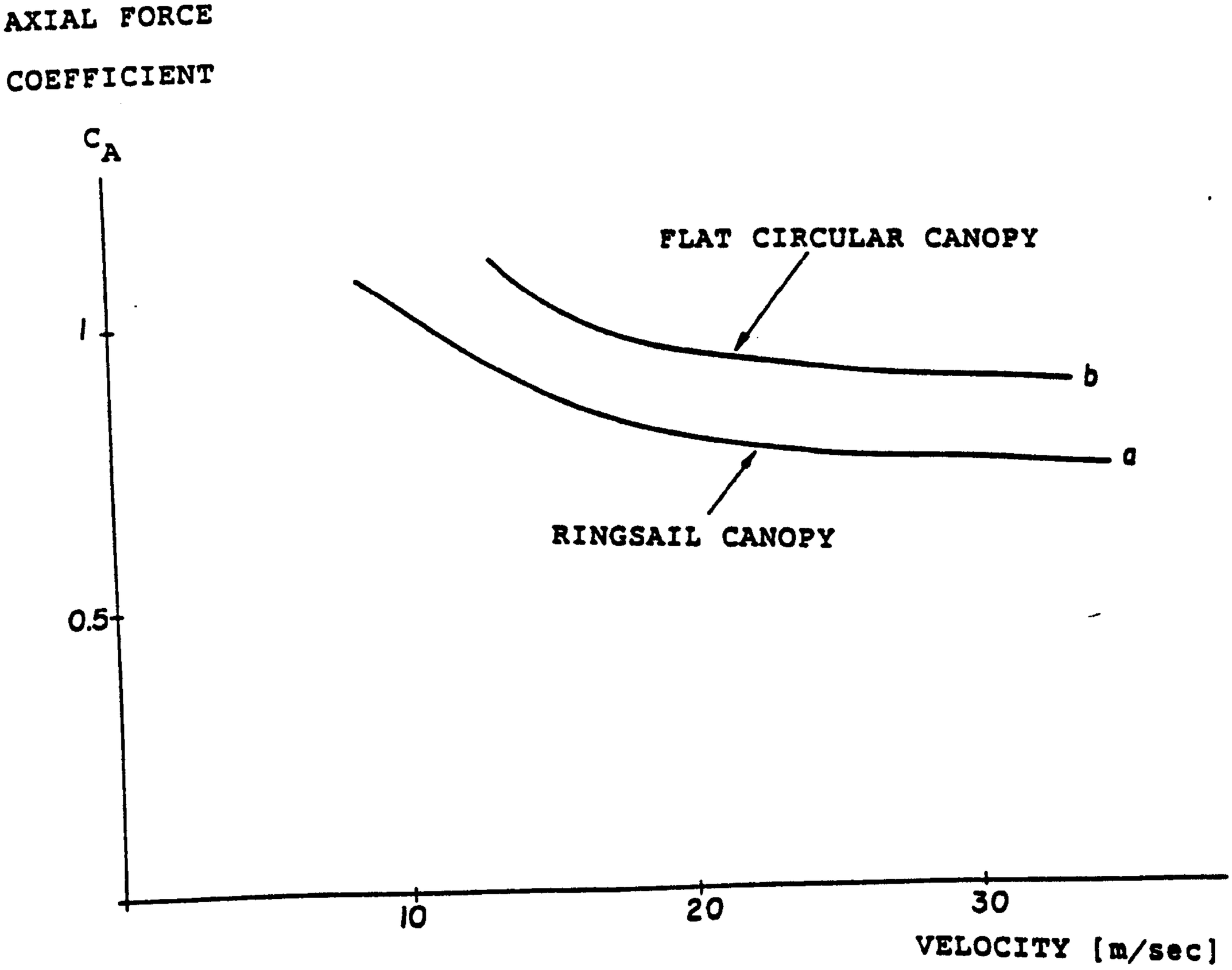


FIGURE 6.26: THE AXIAL FORCE COEFFICIENT, $C_A$, DEVELOPED ON A FREELY-DECELERATING PARACHUTE/PAYLOAD SYSTEM

(based on experimental results reported in:

a) "PERFORMANCE OF AND DESIGN CRITERIA FOR DEPLOYABLE AERODYNAMIC DECELERATORS"-"ASD-TR-61-579,DEC. 1963

b) Ewing E.G. 1972)

## 6.2.4 OSCILLATORY MOTION

Yavuz T. & Cockrell D. (1981) introduced a method for the experimental determination of unsteady aerodynamic load acting on canopy models. The apparatus consisted of a carriage which was capable of towing a canopy model through a ship tank at a desired velocity. An oscillatory motion in different directions could be superimposed on the main axial movement determined by the towing device.

Cockrell D. et al (1986) subsequently improved the apparatus and the data reduction technique.

In 1986 & 1987 Harwood R. performed a series of experiments with several canopy models. Among these were experiments conducted on nominally-hemispherical canopies in axial oscillatory motion.

Figure 6.27 compares the calculated axial force coefficient with two sets of experimental results which he obtained. Owing to the uncertainity in the actual canopy shape (fabric canopy models were used) the ratio between the instantanoeus axial force coefficient to its mean value rather than its absolute value was used in this comparison. The calculated results show good agreement with the experimental measurements.

Figure 6.28 shows the added mass coefficient in this kind of axial oscillatory motion obtained by applying Morison's formula instantaneously. The added mass coefficient changes significantly over a period and is not a single-valued

function of the acceleration modulus.

It is thus apparent that Morison's formula is not suitable for the representation of the axial force generated in motions which are highly flow history dependent, such as oscillatory motions.

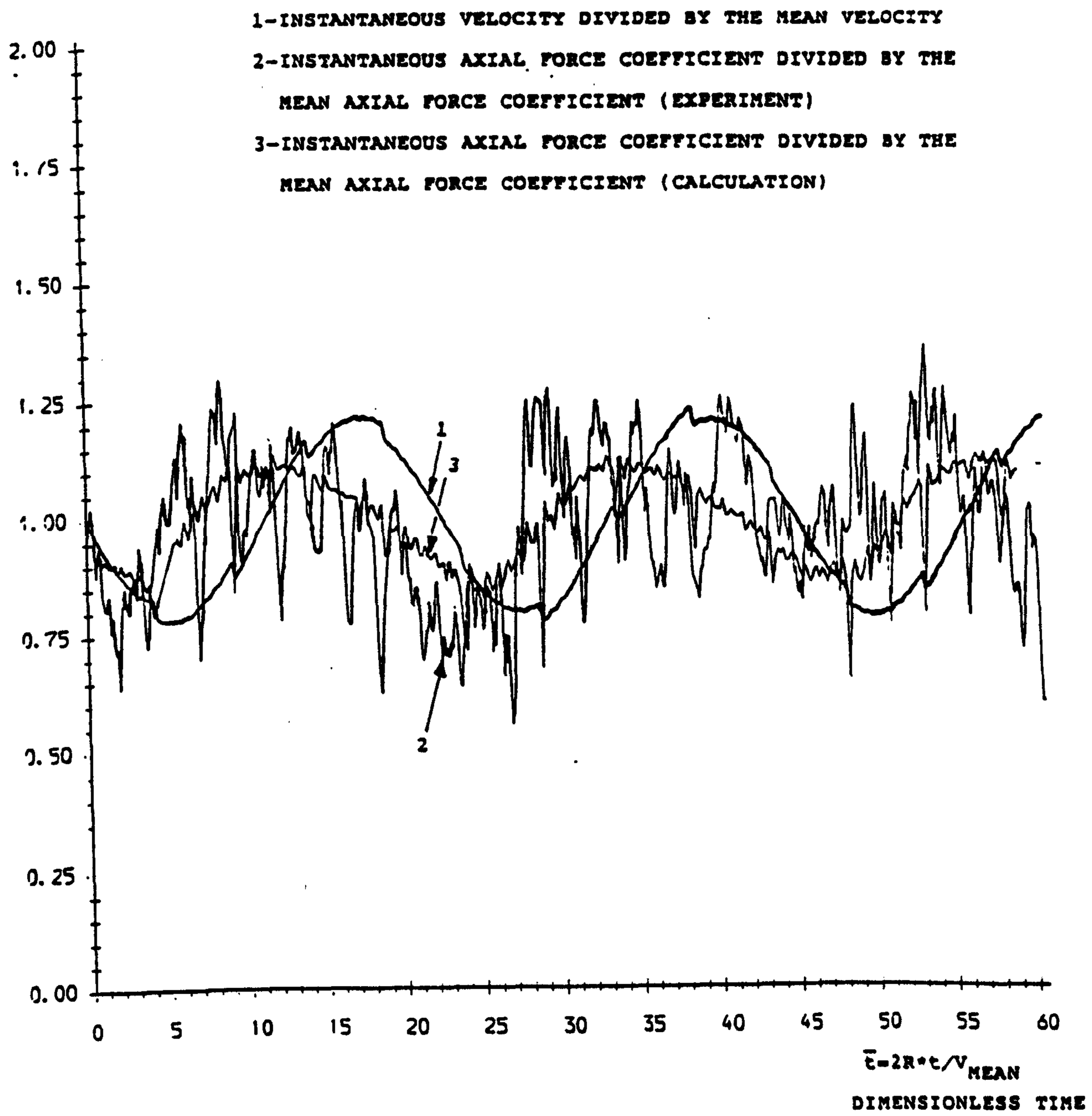


a)1986 EXPERIMENTS

FIGURE 6.27: THE AXIAL FORCE, $C_A$, DEVELOPED ON A HEMISPHERICAL CANOPY IN AXIAL OSCILLATORY MOTION (calculations and Harwood R. 1986-1987 experiments)

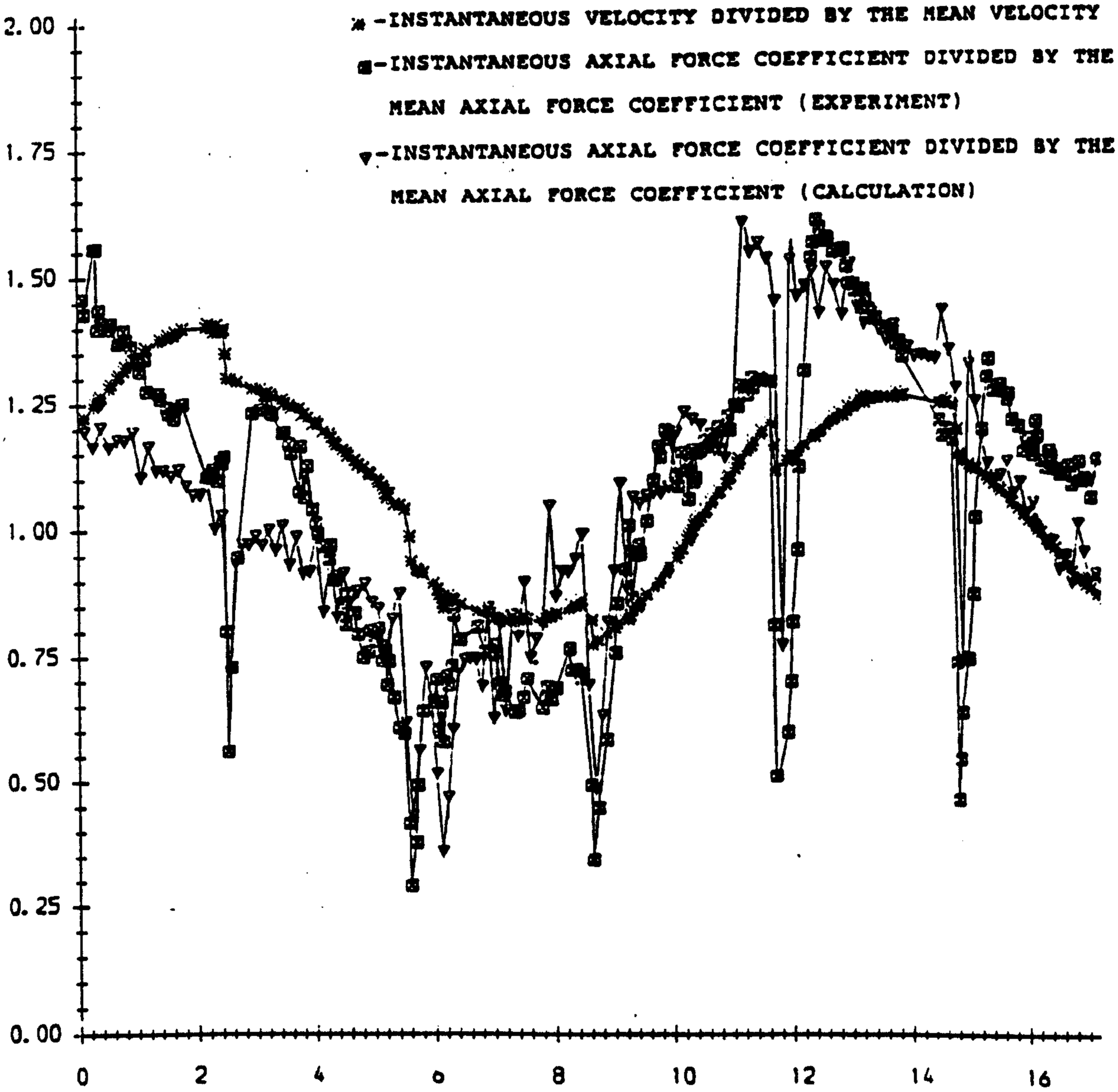


b)1987 EXPERIMENTS

FIGURE 6.27: THE AXIAL FORCE, $C_A$, DEVELOPED ON A HEMISPHERICAL CANOPY IN AXIAL OSCILLATORY MOTION (calculations and Harwood R. 1986-1987 experiments)-continuation

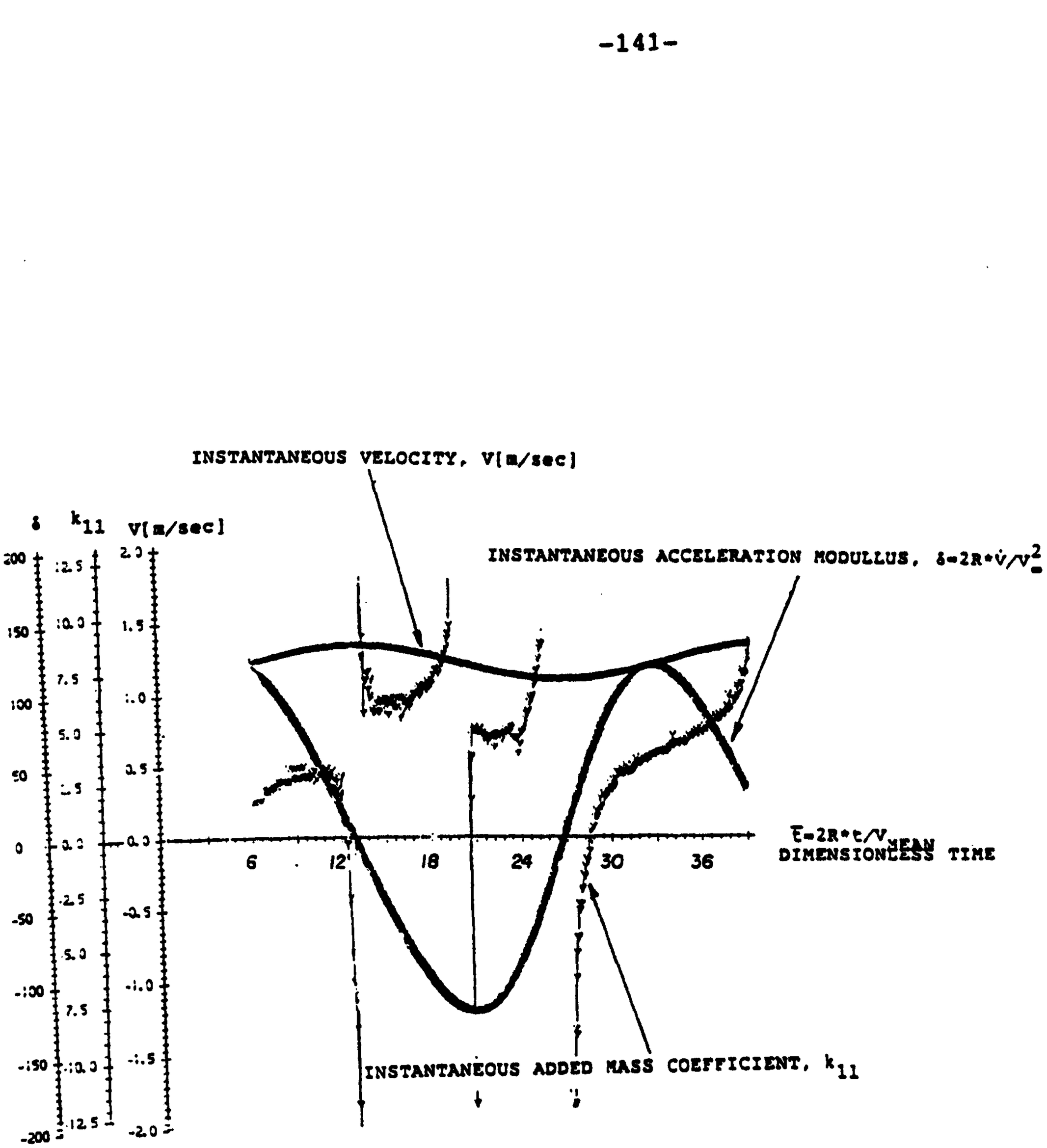


FIGURE 6.28: THE CALCULATED ADDED MASS COEFFICIENT, $k_{11}$, VARIATION DURING THE AXIAL OSCILLATORY MOTION OF A HEMISPHERE

## 6.3 THE PARACHUTE CANOPY INFLATION PROCESS

Engineering interest in the parachute canopy inflation process lies in the high forces which are then generated on the parachute canopy and transferred to the payload. In simulating this process neither the velocity nor the canopy shape can be assumed to have steady values.

The canopy shape variation is determined both by the interaction between the momentary aerodynamic & inertial load and the canopy structural response to these loads. Since canopy structural modelling is beyond the scope of the present research, in this simulation the canopy shape variation with time is assumed to be known.

Mathematically, the changes in the canopy shape are accounted for by including the canopy surface velocity in the flow field boundary conditions (equation 4.5).

By analysing the canopy inflation process photographs presented by Heinrich H.G & Noreen R.R (1970), it appears that the axisymmetric flow assumption might be appropriate only during the last 40% of the inflation time $t_f$. However, the axial force reaches its maximum value within this period, so it is worth simulating this part of the canopy inflation process.

Experimental data which they presented show that the average canopy surface velocity is about one order of magnitude less than the free stream velocity. Thus, in the differential pressure calculation (section 4.9), the square

of the canopy surface velocity can be neglected.

Figure 6.29 shows the calculated axial force during an axisymmetric inflation of an hemispherical canopy. This shape has been assumed since sufficient data to describe the canopy shape during the inflation process are not available.
The velocity and the projected canopy area radius variation with the time are based on the experimental correlation found by Heinrich & Noreen (1970).

The steady shape is achieved at $t/t_f=1$ .

The axial force has a local maximal value at $t/t_f=0.6$. Its absolute maximal value is achieved when $t/t_f=1$.

Although a quantitative comparison with experimental results was not performed, qualitatively the trend in the simulated axial force development agrees with these experiments.

This result shows the ability of the model to cope with the strong simultaneous gradients in both the canopy shape and the free-stream velocity. It would therefore be suitable to use in conjuction with an appropriate structural model in order to obtain a realistic canopy load prediction.

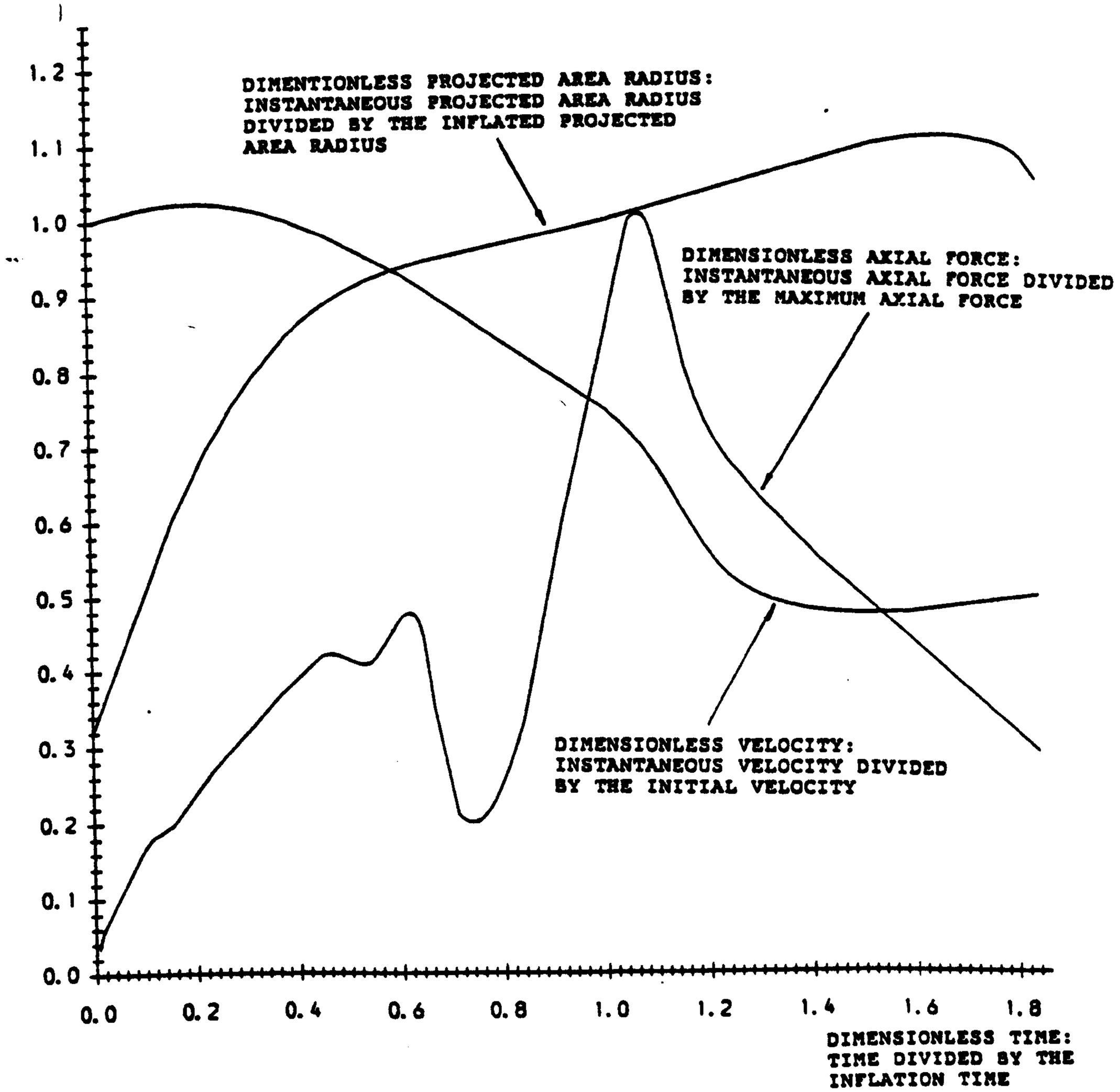


FIGURE 6.29: THE CALCULATED AXIAL FORCE, $C_A$, DEVELOPED ON AN INFLATING CANOPY

## 7. THE MODEL SENSITIVITY

The model sensitivity was checked against free parameters, empirical data and the integration scheme for the convection of the shed vortex rings.

To calculate the aerodynamic load on a given canopy configuration the model requires as input the canopy shape & velocity variation with time, the porosity distribution, the parachute/payload mass (if a free deceleration is simulated) and the desired number of panels (for the sake of abbrevation NP) for canopy discrete representation. Thus, for a given example the model requires only one free parameter, i.e. NP.

The first step in checking the model sensitivity to NP was made by calculating the differential pressure distribution for spherical canopies when attached flow was assumed. Subsequently, the results were compared with Ibrahim's (1965) analytical calculations.

Figure 7.1 shows such a comparison for NP=8. Discrepancies between the model and Ibrahim's (1965) results can be noticed near the skirts of the canopies. These discrepancies are due to the discrete representation of the canopy surface which cannot simulate the large changes in velocity near the canopy hemline.

Both the calculated time step magnitude and the newly-created vortex ring strength depend on NP. Therefore, the next step was to find the sensitivity of the results with

separated flow simulations, to variations in NP.

Figure 7.2 shows the calculated, mean axial force coefficient and the Strouhal number dependence on NP for a hemispherical canopy at a Reynolds number of $1.5*10^5$, based on the projected area diameter. The results presented in figure 7.2 show changes of up to 5% in the mean axial force coefficient with NP from the result obtained when the recommended value for NP, i.e. NP=12, was used. The Strouhal number variations are in the same range as was found for the calculated Strouhal number in section 6.1.1.

Since at every time step a new vortex ring is shed the number of the shed vortex rings is proportional to NP. Thus, the computation time grows as $NP^2$ (chapter 5).

Following the results shown in figure 7.2 and by considering the required computation time, the recommended range for NP is 10-14.

For the shedding frequency evaluation (section 6.6) an experimental axial force coefficient ($C_A$) is required. In equation 5.36 it was assumed that $C_A$, based on the canopy projected area, was 1.3. This was an average value between the extreme experimental values presented by Hoerner (1965) for cup-shaped bodies (i.e $1.20<C_A<1.45$).

When the extreme values for $C_A$ were used to evaluate the shedding frequency, using equation 5.36, the resulting mean axial force coefficient varied by only up to 5%. The calculated Strouhal number was found to vary within +0.02 when $C_A$=1.45 and within 0.01 when $C_A$=1.2 about the mean values shown in figure 6.8 that is, by approximately 10%.

According to equation 4.36 the magnitude of $C_A$ influences the shedding frequency (equation 4.36) in the same manner as does the circulation reduction factor (section 4.3 and 4.6). Therefore, a $\pm$10% uncertainty in the circulation reduction factor affects the axial force development in the same way as the variation in the assumed $C_A$ value used in equation 4.36 for shedding frequency evaluation.

The wake development was calculated using equation 4.37. This equation represents an Eulerian integration scheme. To check the sensitivity of these results to the integration method, several simulations were performed by using the Adam's integration method, whose error is two orders of magnitude less than that of Euler's integration method (Henrici P. 1962), was used. Thus, the shed vortex rings were convected in accordance with :

$$\vec{r}_i=\vec{r}_{i-1}+[\dot{\vec{r}}_{i-1}+0.5*(\dot{\vec{r}}_{i-1}-\dot{\vec{r}}_{i-2})]*\delta t \qquad 7.1$$

where $\vec{r}_k$- is the vector determining the "k"-th vortex ring axial location and radius.

Both the mean axial force and the Strouhal number were unaffected by changing the integration method. Owing to the higher computing resources demanded by Adam's method, Euler's integration scheme (equation 4.37) was maintained.

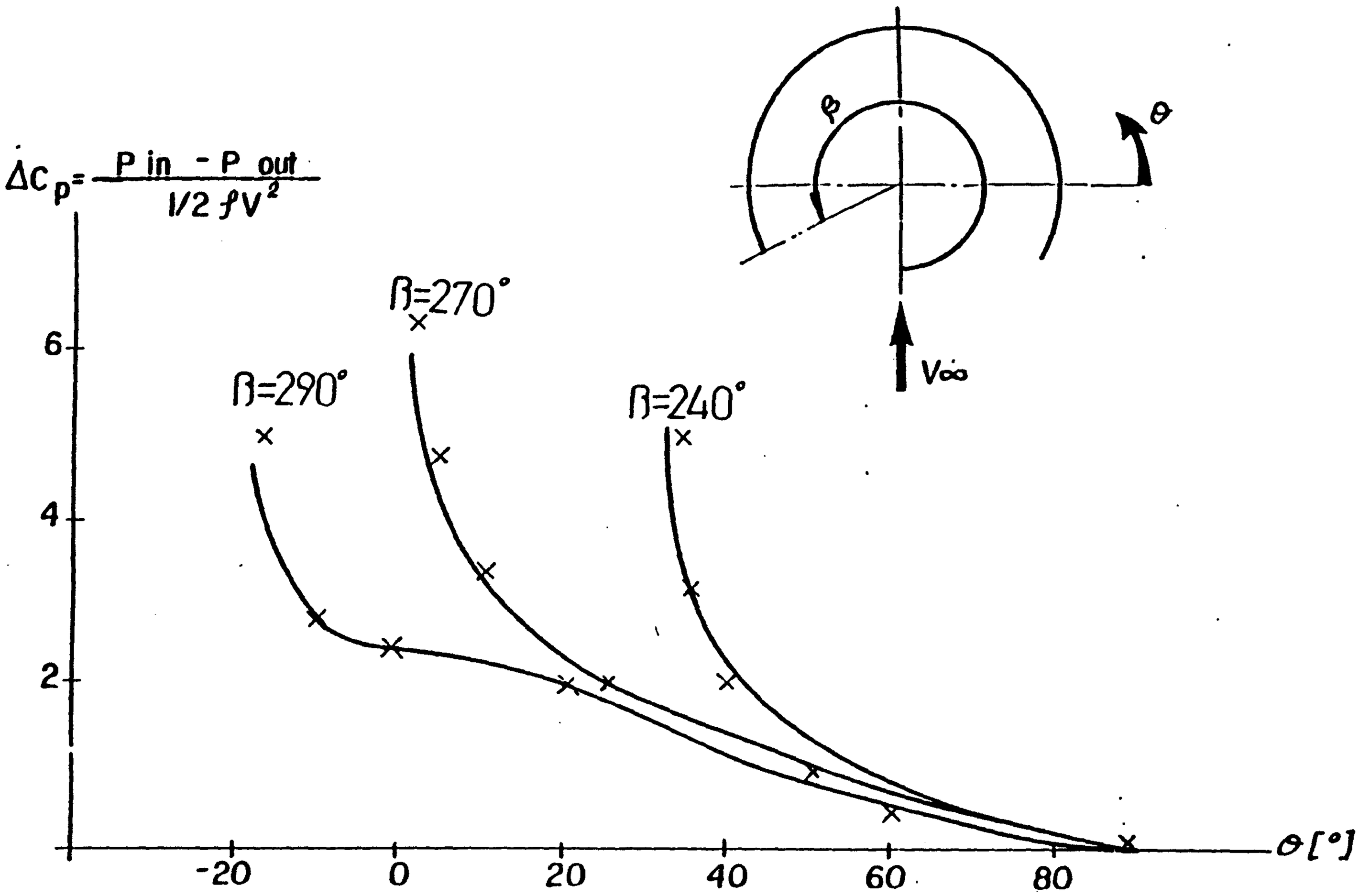


FIGURE 7.1: THE DIFFERENTIAL PRESSURE DISTRIBUTION, $\Delta C_p$, ON SPHERICAL CANOPIES IN ATTACHED FLOW. (comparisson with analytical calculations by IBRAHIM, 1965)

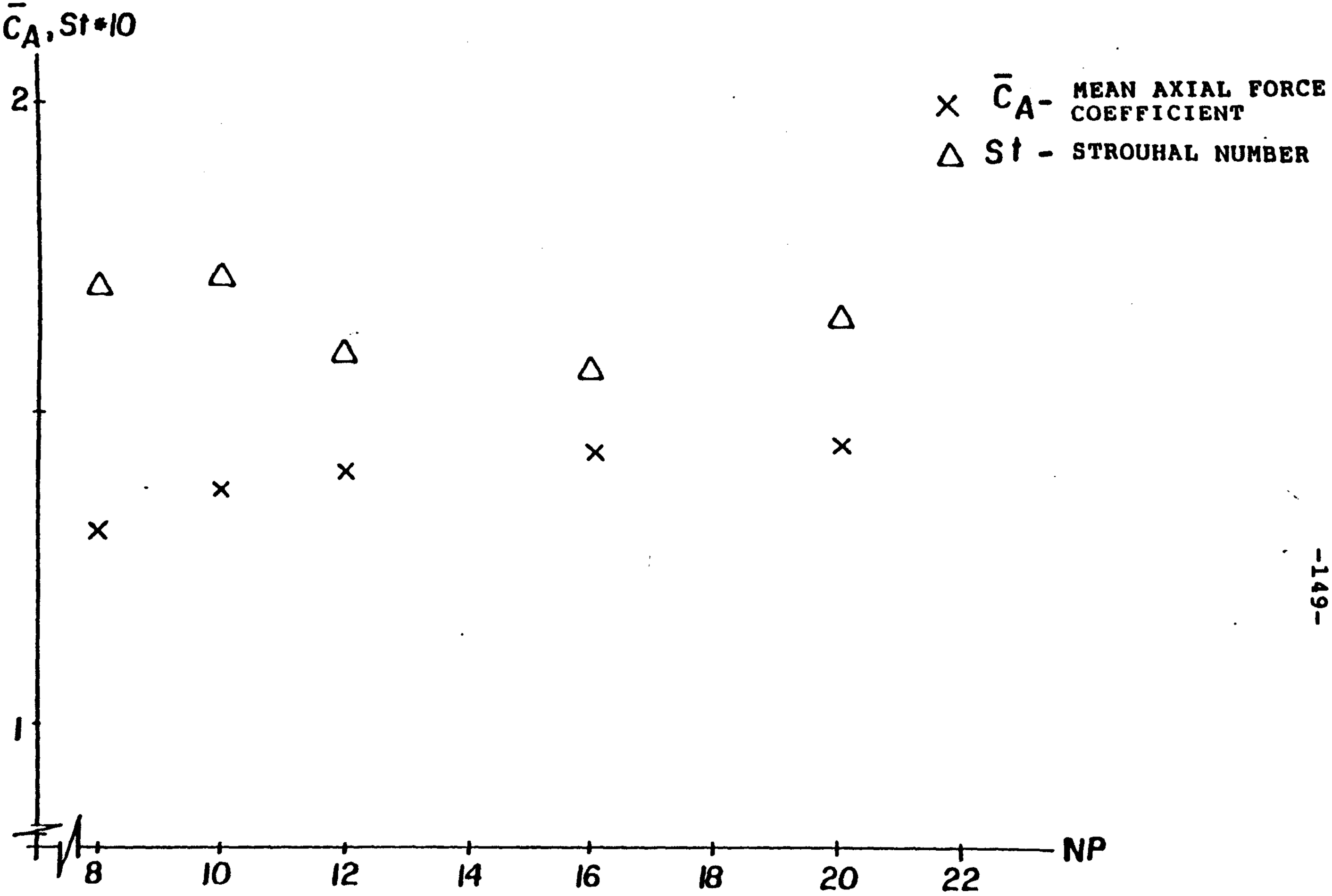


FIGURE 7.2: THE INFLUENCE OF THE NUMBER OF PANELS, NP, ON AXIAL FORCE

# 8. RECOMMENDATIONS FOR FURTHER WORK

As has been already explained, three-dimensional separated flow has not been sufficiently investigated either experimentally or theoretically. Future research effort should therefore be directed in both these two directions.

Owing to the complexity of three-dimensional separated flow at this stage studies should be restricted to incompressible flow.

In view of the theoretical results presented in this research it is recommended that the experimental validation of the present model should be completed prior to undertaking any further theoretical studies.

## 8.1 RECOMMENDATIONS FOR FUTURE EXPERIMENTAL STUDIES

Experimental work should cover both steady and unsteady flows.

It is suggested that the steady flow experiments would investigate both the wake flow and the consequent aerodynamic load generated on the canopy. A simultaneous measurement of the wake flow periodicity and axial force development could explain a significant part of the complex phenomena associated with three-dimensional separated flows.

The porosity influence on both the axial force development and the wake flow influences the design of parachute canopies and therefore, further investigations of the aerodynamic

properties possesed by three-dimensional porous canopies should be performed. It is recommended that experiments such as those performed by Heinrich & Uotilla (1977) are re-examined and that measurements are made of the wake flow properties.

Additional efforts should be directed into unsteady flow experiments such as those conducted by Cockrell D. et.al. (1986) and Harwood R. (1986).

The present research has shown that utilisation of Morison's formula for unsteady separated axisymmetric flows of moderate and small acceleration moduli is unsatisfactory, because the aerodynamic loads developed under these conditions fluctuate strongly. In order to simulate aerodynamic loads generated on full-scale parachute canopies in flight, the canopy models should be tested in velocity profiles which are similar to those which occur in the full-scale flight. If the canopy can be assumed to be rigid, the most significant parameters to model are the canopy shape and the dimensionless time which characterises the velocity variation with time. This similarity in the velocity profiles will account for the fluid flow history. However, it is important to note that although the acceleration modulus does not reflect the fluid flow history, it might be thought of as a first order approximation to it.

## 8.2 RECOMMENDATIONS FOR FUTURE THEORETICAL STUDIES

The recommendations for future theoretical studies lie in the limitations of the present model (section 5.10).

Since the wake flow investigation provides a sufficient data base, the present model can be implemented using empirical methods to model effects such as the viscosity decay and the collision of the vortex rings.

Subsequently, the principles presented in this research could be applied to asymmetrical flows. Flow asymmetry results from both non-zero angle of attack and asymmetric canopy shapes, e.g. cross shaped canopies.

When flow asymmetry arises only from non-zero angles of attack, the canopy surface could be represented by bound vortex rings whose strengths varied around their circumference. Such methods have been used by both Weisinger (1957) and Bagley, Kirby and Marcer (1958) to calculate the aerodynamic load developed on annular aerofoils.

If the flow about asymmetric canopy shapes is to be simulated, the canopy surface could be replaced by a lattice of generally shaped vortex panels such as have been used by Katz & Levin (1980) for a delta wing representation.

In asymmetric flows the shed vortex rings develop non-uniform circumferentially-distributed self-induced velocities (chapter 3). Therefore, every vortex ring must be represented by a grid of several points [ Leonard 1975 ] and the location of each of these points must be tracked. It is

therefore evident that an asymmetrical model will demand much higher computing resources than are required for the present one.

The current model and any future asymmetrical models would possess higher engineering applicability in parachute design if they were to be matched to appropriate structural models.

The flight trajectory of parachute/payload systems could be simulated by building up a computer programme capable of calculating the instantaneous aerodynamic & structural loads and subsequently applying these, togeter with other external loads, in the equations of motion. Although at this present stage this kind of computer programme would be very complex and difficult to develop, its principles are well understood and with continuous effort it could be produced.

# 9. SUMMARY AND CONCLUSIONS

A model for the axisymmetric flow around bluff bodies is presented. This model assumes an incompressible, high Reynolds number flow and its principles are applied to an investigation of the aerodynamic characteristics developed by bluff parachute canopies.

A computer programme which applies these principles has been developed. Subsequently, a numerical investigation of the flow and of the consequent aerodynamic loads generated on an axisymmetric bluff parachute canopy has been performed.

The wake flow created by bluff canopies is found to be characterized by a periodic cluster shedding of vortex rings. Consequently, the calculated axial force coefficient developed on these canopies is also periodic. For steady flow its mean magnitude is in the range of 1.20-1.45 and its Strouhal number is about 0.13. These values are based on the canopy projected area and canopy projected diameter, respectively.

A parametric investigation of the canopy shape influence on both the wake flow & the axial aerodynamic force is presented. It was found that variation of the canopy shape does not have a major influence on the wake flow.

The calculated pressure distribution and wake flow periodicity are in good agreement with established experimental data.

An unsteady flow investigation shows that since the axial aerodynamic force cannot be described as a function of the instantaneous velocity and the instantaneous acceleration

solely, the Morison's formula for its representation is generally unsatisfactory. It provides a better approximation as the acceleration modulus is increased, when the flow history effect becomes of less significance. The calculated results for oscillatory axial motion bear a close resemblance to the sparse relevant experimental results which are available.

The simulated axial force development trend which ocurs during the inflation process, agrees with limited experimental results. However, because these provide insufficient experimental data concerning the simultaneous shape & velocity variation, no quantitative comparisons with experiments can be made.

The present model is basically a potential flow simulation. It includes the effects of fluid viscosity by allowing the fluid to separate from the canopy surface near its discontinuity, i.e. the canopy hemline. Owing to the assumed high Reynolds flow, the shear layer emanating from the hemline is thin. Thus, the vorticity is confined to the thin shear layer and outside it the fluid is irrotational. Consequently, in the irrotational part of the fluid field a velocity potential can be defined.

The canopy surface is replaced by first order ring panels each one containing a bound vortex ring along a circle located at one quarter of the panel length. The flow boundary condition on the canopy surface is determined by the normal velocity requirements at each panel, along a control circle located at three quarters of the panel length. Free-stream velocity variation, porosity effects and canopy shape changes are

accounted for by specifying the normal velocity along the control circle.

By generalizing Rosenhead's discretization of a two-dimensional vortex sheet, the free shear layer emanating from the canopy hemline is represented by discrete vortex rings which leave the canopy surface tangentially, at its hemline. The free vortex rings are convected by the local velocity.

Because of the high Reynolds number flow viscosity dissipation has been neglected.

The standing eddy developed near the separation line, on the canopy unwetted side, is simulated by a standing vortex ring.

In this model, several elements have been introduced which have not been considered previously in the published discrete-vortex separated wake simulation methods:

-improvement of the near wake simulation by accounting for the standing eddy at the flow separation region;

-inclusion of a simple method for calculating the newly-created vortex ring strength & location;

-reduction of the free parameters from two, which are the time step and the number of panels for the canopy representation, to one, the number of panels.

Further studies in model validation & development have been proposed. Owing to an insufficient data base for three-dimensional, separated flows, further experimental studies are certainly desirable and these have been specified.

## REFERENCES

ABERNATHY F.H. AND KRONAKUER R.E.-"THE FORMATION OF VORTEX STREETS" -J. FLUID MECH. 13,1962,pp.1-20

ACHENBACH E. -"EXPERIMENTS ON THE FLOW PAST SPHERES AT VERY HIGH REYNOLDS NUMBERS"-J. FLUID MECH 54,1972,pp.565-575

ATTA E.,KANDIL O.,MOOK D. AND NYFEH A.H. -" UNSTEADY AERODYNAMIC LOADS ON ARBITRARY WINGS INCLUDING WING TIP AND LEADING EDGE SEPARATION" -AIAA 77-156 ,1977

BAGLEY J.A., KIRBY N.B., MARCER P.J.-"A METHOD OF CALCULATING THE VELOCITY DISTRIBUTION ON ANNULAR AIRFOILS IN INCOMPRESSIBLE FLOW" REP.AERO.RES.COUN. LOND.20597, 1958

BATCHELOR G.K.-"AN INTRODUCTION TO FLUID DYNAMICS"- CAMBRIDGE UNIVERSITY PRESS, 1967

BEARMAN P.W. AND FACKRELL J.E.-"CALCULATION OF TWO-DIMENSIONAL AND AXISYMMETRIC BLUFF BODY POTENTIAL FLOW"- J. FLUID MECH. 72,part 2,1975,pp. 229-241

BEARMAN P.W.-" THE EFFECTS OF THE BASE BLEED ON THE FLOW BEHIND A TWO-DIMENSIONAL MODEL WITH A BLUNT TRAILING EDGE"-AERO QUATERLY, vol. 18, pp.207-224, 1967

BERNADIS B. ,GRAHAM J. AND PARKER K.-"OSCILLATORY FLOW AROUND DISKS AND THROUGH ORIFICES"- J. FLUID MECH. 102,1981,pp.279-299

CASTRO I.-"WAKE CHARACTERISTICS OF TWO-DIMENSIONAL PERFORATED PLATES NORMAL TO THE STREAM"-J. FLUID MECH. 46, pp.599-609,1971

CALVERT J.R.-(a)-"EXPERIMENTS ON THE FLOW PAST AN INCLINED DISK"-J. FLUID MECH. 29,pp.691-703,1967

CALVERT J.R.-(b)-"EXPERIMENTS ON THE LOW SPEED FLOW PAST CONES"-J. FLUID MECH. 27,1967,pp.373-289

CHANG P.K.-"SEPARATION OF FLOW", 1970, PERGAMON PRESS

CHIA-SHUN Y.-"FLUID MECHANICS"-Mc GRAW-HILL BOOK COMPANY 1969

CLEMENTS R.R.-"AN INVISCID MODEL OF TWO DIMENSIONAL VORTEX SHEDDING"-J.FLUID MECH. 57,PP.219-243,1973

CLEMENTS R.R AND MAULL D.J.-"THE REPRESENTATION OF SHEETS OF VORTICITY BY DISCRETE VORTICES"-PROG.AERO.SCI. 16,1975,pp.129-146

COCKRELL D.J.-"THE AERODYNAMICS OF PARACHUTES"-AGARD-AG-295 1987

COCKRELL D.J.,SHEN C.Q.,HARWOOD R.J. AND BAXTER A.C.- "AERODYNAMIC FORCES ACTING ON PARACHUTES IN UNSTEADY MOTION AND THE CONSEQUENTAL DYNAMIC STABILITY CHARACTERISTICS"-AIAA 86-2470,OCT 1986

DOHERR K.F.-"THEORETISCH-EXPERIMENTELLE UNTERSUCHUNG DES DYNAMISHEN VERHALTENS VON FALLSHIRM-SYSTEM BEI WINDKANALVERSUCHEN",D.F.V.L.R. INSTITUTE FUR FLUGMECHANIK-BRAUNSCHWEIG-DFVLR-FB81-29,1981

DURAND W.F.-"AERODYNAMIC THEORY-A GENERAL REVIEW OF PROGRESS"-DOVER PUBLICATIONS,NEW YORK,1963.

EDEN G.C.- "INVESTIGATION BY VISUAL AND PHOTOGRAPHIC METHODS OF THE FLOW PAST PLATES AND MODELS"-ADVISORY

COMMITEE FOR AERONAUTICS, R&M 58 ,1911-1912

ERICSSON L.E.-"KARMAN VORTEX SHEDDING AND THE EFFECT OF BODY MOTION" ,AIAA J. ,18,no.8,AUG.1980

EWING E.G.-"RINGSAIL PARACHUTE DESIGN"- AFFDL-TR-72-3 (AD-745-335),1972

EWING E.G., BIXBY K.W. AND KNACKE T.W.-"RECOVERY SYSTEM DESIGN GUIDE"-AFFDL-TR-78-151,DECEMBER 1978

FAGE A. AND JOHANSEN F.C.-"ON THE FLOW OF AIR BEHIND AN INCLINED PLATE OF INFINITE SPAN"-PROC. ROY. SOC. A,116,1927,pp.170-197

FALKNER V.M.-"THE CALCULATION OF AERODYNAMIC LOADING ON SURFACES OF ANY SHAPE"-AERONAUTICAL RESEARCH COMMITEE R&M 1910 AUGUST 1943

FOHL T., TURNER J.S.-"COLIDING VORTEX RINGS" PHYS.FLUIDS 18,1975,PP 433-436

GERRARD J.H.-"THE MECHANICS OF THE FORMATION REGION OF VORTICES BEHIND BLUFF BODIES"-J. FLUID MECH. 28, part 2,1966 pp.401-413

GERRARD J.H.-"NUMERICAL COMPUTATION OF THE MAGNITUDE AND FREQUENCY OF THE LIFT ON A CIRCULAR CYLINDER"-PHIL.TRANS.ROY.SOC. 261,no.1118,1967,pp.137-162

GOLDSTEIN S.-"MODERN DEVELOPMENTS IN FLUID DYNAMICS"- VOL 2, OXFORD UNIVERSITY PRESS,1938

GRADSTEIN I.S. AND RYSHIK I.M.-"SUMEN,PRODUCT UND INTEGRAL TAFELN",VEB DEUTSCHER VERLAG DER WISSENSHAFTEN, BERLIN 1963

HAM N.D.-"AERODYNAMIC LOADING ON A TWO DIMENSIONAL AIRFOIL DURING DYNAMIC STALL"-AIAA J. 6, no.10, OCT.1968,

pp.1927-1937

HARWOOD R.J.-DYNAMIC TESTS ON PARACHUTE CANOPIES, LEICESTER UNIVERSITY, U.K., TO BE PUBLISHED AS A PH.D. THESIS, 1988

HEINRICH G.H. AND UOTILA J.-"PRESSURE AND PROFILE DATA OF $20^0$ CONICAL RIBBON PARACHUTES"- SAND.77-7005, SANDIA LABORATORIES, MAY 1977

HEINRICH H.G. AND NOREEN R.A.-"ANALYSIS OF PARACHUTE OPENING DYNAMICS WITH SUPPORTING WIND-TUNNEL EXPERIMENTS"- J.AIRCRAFT, vol. 7,no.4,JUL-AUG. 1970

HENRICI R.J.-"DISCRETE VARIABLE METHODS IN ORDINARY DIFFERENTIAL EQUATIONS"-1962, JOHN WILEY & SONS

HOERNER S.J.- "FLUID DYNAMIC DRAG",PUBLISHED BY THE AUTHOR,1965

HUME R.G. AND STEVENS G.W.-"OBSERVATION ON BREATHING AND RELATED PHENOMENA IN SOME PARATROOP TYPE PARACHUTES WHEN FREELY DESCENDING"-ROYAL AERONAUTICAL SYMPOSIUM ON PARACHUTES AND RELATED TECHNOLOGIES, LONDON, SEPT. 1971

IBRAHIM S.K.-"APPARENT ADDED MASS AND MOMENT OF INERTIA OF CUP-SHAPED BODIES IN UNSTEADY INCOMPRESSIBLE FLOW"- PH.D. thesis, UNIVERSITY OF MINNESOTA, U.S.A.,1965

IVERSEN H. AND BALLENT R.-"A CORRELATING MODULUS FOR FLUID RESISTANCE IN ACCELERATED MOTION"- J.APP.PHYS.,vol. 22,no.3,March 1951

JORGENSEN D.S. AND COCKRELL D.J.-"AERODYNAMICS OF CRUCIFORM PARACHUTE CANOPIES"-AIAA 81-1919,OCT.1981

JORGENSEN D.S. -"EXPERIMENTAL DETERMINATION OF THE PARACHUTE

EQUATIONS OF MOTIONS"-AIAA 84-0798,OCT. 1984

KARAMCHETI K.-"PRINCIPLES OF IDEAL FLUID AERODYNAMICS"-1966, JOHN WILEY & SONS

KATZ J.-"METHOD FOR CALCULATING WING LOADING DURING MANOEUVRING FLIGHT ALONG A THREE DIMENSIONAL CURVED PATH"-J. AIRCRAFT,16,1979, pp.739-741

KATZ J.-"A DISCRETE VORTEX METHOD FOR THE NON-STEADY SEPARATED FLOW OVER AN AIRFOIL"-J. FLUID MECH. 102,1981,pp.312-328

KIYA M. AND ARIE M.-"A CONTRIBUTION TO AN INVISCID VORTEX SHEDDING MODEL FOR AN INCLINED FLAT PLATE IN UNIFORM FLOW"-J. FLUID MECH. 82,1977,pp.223-240

KLIMAS P. -"FLUID MASS ASSOCIATED WITH AN AXISYMMETRIC PARACHUTE CANOPY"- J. AIRCRAFT,14,no.6,JUNE 1977,pp.577-580

KLIMAS P. -"INFLATING PARACHUTE CANOPY DIFFERENTIAL PRESSURES"-J.AIRCRAFT, 16,no.12,DEC.1979,pp.861-862

KOHIN N.E.,KIBEL I.A. AND ROZE N.V.-"THEORETICAL HYDROMECHANICS" INTERSCIENCE PUBLISHERS,1964

LAMB H.-"HYDRODYNAMICS",6-TH EDITION, CAMBRIDGE UNIVERSITY PRESS, 1932

LEVIN D. AND KATZ.J -"A VORTEX LATTICE METHOD FOR THE CALCULATION OF THE UNSTEADY SEPARATED FLOW OVER DELTA WINGS"- AIAA 80-183 AUG. 1980

LEONARD A.- "NUMERICAL SIMULATION OF INTERACTING THREE-DIMENSIONAL VORTEX FILAMENTS"- LECTURE NOTES IN PHYSICS ,1975,pp 245-250, SPRINGER VERLAG-NEW YORK/BERLIN

LEONARD A.-"SIMULATION OF THREE-DIMENSIONAL SEPARATED FLOWS WITH VORTEX FILAMENTS", LECTURE NOTES IN PHYSICS ,1976,pp 280-284, SPRINGER VERLAG-NEW YORK/BERLIN

LINGARD J.S.-"THE AERODYNAMICS OF PARACHUTE DURING THE INFLATION PROCESS"- PH.D. THESIS, UNIVERSITY OF BRISTOL, 1977

LOW H.T. AND NEWMAN B.G.-"TWO-DIMENSIONAL FLOW PAST BLUFF FLEXIBLE MEMBRANES OF LOW POROSITY"-AERONAUTICAL JOURNAL, pp.313-334,OCT. 1986

MAXWORTHY T.-"THE STRUCTURE AND STABILITY OF VORTEX RINGS"- J.FLUID MECH.,vol. 51,pp.15-32,1972

MAXWORTHY T.-"TURBULENT VORTEX RINGS"-J.FLUID MECH. ,vol. 64,pp.227-230,1974

MODI V.J. AND SLATER J.E.-"UNSTEADY AERODYNAMICS AND VORTEX INDUCED AEROELASTIC INSTABILITY OF A STRUCTURAL ANGLE"-AIAA 77-160,JAN. 1970.

MAULL D.J.-"FLOW MODELS USING VORTEX DYNAMICS-WORKS IN THE UNITED KINGDOM"- paper presented at AGARD ROUND TABLE DISCUSSION, APR. 1986

Mc COY H.H. AND WERME T.D.-"AXISYMMETRIC VORTEX LATTICE METHOD APPLIED TO PARACHUTE SHAPES"-AIAA 86-2456, OCT.1986

MEYER J. AND PURVIS J.W.-"VORTEX LATTICE THEORY APPLIED TO PARACHUTE CANOPY CONFIGURATIONS"-AIAA 84-0795, OCT. 1984

MURAMOTO K. AND GARRARD W.-"A METHOD FOR CALCULATING THE PRESSURE FIELD ABOUT A RIBBON PARACHUTE CANOPY IN STEADY DESCENT"-AIAA 84-0794,APRIL 1984

NEWMAN N.J.-"MARINE HYDRODYNAMICS"-THE MIT PRESS,FOURTH

PRINTING,1982

OSHIMA Y. AND ASAKA S.-INTERACTION OF MULTI-VORTEX RINGS"-
J.PHYS.SOC. JAPAN, 42, 1977, pp 1391-1395

PARKINSON G.V. AND JANDALI T.-"A WAKE SOURCE MODEL FOR BLUFF BODY POTENTIAL FLOW"-J. FLUID MECH.,40,part 3, 1970,pp. 577-594

PAYNE P.R.-"THE THEORY OF FABRIC POROSITY AS APPLIED TO PARACHUTES IN INCOMPRESSIBLE FLOW"-AERONAUTICAL QUARTERLY, AUGUST 1978

"PERFORMANCE OF AND DESIGN CRITERIA FOR DEPLOYABLE AERODYNAMIC DECELERATORS"-"ASD-TR-61-579,DEC. 1963

PEPPER B.W. AND REED J.F.-"PARAMETRIC STUDY OF PARACHUTE PRESSURE DISTRIBUTION BY WIND TUNNEL TESTING"-
J. AIRCRAFT ,13,no.11, NOV. 1976,pp.895-900

PRANDTL L. AND TIETJENS O.G.-"FUNDAMENTALS OF HYDRO- AND AEROMECHANICS",DOVER EDITION,1957

REHBACH C.-"NUMERICAL CALCULATIONS OF THREE DIMENSIONAL UNSTEADY FLOWS WITH VORTEX SHEETS"-AIAA 78-111, JAN.1978

RIABOUCHINSKY D. -"ON SOME CASES OF TWO-DIMENSIONAL FLUID MOTION", PROC. LONDON MATH.SOC.19,1919,pp.206

ROBERTS W.R.-"A CONTRIBUTION TO PARACHUTE INFLATION DYNAMICS"-AIAA 68-928,SEPT.1968

ROBERTS W.R.-"DRAG AND BASE PRESSURE DISTRIBUTION ON A FAMILY OF POROUS,SLOTTED DISKS"-AIAA 79-0462,OCT-1979

ROSENHEAD L.-(a)-APPENDIX TO STANTON T.E. & MARSHAL D. (1931)

ROSENHEAD L.-(b)-"FORMATION OF VORTICES FROM A SURFACE OF DISCONTINUITY" PROC.ROY.SOC.A134,1931,pp.170-192

ROSENHEAD L.-"LAMINAR BOUNDARY LAYERS"-1963, OXFORD CLARENDON PRESS

ROSHKO A.-"ON THE DRAG AND SHEDDING FREQUENCY OF TWO DIMENSIONAL BLUFF BODIES"-NACA TN 3169,JULY,1954 17 no. 10,pp.622-628,OCT. 1950

SARPKAYA T.-"AN INVISCID MODEL OF TWO DIMENSIONAL VORTEX SHEDDING FOR TRANSIENT AND ASYMPTOTICALLY STEADY SEPARATED FLOW ON INCLINED PLATE"-J. FLUID MECH. 68,1975,pp.109-128

SARPKAYA T.-"IMPULSIVE FLOW ABOUT A CIRCULAR CYLINDER"-TECHNICAL REPORT NO. NPS-69SL78-008,NAVAL POSTGRADUATE SCHOOL, MONTEREY, CA.,U.S.,1978

SARPKAYA T. AND SHOAFF R.-"INVISCID MODEL OF TWO-DIMENSIONAL VORTEX SHEDDING BY A CIRCULAR CYLINDER"-AIAA J.,VOL. 17,NO. 11,pp 1193-1200, 1979

SAFFMAN P.G.-"THE VELOCITY OF THE VISCOUS VORTEX RINGS" STUD. APPL. MATH. 49,1970,pp.370-380

SHIRAYAMA S. AND KUWAHARA K.-"COMPUTATION OF FLOW PAST A PARACHUTE BY A THREE DIMENSIONAL VORTEX METHOD"-AIAA 86-0350,JAN.1986

SCHAEFER W.J. AND ESKENAZI S.-"ANALYSIS OF THE VORTEX STREET GENERATED IN A VISCOUS FLUID"-J. FLUID MECH. ,6, 1959,pp.241-260

SHEN C.Q.-"FLOW FIELD CHARACTERISTICS AROUND BLUFF PARACHUTE CANOPIES"-PH.D. THESIS, LEICESTER UNIVERSITY, U.K., 1987

SMITH J.H.B.-"THEORETICAL MODELLING OF THREE DIMENSIONAL VORTEX FLOWS IN AERODYNAMICS"-AER. J. OF ROY.SOC.,

APRIL 1984,pp.101-116

SOVRAN G., THOMAS M. AND MASON W.T.-"AERODYNAMIC DRAG MECHANISMS OF BLUFF BODIES AND ROAD VEHICLES", PLENUM PRESS, NEW YORK-LONDON ,1978

SPAHR R. AND WOLF D.-"THEORETICAL ANALYSIS OF WAKE-INDUCED PARACHUTE COLLAPSE"-AIAA-81-1922, OCT.1981

STANTON T.E. AND MARSHALL D.-"THE EDDY SYSTEM IN THE WAKE OF FLAT CIRCULAR PLATES IN THREE DIMENSIONAL FLOW"-PROC. ROY. SOC. A. ,130,1931,p.295

STREETER V.L. -"FLUID MECHANICS", 1966 Mc GRAW HILL

STRICKLAND J.H.-"ON THE UTILIZATION OF VORTEX METHODS FOR PARACHUTE AERODYNAMICS PREDICTIONS"-AIAA 86-2455, OCT.1986

TANEDA S.-"VISUAL OBSERVATION OF THE FLOW PAST A SPHERE AT REYNOLDS NUMBERS BETWEEN $10^4$ AND $10^6$"-J. FLUID MECH.,85,1978,pp.187-192

TAYLOR G.I. AND DAVIES R.M.-"THE AERODYNAMICS OF POROUS SHEETS" REPORTS AND MEMORANDA OF THE AERONAUTICAL RESEARCH COUNCIL, NO. 2234, 1944

THWAITES B.- "INCOMPRESSIBLE AERODYNAMICS"-OXFORD, CLARENDON PRESS,1960

WEISSINGER J.-"ZUR AERODYNAMIC DES RINGFLUGELS", BER.DTCH.VERS ANT.LUFTFAHRT, MULHEIM 42, 1957

WINDALL S.E.-"THE STRUCTURE AND DYNAMICS OF VORTEX FILAMENTS" ANUAL REVIEW OF FLUID MECHANICS, VOL.7, 1975, pp.141-165

YAVUZ T. AND COCKRELL D.J.-"EXPERIMENTAL DETERMINATION OF PARACHUTE APPARENT MASS AND ITS SIGNIFICANCE IN PREDICTING DYNAMIC STABILITY"- AIAA 81-1920, OCT 198

# APPENDIX :

## COMPUTER PROGRAMME " P A R A C H U T E " LISTING

```
*
*
*                 ================================
*                     PARACHUTE-MAIN PROGRAMME
*                 ================================
*
*
*
*
      PROGRAM PARACHUTE
*
*   " P A R A C H U T E "  SIMULATES THE FLOW FIELD AND CALCULATES THE
*   CONSEQUENT PRESSURE DISTRIBUTION & AXIAL FORCE DEVELOPED
*   AROUND A PARACHUTE CANOPY. THE MAIN ASSUMPTIONS ARE:
*                  - AXISYMMETRIC FLOW
*                  - HIGH REYNOLDS NUMBER INCOMPRESSIBLE FLOW
*   THE MODEL IS BASICALLY, A POTENTIAL ONE.
*   THE CANOPY SURFACE IS REPLACED BY A BOUND VORTEX RING LATTICE.
*   THE SEPARATED WAKE IS SIMULATED BY A FREE VORTEX RING LAYER.
*   THE STANDING EDDY DEVELOPED ON THE CANOPY UNWETTED SIDE, NEAR
*   ITS HEMLINE IS ACCOUNTED FOR BY A STANDING VORTEX RING.
*
*-------------------------------------------------------------------
*
*   THE COMPUTER PROGRAMME CAN BE RUN INTERACTIVELLY. WHEN
*   THIS MODE IS USED THE PROGRAM WILL PROMT WITH QUESTIONS
*   AND HINTS WHICH WILL HELP THE UNEXPERIENCED USER.
*
*-------------------------------------------------------------------
*
      PARAMETER (NPN1=21,NVR1=500,PI1=3.141592654,NMAX1=500)
      DIMENSION C(NPN1,NPN1),CTEMP(NPN1,NPN1),DCP(NPN1),DCPST(NPN1)
     1,GMW(NVR1),CANCELL(NVR1),EP(NVR1),U(NPN1)
     2,C25(NPN1,2),C75(NPN1,2),WKNEW(NVR1,2),WKOLD(NVR1,2)
     3,GMB(NPN1),PANPOR(NPN1),XPN(NPN1),GMBOLD(NPN1),IYG(NVR1)
     4,TIME(NVR1),CA(NVR1),YG(NVR1),IY(NVR1),IX(NVR1)
     5,TVEL(NMAX1),VEL(NMAX1),PX(NVR1),PY(NVR1),DCPOLD(NPN1)
     6,TSHAPE(NMAX1),XMT(NMAX1),YMT(NMAX1),XIT(NMAX1),AXIAL_F(NVR1)
     7,ADD(NVR1),TDEC(NVR1),VDEC(NVR1),C25OLD(NPN1)
      CHARACTER REPLY*3,REPLY1*3,LINE(70),LIN(70),LN(70),TITLE*20
      DATA YMST,XMST,XIST,USTEADY,IPOR,NW,IPR1,IPR2,CASTD,NPAN,
     1IPLOT,IPL1,NPL,NDCUT,IDEC,FYSVR,FQ,
     2ISHAPE_T,IPRSHAPE,IWAKE,IAXIAL_F,TMAX,CASTD,KSHAPE,RO/
     31.,1.,1.,-15.,0,25,999,999,
     41.42,12,0,25,1,4,0,1.12,1,0,0,0,0,1000,1.4,0,1.25/
      NAMELIST/LIST/ TITLE,YMST,XMST,XIST,USTEADY,NW,TMAX,
     1FYSVR,CASTD,RO,
     2IPOR,IDEC,ISHAPE_T,IPRSHAPE,IWAKE,IPR1,IPR2,IPLOT,IPL1,NPL
      NPN=NPN1
      NVR=NVR1
      PI=PI1
      NMAX=NMAX1
*
*
*        ---------------------------
***      THE "DIALOG" WITH THE USER
*        ---------------------------
*
```

```
*
      PRINT 60
      READ(5,'(A)') REPLY1
      IF(REPLY1(1:1).EQ.'N' .OR. REPLY1(1:1).EQ.'n') THEN
          PRINT 70
170       READ*,XMST,YMST,XIST
          CALL SHAPE(XMST,YMST,AL,XIST)
          PRINT 160
          READ(5,'(A)') REPLY
          IF(REPLY(1:1).EQ.'Y' .OR. REPLY(1:1).EQ.'y')
     1    THEN
                PRINT 180
                GO TO 170
          END IF
210       PRINT 90
          READ(5,'(A)') REPLY
          PRINT 80
          PRINT 90
          READ(5,'(A)') REPLY
          PRINT 185
          PRINT 90
          READ(5,'(A)') REPLY
          PRINT 190
          PRINT 90
          READ(5,'(A)') REPLY
          PRINT 110
          PRINT 90
          READ(5,'(A)') REPLY
          PRINT 111
          PRINT 90
          READ(5,'(A)') REPLY
          PRINT 200
          READ(5,'(A)') REPLY
          IF(REPLY(1:1).EQ.'Y' .OR. REPLY(1:1).EQ.'y')
     1    GO TO 210
      END IF
      XMST=1.
      YMST=1.
      XIST=1.
      PRINT 10
      PRINT 90
      READ(5,'(A)') REPLY
      WRITE(6,LIST)
      IF(REPLY1(1:1).EQ.'Y' .OR. REPLY1(1:1).EQ.'y')
     1GO TO 222
      PRINT 100
      READ(5,'(A)') REPLY
      CALL SHAPE(XMST,YMST,AL,XIST)
222   PRINT 20
      READ(5,'(A)') REPLY
      IF(REPLY(1:1).EQ.'y' .OR. REPLY(1:1).EQ.'Y') THEN
           IF(REPLY1(1:1).EQ.'Y' .OR. REPLY1(1:1).EQ.'y')
     1GO TO 333
*
*
*        ----------------
***      READING THE DATA
*        ----------------
*
```

```
*
          PRINT 30
333       READ(5,LIST)
          PRINT 40
          PRINT 90
          READ(5,'(A)') REPLY
          WRITE(6,LIST)
          PRINT 100
          READ(5,'(A)') REPLY
          CALL SHAPE(XMST,YMST,AL,XIST)
          PRINT 90
          READ(5,'(A)') REPLY
          ELSE
             PRINT 50
          END IF
*
*
***       READING THE VELOCITY/TIME TABLE
*
*
          IF(USTEADY.GT.998.)THEN
             PRINT*,' THE NUMBER OF PAIRS IN THE VELOCITY/TIME
         1 TABLE IS:'
             READ*,NVEL
             PRINT*,NVEL
             PRINT 140
             IAXIAL_F=1
             DO 66 I=1,NVEL
66           READ*,TVEL(I),VEL(I)
             PRINT*,'  THE VELOCITY PROFILE IS:'
             PRINT*,'  TIME[SEC]       VELOCITY[M/SEC]'
             DO 77 I=1,NVEL
77           PRINT*,TVEL(I),VEL(I)
             PRINT 90
             READ(5,'(A)') REPLY
          END IF
*
*
***       READING THE CANOPY SHAPE/TIME TABLE
*
*
          IF(ISHAPE_T.EQ.1)THEN
             PRINT*,' THE NUMBER OF SHAPE PARAMETERS IN THE
         1   SHAPE/TIME TABLE IS:'
             READ*,NTSHAPE
             PRINT*,NTSHAPE
             PRINT 240
             DO 85 I=1,NTSHAPE
85           READ*,TSHAPE(I),YMT(I),XMT(I),XIT(I)
             PRINT*,'  THE SHAPE/TIME IS:'
             PRINT*,'  TIME[SEC]       YMT[M]          XMT[M]          XIT[M]'
             DO 87 I=1,NTSHAPE
87           PRINT*,TSHAPE(I),YMT(I),XMT(I),XIT(I)
             PRINT 90
             READ(5,'(A)') REPLY
          END IF
*
*
***       READING THE PARACHUTE/PAYLOAD MASS FOR THE FREE DECELERATION
```

```
***     MODE
*
*
        IF(IDEC.EQ.1)THEN
           PRINT*,' FREE DECELERATION'
           PRINT*,'__PLEASE ENTER THE MASS OF THE DECELERATION
1          SYSTEM.'
           READ*,AMASS
           PRINT*,' THE MASS OF THE DECELERATION SYSTEM IS',
1          AMASS,' KG.'
           PRINT 90
           READ(5,'(A)') REPLY
           UNO=USTEADY
           IAXIAL_F=1
         END IF
*
         IF(IPOR.EQ.0)GO TO 65
*
*
***      READING THE GEOMETRIC POROSITY
*
*
         DO 75 I=1,NPAN
         PRINT*,'PLEASE ENTER THE GEOMETRIC POROSITY OF THE',I,
        1'-TH PANEL'
         READ(5,*)PANPOR(I)
75       WRITE(6,175)I,PANPOR(I)
65       CONTINUE
*
*
*
*       ------------
*       OPENING FILES
*       ------------
*
*       THE FILES CONTEIN RESULTS WHICH CAN BE SUBSEQUENTLY
*       USED FOR PLOTTINGS/PRINTOUTS OR STORED IN AN ARCHIVE:
*            -FLOW.DAT (CHANNEL 1): CONTAINS THE CANOPY & SHED
*                                   VORTEX RING COORDINATES AT
*                                   A GIVEN INSTANT.
*            -CA.DAT (CHANNEL 2): CONTAINTS THE AXIAL FORCE
*                                 COEFFICIENT AND THE TIME.
*            -VEL.DAT (CHANNEL 3): CONTAINS THE VELOCITY IN
*                                  THE WAKE AS  A FUNCTION OF
*                                  Y AT SIX DIFFERENT AXIAL
*                                  STATIONS DOWNSTREAM THE CANOPY.
*                                  THE DISTANCE BETWEEN TWO
*                                  CONSECUTIVE STATIONS IS ONE
*                                  CANOPY PROJECTED AREA RADIUS.
*              -K11.DAT (CHANNEL 4): CONTAINS THE ADDED MASS
*                                    COEFFICIENT AND THE TIME.
*              -AXIAL_F.DAT (CHANNEL 9): CONTAINS THE AXIAL FORCE
*                                        AND THE TIME.
*              -VELDEC.DAT (CHANNEL 10): CONTAINS THE CALCULATED
*                                        DESCENT VELOCITY WHEN THE
*                                        FREE DECELERATION MODE IS
*                                        USED.
*
*       AT THE END OF THE RESULTS THE INPUT DATA IS WROTE.
```

```
*
*
      IF(IPLOT.EQ.1)THEN
              OPEN(UNIT=1,FILE='FLOW',STATUS='NEW')
              OPEN(UNIT=2,FILE='CA',STATUS='NEW')
              IF(IAXIAL_F.EQ.1) THEN
               OPEN(UNIT=9,FILE='AXIAL_F',STATUS='NEW')
               OPEN(UNIT=4,FILE='K11',STATUS='NEW')
               N=1
               WRITE(4,125)N
              END IF
              IF(IDEC.EQ.1) THEN
               OPEN(UNIT=10,FILE='VELDEC',STATUS='NEW')
               N=1
               WRITE(10,125)N
              END IF
              IF(IWAKE.EQ.1)THEN
                 OPEN(UNIT=3,FILE='VEL',STATUS='NEW')
                 NV=6
                 WRITE(3,125)NV
              END IF
              N1=NPAN+1
              WRITE(1,113)N1
              NGR=1
              WRITE(2,125)NGR
      END IF
*
*
      AL=0.
      DO 12 I=1,NVR
12    CANCELL(I)=1.
      IF(ISHAPE_T.EQ.1)THEN
         XI=TB(0.00001,TSHAPE,XIT,NTSHAPE,NMAX1)
         XM=TB(0.00001,TSHAPE,XMT,NTSHAPE,NMAX1)
         YM=TB(0.00001,TSHAPE,YMT,NTSHAPE,NMAX1)
       ELSE
         XI=XIST
         XM=XMST
         YM=YMST
      END IF
      SCALEX=10./YM
      SCALEY=1.75*SCALEX
      YREF=YMST
      YXI=Y(XIST,XIST,XMST,YMST,0)
      IF(XIST.LT.XMST)YREF=YXI
      SREF=PI*YREF*YREF
       VOLCAN=VOL(XIST,PI,XMST,YMST,0)
       SCAN=SURF(XIST,PI,XMST,YMST,0)
       WRITE(6,122)YREF,SREF,VOLCAN,SCAN
       PRINT 130
       PRINT 90
       READ(5,'(A)') REPLY
       U1=UN(0,UNO,0,SREF,0,USTEADY,
     1TVEL,VEL,NVEL,NMAX,IDEC,AMASS,NDT)
       DT=0.1*YM/ABS(U1)
       T=DT
       XCUT=2.*YMST*NDCUT*ABS(U1)/U1
       UNO=USTEADY
*
```

```
*          -------------
***        THE MAIN LOOP
*          -------------
*
          DO 112 NDT=1,NW
*
          UINF=UN(T,UNO,DT,SREF,CAO,USTEADY,
         1TVEL,VEL,NVEL,NMAX,IDEC,AMASS,NDT)
          IF(ABS(UINF).LT.0.000001)THEN
             IF(UINF.LT.O)THEN
                UINF=UINF-0.000001
             ELSE
                UINF=UINF+0.000001
             END IF
          END IF
          IF(ISHAPE_T.EQ.1)THEN
             XI=TB(T̄,TSHAPE,XIT,NTSHAPE,NMAX)
             XM=TB(T,TSHAPE,XMT,NTSHAPE,NMAX)
             YM=TB(T,TSHAPE,YMT,NTSHAPE,NMAX)
             PRINT*,'YM=',YM,'XM=',XM,'XI=',XI
             IF(IPRSHAPE.EQ.1)CALL SHAPE(XM,YM,AL,XI)
          END IF
          IF(NDT.EQ.1)GO TO 44
*
*
***       THE TIME STEP
*
*
          DT=ABS(GMW(NDT-1)/GMWNDT)
*
44        CALL CANOPY(UINF,NPAN,BETA,GMW,CANCELL,EP,NDT,WKOLD,XSHD,
         1YSHD,XI,U,WKNEW,NW,DT,GMB,YREF,XPN,DA,T,IPOR,
         2PANPOR,AXIAL_F,CAO,UNO,CASTD,IPR1,IPR2,ARC,XM,YM,AL,
         3VOLCAN,ACC,P̄I̲,GMWNDT,GMSVR,XSVR,YSVR,NPN,NVR,IYG,
         4DCP,DCPST,DEL,C25,C75,C,CTEMP,TIME,CA,YG,GMBOLD,IPLOT,
         5IPL1,NPL,XCUT,ICORE,FYSVR,ISHAPE_T,DCPOLD,VELDEF,IWAKE,
         6IAXIAL_F,TMAX,ADD,KSHAPE,RO,IDEC,C25OLD)
          IF(T.GT̄.TMAX)GO TO 103
          T=T+DT
*
*
***       CHECKING THE VORTEX RING RADIUS TO ITS CORE RADIUS RATIO
*
*
          DO 33 J=1,NDT
          E=EP(J)/2./YM
          IF(E.GT.0.005)THEN
             PRINT*,'THE SIZE OF THE VORTEX CORE IS TOO BIG',E,J
             PRINT*,'PLEASE INCREASE THE REYNOLDS NUMBER'
             STOP
          END IF
33        CONTINUE
*
*
***       THE CONDITIONAL WRITING OF THE UNCANCELLLED SHED
***       VORTEX RING COORDINATES ON "FLOW.DAT"
*
*
```

```
      IF(IPLOT.EQ.1)THEN
           NPL1=(NDT-IPL1)/NPL
           NPL2=NPL*NPL1
       IF((NDT.GE.IPL1.AND.NPL2.EQ.(NDT-IPL1)).OR.T.GT.TMAX)THEN
             NPLOT=0
             DO 115 IJ=1,NDT
             IF(CANCELL(IJ).GT.0.)THEN
               NPLOT=NPLOT+1
               PX(NPLOT)=WKOLD(IJ,1)
               PY(NPLOT)=WKOLD(IJ,2)
             END IF
115           CONTINUE
              WRITE(1,113)NPLOT
              DO 117 IP=1,NPLOT
117           WRITE(1,114)PX(IP),PY(IP)
            END IF
          END IF
*
*
***     DISPLAYING OR PRINTING ON THE LINE PRINTER THE WAKE FLOW
***     PATTERN AND THE PRESSURE DISTRIBUTION
*
*
116     IF(NDT.LT.IPR1.OR.NDT.GT.IPR2)GO TO 112
        WRITE(6,999)
        WRITE(6,2)XSVR,YSVR,GMSVR
        DO 101 J=1,NDT
        E=EP(J)/2/YM
101     WRITE (6,301) J,WKOLD(J,1),WKOLD(J,2),GMW(J),CANCELL(J),E
521     WRITE (6,201)  DT,T,UINF,ACC
        WRITE(6,401)
         WRITE(6,221) SCALEX,SCALEY
         CALL PLOT(WKOLD,NDT,SCALEX,SCALEY,XI,XM,YM,AL,
       1NVR,IX,IY,XCUT,GMW,CANCELL)
112      CONTINUE
*
*
***     CLOSING THE OUTPUT FILES
*
*
103     IF(IPLOT.EQ.1)THEN
              WRITE(1,LIST)
              WRITE(2,LIST)
              IF(IWAKE.EQ.1)WRITE(3,LIST)
              IF(IAXIAL_F.EQ.1)THEN
                  WRITE(4,LIST)
                  WRITE(9,LIST)
              END IF
              IF(IDEC.EQ.1)WRITE(10,LIST)
              IF(IPOR.EQ.1)THEN
                  DO 176 I=1,NPAN
                  WRITE(2,178)I,PANPOR(I)
                  IF(IWAKE.EQ.1)WRITE(3,178)I,PANPOR(I)
                  IF(IAXIAL_F.EQ.1)THEN
                     WRITE(4,178)I,PANPOR(I)
                     WRITE(9,178)I,PANPOR(I)
                  END IF
                  IF(IDEC.EQ.1)WRITE(10,178)I,PANPOR(I)
176               WRITE(1,178)I,PANPOR(I)
```

```
      END IF
      IF(IDEC.EQ.1)THEN
           WRITE(10,114)AMASS
           WRITE(1,114)AMASS
           WRITE(2,114)AMASS
           IF(IWAKE.EQ.1)WRITE(3,114)AMASS
           IF(IAXIAL_F.EQ.1)WRITE(4,114)AMASS
      END IF
      IF(IAXIAL_F.EQ.1)THEN
           WRITE(2,*)NVEL
           IF(IWAKE.EQ.1)WRITE(3,*)NVEL
           WRITE(4,*)NVEL
           WRITE(9,*)NVEL
           WRITE(1,*)NVEL
           DO 177 I=1,NVEL
           WRITE(2,114)TVEL(I),VEL(I)
           IF(IWAKE.EQ.1)WRITE(3,114)TVEL(I),VEL(I)
           WRITE(4,114)TVEL(I),VEL(I)
           WRITE(9,114)TVEL(I),VEL(I)
177        WRITE(1,114)TVEL(I),VEL(I)
      END IF
      CLOSE(UNIT=1)
      CLOSE(UNIT=2)
      CLOSE(UNIT=3)
      CLOSE(UNIT=4)
      CLOSE(UNIT=9)
      CLOSE(UNIT=10)
 END IF
*
*
*
10    FORMAT(////2X,
     1'THE DEFAULT VALUES USED BY THE PROGRAM ARE:'///)
20    FORMAT(2X,
     1'DO YOU WISH TO CHANGE ANY OF THESE VALUES? (Y/N)')
30    FORMAT(//2X,
     1'IN ORDER  TO CHANGE  THE  VALUE OF  ANY OF'/2X,
     2'THE  CONSTANTS  PLEASE TYPE THE FOLLOWING:'/2X,
     3'         $$LIST'/2X,
     4'         $NAME=VALUE'/2X,
     5'              :'/2X,
     6'              :'/2X,
     7'         $NAME=VALUE'/2X,
     8'         $$'/2X,
     9'WHERE  NAME  IS THE NAME OF THE  CONSTANT,'/2X,
     1'AND VALUE IS THE NEW VALUE TO BE ASSIGNED.'/2X,
     2'       NOTE       THAT THE VALUES OF ONE OR'/2X,
     3'MORE CONSTANTS  CAN BE CHANGED.  THE REST'/2X,
     4'--- OF THE VALUES REMAINE UNALTERED. ----')
40    FORMAT(//2X,
     1'THE VALUES OF THE CONSTANTS HAVE CHANGED'/2X,
     2'--------- THE NEW VALUES ARE -----------'////)
50    FORMAT(2X,
     1'THE VALUES OF CONSTANTS ON $$LIST REMAIN UNALTERED.')
60    FORMAT(//2X
     1'DO YOU KNOW HOW TO RUN THE PROGRAM ? (Y/N)'////)
70    FORMAT(
     1' THE PROGRAM CALCULATES THE AERODYNAMIC LOADS DEVELOPED
                                                    ON AN'/,
```

```
     2' AXISYMMETRIC CANOPY IN AXISYMMETRIC, INCOMPRESSIBLE,'/,
     3' HIGH REYNOLDS NUMBER FLOW. THE DIMENSIONS ARE IN S.I.
                                                        SYSTEM.'/,
     4' THE DATA IS INTRODUCED BY USING THE "NAMELIST"
                                                      FUNCTION.'/,
     5' IN THE FOLLOWING THE INPUT PARAMETERS ARE EXPLAINED:'/,
     6'     -"TITLE"-A STRING OF UP TO 20 CHARACTERS.'/,
     7'     -THE CANOPY IS APPROXIMATED BY AN ELLIPTIC SHELL.'/,
     8'      IN THE NAMELIST THE STEADY VALUE OF THOSE
                                                      PARAMETERS'/,
     9'      ARE INTRODUCED:'/,
     1'          -"XMST" IS THE RADIUS PARALLEL WITH X AXIS.'/,
     2'           THE FLOW IS PARALLEL WITH X AXIS. THE '/,
     3'           THE CANOPY APPEX IS THE ORIGIN.'/,
     4'          -"YMST" IS THE RADIUS PERPENDICULAR TO THE
                                                        FLOW.'/,
     5'          -"XIST" IS THE X COORDINATE OF THE CANOPY'/,
     6'           HEMLINE (THE SKIRT).'/,
     7'        FOR EXAMPLE : XM=0.5,YM=0.5,XI=0.5 DESCRIBE A '/,
     8'        HEMISPHERICAL CANOPY WITH RADIUS 0.5 METERS.'/,
     9'        AS AN ADDITIONAL EXAMPLE, PLEASE --ENTER--
                                                        VALUES'/,
     1'        FOR XM,YM,XI( E.G. 1.,0.5,0.8). THE PICTURE ON'/,
     2'        THE SCREEN WILL SHOW THE CANOPY ( THE ARROW
                                                         THE '/,
     3'        FLOW DIRECTION).')
  80  FORMAT(//2X' THE REMAINING PARAMETERS ARE:'/,
     1'   -"USTEADY": THE VELOCITY (FOR A BLUFF PARACHUTE
                                                        CANOPY'/,
     2'               IT IS USUALLY, NEGATIVE).'/,
     2'               THE DIMENSIONS METERS/SECOND. WHEN A '/,
     3'               TIME-DEPENDENT VELOCITY PROFILE IS TO BE'/,
     4'               SIMULATED USTEADY=999 ( YOU WILL BE'/,
     5'               ASKED TO ENTER THE VELOCITY PROFILE.)'/,
     6'               WHEN FREE DECELERATION IS SIMULATED, '/,
     7'               "USTEADY" IS THE INITIAL VELOCITY'/,
     8'               OF THE PARACHUTE/PAYLOAD SYMSTEM.'/,
     9'   -"NW": THE MAXIMUM NUMBER OF SHED VORTEX RINGS.'/,
     1'          (STOPPING CRITERIA). FOR THE AVERAGE
                                                      AERODYNAMIC'/,
     2'          LOAD NW ~ 40 ; FOR TIME-DEPENDENT
                                                    CHARACTERISTICS'/,
     3'          NW ~ 250.'/,
     4'   -"TMAX": THE MAXIMUM TIME (ADDITIONAL STOPPING
                                                      CRITERIA. ')
  90  FORMAT(' PLEASE PRESS RETURN TO CONTINUE.')
 100  FORMAT('  PLEASE PRESS RETURN AND THE CANOPY SHAPE
     1 WILL BE DISPLAYED.')
 110  FORMAT(
     1' -"IPR1","IPR2": THE FIRST AND THE LAST TIME STEP WHEN
                                                        THE '/,
     2'                 FLOW PATTERN IS TO BE PRINTED OR
                                                      DISPLAYED'/,
     3'                 ON THE TERMINAL SCREEN. IN ADDITION
                                                      TO THAT'/,
     4'                 ALSO A DETAILED OUTPUT INCLUDING
                                                      PRESSURE'/,
     5'                 DISTRIBUTION AND SHED VORTEX RINGS '/,
     6'                 COORDINATES ARE DISPLAYED OR PRINTED.'/,
```

```
     7' -"IPLOT": IF IPLOT=1 THE OUTPUT IS DIRECTED TO OUTPUT
                                                        FILES.'/,
     8'           THE RESULTS CAN BE SUBSEQUENTLY USED FOR P'/,
     9'           PLOTTINGS/PRINTOUTS OR STORED IN AN ARCHIVE:'/,
     1'     -FLOW.DAT (CHANNEL 1): CONTAINS THE CANOPY & SHED'/,
     2'                            VORTEX RING COORDINATES AT'/,
     3'                            A GIVEN INSTANT'/,
     4'     -CA.DAT (CHANNEL 2): CONTAINTS THE AXIAL FORCE'/,
     5'                          COEFFICIENT AND THE TIME'/,
     6'     -VEL.DAT (CHANNEL 3): CONTAINS THE VELOCITY IN
                                                      THE WAKE A '/,
     7'                          A FUNTION OF Y AT SIX DIFFERENT A'/
     8'                          AXIAL STATIONS DOWNSTREAM THE
                                                        CANOPY.'/,
     9'                          THE DISTANCE BETWEEN TWO
                                                      CONSECUTIVE'/
     1'                          STATIONS IS ONE CANOPY PROJECTED'/,
     2'                          AREA RADIUS.')
   111  FORMAT(
     1'      -K11.DAT (CHANNEL 4): CONTAINS THE ADDED MASS
                                                      COEFFICIENT'/
     2'                           AND THE TIME.'/,
     3'     -AXIAL_F.DAT (CHANNEL 9): CONTAINS THE AXIAL FORCE AND'/,
     4'                               THE TIME.'/,
     5'      -VELDEC.DAT (CHANNEL 10): CONTAINS THE CALCULATED
                                                        DESCENT'/
     6'                                VELOCITY WHEN THE FREE '/,
     7'                                DECELERATION MODE IS USED.'/,
     8'       '/,
     9'     AT THE END OF THE RESULTS THE INPUT DATA IS WROTE.'/,
     1'          '/,
     2'   -"IPL1" : AS "IPR1" WHEN IPLOT=1'/,
     3'   -"NPL" : PLOTTING FREQUENCY (E.G. WHEN NPL=5 EVERY 5 TIME'/,
     4'            STEPS AFTER THE IPL1-TH TIME STEP,THE FLOW PATERN'/
     5'            WILL BE WROTE ON "FLOW.DAT".')
   175  FORMAT(' THE GEOMETRIC POROSITY OF THE',I3,'-TH PANEL IS ',F6.4
   185  FORMAT(//,
     1'    -"FYSVR": DIMENSIONLESS PARAMETER DETERMINING THE'/,
     2'              STANDING VORTEX RING LOCATION. IT IS TO BE'/,
     3'              SET TO ENSSURE MINIMUM LOAD ACROSS THE NEAR'/,
     4'              HEMLINE PANEL.   1.25> FSVR>1.01'/,
     5'    -"CASTD": THE STEADY AXIAL FORCE COEFFICIENT USED FOR'/,
     6'              ADDED MASS COEFFICIENT CALCULATION.'/,
     7'    -"RO": FLUID DENSITY.')
   190  FORMAT(//,
     1'    -"IPOR": FOR IPOR=1 THE FLOW AROUND A POROUS CANOPY IS'/,
     2'              SIMULATED. YOU WILL BE ASKED TO ENTER THE '/,
     3'              GEOMETRIC POROSITY OF EACH PANEL.'/,
     4'    -"IDEC": FOR IDEC=1, THE DECELERATION OF A PARACHUTE-'/,
     5'              -PAYLOAD SYMSTEM IS SIMULATED. YOU WILL BE'/,
     6'              ASKED TO ENTER THE DECELERATION SYSTEM MASS.'/,
     7'    -"ISHAPE_T": FOR ISHAPE_T=1 THE FLOW AROUND A
                                                      TIME-DEPENDENT'/,
     8'                 CANOPY SHAPE IS SIMULATED. YOU WILL BE
                                                        ASKED TO'/,
     9'                 ENTER THE TABLE CONTAINING THE
                                                      TIME AND THE'/,
     1'                 PARAMETERS DETERMINING THE CANOPY SHAPE'/,
     2'     -"IPRSHAPE": FOR IPRSHAPE=1 THE CANOPY SHAPE IS
```

```
     3'                    AT EVERY TIME STEP. THIS PARAMETER
                                                          IS RELEVANT'/,
     4'                    ONLY WHEN ISHAPE_T=1.')
130   FORMAT(/' IN THE FOLLOWING OUTPUT:'/,
     1'                  -N  = TIME STEP NUMBER'/,
     2'                  -T  = TIME [SECOND]'/,
     3'                  -U  = VELOCITY [METER/SECOND]'/,
     4'                  -CA = AXIAL FORCE COEFFICIENT'/,
     5'                  -AM = ADDED MASS COEFFICIENT'/,
     5'                  -A  = AXIAL FORCE [NEWTONS]'/,
     5'                -P1,P8,P12= THE DIFFERENTIAL PRESSURE'/,
     6'                            COEFFICIENT AT PANELS 1,8,12'//)
140   FORMAT(/' PLEASE ENTER THE PAIRS (TIME,VELOCITY).'/,
     1' FOR EXAMPLE IF AT TIME=5SEC THE VELOCITY IS -2 M/SEC'/,
     2' THEN ENTER 5,-2 AND PRESS RETURN. REPEAT THIS FOR EACH'/,
     3' ONE OF THE PAIRS IN THE TABLE.'//)
160   FORMAT(/'  DO YOU WANT AN ADDITIONAL TRY ? (Y/N)'/)
180   FORMAT(/' PLEASE ENTER XM,YM,XI .'/)
200   FORMAT(/' DO YOU WANT TO READ THIS SECTION AGAIN ? (Y/N)'/)
240   FORMAT(/' PLEASE ENTER THE SHAPE PARAMETERS :'/,
     1' TIME,YM,XM,XI.'/,
     2' FOR EXAMPLE IF AT TIME=5SEC THE SHAPE IS DETERMINED BY:'/,
     3' YM=1,XM=1.5,XI=1.2,'/,
     4' THEN ENTER 5,1,1.5,1.2 AND PRESS RETURN. REPEAT THIS
                                                        FOR EACH'/,
     5' ONE OF THE PAIRS IN THE TABLE.'//)
999   FORMAT(51(1H*))
221   FORMAT(24(1H ),'SCALEX=',F8.2,' SCALEY=',F8.2)
421   FORMAT('  NDT=',I5)
2     FORMAT('  XSVR=',F10.5,'  YSVR=',F10.5,' GMSVR=',F10.5)
201   FORMAT ('                              DT=',F8.5,'   T=',F12.4,
     1' UINF=',F7.2,'  ACC=',F7.4)
401   FORMAT (23(1H ),54(1H=))
301   FORMAT (' J=',I5,'  XVR=',F10.4,'  YVR=',F10.4,'  GMW=',
     1F6.3,' CANCELL=',F3.0,' EP=',F9.6)
113   FORMAT(I10)
114   FORMAT(2F20.5)
122   FORMAT(//2X'THE FOLLOWING QUANTITIES ARE EXPRESSED IN
                                                        METERS'//,
     1'    YREF (reference length -projected area radius)=',F6.3,/,
     2'    SREF (projected area)=',F7.3,/,
     3'    VOLCAN (enclosed volume)=',F7.3,/,
     4'    SCAN (constructed area)=',F7.3)
125   FORMAT(I20)
178   FORMAT(I10,F10.5)
      STOP
      END
```

```
*
*              ------------------------------
*              CANOPY-THE MAIN SUBPROGRAMME
*              ------------------------------
*
*
*
```

```
*       "C A N O P Y" CALCULATES THE AXIAL FORCE DEVELOPED ON THE
*       PARACHUTE CANOPY AT THE INSTANT "T". IT IS DONE BY CALLING
*       ON SUBROUTINES WHICH DETERMINE THE BOUNDARY CONDITIONS
*       ON THE CANOPY SURFACE, SOLVES THE LINEAR SYSTEM OF EQUATION
*       WHICH GIVES THE BOUND VORTEX RING STRENGTH AND FINALLY
*       INTEGRATES THE DIFFERENTIAL PRESSURE DISTRIBUTION.
*
*
*
*
      SUBROUTINE CANOPY(UINF,NPN,BETA,GMW,CANCELL,EP,NDT,WKOLD,XSHD,
     1YSHD,XI,U,WKNEW,NW,DT,GMB,YREF,XPN,DA,T,IPOR,
     2PANPOR,AXIAL_F,CAO,UNO,CASTD,IPR1,IPR2,ARC,XM,YM,AL,
     3VOLCAN,ACC,PI,GMWNDT,GMSVR,XSVR,YSVR,NPN,NVR,IYG,
     4DCP,DCPST,DEL,C25,C75,C,CTEMP,TIME,CA,YG,GMBOLD,IPLOT,
     5IPL1,NPL,XCUT,ICORE,FYSVR,ISHAPE_T,DCPOLD,VELDEF,IWAKE,
     6IAXIAL_F,TMAX,ADD,KSHAPE,RO,IDEC,C25OLD)
*
      DIMENSION GMW(NVR),CANCELL(NVR),EP(NVR),WKOLD(NVR,2),DCP(NPN)
     1,WKNEW(NVR,2),GMB(NPN),XPN(NPN),C25(NPN,2),DCPST(NPN),
     2C75(NPN,2),C(NPN,NPN),PANPOR(NPN),CTEMP(NPN,NPN),U(NPN)
     3,TIME(NVR),IYG(NVR),CA(NVR),YG(NVR),GMBOLD(NPN)
     4,DCPOLD(NPN),AXIAL_F(NVR),ADD(NVR),C25OLD(NPN)
*
      UNI=UNO
      UNO=UINF
      IF(NDT.EQ.1.OR.ISHAPE_T.EQ.1) THEN
*
*
***   CANOPY DIVISION IN PANELS OF EQUAL LENGTH
*
*
         CALL PANEL(XI,XM,YM,AL,NPAN,XPN,DA,ARC,PI,NPN)
         AL=ALFA(NPN,XPN,NPAN,XI,XM,YM,AL)
*
*
***   CANOPY INFLUENCE COEFFICIENTS DETERMINATION
*
*
         CALL CIC(XI,NPAN,C,XPN,DA,C25,C75,XM,YM,AL,PI,NPN
     1           ,IPLOT,IPL1,NPL,XCUT,NDT,ISHAPE_T,T,TMAX
     2           ,KSHAPE)
      END IF
*
*
***   THE BOUNDARY CONDITION  (THE NORMAL VELOCITY) ON
***   THE CANOPY SURFACE. VECTOR "U" CONTAINS THE NORMAL VELOCITY.
*
*
      CALL BC(XI,U,GMW,CANCELL,EP,NDT,WKOLD,UINF,WKNEW,NW,XSHD,
     1YSHD,DT,NPAN,GMB,DCP,YREF,XPN,DA,T,
     2CA1,C25,C75,IPOR,PANPOR,
     3XM,YM,AL,GMSVR,XSVR,YSVR,GMWNDT,PI,NPN,NVR,XCUT,
     4FYSVR,DCPOLD,VELDEF,IWAKE,IPLOT,TMAX,C25OLD,ISHAPE_T)
      NG=NPN+1
      DO 666 I=1,NG
      DO 666 J=1,NG
666   CTEMP(I,J)=C(I,J)
*
```

```
*
***    SOLVES THE LINEAR SYSTEM OF EQUATION GIVING THE BOUND VORTEX
***    RING STRENGTH. ON RETURN VECTOR "U" CONTAINS THE BOUND VORTEX
***    RING STRENGTH.
*
*
      CALL SOLVE(NG,CTEMP,U,NPN)
      DO 800 I=1,NG
      GMB(I)=U(I)
800   CONTINUE
*
*
***    THE NEWLY-CREATED VORTEX RING STENGTH
*
*
      GMW(NDT)=GMB(NPAN+1)
*
      TIME(NDT)=T
*
*
***    THE DIFFERENTIAL PRESSURE DISTRIBUTION
*
*
      CALL CP(NPAN,GMB,DCP,DCPST,XI,UINF,GMW,CANCELL,EP,
     1NDT,DT,XPN,DA,T,IPOR,PANPOR,GMSVR,XSVR,YSVR,XM,YM,
     2AL,NPN,NVR,GMBOLD,XCUT)
*
      IF(NDT.LT.IPR1.OR.NDT.GT.IPR2)GO TO 4
      WRITE(6,900)
      AR=0
      DO 555 I=1,NG
      X=XPN(I)
      AR=AR+DA
      ARD=AR/ARC
555   WRITE (6,222) I,X,Y(X,XI,XM,YM,AL),AR,ARD,GMB(I),DCP(I),
     1DCPST(I)
      CALL GRAPH(DCP,NPAN,TIME,0,1,NVR,IYG)
4     CONTINUE
*
*
***    AXIAL FORCE COEFFICIENT CALCULATION.
*
*
      CA(NDT)=0
      DO 930 I=1,NPN
      X=XPN(I)-0.5*DA*COS(ALFA(NPN,XPN,I,XI,XM,YM,AL))
      CA(NDT)=CA(NDT)+DCP(I)*DA*SIN(ALFA(NPN,XPN,I,XI,XM,YM,AL))*2*
     *Y(X,XI,XM,YM,AL)/YREF/YREF
930   CONTINUE
      CAO=CA(NDT)
*
*
***    AXIAL FORCE CALCULATION.
*
*
      AXIAL_F(NDT)=0.5*RO*UINF*UINF*YREF*YREF*PI*CA(NDT)
*
*
***    ADDED MASS COEFFICIENT CALCULATION.
```

```
*
*
      ACC=(UINF-UNI)/DT*ABS(UINF)/UINF
      ADD(NDT)=0
      IF(NDT.GT.5.AND.ABS(ACC).GE.0.0000001)ADD(NDT)=0.5*(UINF**2)*
     1PI*YREF*YREF/VOLCAN/ACC*(CA(NDT)+CASTD*UINF/ABS(UINF))-1.
*
*
***   AVOIDING PRINT-OUT FORMAT MISMATCH.
*
*
      AXIAL_FPR=AXIAL_F(NDT)
      IF(AXIAL_F(NDT).GT.9999.9)AXIAL_FPR=9999.9
      IF(AXIAL_F(NDT).LT.-999.9)AXIAL_FPR=-999.9
      ADDPR=ADD(NDT)
      IF(ADD(NDT).GT.999.9)ADDPR=999.9
      IF(ADD(NDT).LT.-99.9)ADDPR=-99.9
      CAPR=CA(NDT)
      IF(CA(NDT).GT.999.9)CAPR=999.9
      IF(CA(NDT).LT.-99.9)CAPR=-99.9
      D1=DCP(1)
      IF(D1.GT.9.9)D1=9.9
      IF(D1.LT.-9.9)D1=-9.9
      DN=DCP(NPAN)
      IF(DN.GT.9.9)DN=9.9
      IF(DN.LT.-9.9)DN=-9.9
      NCP=NPAN*2/3
      DM=DCP(NCP)
      IF(DM.GT.9.9)DM=9.9
      IF(DM.LT.-9.9)DM=-9.9
      WRITE(6,931)NDT,TIME(NDT),UINF,CAPR,AXIAL_FPR
     2,ADDPR,D1,NCP,DM,NPAN,DN
      IF(IPLOT.EQ.1.AND.IDEC.EQ.1)WRITE(10,777)TIME(NDT),UINF
213   CONTINUE
*
*
***   DIRECTING RESULTS TO THE LINE PRINTER & OUTPUT FILES
*
*
      IF(NDT.EQ.NW.OR.T.GE.TMAX)THEN
       IF(IPR1.LE.NW)CALL GRAPH(CA,NDT,TIME,0,2,NVR,IYG)
       IF(IPLOT.EQ.1)THEN
          IF(IAXIAL_F.EQ.1)THEN
               WRITE (4,444)NDT
               WRITE (9,444)NDT
          END IF
          WRITE (2,444)NDT
          DO 333  ICA=1,NDT
            IF(IAXIAL_F.EQ.1)THEN
                 WRITE(4,777)TIME(ICA),ADD(ICA)
                 WRITE(9,777)TIME(ICA),AXIAL_F(ICA)
            END IF
333       WRITE(2,777)TIME(ICA),CA(ICA)
       END IF
      END IF
931   FORMAT(' N=',I3,' T=',F6.3,' U=',F6.1,' CA=',F8.4,' A=',
     1F6.1,' AM=',F5.1,' P1=',F4.1,' P',I1,'=',F5.1,' P',I2,
     2'=',F5.1)
900   FORMAT ( '    I    X     Y     L    L*        GMB                DCP
```

```
     1    DPSTDY')
222   FORMAT (I3,F6.2,3F5.2,F10.3,2F14.3)
444   FORMAT (I20)
777   FORMAT (2F20.5)
      RETURN
      END
*                              ----
*                               CP
*                              ----
*
*      SOUBROUTINE " C P " CALCULATES THE DIFFERENTIAL PRESSURE
*      DISTRIBUTION. IT IS DONE BY SUMMING UP THE STEADY-BOUND
*      VORTEX SHEET AND THE INSTANTANEOUS VARIATIONS IN THE FLOW
*      FIELD CIRCULATION CONTRIBUTIONS.
*
*
*
      SUBROUTINE CP(NPAN,GMB,DCP,DCPST,XI,UINF,GMW,CANCELL,EP,NDT,
     1DT,XPN,DA,T,IPOR,PANPOR,GMSVR,XSVR,YSVR,XM,YM,AL,NPN,NVR,
     2GMBOLD,XCUT)
      DIMENSION GMBOLD(NPN),GMW(NVR),CANCELL(NVR),EP(NVR),XPN(NPN)
     1,GMB(NPN),PANPOR(NPN),DCP(NPN),DCPST(NPN)
*
*
***   THE WAKE CIRCULATION VARIATION
***   (THE NEWLY CREATED VORTEX RING STRENGTH)
*
*
      IF(CANCELL(NDT).LT.0.)THEN
         GWT=0
        ELSE
         GWT=GMW(NDT)
      END IF
*
      DO 109 I=1,NPAN
      IF(NDT.EQ.1)GWT=0.
      XX=0
      IF(I.GT.1)XX=XPN(I-1)
*
*
***   THE DIFFERENTIAL PRESSURE DUE THE INSTANTANEOUS
***   BOUND VORTEX SHEET STRENGTH.
*
*
       DCPST(I)=-1.*GMB(I)*2/DA/UINF*
     1((COS(ALFA(NPN,XPN,I,XI,XM,YM,AL))**2))
*
*
***   BOUND VORTEX SHEET STRENGTH VARIATION
*
*
       SGDGDT=0
       IF(NDT.EQ.1) GO TO 115
       DO 116 J=1,I
```

```
116     SGDGDT=SGDGDT+GMB(J)-GMBOLD(J)
*
*
***   STANDING VORTEX RING STRENGTH VARIATIAN
*
*
115     DIF=GMSVR-GMTOLD
        SGDGDT=SGDGDT+DIF
*
*
***     SUMMING UP THE VARIOUS DIFFERENTIAL PRESSURE
***     COEFFICIENT CONTRIBUTIONS.
*
*
        DCP(I)=DCPST(I)+(GWT+SGDGDT)*2./(UINF**2)/DT
109     CONTINUE
*
        DO 111 I=1,NPAN
111     GMBOLD(I)=GMB(I)
        GMTOLD=GMSVR
        RETURN
        END
```

```
*
*
*                    -----
*                     CIC
*                    -----
*
*
*       SUBROUTINE " C I C " CALCULATES THE CANOPY INFLUENCE
*       COEFFICIENTS MATRIX. A BOUND VORTEX RING OF UNIT STRENGTH
*       IS LOCATED AT 0.25 PANEL LENGTH AND THE BOUNDARY CONDITIONS
*       ARE FULFILLED AT 0.75 PANEL LENGTH. THE NEWLY-CREATED
*       VORTEX RING IS ACCOUNTED FOR BY AN ADDITIONAL FICTITIOUS
*       PANEL TANGENT TO THE CANOPY SURFACE AT ITS HEMLINE.
*
*
*
        SUBROUTINE CIC(XI,NPAN,C,XPN,DA,C25,C75,XM,YM,AL,PI,NPN,IPLOT,
      1IPL1,NPL,XCUT,NDT,ISHAPE_T,T,TMAX,KSHAPE)
        DIMENSION C(NPN,NPN),C25(NPN,2),C75(NPN,2),XPN(NPN)
*
*
***     CANOPY BOUND VORTEX SHEET & CONTROL CIRCLES COORDINATES
*
*
        DO 5 I=1,NPN
        DC=DA*COS(ALFA(NPN,XPN,I,XI,XM,YM,AL))
        C25(I,1)=XPN(I)-0.25*DC
        C75(I,1)=XPN(I)-0.75*DC
        C25(I,2)=Y(C25(I,1),XI,XM,YM,AL)
        C75(I,2)=Y(C75(I,1),XI,XM,YM,AL)
        IF(IPLOT.EQ.1.AND.KSHAPE.EQ.0)THEN
           IF(I.EQ.1)WRITE(1,111)0.00001,0.00001
```

```
         WRITE(1,111)C25(I,1),C25(I,2)
       END IF
5      CONTINUE
       KSHAPE=1
*
*
***    THE NEWLY CREATED FICTITIOUS PANEL
*
*
       C25(NPAN+1,1)=XPN(NPAN)+0.75*DC
       C75(NPAN+1,1)=XPN(NPAN)+0.25*DC
       C25(NPAN+1,2)=Y(C25(NPAN+1,1),XI,XM,YM,AL)
       C75(NPAN+1,2)=Y(C75(NPAN+1,1),XI,XM,YM,AL)
*
*
***    CANOPY IFLUENCE COEFFICIENTS  MATRIX
*
*
       DO 20 NY=1,NPAN+1
       DO 20 NX=1,NPAN+1
       NNX=NX
       IF(NX.GT.NPAN)NNX=NPAN
       C(NY,NX)=UVR(PI,C75(NY,1),C75(NY,2),C25(NX,1),C25(NX,2))*
      1SIN(ALFA(NPN,XPN,NNX,XI,XM,YM,AL))-
      2VVR(PI,C75(NY,1),C75(NY,2),C25(NX,1),C25(NX,2))
      3*COS(ALFA(NPN,XPN,NNX,XI,XM,YM,AL))
 20    CONTINUE
111    FORMAT(2F20.5)
       RETURN
       END
```

```
*
*
*                          ----
*                           BC
*                          ----
*
*
*      SUBROUTINE " B C "  DETERMINES THE BOUNDARY CONDITION
*      ON THE CANOPY SURFACE. IT IS DONE BY SUMMING UP THE WHOLE
*      VORTEX SYSTEM INDUCED-VELOCITY & THE FREE STREAM VELOCITY
*      NORMAL TO THE CANOPY SURFACE, ALONG THE CONTROL CIRCLES.
*
*
*
       SUBROUTINE BC(XI,U,GMW,CANCELL,EP,NDT,WKOLD,UINF,WKNEW,NW,XSHD,
      1YSHD,DT,NPAN,GMB,DCP,YREF,XPN,DA,T,
      2CA1,C25,C75,IPOR,PANPOR,
      3XM,YM,AL,GMSVR,XSVR,YSVR,GMWNDT,PI,NPN,NVR,XCUT,
      4FYSVR,DCPOLD,VELDEF,IWAKE,IPLOT,TMAX,C25OLD,ISHAPE_T)
       DIMENSION GMB(NPN),C25(NPN,2),C75(NPN,2),DCP(NPN)
      1,GMW(NVR),CANCELL(NVR),EP(NVR),WKOLD(NVR,2),WKNEW(NVR,2)
      2,U(NPN),PANPOR(NPN),XPN(NPN),DCPOLD(NPN)
      3,C25OLD(NPN)
```

```
*
      CALL WAKE(WKOLD,WKNEW,GMW,CANCELL,EP,NW,XSHD,YSHD,UINF,DT,
     1NDT,NPAN,U,XI,GMB,YREF,XPN,DA,T,CA1,C25,C75,
     2PI,XM,YM,AL,GMWNDT,GMSVR,XSVR,YSVR,NPN,NVR,XCUT,
     3FYSVR,VELDEF,IWAKE,IPLOT,TMAX)
*
      DO 25 I=1,NPN+1
*
*
***   CANOPY SURFACE CONTRIBUTION
*
*
      IF(I.GT.NPN.OR.NDT.EQ.1)GO TO 95
      IF(ISHAPE_T.EQ.1)THEN
         VSURF=(C25OLD(I)-C25(I,2))/DT
        ELSE
         VSURF=0
      END IF
*
*
***   WAKE CONTRIBUTION
*
*
95    UIND=0
      VIND=0
      IF(NDT.EQ.1)GO TO 60
      DO 13 J=1,NDT-1
      IF(CANCELL(J).LT.0.)GO TO 13
      DISCOR=SQRT((WKOLD(J,1)-C75(J,1))**2+(WKOLD(J,2)-C75(J,2))**2)
*
**    CUTOFF DISTANCE
*
      IF(DISCOR.LE.(EP(J)))GO TO 13
      UIND=UIND+UVR(PI,C75(I,1),C75(I,2),WKOLD(J,1),WKOLD(J,2))*GMW(J
      VIND=VIND+VVR(PI,C75(I,1),C75(I,2),WKOLD(J,1),WKOLD(J,2))*GMW(J
13    CONTINUE
*
*
***   POROSITY REQUIREMENTS
*
*
60    IF(NDT.EQ.1.OR.DCP(I).LT.0.
     1OR.I.GT.NPN.OR.IPOR.EQ.0)THEN
           FCT=0.
        ELSE
           FCT=SQRT(DCP(I))*PANPOR(I)
           IF(FCT.GT.0.15)THEN
              WRITE(6,100)I
            END IF
      END IF
      VNPOR=-1.*UINF*FCT
*
*
***   STANDING VORTEX RING CONTRIBUTION
*
*
      IF(NDT.EQ.1)GO TO 55
      UIND=UIND+UVR(PI,C75(I,1),C75(I,2),XSVR,YSVR)*GMSVR
      VIND=VIND+VVR(PI,C75(I,1),C75(I,2),XSVR,YSVR)*GMSVR
```

```
55      II=I
        IF(I.GT.NPN) THEN
              II=NPN
              VNPOR=0
        END IF
25      U(I)=VIND*COS(ALFA(NPN,XPN,II,XI,XM,YM,AL))-
       1(UIND+UINF)*SIN(ALFA(NPN,XPN,II,XI,XM,YM,AL))-VNPOR-VSURF
*
*
        DO 75 I=1,NPN
75      DCPOLD(I)=DCP(I)
        IF(ISHAPE T.EQ.1)THEN
           DO 90 J=1,NPN
90         C25OLD(J)=C25(J,2)
        END IF
100     FORMAT('THE NORMAL VELOCITY AT PANEL',I3,' IS TOO HIGH.')
        RETURN
        END
```

```
*
*
*           -------
*            SOLVE
*           -------
*
*
*       SUBROUTINE " S O L V E "  SOLVES A LINEAR SYSTEM OF
*       EQUATIONS BY USING GAUSS ELIMINATION METHOD.
*
*
*
*
        SUBROUTINE SOLVE(N,B2,B1,NPN)
        DIMENSION B2(NPN,NPN),B1(NPN)
        DO 60 K=1,N
        A1=B2(K,K)
        DO 60 I=1,N
        IF(I.EQ.K) GO TO 60
        A2=B2(I,K)
        IF(A2.EQ.0) GO TO 60
        B1(I)=B1(I)/A2-B1(K)/A1
        DO 60 J=1,N
        B2(I,J)=B2(I,J)/A2-B2(K,J)/A1
60      CONTINUE
        DO 80 I=1,N
80      B1(I)=B1(I)/B2(I,I)
        RETURN
        END
```

```
*
*
*              ---
*               Y
*              ---
*
*
*       FUNCTION " Y "  GENERATES THE CANOPY SHAPE BY ASSUMING
*       AN ELLIPTICAL SHAPE. IT MAY BE CHANGED TO ANY OTHER
*       DESIRED CANOPY REPRESENTATION.
*
*
*
      FUNCTION Y(X,XI,XM,YM,AL)
      Y=0.5*YM
      IF(X.GE.(2.*XM))RETURN
      IF(X.GT.XI) GO TO 1
      Y=YM/XM*SQRT(X*(2*XM-X))
      RETURN
1     Y=YM/XM*SQRT(XI*(2*XM-XI))+(X-XI)*SIN(AL)
      RETURN
      END
*
*
*              ------
*               ALFA
*              ------
*
*
*
*
*       FUNCTION " A L F A "  CALCULATES THE LOCAL CANOPY INCLINATION.
*
*
*
*
      FUNCTION ALFA(NPN,XPN,N,XI,XM,YM,AL)
      DIMENSION XPN(NPN)
      X1=0
      IF(N.GT.1)X1=XPN(N-1)
      DYDX=(Y(XPN(N),XI,XM,YM,AL)-Y(X1,XI,XM,YM,AL))/(XPN(N)-X1)
      ALFA=ATAN(DYDX)
      RETURN
      END
*
*
```

```
*
*                    -------
*                     PANEL
*                    -------
*
*
*
*       SUBROUTINE " P A N E L "  DETERMINES THE FORWARD PANELS
*       AXIAL COORDINATE BY DIVIDING THE CANOPY IN EQUAL LENGTH
*       PANELS.
*
*
*
      SUBROUTINE PANEL(XI,XM,YM,AL,NPAN,XPN,DA,ARC,PI,NPN)
      DIMENSION XPN(NPN)
      ARC=0
      DO 1 I=1,100
      XXI=0.01*XI*(I-1)
      XX2=0.01*XI*I
    1 ARC=ARC+SQRT((Y(XXI,XI,XM,YM,AL)-Y(XX2,XI,XM,YM,AL))**2+
     1(0.01*XI)**2)
      DA=ARC/NPAN
      XPN(1)=0
      DX=XI/NPAN/500.
      XS=0
      DO 4 I=1,NPAN
      DD=0
      DO 3 J=1,10000
      XS=XS+DX
      DD=DD+SQRT((Y(XS,XI,XM,YM,AL)-Y((XS-DX),XI,XM,YM,AL))**2+DX**2)
    3 IF(DD.GE.DA.OR.XS.GE.XI)GO TO 5
    5 XPN(I)=XS
      IF(XPN(I).GT.XI)XPN(I)=XI
    4 CONTINUE
      RETURN
      END
*
*
*                    -----
*                     VOL
*                    -----
*
*       FUNCTION " V O L "  CALCULATES THE CANOPY INCLUDED VOLUME
*
*
*
      FUNCTION VOL(XI,PI,XM,YM,AL)
      VOL=0
      DO 1 I=1,20
    1 VOL=VOL+(Y((I*XI/20),XI,XM,YM,AL)**2)*XI/20
      VOL=PI*VOL
```

```
      RETURN
      END
```

```
*
*
*                ------
*                 SURF
*                ------
*
*
*       FUNCTION " S U R F "  CALCULATES THE CANOPY CONSTRUCTED
*       SURFACE.
*
*
*
      FUNCTION SURF(XI,PI,XM,YM,AL)
      X=XM/I
      SURF=0
      DO 2 I=1,20
      XII=XI
    2 SURF=SURF+XI/20*Y(I*XI/20,XI,XM,YM,AL)*SQRT(1+((XM-I*XI/20)/
     1XM*YM/XM*YM/Y(I*XI/20,XI,XM,YM,AL))**2)
      SURF=SURF*2*PI
      RETURN
      END
```

```
*
*
*                      ------
*                       WAKE
*                      ------
*
*       SUBROUTINE " W A K E "  SIMULATES THE WAKE FLOW. IT CALCULATES
*       THE SHED VORTEX RING LOCATION AT EVERY TIME STEP.
*
*
*
*
*
      SUBROUTINE WAKE(WKOLD,WKNEW,GMW,CANCELL,EP,NW,XSHD,YSHD,UINF,DT
     1NDT,NPAN,U,XI,GMB,YREF,XPN,DA,T,CA1,C25,C75,
     2PI,XM,YM,AL,GMWNDT,GMSVR,XSVR,YSVR,NPN,NVR,XCUT,
     3FYSVR,VELDEF,IWAKE,IPLOT,TMAX)
      DIMENSION GMB(NPN),C25(NPN,2),C75(NPN,2),XPN(NPN)
```

```
     1,CANCELL(NVR),GMW(NVR),EP(NVR),U(NPN),WKOLD(NVR,2),WKNEW(NVR,2)
*
*
***      THE SHEDDING POINT
*
*
       XSHD=C25(NPAN+1,1)
       YSHD=C25(NPAN+1,2)
*
*
***    INITIAL VORTEX RING CORE DIAMETER
*
*
       EP(NDT)=0.02*SQRT(DT)
*
*
***    THE SHEDDING FREQUENCY
*
*
       GMWNDT=0.5*UINF*UINF
*
*
***    STANDING VORTEX RING STRENGTH AND POSITION
*
*
       IF(NDT.EQ.1)THEN
            XSVR=0
            YSVR=0
            GMSVR=0
            GO TO 58
       END IF
       XSVR=XPN(NPAN)-0.5*DA*COS(ALFA(NPN,XPN,NPAN,XI,XM,YM,AL))
       GMSVR=-0.84*Y(XI,XI,XM,YM,AL)*UINF-GMW(NDT-1)
       IF((ABS(UINF)/UINF).LT.0)THEN
            FY=FYSVR
               ELSE
            FY=2.-FYSVR
       END IF
       YSVR=Y(XSVR,XI,XM,YM,AL)*FY
*
*
***    WAKE DEVELOPMENT
*
*
       DO 14 M=1,NDT-1
       XVR=WKOLD(M,1)
       YVR=WKOLD(M,2)
       UIND=0
       VIND=0
       IF(CANCELL(M).LT.0.) THEN
              WKNEW(M,1)=WKOLD(M,1)
              WKNEW(M,2)=WKOLD(M,2)
          GO TO 14
       END IF
*
*
***   THE VELOCITY UNDUCED BY THE WAKE AT A CERTAIN VORTEX RING
***   CIRCOMFERENCE ( XVR & YVR).
*
```

```
*
      DO 13 N=1,NDT-1
      B=WKOLD(N,1)
      IF(CANCELL(N).LT.0.) GO TO 13
      AB=WKOLD(N,2)
      IF(N.EQ.M) GO TO 12
      DISCOR=SQRT((XVR-B)**2+(YVR-AB)**2)
*
*
***   CUTOFF DISTANCE
*
*
      IF(DISCOR.LE.(EP(N)+EP(M)))GO TO 13
      VIND=VIND+VVR(PI,XVR,YVR,B,AB)*GMW(N)
      UIND=UIND+UVR(PI,XVR,YVR,B,AB)*GMW(N)
      GO TO 13
*
*
***   VORTEX RING SELF INDUCED  VELOCITY
*
*
12    IF(EP(N).LT.0.0000001)GO TO 13
      UIND=UIND+GMW(N)*(ALOG(16.*(ABS(AB))/EP(N))-0.25)/
     1(4.*PI*(ABS(AB)))
13    CONTINUE
*
*
***   THE VELOCITY INDUCED  BY THE CANOPY AT XVR & YVR.
*
*
      DO 79 IB=1,NPAN
      DISCOR=SQRT((XVR-C25(IB,1))**2+(YVR-C25(IB,2))**2)
*
*
***   CUTOFF DISTANCE
*
*
      IF(DISCOR.LE.(EP(M)))GO TO 79
      UIND=UIND+UVR(PI,XVR,YVR,C25(IB,1),C25(IB,2))*GMB(IB)
      VIND=VIND+VVR(PI,XVR,YVR,C25(IB,1),C25(IB,2))*GMB(IB)
79    CONTINUE
      IF(NDT.LT.3)GO TO 998
*
*
***   THE VELOCITY INDUCED AT XVR & YVR BY THE STANDING VORTEX
***   RING.
*
*
      DISCOR=SQRT((XVR-XSVR)**2+(YVR-YSVR)**2)
*
*
***   CUTOFF DISTANCE
*
*
      IF(DISCOR.LE.(EP(M)))GO TO 998
*
*
***   THE RESULTING INDUCED VELOCITY AT XVR & YVR
*
```

```
*
      UIND=UIND+UVR(PI,XVR,YVR,XSVR,YSVR)*GMSVR
      VIND=VIND+VVR(PI,XVR,YVR,XSVR,YSVR)*GMSVR
*
*
***   SHED VORTEX RINGS CONVECTION
*
*
998   WKNEW(M,2)=DT*VIND+WKOLD(M,2)
      WKNEW(M,1)=DT*(UINF+UIND)+WKOLD(M,1)
14    CONTINUE
58    CONTINUE
*
*
***   CONDITIONAL VELOCITY DISTRIBUTION IN THE WAKE
*
*
      IF((NDT.EQ.NW.OR.T.GT.TMAX).AND.IPLOT.EQ.1.AND.IWAKE.EQ.1)THEN
      NJ=6
      DO 100 I=1,NJ
      XWAKE=-I*YSHD
      NY=11
      WRITE(3,104)NY
      DO 110 JJ=1,NY
      VX=0
      VY=0
      E=YSHD*((JJ-1)*0.15+0.01)
      DO 101 II=1,NPAN
      VY=VVR(PI,XWAKE,E,C25(II,1),C25(II,2))*GMB(II)+VY
101   VX=UVR(PI,XWAKE,E,C25(II,1),C25(II,2))*GMB(II)+VX
      DO 102 II=1,NDT-1
      IF(CANCELL(II).LT.0.)GO TO 102
      VY=VVR(PI,XWAKE,E,WKOLD(II,1),WKOLD(II,2))*GMW(II)+VY
      VX=UVR(PI,XWAKE,E,WKOLD(II,1),WKOLD(II,2))*GMW(II)+VX
102   CONTINUE
      VY=VVR(PI,XWAKE,E,XSVR,YSVR)*GMSVR+VY
      VX=UVR(PI,XWAKE,E,XSVR,YSVR)*GMSVR+VX+UINF
      DY=E/YSHD
      VELDEF=(SQRT(VX*VX+VY*VY))/ABS(UINF)
110   WRITE(3,105)VELDEF,DY
100   CONTINUE
      END IF
*
*
***   THE NEWLY CREATED VORTEX RING LOCATION
*
*
103   WKNEW(NDT,1)=XSHD
      WKNEW(NDT,2)=YSHD
*
      X1=0.8*XI
      X2=-0.1*YSHD
      Y1=YM
      DO 17 J=1,NDT
      IF(CANCELL(J).LT.0.OR.NDT.EQ.1)GO TO 993
*
*
***   FREE VORTEX RINGS CANCELLATION DUE THEIR DISTANCE
***   TO THE CANOPY EXCEEDING
```

```
*
*
      IF(UINF.LT.0)THEN
        IF(WKNEW(J,1).LT.XCUT)THEN
            CANCELL(J)=-1.
            GO TO 993
        END IF
      ELSE
         IF(WKNEW(J,1).GT.XCUT)THEN
            CANCELL(J)=-1.
            GO TO 993
         END IF
      END IF
      IF(J.EQ.NDT)GO TO 993
*
*
***   FREE VORTEX RINGS CANCELLATION DUE COLLISION WITH
***   THE CANOPY SURFACE
*
*
       IF(WKNEW(J,1).LT.X1.AND.WKNEW(J,1).GT.X2.AND.
     1WKNEW(J,2).LT.Y1)GO TO 889
       GO TO 999
889    WRITE(6,2)J
       CANCELL(J)=-1.
       GO TO 993
999    EP(J)=EP(J)*SQRT(ABS(WKOLD(J,2)/WKNEW(J,2)))
993    WKOLD(J,1)=WKNEW(J,1)
       WKOLD(J,2)=WKNEW(J,2)
17     CONTINUE
2      FORMAT(' !! THE',I5,'-TH V.R. WAS CANCELLED DUE ITS DISTANCE
     1 FROM THE CANOPY')
       RETURN
104    FORMAT(I10)
105    FORMAT(2F20.5)
       END
```

```
*
*
*              -----
*               UVR
*              -----
*
*
*      FUNCTION " U V R "  CALCULATES THE AXIAL VELOCITY
*      INDUCED BY A VORTEX RING OF UNIT STRENGTH AT A GIVEN
*      LOCATION
*
*
*
*
       FUNCTION UVR(PI,X,YX,B,AB)
       AE=4.*AB*YX/((X-B)**2+(YX+AB)**2)
```

```
*
*
***    TO AVOID THE NEED OF DOUBLE PRECISION
*
*
       A1=ABS(1.-AE)
       IF(A1.LT.0.000001)AE=0.999999
*
       AR=SQRT(ABS(AE))
       AW=1./((X-B)**2+(YX+AB)**2)**1.5
       UVR=AB*AW/(PI*AE*(1-AE))*((AB*AE-2*YX+YX*AE)*
      1E2(AR)+2*YX*(1-AE)*E1(AR))
       RETURN
       END
```

```
*
*
*              -----
*               VVR
*              -----
*
*
*     FUNCTION " U V R "  CALCULATES THE AXIAL VELOCITY
*     INDUCED BY A VORTEX RING OF UNIT STRENGTH AT A GIVEN
*     LOCATION
*
*
*
*
       FUNCTION VVR(PI,X,YX,B,AB)
       AE=4.*AB*YX/((X-B)**2+(YX+AB)**2)
*
*
***    TO AVOID THE NEED OF DOUBLE PRECISION
*
*
       A1=ABS(1.-AE)
       IF(A1.LT.0.000001)AE=0.999999
*
       AR=SQRT(ABS(AE))
       AW=1./((X-B)**2+(YX+AB)**2)**1.5
       VVR=AB*AW*(X-B)/(PI*AE*(1-AE))*((2-AE)*E2(AR)
      1-2*(1-AE)*E1(AR))
       RETURN
       END
```

```
*
*
*            ----
*             UN
*            ----
*
*
*      FUNCTION " U N "  DETERMINES THE INSTANTANEOUS VELOCITY
*
*
      FUNCTION UN(T,UNO,DT,SREF,CAO,USTEADY,
     1TVEL,VEL,NVEL,NMAX,IDEC,AMASS,NDT)
      DIMENSION TVEL(NMAX),VEL(NMAX)
      IF(USTEADY.LT.998.)THEN
*
*
***   FREE DECELERATION
*
*
            IF(IDEC.EQ.1)THEN
                  UN=UNO-DT*(9.8-0.5*1.25*(UNO**2)*SREF*CAO/AMASS)
                  RETURN
            END IF
            UN=USTEADY
            RETURN
      END IF
*
*
***   TABULATED VELOCITY/TIME FUNCTION
*
*
      UN=TB(T,TVEL,VEL,NVEL,NMAX)
      RETURN
      END
```

```
*
*
*            ----
*             E1
*            ----
*
*      FUNCTION " E 1 "  CALCULATES THE FIRST KIND
*      ELLIPTIC INTEGRAL
*
*
*
*
       FUNCTION E1(A1)
       ARGUM=A1
             ARGUM1=DSQRT(1.0D+00-DBLE(ARGUM)**2)
             ARGUM=(1.0E+00-ARGUM1)/(1.0E+00+ARGUM1)
             SERIES=0.0E+00
             COUNT=1.0E+00
```

```
      TERM=1.0E+00
      TEST=1.0E+30
      DO WHILE(TEST.GT.1.E-8)
            SERIES=SERIES+TERM
            COE=ARGUM*COUNT/(COUNT+1.0E+00)
            TERM=TERM*COE*COE
            COUNT=COUNT+2.0E+00
           IF(ABS(ARGUM**2-1.).LT.0.0000001)GO TO 1
            TEST=TERM/((1.0E+00-ARGUM**2)*SERIES)
      END DO
 1     SERIES=6.0E+00*ASIN(0.5E+00)*SERIES/(1.0E+00+ARGUM1)
      E1=SERIES
      RETURN
      END
*
*
*           ----
*            E2
*           ----
*
*
*     FUNCTION " E 2 "  CALCULATES THE SECOND KIND
*     ELLIPTIC INTEGRAL
*
*
*
      FUNCTION E2(A2)
      ARGUM=A2
            ARGUM1=DSQRT(1.0D+00-DBLE(ARGUM)**2)
            ARGUM=(1.0E+00-ARGUM1)/(1.0E+00+ARGUM1)
            SERIES=1.0E+00
            COUNT=1.0E+00
            TERM=ARGUM*ARGUM/4.0E+00
            TEST=1.0E+30
            DO WHILE(TEST.GT.1.E-8)
                  SERIES=SERIES+TERM
                  COE=ARGUM*COUNT/(COUNT+3.0E+00)
                  TERM=TERM*COE*COE
                  COUNT=COUNT+2.0E+00
                  IF(ABS(ARGUM**2-1.).LT.0.0000001)GO TO 1
                  TEST=TERM/((1.0E+00-ARGUM**2)*SERIES)
            END DO
 1          SERIES=1.5E+00*ASIN(0.5E+00)*(1.0E+00+ARGUM1)*SERIES
      E2=SERIES
      RETURN
      END
```

```
*
*
*              ----
*               TB
*              ----
*
*
*       FUNCTION " T B "  PERFORMS LINEAR INTERPOLATION
*
*
*
      FUNCTION TB(X1,XX,YY,M,NMAX)
      DIMENSION XX(NMAX),YY(NMAX)
      IF((X1-XX(1)).LT.0)GO TO 2
      DO 1 I=1,M
      IF(XX(I).GE.X1)THEN
          IF(I.EQ.1)THEN
              TB=YY(1)
              RETURN
          END IF
          A=(YY(I)-YY(I-1))/(XX(I)-XX(I-1))
          B=X1-XX(I-1)
          TB=B*A+YY(I-1)
          RETURN
      END IF
1     CONTINUE
2     PRINT*,' ARGUMENT TB=>',X1,', IS OUT OF RANGE.'
      STOP
      END
*
*
*              ------
*               PLOT
*              ------
*
*
*       SUBROUTINE " P L O T "  PRODUCES A ROUGH DRAW OF THE
*       WAKE FLOW PATTERN ON THE LINE PRINTER OR ON THE TERMINAL
*       SCREEN.
*
*
*
      SUBROUTINE PLOT(WKOLD,NDT,SCALEX,SCALEY,XI,XM,YM,AL,
     1NVR,IX,IY,XCUT,GMW,CANCELL)
      CHARACTER LINE(70)
      DIMENSION IX(NVR),IY(NVR),WKOLD(NVR,2),GMW(NVR),CANCELL(NVR)
      IXM=0
      MAXIX=1
      ICC=(3*XI-XI)*SCALEX
```

```
      IF((3*XI-XI).LE.0.)IXM=1
      ICY=Y(XI,XI,XM,YM,AL)*SCALEY
      IC=3*XI*SCALEX
      DO 17 I=1,NDT
      IF(CANCELL(I).LT.0.)GO TO 17
      WKOLD1=3*XI-WKOLD(I,1)
      IX(I)=ABS(SCALEX*WKOLD1)
      IY(I)=SCALEY*WKOLD(I,2)
      IF(IX(I).GT.MAXIX)MAXIX=IX(I)
      IF(IY(I).GT.34)IY(I)=34
17    CONTINUE
      M5=MAXIX+5
      DO 12 K=1,M5
      DO 30 I=1,70
30    LINE(I)=' '
      DO 21 J=1,70
      IF(K.EQ.1)LINE(J)='-'
21    IYC=Y(XI,XI,XM,YM,AL)*SCALEY
      ISC=SCALEX*(3*XI-XI)
      IF(K.EQ.ISC)LINE(35+IYC)='#'
      IF(K.EQ.ISC)LINE(35-IYC)='#'
      IF(K.GT.MAXIX)GO TO 12
      IJ=0
      DO 19 J=1,NDT
      LINE(35)='|'
      IF(IC.EQ.K)LINE(35)='#'
      IF(ICC.EQ.K.AND.IXM.NE.1)LINE(35+ICY)='#'
      IF(ICC.EQ.K.AND.IXM.NE.1)LINE(35-ICY)='#'
      IF(IX(J).NE.K)GO TO 19
      IJ=J
      LINE(35+IY(J))='*'
      LINE(35-IY(J))='*'
      DO 50 NPL=36-IY(J),34
50    LINE (NPL)='.'
      DO 60 NPL=36,34+IY(J)
60    LINE(NPL)='.'
19    CONTINUE
12    WRITE (6,20)LINE,IJ
20    FORMAT (1X,70A1,I5)
      RETURN
      END
```

```
*
*
*              -------
*               GRAPH
*              -------
*
*
*       SUBROUTINE " G R A P H "  PRODUCES A ROUGH GRAPH OF THE
*       AXIAL FORCE AND DIFFERENTIAL PRESSURE COFFICIENTS
*       ON THE LINE PRINTER OR ON THE TERMINAL SCREEN.
*
*
*
```

```
      SUBROUTINE GRAPH(YG,N,TIME,KG,IGR,NVR,IYG)
      DIMENSION TIME(NVR),YG(NVR),IYG(NVR)
      CHARACTER LIN(70)
      IF(KG.NE.1)GO TO 100
      DO 30 I=1,N
30    IYG(I)=64*(YG(I)-1)+5
      DO 20 J=1,70
20    LIN(J)='-'
      LIN(5)='0'
      LIN(36)='1'
      LIN(38)='5'
      LIN(37)='.'
      LIN(67)='2'
      GO TO 200
100   DO 31 I=1,N
31    IYG(I)=10*YG(I)+5
      DO 21  J=1,70
21    LIN(J)='-'
      LIN(15)='1'
      LIN(25)='2'
      LIN(35)='3'
      LIN(45)='4'
      LIN(55)='5'
      LIN(65)='6'
200   CONTINUE
      LIN(69)='C'
      LIN(70)='D'
      IF(IGR.EQ.1)LIN(70)='P'
500   WRITE(6,80)LIN
      DO 90 I=1,N
      DO 60 IJ=1,70
60    LIN(IJ)=' '
      DO 40 J=1,70
      LIN(5)='|'
      NT=I/5
      N1=NT*5
      IF(N1.EQ.I)LIN(5)='-'
      IF(IYG(I).GT.70)GO TO 71
      IF(IYG(I).LT.5)GO TO 70
      LIN(IYG(I))='.'
      GO TO 40
70    LIN(3)='!'
      GO TO 40
71    LIN(69)='!'
40    CONTINUE
      IF(IGR.EQ.2)GO TO 99
      WRITE(6,80)LIN
      GO TO 90
99    TT=TIME(I)
      WRITE(6,88)LIN,TT
90    CONTINUE
      DO 300 I=1,5
      DO 101 II=1,70
101   LIN(II)=' '
300   WRITE(6,80)LIN
80    FORMAT(1X,70A1)
88    FORMAT(1X,70A1,F8.3,'S')
      RETURN
      END
```

```
*
*
*                -------
*                 SHAPE
*                -------
*
*
*       SUBROUTINE " S H A P E " PRODUCES A ROUGH DRAW OF THE
*       CANOPY SHAPE ON THE LINE PRINTER OR ON THE TERMINAL
*       SCREEN.
*
*
*
      SUBROUTINE SHAPE(XM,YM,AL,XI)
      CHARACTER LN(69)
      DO 1 I=1,69
1     LN(I)=' '
      DO 2 I=1,7
      IF(I.LT.5)LN(35)=':'
      IF(I.EQ.6)LN(35)='V'
      IF(I.EQ.5)LN(35)='_'
2     WRITE(6,10)LN
      DO 5 I=1,69
5     LN(I)=' '
      DO 3 I=1,69
      YII=Y(XI,XI,XM,YM,AL)
      LN(I)='-'
      LN(35)='|'
      IL=30*Y(XI,XI,XM,YM,AL)/YM
      LN(IL+35)='.'
3     LN(35-IL)='.'
      WRITE(6,20)LN
      IXI=18*XI/YM
      DO 4 J=1,IXI
      DO 6 IJ=1,69
6     LN(IJ)=' '
      XX=XI-XI/IXI*J
      XX=ABS(XX)
      DO 7 I=1,69
      LN(35)='|'
      YII=Y(XX,XI,XM,YM,AL)
      IS=30*YII/YM
      LN(35+IS)='.'
7     LN(35-IS)='.'
4     WRITE(6,22)LN,XX,YII
10    FORMAT(69A1)
20    FORMAT(69A1,'   X       Y')
22    FORMAT(69A1,2F6.3)
      RETURN
      END
```